RIGA TECHNICAL UNIVERSITY
Faculty of Power and Electrical Engineering
Institute of Industrial Electronics and Electrical Engineering

ANDREJS STEPANOVS
Doctoral student of program “Computer control of electrical technology”

RESEARCH AND DEVELOPMENT OF MODULAR UNINTERRUPTIBLE POWER SUPPLY SYSTEM WITH VARIED ENERGY SOURCES AND STORAGES

Doctoral thesis

Scientific supervisor
Dr. sc. ing., professor
I. GALKIN

Riga 2011

Annotation

The doctoral thesis is dedicated to the elaboration of modular uninterruptible power supply system that utilizes versatile power module (VPM). The novelty of the work and difference from many existent modules of UPS is in multifunction of the VPM. Existent UPS modules allow only to increase power or to add module for system redundancy for higher reliability. The VPMs allows connection of alternative energy sources and storages like supercapacitor, flywheels, fuel-cells, photovoltaic panel, wind-turbines and etc. At the given moment on the market there are many different types of UPS systems. Some of them are not expandable at all. Some of them can be parallel for higher power and reliability increase. Some of them utilize alternative storage like supercapacitors and flywheels. Most advanced UPS system even switches between operation modes (“online” mode or ”line-interactive” mode) for higher efficiency or higher protection. The modular UPS system that is researched in the thesis combines most features of the UPS systems mentioned above.

It allows:

- To build stand alone converters like invertors, active rectifiers, DC/DC converters;
- To build different UPS topologies like “standby UPS”, “on-line UPS”, “DC-UPS”;
- To utilize different energy storages like supercapacitor, flywheels;
- To utilize different energy sources like photovoltaic panels, wind-turbines, fuel-cells;
- To build UPS systems for remote places with alternative primary energy source where does not available power grid;
- Power converters that are built with VPM can be easily rebuild to any another system.

The first chapter describes grid problems. There are given short UPS topologies description. Energy sources and storages which can be utilized in UPS systems are described as well. At the end of the first chapter there are given the reasons of modular system utilization.

In the second chapter VPM development stages are given.

In the third chapter development of Matlab-simulink model of VPM and its control algorithms are described.

The forth chapter considers the proof of possibility of usage of VPM for UPS systems assembly by means of simulations and experiments.

In the last chapter price of VPM and UPS system that are built with VPM are calculated.

The thesis, written in English, contains: 190 pages, introduction, 5 chapters, conclusions, 190 figures, 72 formulas, 29 tables, 68 references and 4 appendixes.

Anotācija

Šī doktora disertācija ir veltīta uz universāliem spēka moduļiem (USM) veidotas modulāras nepārtrauktās barošanas bloka (NBB) sistēmas izstrādei. Darba novitāte un atšķirība no citiem jau eksistējošiem NBB moduļiem ir USM multifunkcionalitāte. Esošie NBB moduļi ļauj palielināt jaudu vai apvienot vairākus moduļus sistēmas drošuma palielināšanai. Ar USM palīdzību arī var izmantot tādus alternatīvās enerģijas avotus un uzkrājējus kā superkondensatorus, spararatus, kurināmā elementus, saules paneļus, vēja ģeneratorus un citus. Tirgū šobrīd ir pieejamas dažādu veidu NBB sistēmas. Dažas no tām nav paplašināmas. Dažas no tām var slēgt paralēli, lai palielinātu jaudu un drošumu. Dažas no tām izmanto tādus alternatīvos enerģijas uzkrājējus kā superkondensatorus un spararatus. Visattīstītākās NBB sistēmas pat var pārslēgties starp darbības režīmiem(dubultās pārveidošanas režīms vai mijiedarbības ar tīklu režīms), lai uzlabotu lietderību vai palielinātu drošumu. Disertācijā pētītā modulārā NBB sistēma apvieno lielāko daļu iepriekš minēto funkciju.

Ar to var:

- izveidot invertorus, aktīvos taisngriežus, līdzstrāvas pārveidotājus;
- izveidot dažādas NBB topoloģijas, piemēram, “NBB ar pārslēgšanos”, “dubultās pārveidošanas NBB”, “līdzstrāvas NBB”;
- izmantot tādus enerģijas uzkrājējus kā superkondensatorus un spararatus;
- izmantot tādus enerģijas avotus kā saules paneļus, vēja turbīnas, kurināmā elementus;
- izveidot NBB sistēmas priekš attālinātām vietām, kur nav pieejams tīkla spriegums, bet ir pieejami alternatīvie enerģijas avoti;
- veidot spēka pārveidotājus, kurus viegli pārveidot par citām sistēmām.

Pirmajā nodaļā ir aprakstītas tīkla problēmas. Ir dots īss NBB topoloģiju apraksts. Ir aprakstīti arī NBB sistēmās izmantojamie enerģijas avoti un uzkrājēji. Pirmās nodaļas beigās ir doti iemesli modulārās sistēmās izmantošanai.

Otrajā nodaļā ir aprakstītas USM izstrādes stadijas.

Trešajā nodaļā ir aprakstīta Matlab-simulink modeļu izstrāde priekš USM un tā vadības algoritmiem.

Ceturtajā nodaļā ir apskatīti modelēšanas un eksperimentālie pierādījumi iespējamajai USM izmantošanai NBB sistēmu veidošanā.

Pēdējā nodaļā ir aprēķinātas USM un ar USM veidotas NBB sistēmas izmaksas.

Disertācija ir rakstīta angļu valodā. Tā satur: 190 lapaspuses, ievadu, 5 nodaļas, secinājumus, 190 attēlus, 72 formulas, 29 tabulas, 68 literatūras avotus un 4 pielikumus.

Content

List of Abbreviations

AC – alternative current
DC – direct current
AC/DC – rectifier
DC/AC – inverter
DC/DC – direct current converter
PSU – power supply unit
PDU – power distribution unit
UPS – uninterruptible power supply
MTTR - Mean Time To Repair
UPSs - uninterruptible power supplies
UPSS - uninterruptible power supply system
VRM – voltage regulation module
VRMs - voltage regulation modules
SC – supercapacitor
EDLC – electric double layer capacitor
LAB – lead –acid battery
VRLA – valve regulated lead-acid
SLA – sealed lead-acid
PV – photovoltaic
DG – diesel-generator
PFC – power factor corrector (correction)
VFD – Voltage and frequency dependent
VI - Voltage independent
VFI - Voltage and frequency independent
DIN rail - is a metal rail of a standard type widely used for mounting circuit breakers and industrial control equipment inside equipment racks
BJT - bipolar junction transistor
IGBT - insulated-gate bipolar transistor
MOSFET - metal-oxide-semiconductor field-effect transistor
EMI - Electromagnetic Interference
EMC - electromagnetic compatibility
PCB – printed circuit board
ESR – equivalent series resistance
IC – integrated circuit
IO – inputs, outputs
DSP – digital signal processor
LED – light-emitting diode
RMS - root-mean-square
THD - Total Harmonic Distortion
PWM – pulse width modulation
PID – proportional-integral-differential
PI – proportional-integral
MBd - mega baud
VPM – versatile power module

Acknowledgements

Firstly, I would like to express my appreciation to Professor Ilja Galkin my supervisor for support during the last few years.
Secondly, I would like to thank all my colleagues, who gave their time and helped me to do my work better.
Finally, I would like to express my sincere acknowledgement to my dear parents and my wife, who always support me.

This work has been performed within the framework of the project “Support for the development of doctoral studies at Riga Technical university” supported by the European Social Fund within the National Programme “Support for carrying out doctoral study programmes and post-doctoral researches.

ESF
EIROPAS SOCIĀLAIS FONDS

EIROPAS SAVIENĪBA

Introduction

The electric power in the modern world is necessary everywhere. Without it any manufacturing, hospitals, banks etc cannot operate. Modern electrical equipment gives many advantages to us, but for correct operation this electrical equipment needs qualitative power supply. Good example computer, which gives us infinite opportunities: assistance in many jobs, help in studies, communications with the world, entertainment, etc. But many people also know disappointment and sorrow when due to grid fault they lose many hours of work. The best possibility to prevent grid outages is to connect load through uninterruptible power supply (UPS). There are different topologies of UPS (discussed in chapter 1.2) that give different class of protection and protect from different grid events. Each topology has advantages and disadvantages. To understand which type of protection needs load it is necessary to understand common grid faults and its danger (discussed in chapter 1.1).

Generally speaking there is no cost-effective and versatile solution for all types of loads (equipment) and each type of UPS better fits to particular loads and cases. AC motors work better with pure sine-wave, but mostly pure sine-wave has on-line topologies and sometimes line-interactive UPS. Most equipment with switching mode power supplies (SMPS) can be supplied with any form of voltage: square, stepped square (quasi sine-wave), sine-wave and even DC voltage. That is why for high efficiency and high reliability UPS system with different topologies can be used.

Another topical point is environmentally friendly devices with alternative energy sources like wind-turbines and photovoltaic panels that reduce CO_2 emission. Nowadays on the market many different solutions for solar and wind energy harvesting can be found. But these systems cannot be easily integrated in UPS system. Only some manufactures offer quite flexible solutions allowing assemble of different systems and managing of harvested energy in many ways. Its solutions allow assemble of supply systems that:

- - can operate as a stand alone systems;
- - can recuperate harvested energy to the grid;
- - system can operate as a backup system.

To realize these systems the manufacturers offer many types of inverters for each type of system:

- Inverter for grid-tied system
- Inverter for off-grid system

- Inverter for backup system

The inverters that are designed for backup systems have additional inputs and outputs for diesel-generator interfacing. In case of grid outage and lack of power generated by photovoltaic system it starts DG or use energy stored in batteries. Such systems in future will become more and more popular. But nowadays most of the systems are designed to use lead-acid batteries as backup storage.

As it will be discussed in the next chapters in some cases higher reliability can be given by such alternative backup storages like supercapacitors and flywheels. In future the interest to the alternative energy storages will increase due to its high reliability and environment friendly technology. It means that also the needs in UPS systems with these energy storages will increase.

As it can be seen there is a need in many different converters that interconnect all above mentioned energy sources and storages. But it is hard to find a manufacturer that offers all these kinds of converters for UPS system.

That’s why it was decided to develop versatile power module which can be used to assemble different UPS systems or many another power converters.

1. Research of grid problems and methods of its solving

1.1. Classification of grid problems

All grid events except one are characterized by a change in the magnitude of the voltage and they can have different time durations from milliseconds up to hours. Based on this the voltage events are classified by standard EN 50160 [2]:

1) **Power frequency**

In power grids frequency variation (Fig. 1.1) is extremely rare. Frequency variations can be in systems with standby diesel-generator especially if it runs on full power or overloaded. Mostly modern SMPS is frequency tolerant, and generally not affected by minor frequency shifts. Frequency variations are more dangerous in systems with motors, because it changes motor rate of rotation and other parameters like torques and power.

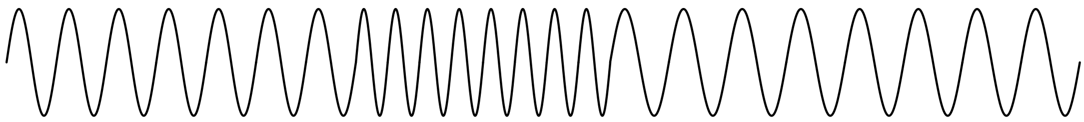

Fig. 1.1. Frequency variations

a) by standard EN 50160 frequency in the systems with synchronous connection to an interconnected system has to be in range:

±1% (49.5 - 50.5 Hz) for 99.5% of a year

-6%/+4% (47- 52 Hz) for 100% of the time

b) in the systems with no synchronous connection to an interconnected system has to be in range:

±2% (49 - 51 Hz) for 99.5% of a year

-15%/+15% (42.5- 57.5 Hz) for 100% of the time

2) **Voltage magnitude variations**

Voltage deviation within the range ±10% of rated voltage is acceptable.

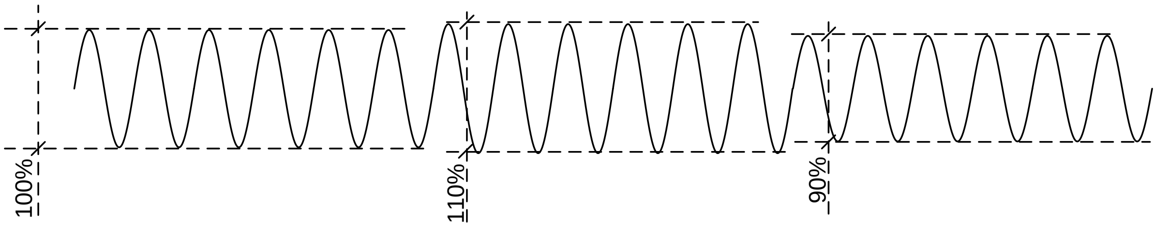

Fig. 1.2 Voltage acceptable variations

3) **Rapid voltage changes**

The same as voltage magnitude variations, but in short time. Usually caused by fast load changes in user grid.

4) **Supply voltage dips**

Voltage dip is a reduction of AC voltage below 90% for the duration 0.5 cycle to 1 minute. Dips are usually caused by “short circuits” in the grid and connecting of a load with heavy startup current. They are not predictable. Number of voltage dips per year may be from 10 to 1000.

By standard EN 50160 it must be:

Majority: duration <1s, amplitude >40%.

Locally limited dips caused by load switching on: 10 - 50%,

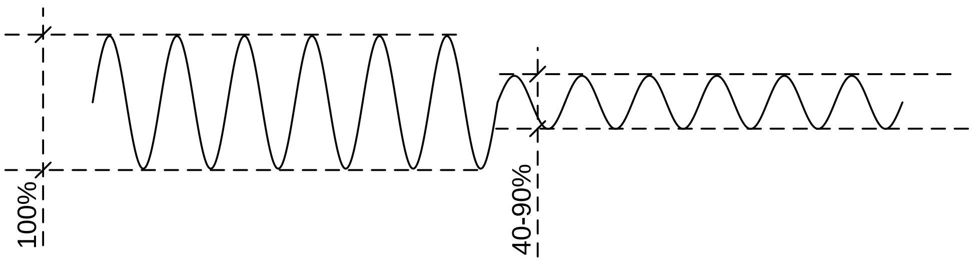

Fig. 1.3. Supply voltage dips

5) **Short interruptions of supply voltage**

An interruption is a complete loss of supply voltage or load current. Duration of it can be from 10 milliseconds to 3 minutes. It is usually caused by electrical grid damage: lightning strikes, trees, vehicle accidents, animals, destructive weather (fast wind, ice on wires) or basic circuit breaker tripping.

By standard EN 50160 it must be:

up to 1 minutes and few tens - few hundreds per year with duration 70% of them below 1 s

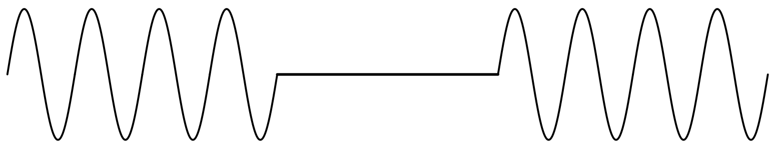

Fig. 1.4. short voltage interruption

6) Long interruption of supply voltage

Long interruptions are accidental interruptions that are not prevented by the distribution network operator. In principle it is the same as “short interruptions” but duration of it 3 minutes and above.

By standard EN 50160 it is:

longer than 1 minute (in some cases 3 minutes)

number of it is 10 – 50 per year

7) Temporary overvoltage

Overvoltage is an increase in voltage amplitude over 10% for the duration 10 milliseconds to 1 minute. They can be caused by large load disconnection or fault of one phase in a 3-phase system. High overvoltages can damage electrical equipment.

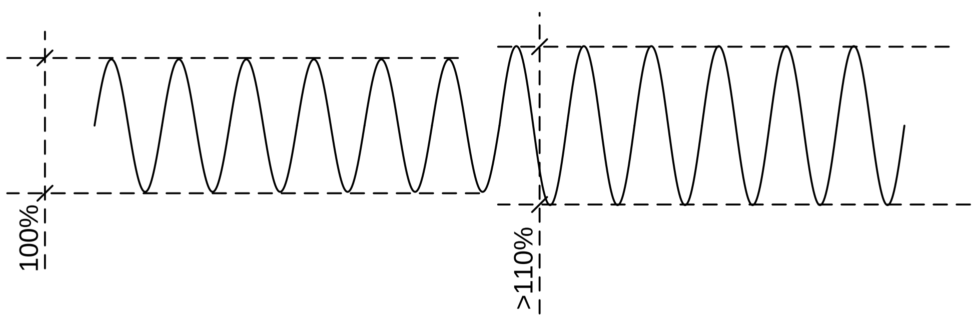

Fig. 1.5. temporary overvoltage

8) Transient overvoltages

These are very short high voltage or voltage peaks (fig.1.6). It must not exceed 6kV. They can be caused by electrostatic discharge, lightning, poor grounding, switching of inductive loads.

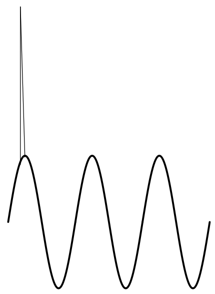

Fig. 1.6. Transient overvoltage

9) Supply voltage unbalance

Voltage unbalance of RMS value of sine-waves between phases that not exceed 2%.

By standard EN 50160 it must be:

up to 2% of RMS for 95% of time

up to 3% at some locations

10) Harmonic voltage

Harmonic distortion is the corruption of the fundamental sine-wave harmonic. Usually they are caused by SMPS of economical bulb, TV , computer, etc. Harmonic distortion can be dangerous for transformers, inductor motors, neutral wires in 3-phase systems.

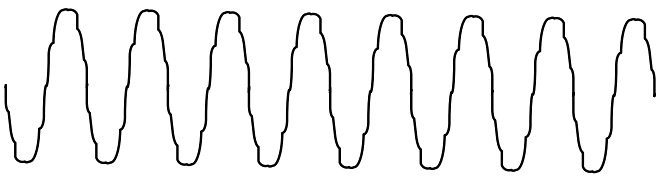

Fig. 1.7. Harmonically distorted voltage

By standard EN 50160 THD must be below 8% (including all harmonics up to the order 40)

Table 1.1:

Harmonic values percentage values according to fundamental voltage

Odd harmonics		Even harmonics	
Order	Relative voltage (%)	Order	Relative voltage (%)
3	5	2	2
5	6	4	1
7	5	6…24	0.5
9	1.5		
11	3.5		
13	3		
15	0.5		
17	2		
19	1.5		
21	0.5		
23	1.5		
25	1.5		

11) Interharmonic voltage

Interharmonics is a result of electrical equipment such as cicloconverters, static frequency converters, inductor motor and arcing device. Interharmonic can cause bulb or monitor flickering.

In theory, all of these grid events (voltage deviation outside $\pm 10\%$ of rated voltage) can cause electrical equipment fault, especially in sensitive electronic equipment. Often overvoltages above +10% cause reduction of equipment lifetime, but high overvoltages can damage equipment. In switching mode power supplies (SMPS) undervoltages below -10% cause consumption of higher current from grid, but due to that, conductors, inductors and other elements can have temperature rise, that in longer time also can cause equipment damage. Large undervoltage can cause equipment immediate shutdown. Undervoltages take up large part (as it is shown in fig.1.8. up to 95%) of grid faults and they are classified in a power quality category as voltage dips. Voltage dips are probably the most annoying of all power quality problems [3].

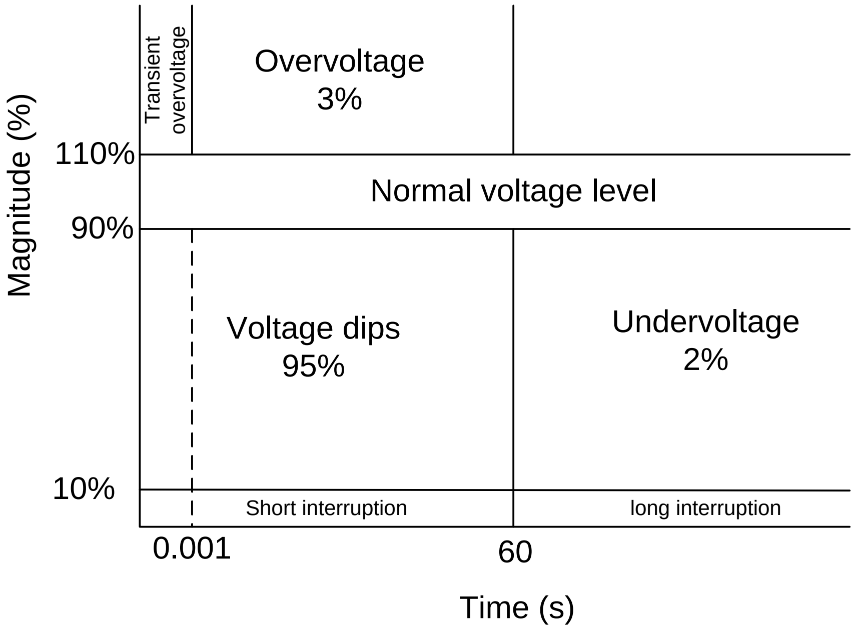

Fig. 1.8. Distribution of voltage problems [1, 4, 7]

As an example statistics which shows that outage cost for US industry estimated at 79$ billions annually can be given. It must be noted that voltage dips and short interruptions of supply voltage cause 2/3 of all damages (losses) [4].

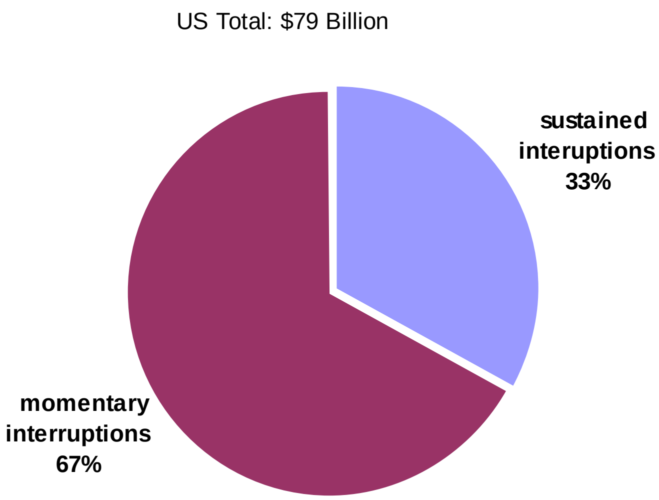

Fig. 1.9. Money damage due to interruptions [4]

Very good protections from short interruptions is provided by means of UPS. UPS and its classification are discussed in the next subchapter.

1.2. Classification of UPS

Classification of UPS by performance clarifies standard EN 620040-3 [3, 6]. Table 1.2. shows explain classification code.

Table 1.2.

Explanation of classification code

X X X -	X X -	X X X
Output dependency	Output waveform	Output dynamic performance
Describes output voltage dependence on input voltage in normal operation mode (supplied from grid)	- The first character describes waveform in normal or bypass mode - The second character describes waveform in battery (stored energy) mode	- the first character describes output voltage dynamic performance in case of switching between operation modes (for example switching from grid to battery mode) - the second character describes output voltage dynamic performance for step change of linear load (in all operation modes) - the third character describes output voltage dynamic performance for step change of non-linear load (in all operation modes)
VFI – voltage and frequency independent VFD – voltage and frequency dependent VI – voltage independent	S – sinusoidal voltage with THD<8%. All harmonics have to be in the range of standard EN 61000-2-2 X- generated waveform is sinusoidal with linear loads. With non-linear loads waveform THD will exceed 8% and can be in the range stated by manufacturer Y – Generated waveform is non-sinusoidal with THD that exceeds the range of EN 61000-2-2.	1 – no break of voltage (fig.1.10) 2 –voltage break up to 1 ms (fig.1.11) 3 –voltage break up to 10 ms (fig.1.12)

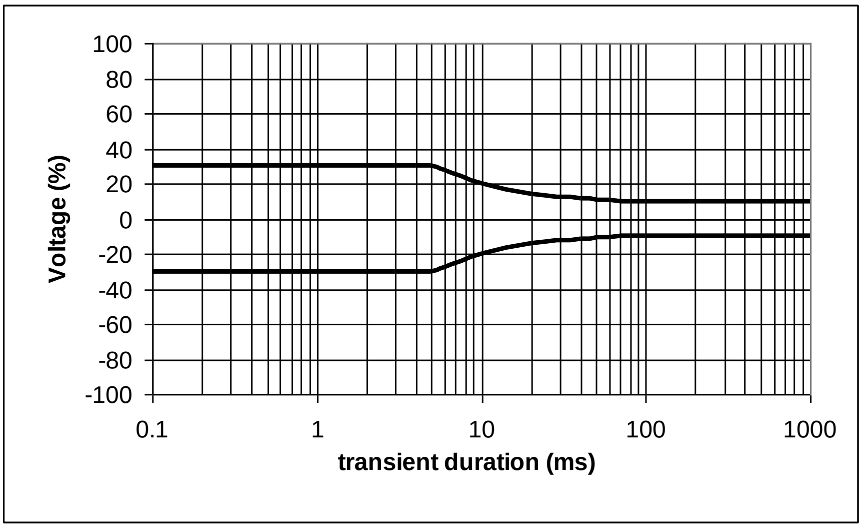

Fig. 1.10. UPS output voltage dynamic performance Classification 1 [LVS EN 62040-3]

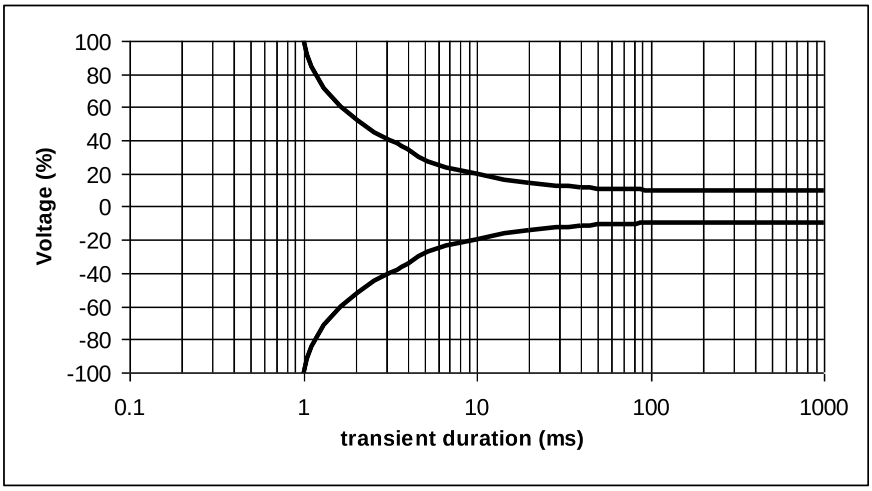

Fig. 1.11. UPS output voltage dynamic performance classification 2 [LVS EN 62040-3]

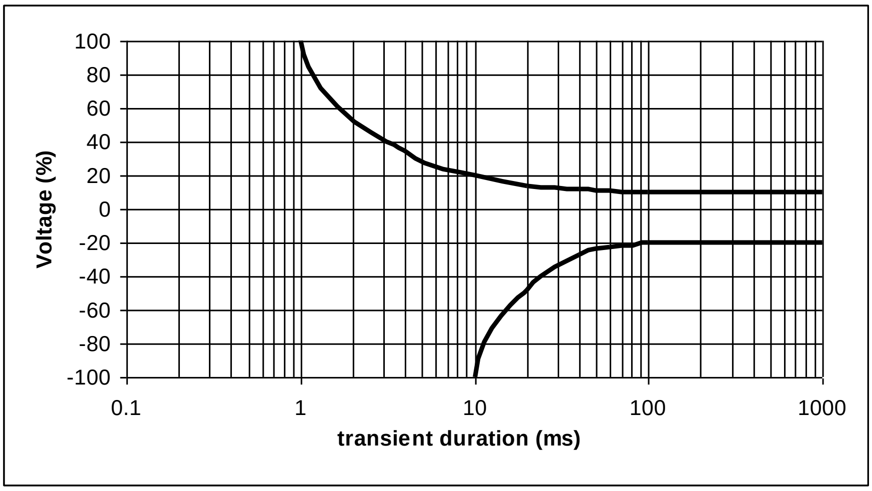

Fig. 1.12. UPS output voltage dynamic performance classification 3 [LVS EN 62040-3]

From all the above mentioned it can be concluded that best protection is provided by means of UPS with classification code “VFI-SS-111”. This means that output voltage:

- does not depend on input voltage
- output voltage in all operations mode (battery, grid, bypass) is sinusoidal
- output voltage has no interruption in the case of switching between modes
- in transient regimes output voltage changes do not exceed ±30% of rated voltage

Mostly such high protection level has online (double conversion) UPS topology.

Standard “LVS EN 62040-3” classification can be matched to classical UPS topology classification (table.1.3.).

Table1.3.

UPS topologies comparison with LVS EN 62040-3 classification

Class	LVS EN 62040-3 classification	Protection form grid events	Comments
Offline or Stand by	VFD - Voltage and frequency dependent	1) Grid failure 2) Voltage dips 3) Voltage peak	In normal operation mode load is connected directly to grid. In case of any grid failures it switches to battery mode. Protection time depends on battery capacity.
Line interactive	VI - Voltage independent	1) Mains failure 2) Voltage dips 3) Voltage peak 4) Undervoltage 5) Overvoltage	In normal operation mode load is connected to grid through transformer. In the case of most grid failures it is switched to battery mode. Only in undervoltage or overvoltage case it regulates output voltage using built-in transformer.
Online or double conversion	VFI –Voltage and frequency independent	1) Mains failure 2) Voltage dip 3) Voltage peak 4) Undervoltage 5)Overvoltage 6) Surges 7) Frequency variations 8) Voltage distortions 9) Voltage harmonics	In normal operation mode load is supplied from inverter that is supplied by rectifier. Only in the case of grid full outage or at very low undervoltage it switches to battery mode

There are also many another types of UPS, but they all will not be discussed. From all another types it will be noticed only “hybrid UPS” (also known as double conversion on demand) and DC-UPS [8, 9], because they have prospects in future due to high efficiency.

Table 1.4.

Other types of UPSs

Hybrid or Double Conversion on Demand	VFI –Voltage and frequency independent (in online mode)	The same as on-line UPS	In normal operation mode operates as line-interactive with high efficiency, but in case of any input voltage deviation it is switched to online mode
DC UPS	VFI –Voltage and frequency independent	The same as on-line UPS	Rectifier operates permanently.

1.2.1. Standby UPS

Stand-by UPS also known as “off-line UPS” or “line-preferred UPS”. It is most common type of UPS for home use. But due to sheer fall in prices of notebook and increased selling of it, seems that home workstations in future will be not so popular and due to that popularity of standby UPS also will decrease.

Figure 1.13 shows the bock diagram of a standby UPS. It consists of an AC/DC converter (battery charger), a battery bank, a DC/AC inverter, and a static switch. A passive filter and surge circuitry may also be used in the UPS.

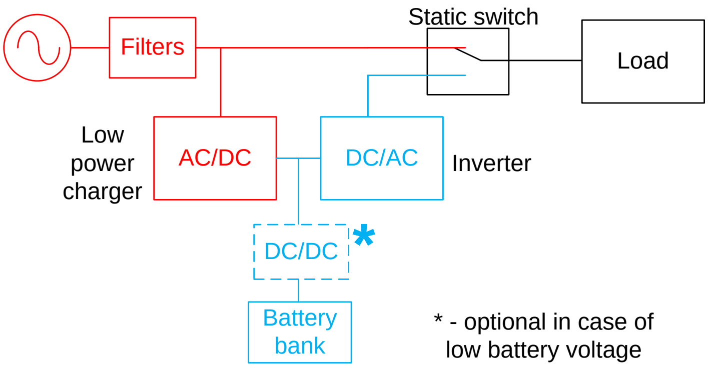

Fig. 1.13. Standby UPS system

Red – normal operation mode. Blue – battery operation mode (DC-DC converter is optional and is required in case of low battery voltage).

The static switch connects load to grid in normal mode of operation. In this mode load is supplied from the AC line directly or through passive filter. AC/DC converter (battery charges) charges the battery as well. Usually the power of charger is many times lower that that of UPS, that is why it charges battery during about 5-6 hours, but battery usually can supply load during 5-10 minutes only.

In the case of power outage or voltage dips the static switch is opened and the DC/AC inverter starts to supply load from the batteries. Inverter power is rated at 100% of the load power demand.

Switching time (transition time) from fault to DC/AC inverter start supply load usually is 4-15ms, that is quite short time for the most of modern SMPS and personal computers power supply unit (PSU) to not-shutdown. The main advantages of this topology are simple design, low cost, and small size.

1.2.2. Line interactive UPS

Line-interactive UPS is most common UPS for small business, WEB, departmental servers in power range from 0.5 to 5kW.

This UPS consists of a static switch, a DC/AC reversible converter, a battery bank. The DC/AC reversible converter is always connected to load. Due to that it could be used to improve the power factor and compensate the load current harmonics of the load. In normal mode DC/AC converter work as battery charger and/or active filter.

When grid fails “transfer switch” is opened and DC/AC converter starts to supply load from the batteries. Typical configuration of a line-interactive UPS is shown in Fig. 1.14 [3, 8]

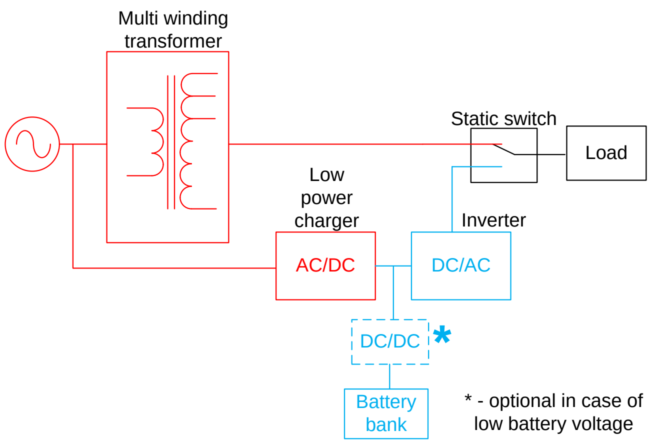

Fig. 1.14. A typical configuration of a line-interactive UPS system.

Red – normal operation mode. Blue – battery operation mode (DC-DC converter is optional and is required in case of low battery voltage).

Line-interactive UPS can have autotransformer or tap-changing transformer as well. It allows output voltage regulation when input voltage is out of rated range (usually +10 and -25%). Due to this UPS is switched to battery rarer and battery life increases. The main advantage of the line-interactive UPS is high efficiency and low cost. Usually its price is a bit higher than a standby UPS has, but lower than other UPS topologies.

1.2.3. Online UPS

On-line UPS also known as "double conversion" or "inverter preferred UPS" or "true UPS" consists of a AC/DC converter, a battery set, an DC/AC inverter, and a static switch (bypass). It is most common for large server room or data centres with power above 10 kW. Figure 1.15 shows the block diagram of a typical on-line UPS. At first sight it is identical to standby UPS topology, but there is principle difference that in normal mode "static switch" connects load to inverter and all power flows through rectifier and inverter. In the case of grid fault static "switch also" is connected to inverter, but the battery bank start supply the load through the same inverter. As a result the load voltage is sinusoidal without interruptions. The "Static switch" can be closed only in the case of UPS malfunction or UPS maintenance. For simple and easy switching to bypass mode UPS inverter output frequency is synchronised with that of grid. Synchronisation is interrupted only in the case of large deviation from grid frequency. Synchronisation also can be switched "OFF" when UPS runs as an international frequency adaptor (50Hz to 60Hz or vice versa).

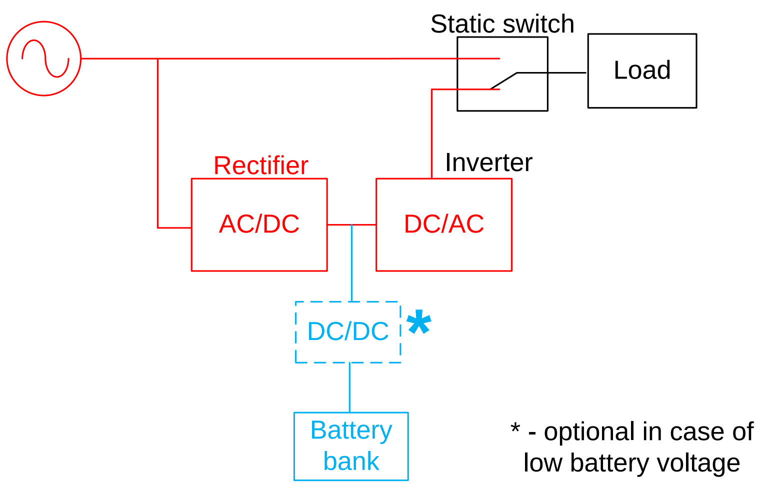

Fig. 1.15. Block diagram of an on-line UPS system.

Red – normal operation mode. Blue – battery operation mode (DC-DC converter is optional and is required in case of low battery voltage).

The AC/DC rectifier has to have power higher than load power, because in normal mode it supplies load through the inverter and in addition it can charge the battery.
Advantage of online UPS is very good power conditioning and protection from all grid failures (chapter 1.1). It uses battery very rarely as well, only in the case of deep voltage dips or full power interruption that results in the increasing of battery lifetime.
But due to double energy conversion it has low efficiency (usually 85-92%, and the newest one can have up to 95%).

1.2.4. Hybrid UPS

This type of UPS has no official "name", but HP and Eaton name it as "Double Conversion on Demand". In normal mode it connects load to grid directly like the standby UPS does, but in the case of some deviation from grid voltage it is switched to double conversion mode. In latest versions of UPS it can be forced to double conversion. It can be used in the case of prognoses (predicted) problems in grid power such as grid maintenance repair or in the case of lightning.
Examples of this hybrid/double conversion on demand UPS design are the HP R8000, HP R12000, HP RP12000/3 and the Eaton BladeUPS [9].

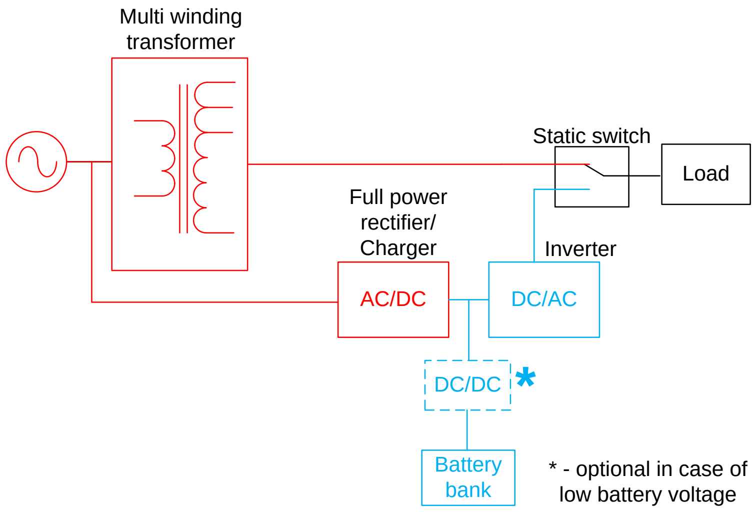

Fig. 1.16. Block diagram of an hybrid UPS (Online on demand) system.
Red – normal operation mode. Blue – battery operation mode (DC-DC converter is optional and is required in case of low battery voltage).

1.2.5. DC UPS

As a separate type of UPS the DC UPS can be mentioned (fig.1.17).

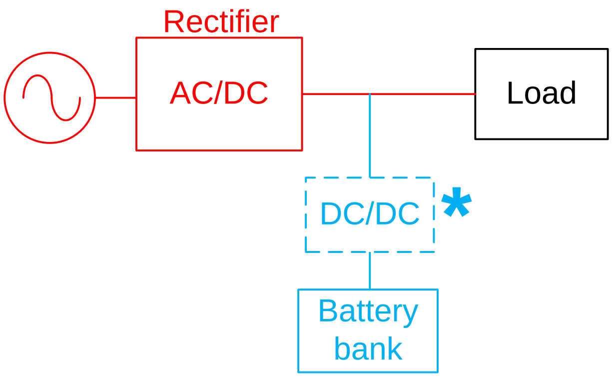

Fig. 1.17. Block diagram of DC UPS.

Red – normal operation mode. Blue – battery operation mode (DC-DC converter is optional and is required in case of low battery voltage).

Low voltage (12V,24V) DC UPSs are widely used as a backup supply for small technological processes and building security systems (alarm system, access control systems, video surveillance systems, alarm lighting systems and etc). This UPS is very small in size and can be mounted on DIN rail. Its rated power may vary from ten to hundreds watts. Most of all lead-acid batteries are used as energy storage.

Recently few companies began to offer DC UPS with supercapacitors. Example is innovative Siemens SITOP UPS500. Due to the supercapacitor this UPS is maintenance free and has very long service life. Even running at high ambient temperature (50 °C) after 8 years it will have 80% of their backup time. The supercapacitor is absolutely sealed and no ventilation of the mounting location is necessary (standard VDE 0510 Part 2 / EN 50272-2).

The backup time is not so long as with lead-acid battery, but in many cases it is enough to back up data and correctly shut down the equipment. For longer backup time supercapacitor modules can be connected in parallel. Minimum backup time is 3 seconds and up to 15 minutes for small load.

The DC UPSs with output voltage 48V in telecommunication and datacentrs are commonly used, but nowadays the DC UPS with output voltage 400V become more and more popular [57]. In 2007-2008 large project “DC Power for Improved Data Center Efficiency“ was realized which compared efficiency of DC based UPS systems and AC based UPS systems. The fact that AC based system (fig.1.18) has too many energy conversions (up to 6) before it reaches load is discussed there.

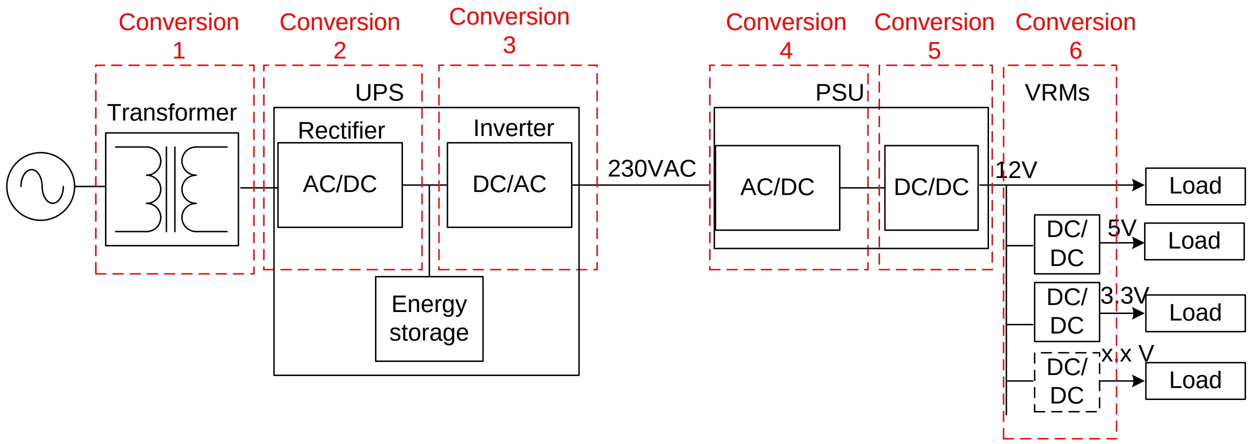

Fig. 1.18. AC based UPS system

In DC based UPS system (fig.1.19) there are two less voltage conversions. It allows increasing of total efficiency (usually for 5-7%) of energy from grid to load.

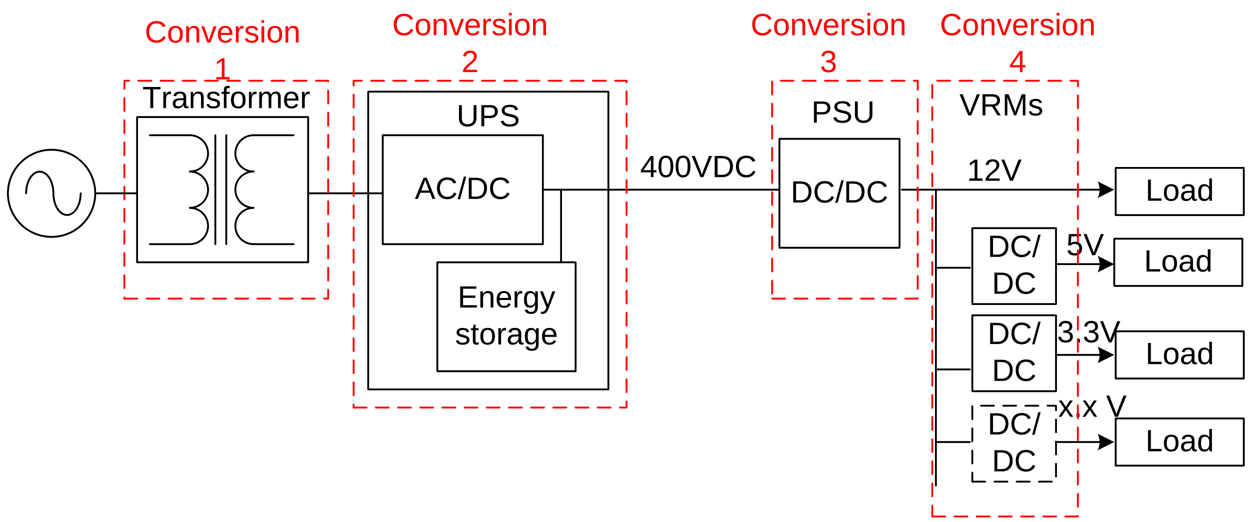

Fig. 1.19. DC based UPS system

Another advantages of DC based UPS system are:

- Gain in the efficiency is given without taking into account reduction of produced heat and reduction of power consumption of cooling system.
- Increase of efficiency of distribution system due to higher voltage and lower current in conductors
- Theoretical higher reliability due to fewer number of parts that can failure

1.3. Review of energy sources for uninterruptible power supply system and their interfacing converters

Main energy source of all uninterruptible power supplies in normal operation mode is power grid. When power grid operates normally some types of UPS connect load to grid directly without any conversion, but another types of UPS convert grid voltage (step-down, step-up, step-down and rectify, rectify and invert and etc). When power grid is inaccessible UPS supplies load from another energy source (in general all energy storages are energy sources, but with limited capacity).

This chapter will discuss most common UPS energy sources. They can be divided into two groups: AC sources and DC sources (table 1.5).

Table.1.5.

Energy sources

AC sources	DC sources
- grid - diesel-generator - wind turbine - flywheel*	- battery - supercapacitor - photovoltaic panel - fuel-cell - flywheel*

*- flywheel operates with AC voltage, but some manufacturers have developed flywheels with integrated DC/AC converter. In this case flywheel behaves like a DC source.

1.3.1. AC sources and their converters

To AC energy sources refer power grid, diesel-generator, wind-turbine and another sources where mechanical energy in converted into electrical with electrical generators. The mentioned sources have advantages and disadvantages. Main advantages and disadvantages of commonly used AC sources are given in table 1.6.

Table.1.6.

Comparison of commonly used AC energy sources

Energy sources	Advantages	Disadvantages
Grid	- power source with availability close to 99-99.9% - almost unlimited energy source (maximum power depends on safety device amperage) - relatively cheap energy source - does not need power converter for interfacing with AC loads	- for some cases (datacenter, hospitals etc supply) grid energy availability is not enough - voltage form can be distorted - There are places where the power grid isn't available. In this case they are usually replaced with another energy sources like diesel-generator, photovoltaic panels, wind-turbines etc
Diesel-generator	- highly reliable energy source - energy amount theoretically unlimited (practically limited with fuel tank) - does not need power converter for interfacing with AC loads - can be used in remote places instead of grid	- high price of generated electrical energy - in case of usage inside buildings a specially designed room (or container) for noise and vibration reduce has to be used
Wind turbine	- environment friendly energy source - can be used in remote places instead of grid	- non-constant power source - need power converter to interface with load
flywheel	- environment friendly energy source (energy storage) - high power density - high reliability - for short time (up to 30sec) backup can be cheaper power source that battery	- low energy density (backup time is below 30s mostly) - need quite complex bidirectional DC/AC converter

Independently on UPSS topology it has energy storage that has to be charged. As most of the energy storages need DC power the AC/DC converters (rectifier) must be used for energy conversion.

Some UPS have only small power rectifier to charge batteries, but some have powerful rectifier that also supply inverter like in online UPS. There are many types of rectifiers (fig. 1.20) that can be divided into many subgroups. Most rectifiers are unidirectional, but also can be bidirectional rectifiers/inverters like active front-end IGBT converter (fig.1.31., fig.1.32) that are used in most advanced and most expensive UPSS. Some rectifiers can have power factor correction (PFC), but some can be without it.

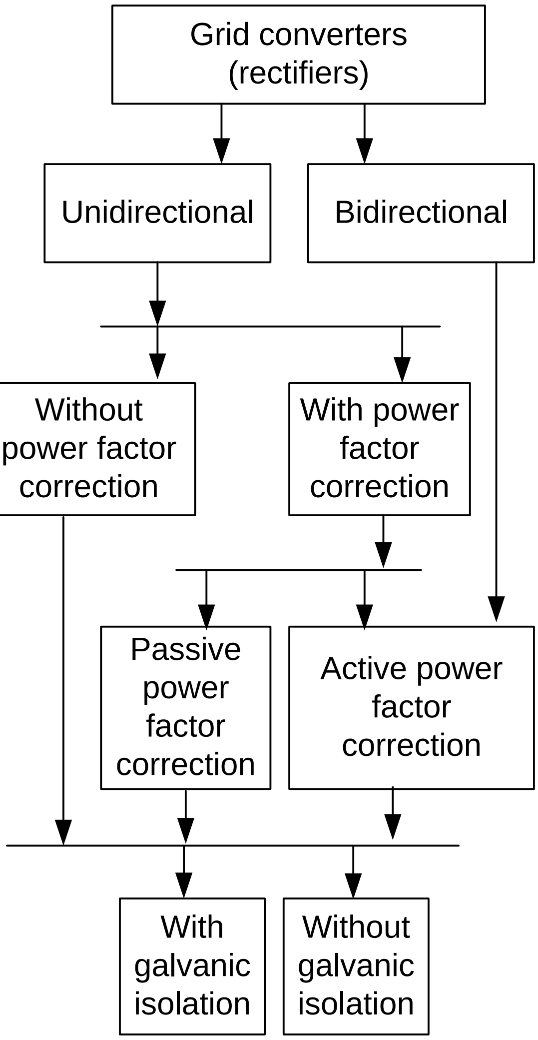

Fig. 1.20. Rectifier types

Unidirectional rectifiers without PFC

Simplest rectifiers consist only of diodes, but more often diodes and capacitors are used (fig.1.22, fig.1.24), but it has very important disadvantage. These topologies consume from the grid non-sinusoidal current with low power factor (PF) 0.5-0.7 (fig. 1.23. and fig.1.24).

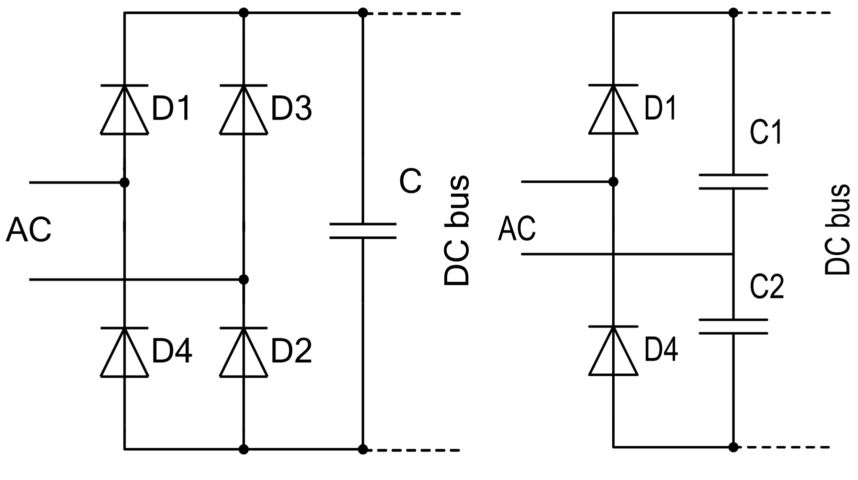

a) b)

Fig. 1.21. Rectifier a) full-bridge rectifier, b) half-bridge rectifier

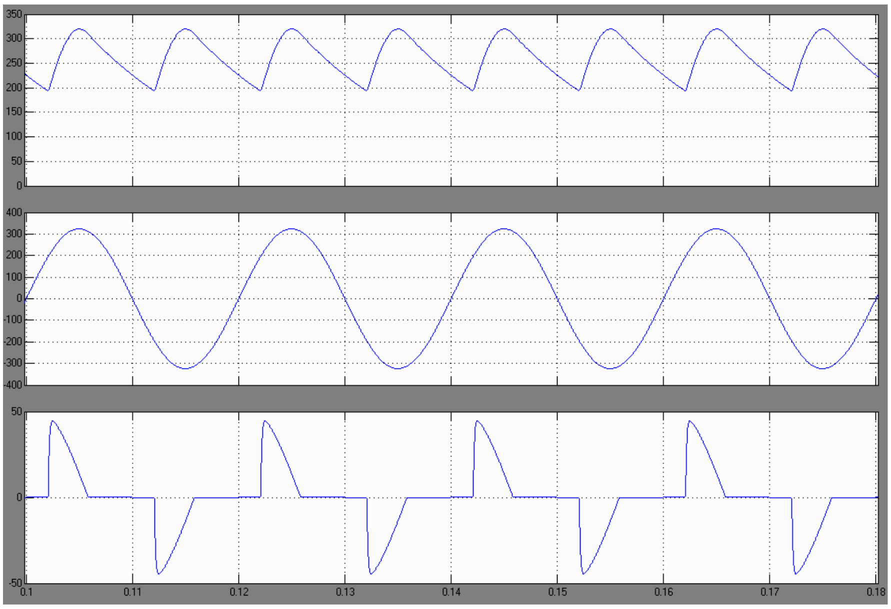

Fig. 1.22. Full-bridge DC-link voltage, grid voltage, grid current (from above respectively) COS(f)=0.88, Current THD = 90%, PF=0.66

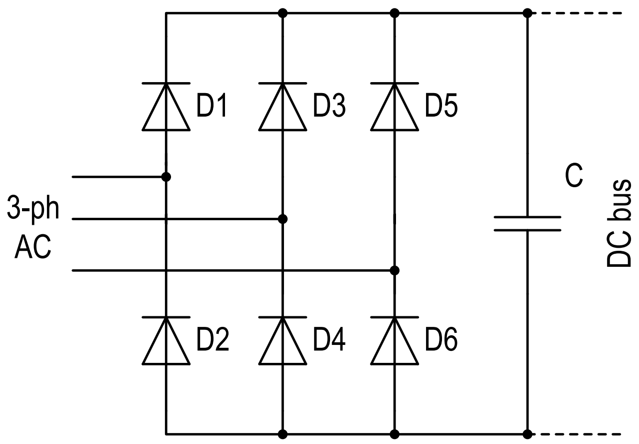

Fig. 1.23. 3-phase diode rectifier

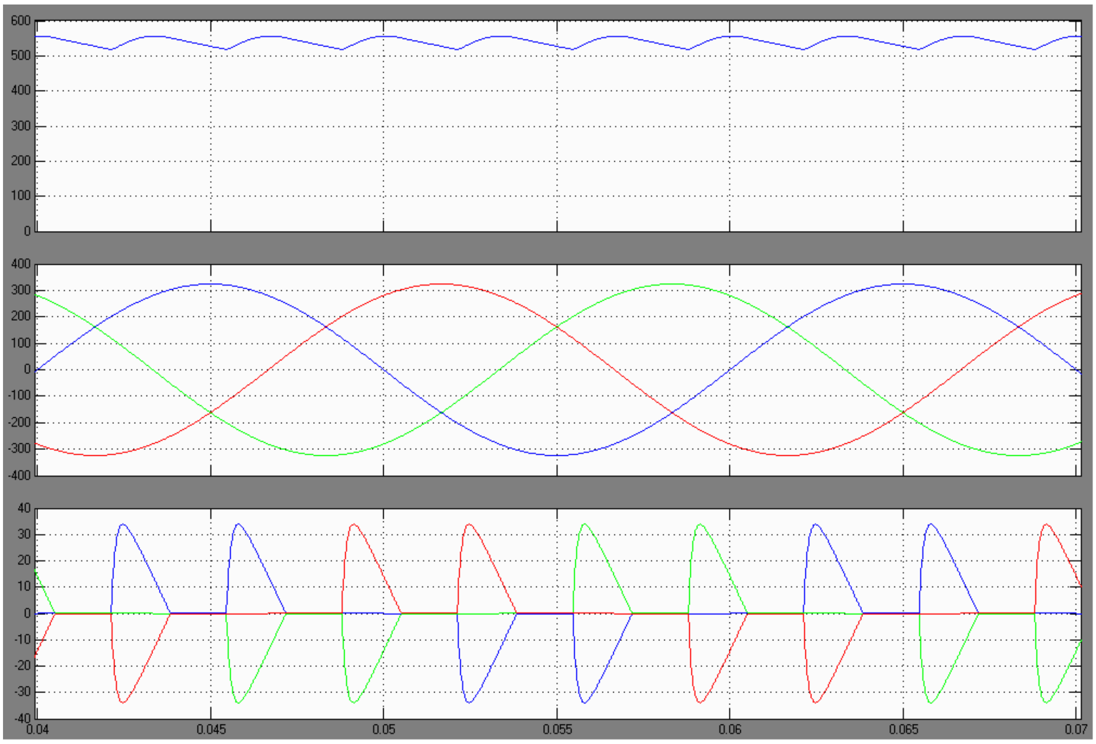

Fig. 1.24. DC-link voltage, grid voltage, grid current (from above respectively) of 3-phase diode rectifier

Shown signals has: COS(f)=0.98, Current THD = 123%, PF=0.62

In practice they are used very rarely due to the currents high harmonic distortions and low PF. Such rectifiers do not meet European standards EN 61000-3-2 [21]. Fig. 1.25 shows examples of rectifier's harmonics and standard EN 61000-3-2 for the devices with power below 600W.

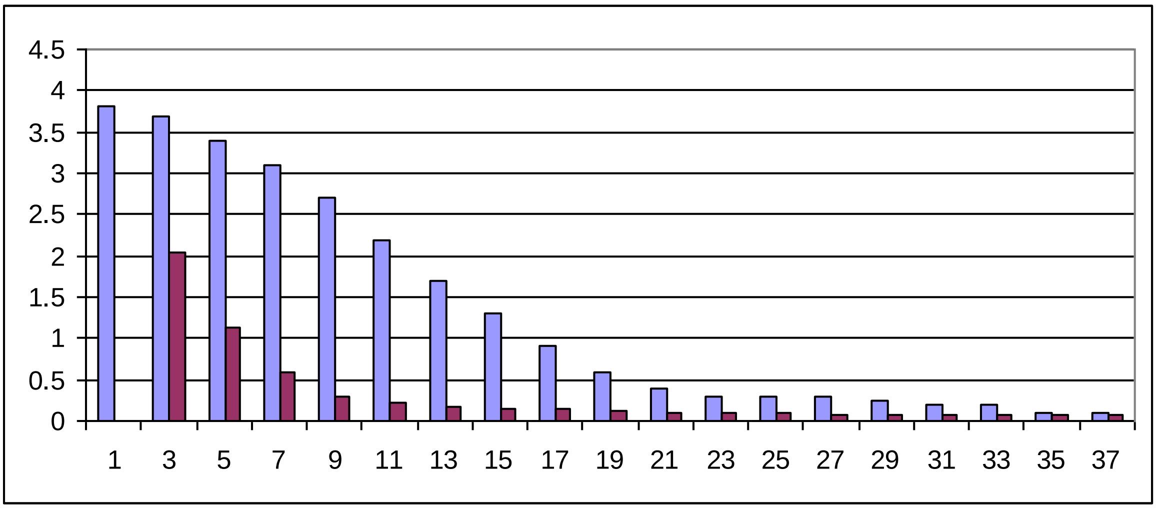

Fig. 1.25. Diode rectifier harmonics and Standarts EN 61000-3-2 Class D
(blue – rectifier current, red – standard EN 61000-3-2 class D)

Unidirectional rectifiers with passive PFC

To increase power factor and to fit European standards EN 61000-3-2 there are used passive or active power factor correctors. One-phase rectifiers with passive power factor corrector is shown in figure 1.26.a,b. Such rectifiers can have power factor about 0.7-0.9 (fig.1.27).

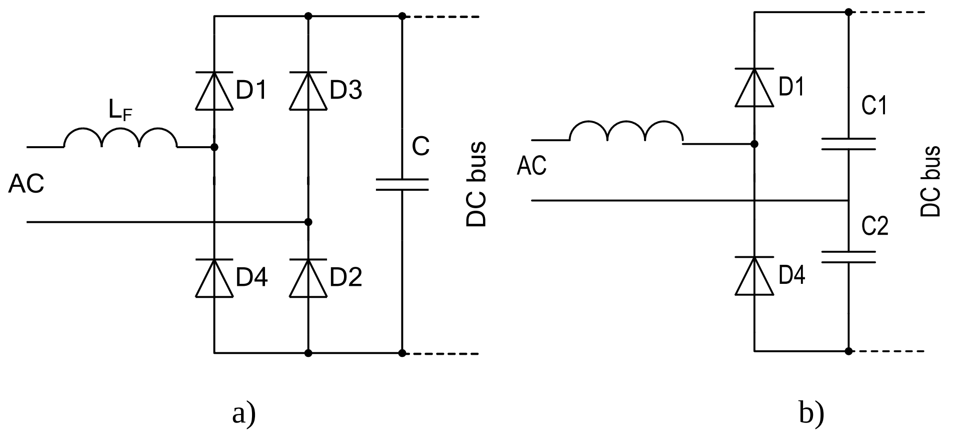

Fig. 1.26. a) Full-bridge diode rectifier with passive PFC, b) Half-bridge diode rectifier with passive PFC

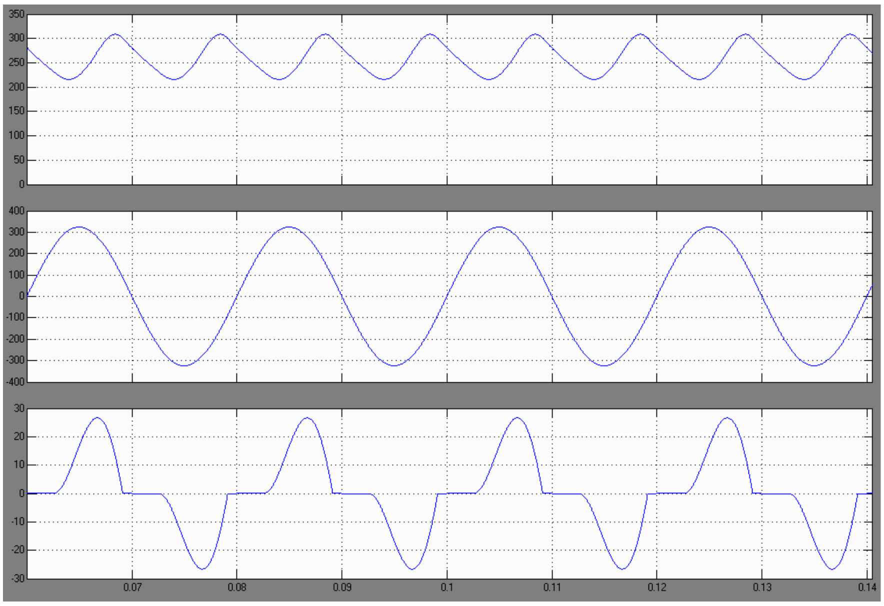

Fig. 1.27. Full-bridge DC-link voltage, grid voltage, grid current
COS(f)=0.99, Current THD = 49%, PF=0.9

Three-phase rectifier with passive power factor corrector is shown in figure 1.28. Such rectifiers also can have power factor about 0.9 (1.29).

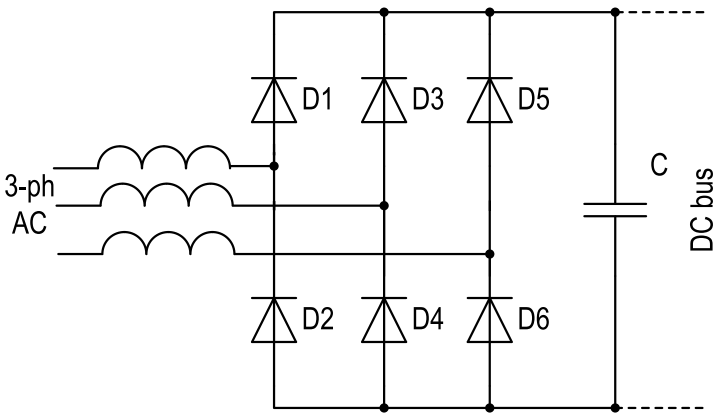

Fig. 1.28. 3-phase diode rectifier with passive PFC

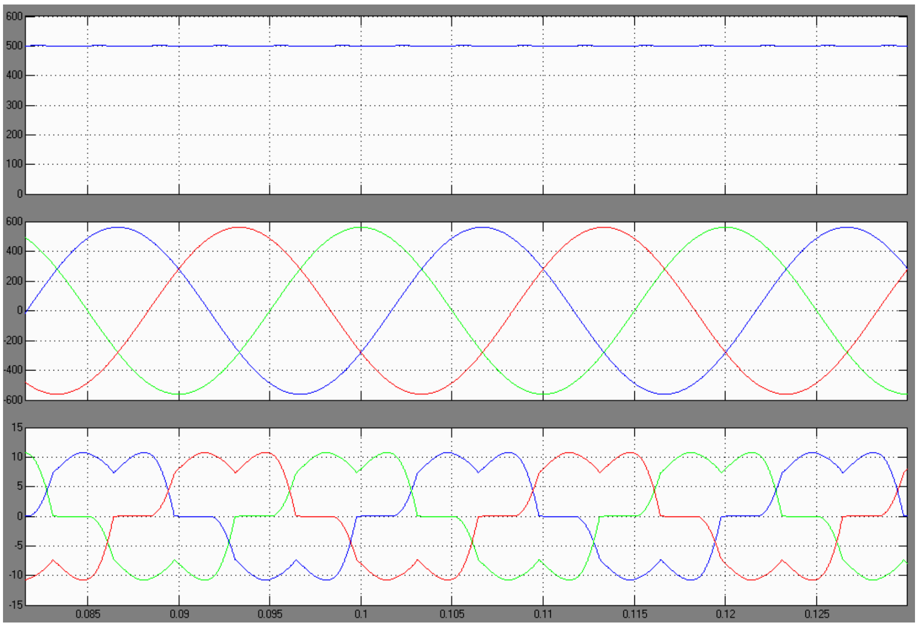

Fig. 1.29. DC-link voltage, grid voltage, grid current (COS(f)=0.94, Current THD = 25%, PF=0.91)

Due to better PF such rectifiers practically can be used in UPS.

Unidirectional rectifiers with active PFC

Unity power factor has rectifiers with active power factor correction. There are many different topologies of active PFC circuits. Most commonly used active PFC topology (boost PFC) is shown in fig.1.30. Power factor of active PFC usually is in the range from 0.95 to 1.

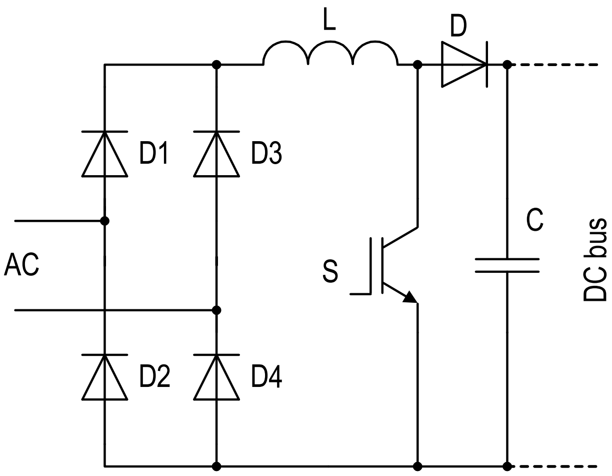

Fig. 1.30. Rectifier with active PFC

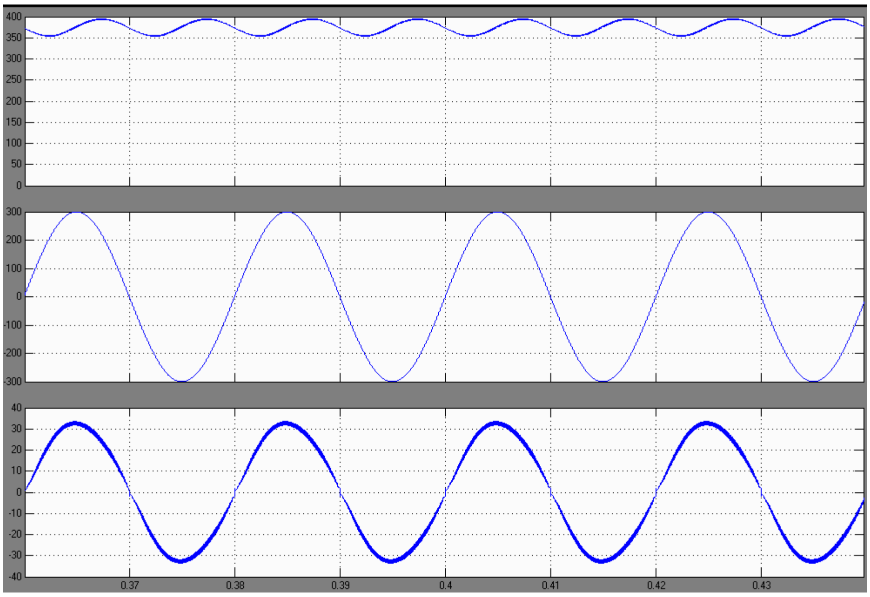

Fig. 1.31. DC-link voltage, grid voltage, grid current of boost PFC rectifier
COS(f)=0.99, Current THD < 5%, PF=0.99

More advanced PFC topology (boost interleaved PFC) is shown in fig.1.32. Due to interleaved PWM control signals pulsations in each inductor are also interleaved (fig.1.33. green and violet curves), that gives total input current with lower pulsations (fig.1.33. red curve).

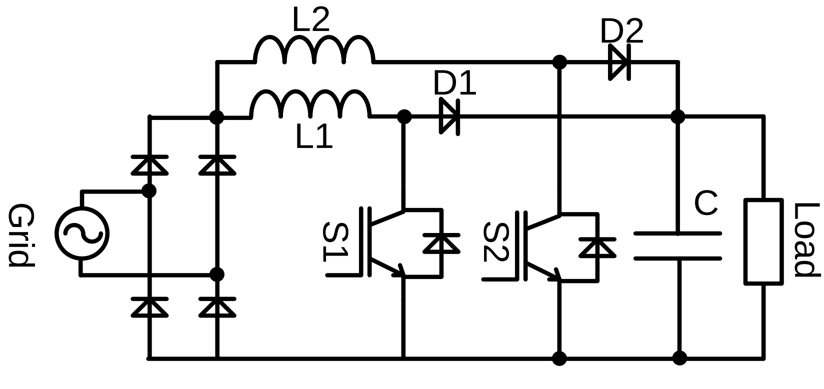

Fig. 1.32. Boost interleaved PFC converter

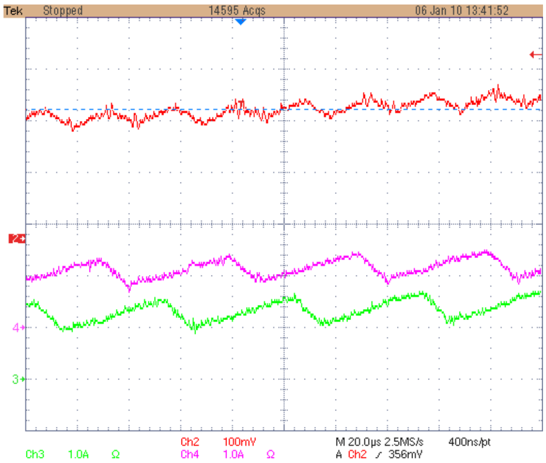

Fig. 1.33. Inductor currents of boost interleaved PFC converter
red – total current, green and violet – inductors current

Next PFC topology (bridgeless PFC) has no diode bridge (fig.1.34.). Current path goes though only 2 semiconductors and due to this the topology has higher efficiency. Another advantage of this topology is that transistors can be driven by one control signal and even by one driver.

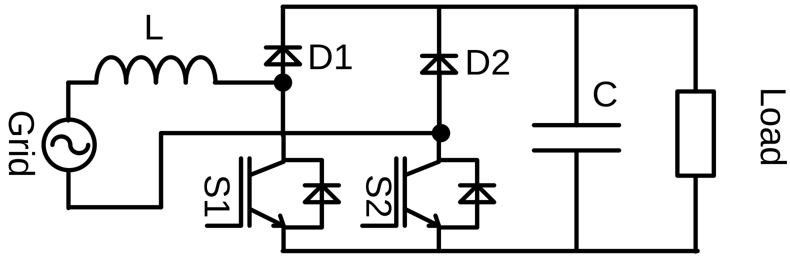

Fig. 1.34. Bridgeless PFC converter

Next PFC topology (bridgeless-totem PFC) has similar to the previous parameters but the transistors can not be driven by one control signal or one driver (fig.1.35.).

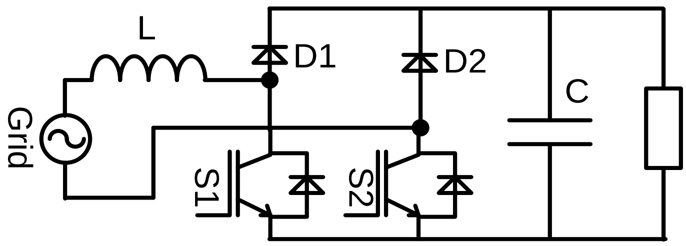

Fig. 1.35. Bridgeless totem PFC converter

Bidirectional rectifiers with active PFC

Full-bridge PFC (fig.1.36) is bidirectional rectifier/inverter. This topology is very versatile and can be used in many different applications. In addition, this rectifier/inverter can be used as a reactive power compensator or active filter.

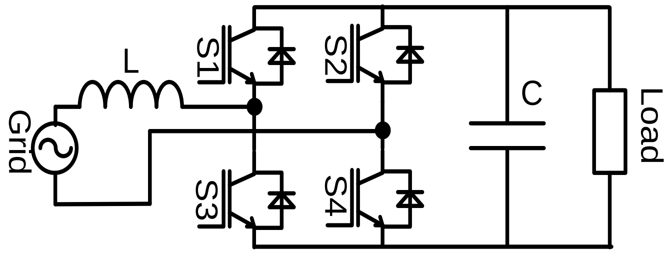

Fig. 1.36. Full-bridge PFC rectifier/inverter

Half-bridge PFC (fig.1.37) is also bidirectional rectifier/inverter and can be used in the same applications as full-bridge. Advantage of this topology is lower number of semiconductors. Disadvantage of it is high DC-link voltage (700-800V).

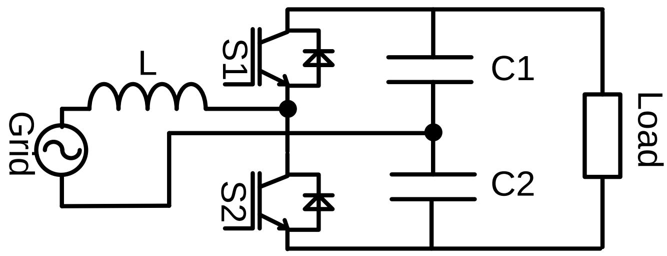

Fig. 1.37. Half-bridge PFC rectifier/inverter

In fig.1.38. 3-phase bidirectional PFC rectifier/inverter is shown. Similar to one-phase bidirectional PFC rectifiers it can consume fully sinusoidal current and compensate reactive currents. Such power converter type is integrated in flywheels that have DC output.

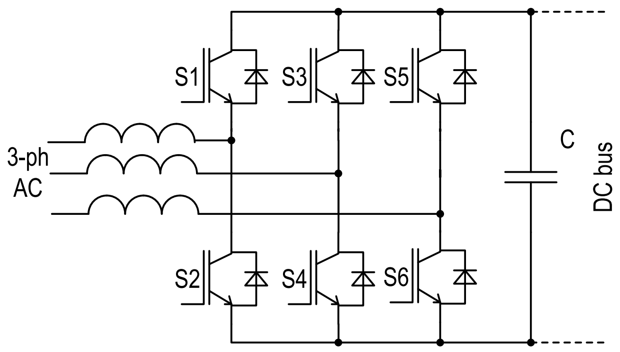

Fig. 1.38. 3-phase PFC rectifier/inverter

Galvanic isolated rectifiers

Galvanic isolated rectifiers are commonly used in most power supplies for home use (computer's power supply, mobile phone's chargers, audio and video device's power supplies). It is necessary to ensure the user safety. In older power supplies low frequency transformers (fig.1.39) were used. Due to that power supplies were bulky and heavy.

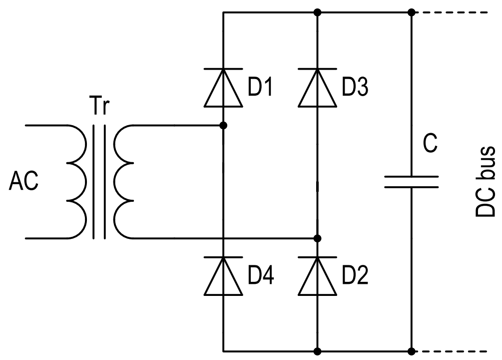

Fig. 1.39. Galvanic isolated rectifier with low frequency transformer

1.3.2. DC sources

Lead-acid battery, supercapacitor, fuel-cell, flywheel*, photovoltaic panels and others refer to DC energy sources. Mentioned sources have advantages and disadvantages. Main advantages and disadvantages of commonly used DC sources are given in table 1.7.

Table.1.7.

Common used DC voltage sources

Energy sources	Advantages	Disadvantages
Lead-acid batteries	- Cheap power source at longer backup time	- low power density - necessity of power converter to interface with AC load -
Supercapacitor	- highly reliable energy source - many charge/discharge cycles	- high price at longer backup times - necessity of power converter to interface with AC load
Fuel-cell	- theoretically unlimited energy source (practically limited with hydrogen fuel tank) - environmentally friendly	- Very expensive energy source - necessity of power converter to interface with AC load
Flywheel	- environmentally friendly energy storage - high power density - high reliability - for short time (up to 30sec) backup can be cheaper power source that battery	- low energy density (backup time is below 30s mostly) - necessity of power converter to interface with AC load
Photovoltaic panels	- environment friendly energy source - can be used in remote places instead the power grid	- non-constant energy source - Expensive energy source

a) Lead-acid batteries

Today lead acid batteries are more common secondary energy source and more often used type of rechargeable batteries in UPS.

There are few common types of lead-acid batteries [58]:

a. gel cell
b. absorbed glass mat (AGM)
c. vented (wet cell, flooded)

Flooded may be standard, with removable caps, or the so-called "maintenance free". Gel lead-acid batteries usually are sealed. AGM lead-acid batteries are valve regulated (commonly referred to as "VRLA" - Valve Regulated Lead-Acid).

Unfortunately lead-acid batteries (all types) have quite many disadvantages and only few advantages. Main advantage is low price of lead-acid batteries. Significant disadvantage of lead-acid battery describe Peukert's law.

That expresses the capacity of a lead-acid battery in terms of the rate at which it is discharged. At higher discharge rate, the battery's available capacity decreases.

Peukert's law equation is:

$$C_p = I^k t \tag{1.1}$$

where:

Cp - is the capacity according to Peukert, at a one-ampere discharge rate, expressed in (A·h).

I - is the discharge current in (A).

k - is the Peukert constant (dimensionless)

T -time of discharge (h).

In practice more often the capacity of a battery is given with reference to a discharge time:

$$t = H\left(\frac{C}{IH}\right)^k \tag{1.2}$$

where:

H - is the hour rating that the battery is specified against

C - is the rated capacity at that discharge rate.

For an ideal battery, the constant “k” is equal to one, and the capacity does not depend on the discharge current. For a real lead-acid battery, the value of k is usually in range between 1.1 and 1.3. In addition the Peukert constant is increasing with age of battery.

The Peukert law is very important in UPS systems where batteries discharge rated is usually between 1C-5C [15].

Graphical representation of Peukert’s law is given in fig. 1.40. In case of discharge current 0,1C the battery discharge time is 10 hours and battery capacity efficiency is close to 100 percent. If output current is 2C(20 time bigger) the battery discharge time is 15 minutes and battery capacity efficiency is close to 50 percents. At the biggest discharge currents this value is even less.

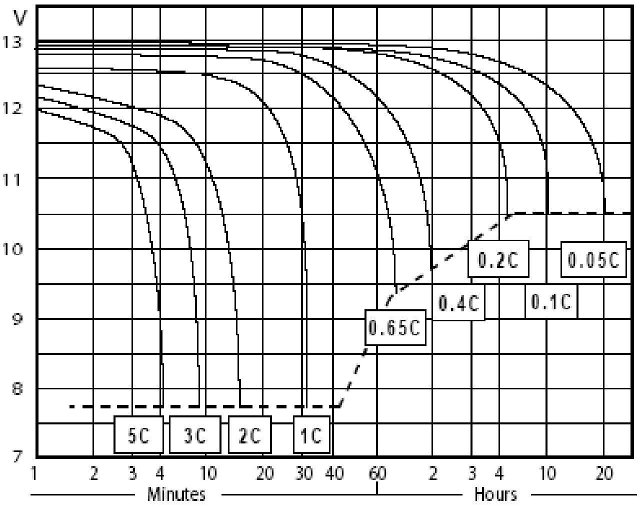

Fig. 1.40. Discharge characteristic of a lead-acid battery

Another disadvantage is that batteries life also depends on discharge depth. The deeper discharge, the longer time the battery is in discharging state, the fewer charge-discharge the battery can experience.

In the UPS which are used at home and office because of short operating time which is only enough for correct computer shutdown, deep discharge usually takes place. That can reduce a battery life up to 5 times (fig.1.41.).

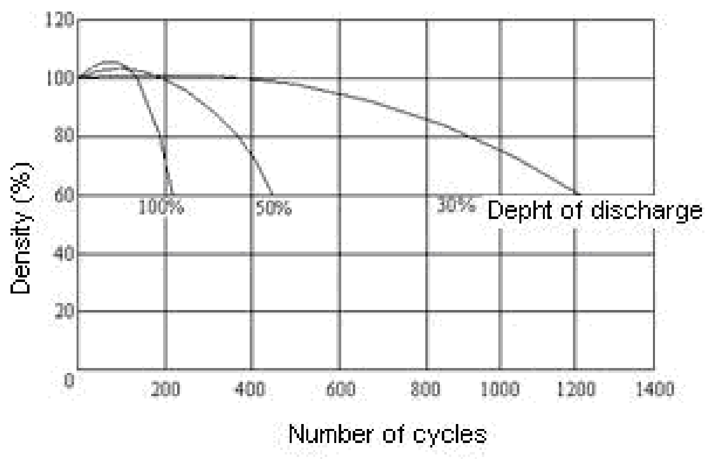

Fig. 1.41. Lifetime versus depth of discharge

Another factor that depends on battery lifetime is ambient temperature. Each $10C^0$ results in double decreasing of its lifetime.

One more factor which can affect a battery life is charging current. In order to the battery could accumulate maximum of its capacity, it is necessary to charge it correctly. There are few charging methods:

1. with constant voltage
2. with constant current at the beginning and with constant voltage at the end
3. with constant current at the beginning, with constant voltage in the middle, and with floating voltage level at the end (fig.1.42.)

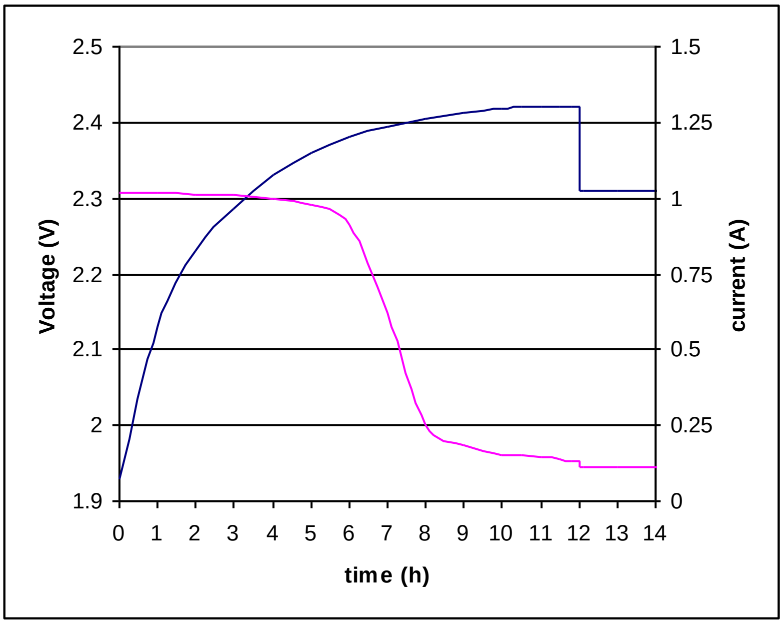

Fig. 1.42. Lead-acid battery charging algorithm

The best charging algorithm is the third method. At the initial stage high current can pass through the discharged battery which can cause overheating of the battery and consequently it is necessary to reduce value of charging current to 0,25C as a rule. At the second step, value of the charging current is reduced to prevent overvoltage in that way to keep the voltage constant about 2.4 volt per cell. And at the end of charging cycle the charging voltage is reduced to floating battery voltage that is usually 2.2-2.3V per cell.

b) Supercapacitors

The first record of the structure of electric double layer and possibility of it usage to store energy belongs to Hermann Ludwig Ferdinand von Helmholtz and dates back to 1879. The practical use of electric double layer in capacitors began only in the second half of the 20th century. It is powerful, quickly chargeable sources of energy with a long lifetime for the decision of great number of technical tasks.

The first capacitor with an electric double layer was developed in corporation "General Electric" and patented on July, 23, 1957 [14].

An electrochemical double layer supercapacitor consists of two carbon electrodes, electrolyte and separator. As well as traditional capacitor, EDLCs store charge in electrostatic field, it means that a charge does not pass from an electrolyte on an electrode or vice versa. When voltage is applied to capacitor, ions settle on electrodes due to attraction of opposite charges. Negative ions are accumulated near positive electrode and positive ions are accumulated near negative electrode.

Distances between layers accumulating the charge is measured with a few angstroms (1 And = 10-10 m = 0,1 nm), and the area of electrodes from a carbon can achieve 500 – 2000 m^2/gram.

Due to capacitor the capacity depends on area (S), distance between the layers accumulating the charge (d) and dielectric conductivity (e),

$$C = \varepsilon \frac{S}{d} \tag{1.3}$$

the capacity of such capacitors achieve enormous values (hundreds farads per gram).

Stored energy in the capacitor can be calculated

$$E=CU^2/2 \tag{1.4}$$

where: C – capacitance (F);

U – capacitor voltage.

Discharge time at constant current can be calculated using:

$$t = \frac{C(V_s - V_f)}{I} \tag{1.5}$$

where: t- time in seconds;

V_s – voltage in volts at the beginning of discharge;

V_f – voltage in volts at the end of discharge;

I – discharge current in amperes.

Supercapacitor discharging curves for constant current are depicted in fig.1.43. The example is given for Maxwell capacitor with capacitance - 3000F, rated voltage - 2.7V, ESR – 0.29mOhm [60].

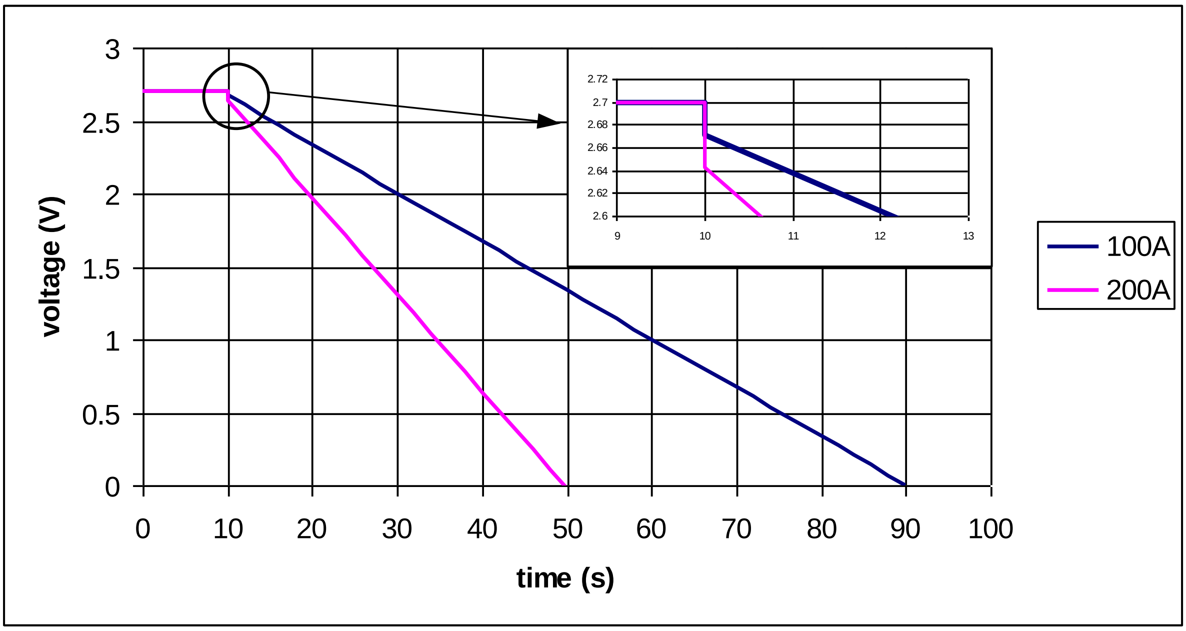

Fig. 1.43. Supercapacitor constant current discharge curves. Discharge starts at 20s.

In power electronics more actual is a discharge at constant power. Discharge time in the case of constant power can be found using:

$$t = \frac{CV_s}{2P}(1-(\frac{V_f}{V_s})^2) + CR_{ESR}\ln\frac{V_f}{V_s} \tag{1.6}$$

where: P – discharge power,

R_{ESR} – equivalent series resistance of supercapacitor.

Supercapacitor discharging curves for constant power are depicted in fig.1.44. The example is given for the same Maxwell capacitor.

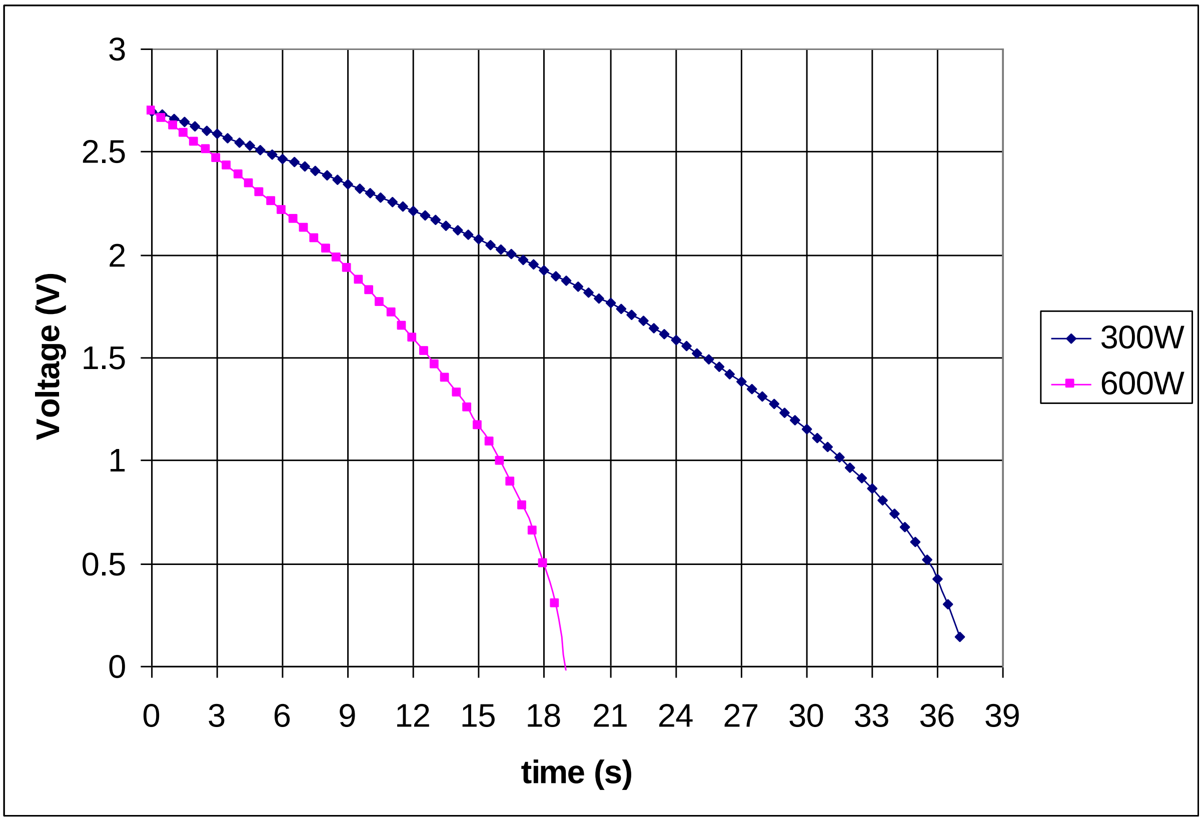

Fig. 1.44. Capacitor discharge curves at constant power

As charging and discharging processes are not chemical it is stable and supercapacitors are capable to do a lot of numbers of recharging cycles (up to 1 000 000 cycles). Also supercapacitors are less sensitive to the temperature conditions.

As soon as supercapacitors were developed it became possible to use them as energy sources. Supercapacitors have some advantages over batteries:

- Rapid recharge capability within minutes
- Wider temperature range (-40^{0}C - +65^{0}C)
- Low degradation after 1 000 000 cycles
- Environment safety
- High efficiency (above 95%)
- No maintenance

But there are also some disadvantages:

- High price
- Energy density lower that the batteries have
- Voltage depends on a degree of charge

c) Flywheel

Flywheels are known hundreds of years, but new material development and power electronics development gave new possibilities for this storage device. Flywheels store energy as kinetic energy in rotating objects. Stored energy depends on the moment of inertia of the rotating mass and on the RPM of the flywheel:

$$E = \frac{1}{2} J\omega^2 \tag{1.7}$$

where: E - the kinetic energy,

J -the moment of inertia of the rotating mass

Ω - the rotational velocity of the flywheel.

From (1.7) it follows that to increase (gravimetric) energy density of flywheel it is necessary to increase radius of flywheel or its rotation speed. For the first approach usually large iron pr steel disk is used and its rotation velocity can be up to 10 000 rpm. In the second approach usually carbon or other modern materials are applied with rotation velocity up to 100 000 rpm or even higher. Due to square-law of stored energy from RPM, such flywheels allow store much more energy in the same mass. Modern flywheel can have energy density close to the lead acid battery.

Disadvantage of flywheel is relatively large self-discharge (standby loses) up to 2%. To reduce air resistance and bearing frictional force for high speed flywheels vacuum containers (0.1 Pa) and magnetic bearings (flywheel-rotor levitate and due to it have not friction force) are used. Using these methods the standby loses can be reduced up to 0.1%.

Advantages of flywheel over lead-acid battery:

- Higher power density
- Fast recharge after use
- Wide temperature range

- Lifetime of more than 20 year

Disadvantages of flywheel over lead-acid battery:

- Lower energy density
- Higher price at longer backup time

Nowadays many manufacturers [53,54] offer flywheels with integrated DC/AC power converter, thus flywheel behave like a constant voltage source. Mostly the flywheels are designed to supply rated power only short moment (10-30 seconds). In most cases it is enough to start another voltage source like diesel-generator or fuel-cell. Due to flywheel advantages it became more and more popular in UPS systems.

d) Fuel cells

Nowadays the use of traditional batteries (lead-acid) and diesel-generator set is not always the best choice. It should be noted that the batteries are sensitive to ambient temperature, but diesel-generator can be very noisy and has high maintenance requirements. Today on the market various chemical, mechanical and electrical energy storage and different energy sources could be found as an alternative for diesel-generator and lead-acid battery. In some cases fuel-cells can be used as a backup energy source. It has many advantages, but a significant disadvantage as well - it is of very high price.

Volt-ampere curve for fuel-cell is depicted in fig. 1.45.

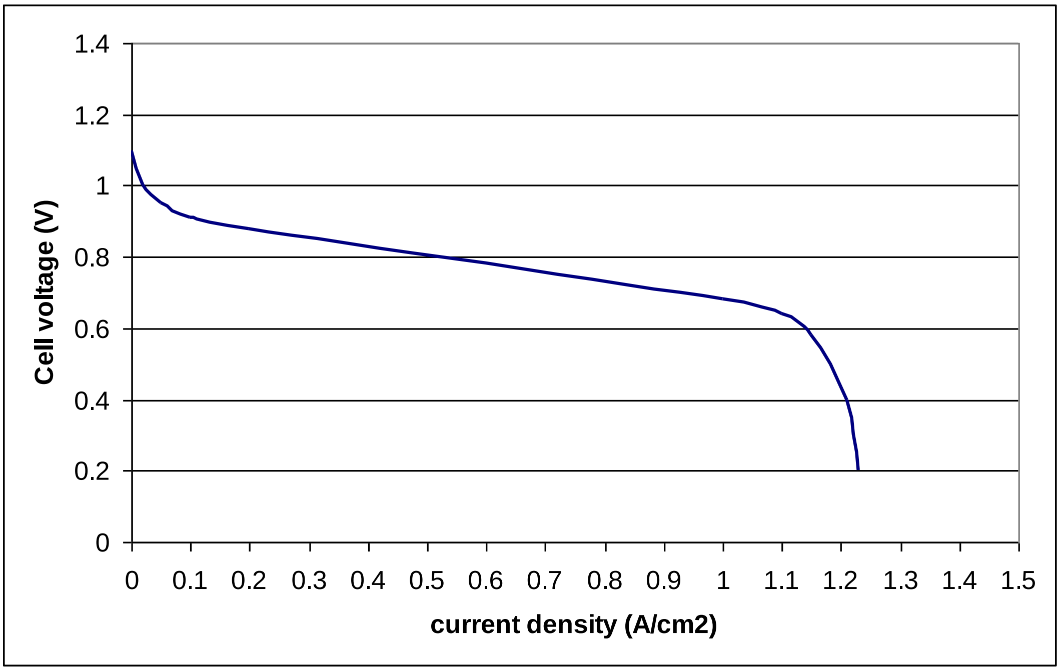

Fig. 1.45. Fuel-cell V-I curve

As it can be seen at higher currents the output voltage decreases due to internal resistance. It means that power converter has to have wide input voltage range.

e) Photovoltaic panels

In some cases when power grid is not accessible as a primary power source photovoltaic panels can be used. Low power system examples are parking automats, road marking, and weather stations. Another example of photovoltaic powered system is remote cottages which have no grid connection. In such applications the photovoltaic powered systems can be considered as the "UNINTERRUPTIBLE POWER SUPPLY SYSTEMS" that provides power to load without interruptions.

There are many different methods of photovoltaic panel connection to any load or grid (fig.1.46).

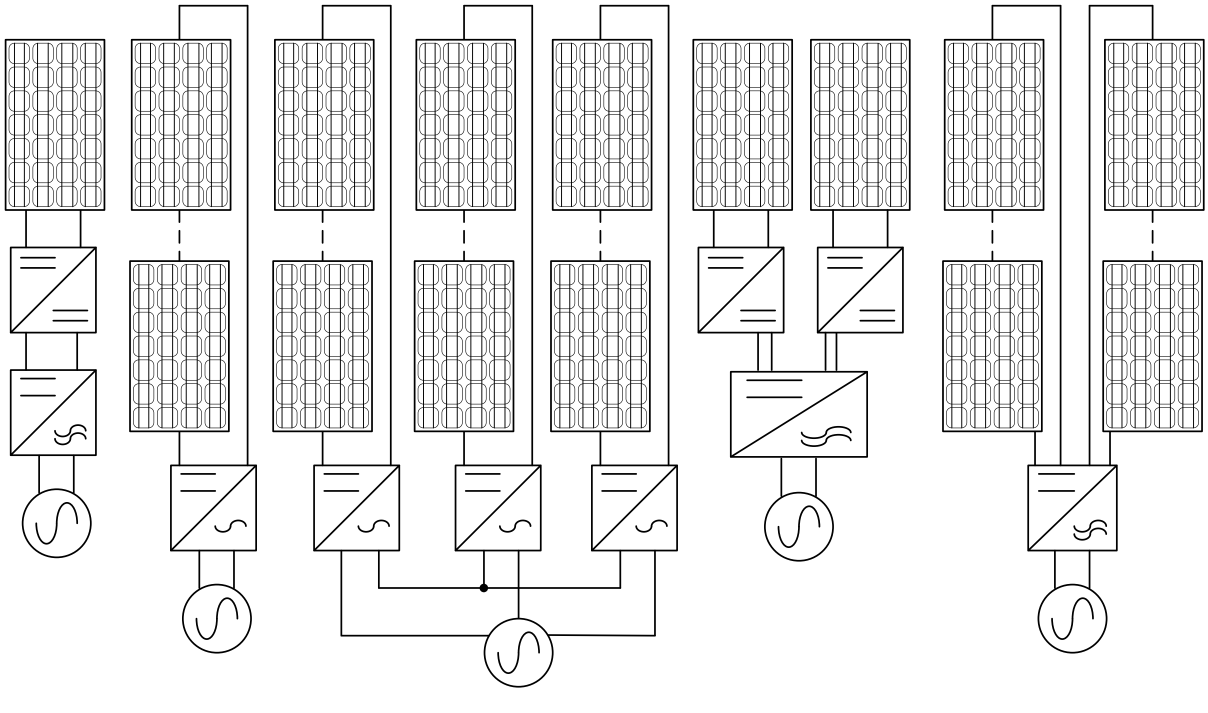

Fig. 1.46. Photovoltaic system connection methods: a) module integrated, b) string, c) mini-central, d) multi-string, e) central inverter concept [40]

Fig. 1.47. provides an example of volt-ampere and power curves of 90W monocrystalline photovoltaic panel at rated illumination (1000W/m^2). As it can be seen the maximum power is about 16V, but it can vary from panel temperature and illumination intensity. It means that to take maximum power from panel power converter has to operate at maximum power point.

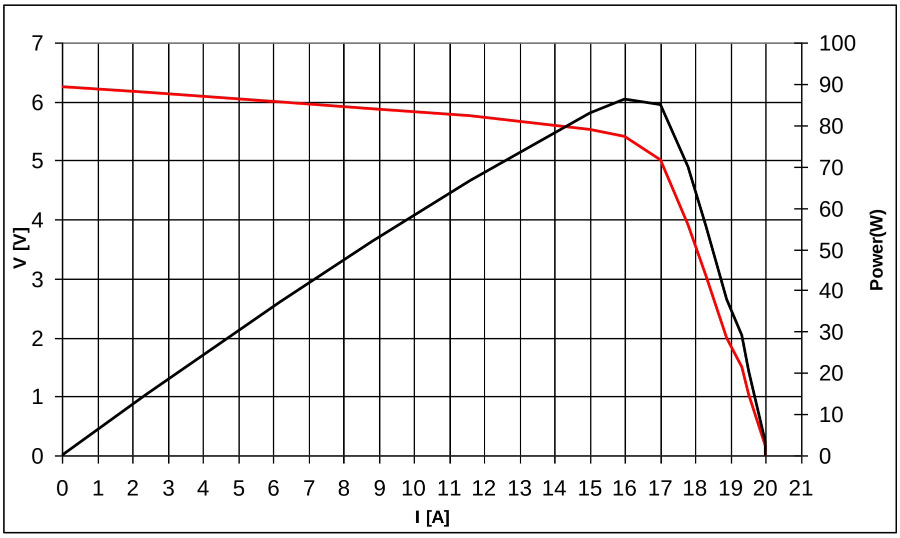

Fig. 1.47. Photovoltaic panel V-I curve and power curve

Depending on photovoltaic panel's power, voltage and the chosen photovoltaic connection method will depend on converter topology.

Main photovoltaic system advantages are:

- environmently friendly and clean energy
- almost unlimited energy source
- can be built in remote places where connection to the grid is impossible

Disadvantages:

- high capital investment
- intermittent energy source (depends on weather conditions, day time, longitude)

1.3.3. DC source converters

As it was shown there are many different DC voltage sources and some sources are storages. As it can be seen from voltage sources description their output voltage can depend on many parameters. Some voltage source voltage level depends on current, in some sources (that is storage) the voltage depends on state-of-the-charge and in some cases voltage is constant.

The market mostly offers power converters that are capable to operate with definite type of DC sources. Due to that in the systems with many different sources many different power converters will take place that in some cases may have compatibility problems.

Power converters types are depicted in fig.1.48.

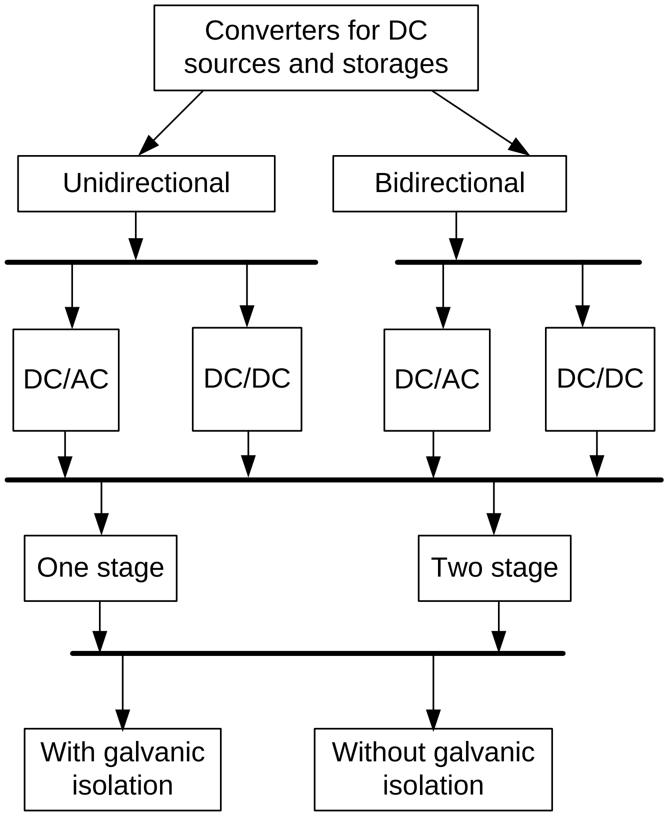

Fig. 1.48. Converters types for DC sources and storages charging and discharging

Unidirectional DC/DC converters

Widely used step-down converter (buck converter) is shown in fig. 1.49. Usually it is used when output and input voltage difference does not exceed 10 (practically 3-5). Output voltage (for continuous current in inductor) depends on duty cycle of transistor:

$$V_{0,ave} = d \cdot V_{in} \tag{1.8}$$

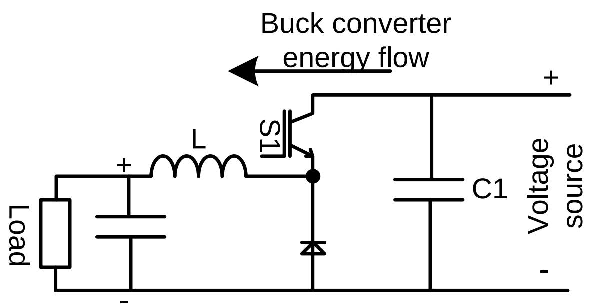

Fig. 1.49. step-down (buck) converter

Step-up converter topology (also known as boost converter) (fig.1.50) usually is used when there is a need to step-up the voltage. Practical difference between input and output voltage is up to 5. Output voltage (for continuous current in inductor) depends on transistor duty cycle:

$$V_{0,ave} = \frac{1}{1-d} V_{in} \tag{1.9}$$

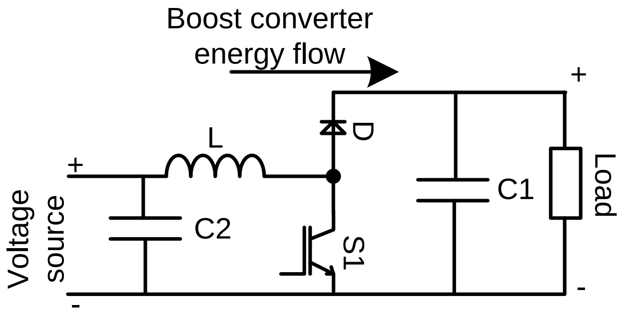

Fig. 1.50. Step-up (boost) converter

In the case of necessity in galvanic isolation between input and output power converter with pulse transformer (fig. 1.51) can be used. Voltage difference between input and output depends on the ratio of turns number of the pulse transformer primary and secondary coils.

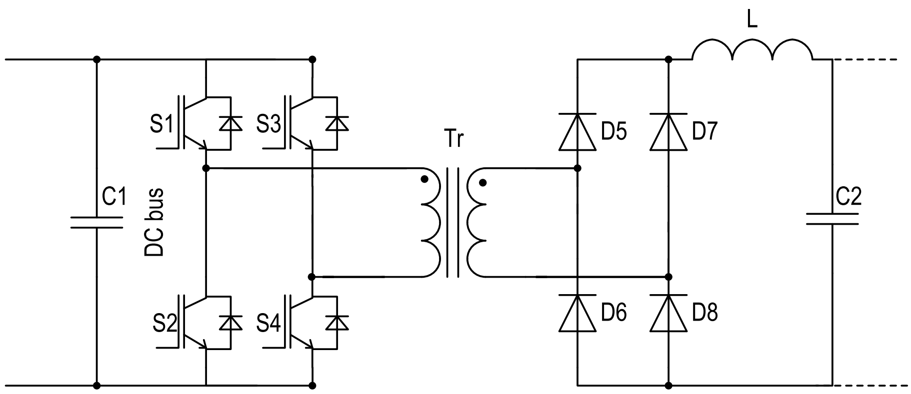

Fig. 1.51. Galvanic isolated power converter with high frequency transformer (full-bridge topology)

Bidirectional DC/DC converters

Topology that is shown in figure 1.52 can be used as a bidirectional converter. In one direction it can step up the voltage and in the other direction step it down. When it steps up the voltage S2 switch and free-wheeling diode in S1 operate. In step-down mode S1 switch and free-wheeling diode in S2 operate. Most common use is battery charger/discharger when voltages difference between output voltage and input is not very high (usually up to 5 times). Voltage dependence is the same as for conventional step-down and step-up converter.

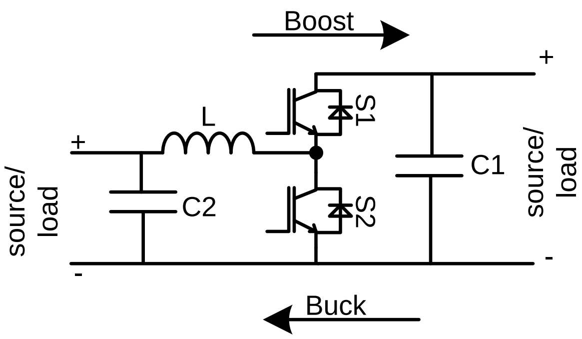

Fig. 1.52. Step-down/up (buck/boost) converter

The example of galvanic insulated power converter is depicted in fig.1.53. Voltage difference between input and output depends on the ratio of turns number of the pulse transformer primary and secondary coils.

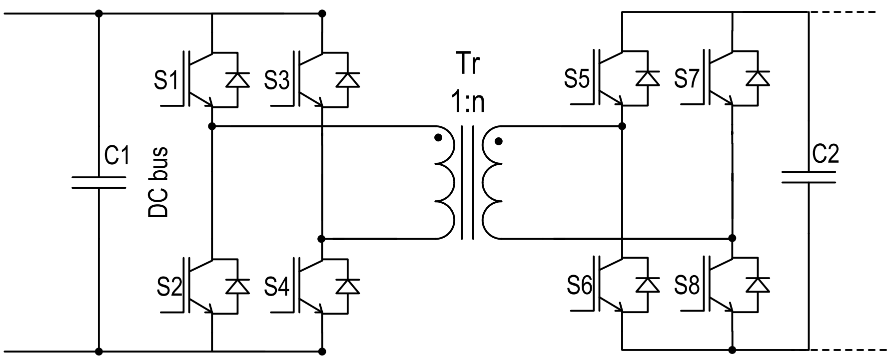

Fig. 1.53. Galvanic isolated bidirectional power converter

DC/AC power converters

Very often the power from DC source has to be inverted to AC, because in most of the cases a load has to be supplied with AC voltage.

The simplest full-bridge topology (fig.1.54) can be applied in the case if there is a high DC source voltage (350V-600V) that can be inverter directly.

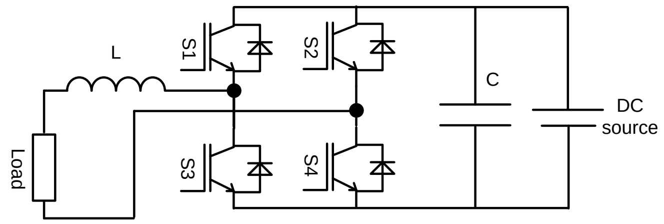

Fig. 1.54. Full-bridge inverter topology

Half-bridge topology can be applied in the case if DC source has voltage within the range of 700V-800V.

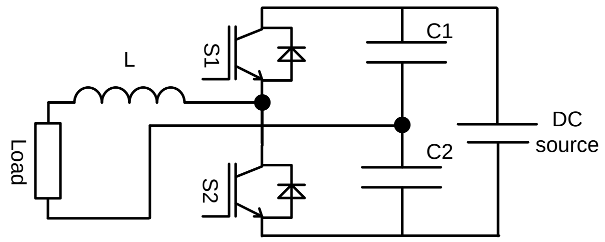

Fig. 1.55. Half-bridge inverter topology

But in most of the cases DC source has low voltage. So there is a necessity in two stage converters (fig.1.56). The first stage (converter) steps up the voltage, but the second stage (converter) inverts the voltage. For the first stage the mentioned before DC/DC boost converter can be chosen, if DC source output voltage and inverter input voltage difference is below 5. In the case of higher voltage difference than 5 it is better to chose DC/DC converter with pulse transformer. In the case if the voltage source is storage the step-up converter has to be bidirectional (fig.1.52., fig.1.53.).

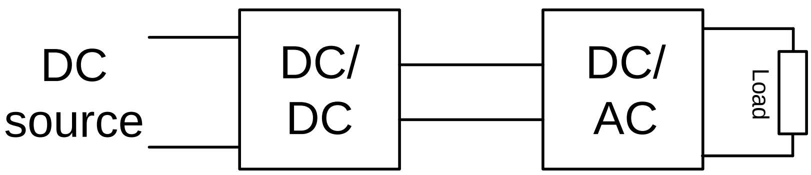

Fig. 1.56. Two stage converter

DC/AC power converters with low frequency galvanic isolation

To get high frequency galvanic isolation can be used DC/DC converters depicted in fig.1.51 and 1.53. For low frequency galvanic isolation can be used inverter with connected to output transformer (fig.1.57). Disadvantage of this converter is high weight of transformer, but advantage is lack of step-up power converter. This topology can be used even in the case of lower DC-link voltage, but the transformer turn ratio must be properly chosen.

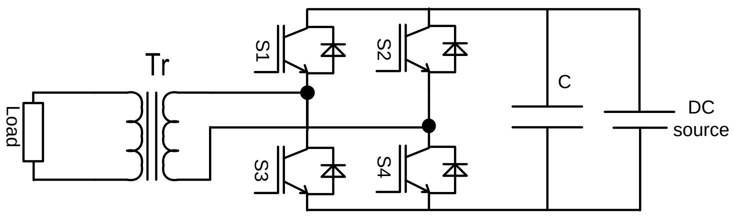

Fig. 1.57. Full-bridge topology with low frequency transformer

1.4. UPS system reliability

Taking into account all the above written it can be concluded that especially profitable alternative storages (flywheels or supercapacitors) are in the systems where energy storage provides short backup time. Example of such system can be uninterruptible power supply systems with additional local energy source as diesel-generator or fuel-cell. In this case UPS must supply critical load only the time that required for start up diesel-generator or fuel-cell (usually 20-30 seconds).

“When a standby diesel-generator (or alternative system) is necessary for backup system?” Most domestic UPS can back up load 5-7 minutes at full load. For small data centre UPS system (without diesel-generator) usually has back up time about 1 hour. According to statistical data in the first case the equipment is protected from 90% of all grid problems, but in the second case from 99% of all grid problems.

Grid can have reliability from 99% (downtime 87.6 h per year) up to 99.99% (downtime 0.876 h per year). But usually it is accepted that grid power has reliability of 99.9%.

To increase power supply reliability usually critical loads are supplied though UPS. Simple UPS can improve power reliability up to 99.99%. As it was mentioned above, usually UPS backup time does not exceed 1 hour. To ensure 1 hour or above backup time large amount of batteries is necessary, but this greatly increases the cost of UPS. In such cases for increasing of backup time additional voltage sources such as a diesel-generators, fuel-cells, etc are used.

This ensures almost unlimited backup time and can increase power availability up to 99.999%. It seems that five 9's it is very reliable system, but five 9's means that system's downtime can be up to 5.256 minutes per year. For some sphere of activity or services stop for 5 minutes can cause huge loses.

Modern datacenters and server-rooms need power availability for 99.9999% or even higher. To get such high UPS system reliability it is necessary to use redundant (parallel) systems (fig.1.58).

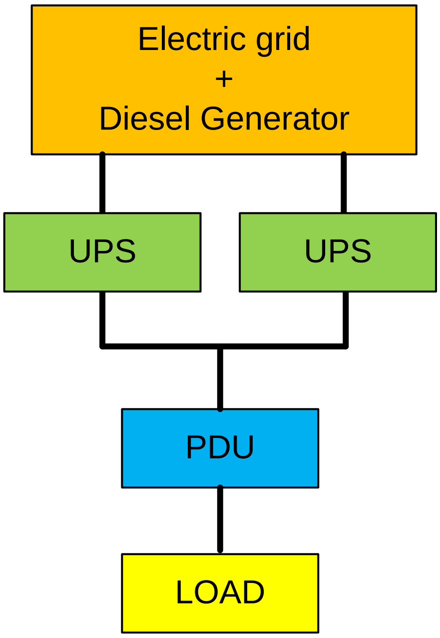

Fig. 1.58. Redundant (1+1) parallel supply system [16]

To get availability higher than seven 9's (99.99999% or downtime below 3 seconds per year) there is a necessity in two independent supply systems with two independent UPS. In fig.1.59 [16] the system with two independent grid sources, two independent diesel-generators, two independent UPS, dual supply cord and dual input loads is shown. Such system can give up to 9 9's (99.9999999% or downtime 0.03 second per year) reliability.

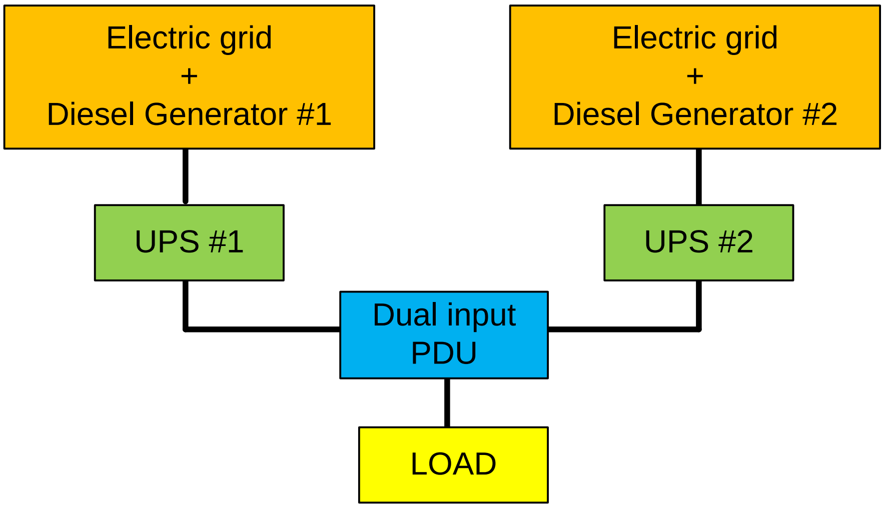

Fig. 1.59. Two independent supply systems with two independent UPS and double input PDU

Back to the question about: “When a standby diesel-generator (or alternative system) is necessary for backup system?”

As fact, diesel-generator can increase supply system reliability, but if there is a need only in system availability between 99.99% and 99.999%. In such case might be more reasonable to increase battery and built system without diesel-generator. In fig.1.60 comparison of UPS system with DG and without [17] is shown.

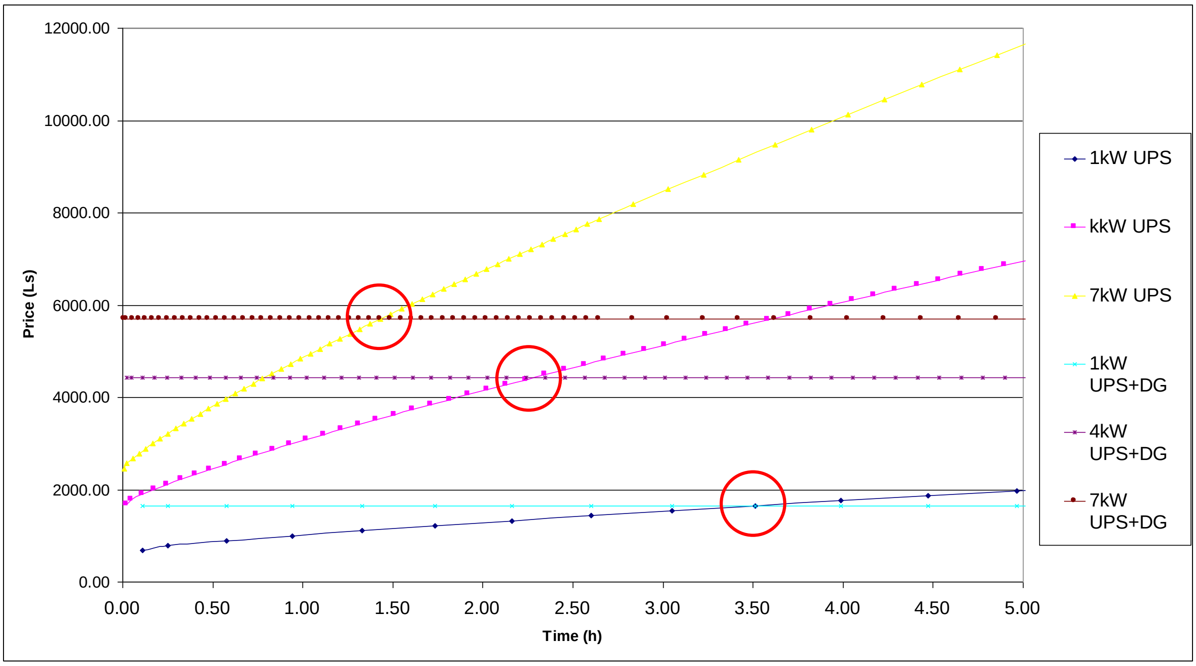

Fig. 1.60. Comparison of prices of UPS system with DG and without DG depending on backup time (DG, UPS and battery prices are taken from http://www.powerall.lv/)

As it can be seen the higher datacenter power the shorter time is when supplemental batteries reasonable. For 7kW after 1 hour it is more reasonable to put diesel-generator. For higher powers (100 kW to 1 MW) this time can be 1 minute and less.

Another question is: “What energy storage is better for reliable and cost effective system”? As it was considered most UPS systems with long back up time must have diesel-generator or alternative voltage source. Table 1.8 provides the comparison of storage devices in context of 4kW UPS system with diesel-generator (6 kVA).

Table. 1.8.

Lead-acid battery and supercapacitor comparison.

	Lead acid battery 120V, 10Ah	Maxwell technology Supercapacitor; 48.6V, 165F[18]
Stored energy	1200 Wh Useful 350-400 Wh	54,1 Wh Useful 40.9 Wh (48.6-24V)
Weight (kg)	25	14.2
Backup time	4-5 min	29 s (48.6V-24V)
Lifetime	3-5 year	More than 10 years
Cycle number	200-1000	Up to 1 000 000 at 25°C
Operating temperature	Best at 15-25°C	-40°C to +65°C
Reliability	middle	Very high
Maintenance cost for 3-5 years	100	0
Price (Ls)	250	900
Total cost for 10-15 years	950-1400	900

As it can be seen from the comparison for 10-15 years of operation, battery and supercapacitor have similar cost of usage. In the case of higher power the supercapacitor will have savings. Due to all the above written and supercapacitor high reliability it is good candidate to be used in highly reliable UPS systems.

It seems that 29 seconds for backup time is not enough! As a matter of fact diesel-generator can start the operation at full power in 8-15 seconds. Due to that 1-3 seconds (as was written in previous chapters 80-90 % of all problem last below 3 second) can be checked grid status (minimises diesel-generator start number) and if the grid does not restore to normal condition then diesel-generator engine starts. It must be noted that 29 seconds also is enough for two starting attempts, but usually systems are calculated for 1 attempt. Good and in time maintained diesel-generator has start reliability about 99.5% [19].

Today 5-15 minutes of battery backup time in the system with diesel-generator is unreasonable. 10-20 years ago such time was enough for system soft shutdown, but today such approach is intolerable [19]. In addition, as practice shows if diesel-generator does not start in first seconds it probably does not start in 15 minutes also.

In complex systems with reliability above 99.999% each UPS part (rectifier, inverter, energy storage charger) and switch mode power supply (SMPS) parts reliability (rectifier, pfc, step-down converter) is important. That is why a UPS system with smaller number of conversions (like DC UPS system) theoretically can have higher reliability. As it was already mentioned the DC UPS system has other advantages over AC UPS system:

- higher efficiency of UPS system
- smaller number of parts in DC UPS system that means lower price of UPS system
- higher voltage (400V) means lower loses in wires
- simplify integration of alternative energy sources like solar, power, fuel cell and other DC-based distributed generation systems
- higher efficiency and lower loses in wires also means lower power of cooling system

1.5. Reasons for versatile power modules utilization for UPS system assembling

As it was mentioned above there are many different energy sources that could be used in UPS systems. Each of them has disadvantages and advantages. Due to that UPS system never contains only one energy source. In this case each energy source completes another and systems become more reliable. In a system with not very high reliability usually only 2 energy sources are used (most common grid and lead-acid batteries are). In more reliable systems in most cases there are 3 energy sources (most common are: the grid, the lead-acid battery and the diesel-generator) [5].

Nowadays on the market there are many types of UPS systems with different combinations of energy sources like supercapacitors, flywheels, fuel-cells, photovoltaic panels and wind turbines [11,51,52,53,54,55]. But most of these systems even now are not extendable with another kind of energy source. For example, UPS systems which are designed to use lead-acid batteries, as a backup storage, can not be easily rebuilt for supercapacitor (or another storage) utilization. This means that for a system with many different energy sources many different converters are necessary. Many different types of converters complicate system and make it unstable.

Thus it was decided to develop versatile power module (VPM) that simplifies system assembly with any energy sources or storages.

As it was shown in chapter 1.3 basically power converters (common configurations of converters like rectifier, inverter, step-down DC/DC, step-up DC/DC and etc) consist of one or few half-bridge legs (two connected in series transistors with free-wheeling diodes) that allow assembling almost any converter containing n-number of VPM.

In the thesis "*VERSATILE POWER MODULE"* is proposed that has all necessary parts to operate like a simple power converter. Few interconnected power modules can operate like most of UPS topologies (also 3-phase topologies), frequency converter, active filter etc.

The proposed VPM must contain:

- two power switches with anti-parallel diodes that are connected as half-bridge leg
- Transistor's drivers
- DC –link capacitors
- Measurement elements
- Cooling system
- Auxiliary power supply
- Control device

The proposed circuit of modular power converter is depicted in fig. 1.61.

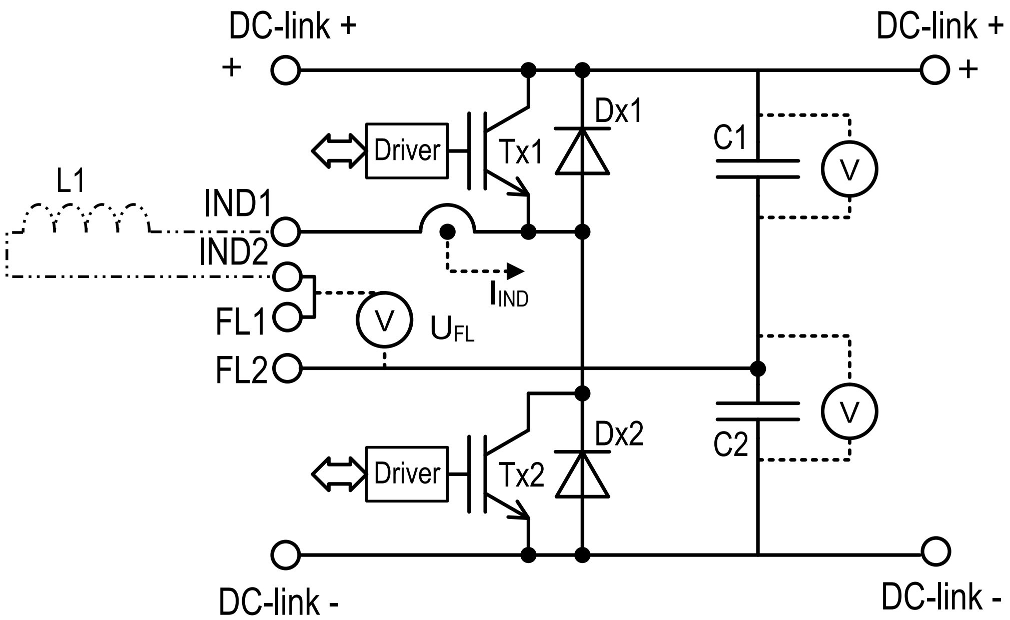

Fig. 1.61. Power circuit of versatile power module

Power converter assembled with VPMs gives the possibility to choose UPS topology, but this gives the possibility to make a choice between power quality or efficiency. Most of the UPS available on the market are designed to operate only in one mode and it can not operate in another mode (exception is “hybrid” UPS topology [9] that can operate as “line-interactive” UPS or “online” UPS).

Modern customers prefer systems that are versatile, flexible and upgradable. For example new growing companies at the beginning have small data centers with cheaper UPS that can provide only basic protection (for example stand-by UPS). When the company is developed it needs more powerful data center, but it increases its power. In additional to this requirement for power quality can be increased. Higher power quality means more expensive “online” UPS. So, in this case huge money investments are required for UPS upgrade.

IN fig.1.62 example of VPM implementation is given. Let us assume that VPM power is “X”. Using 3 VPM “2X” powerful “standby” UPS can be built - one module for charger and two modules for parallel inverters for higher power. In the case of higher (3X) power necessity and protection level it is possible to add only 3 VPM and assemble “on-line” UPS topology. In this case only half of investments are necessary.

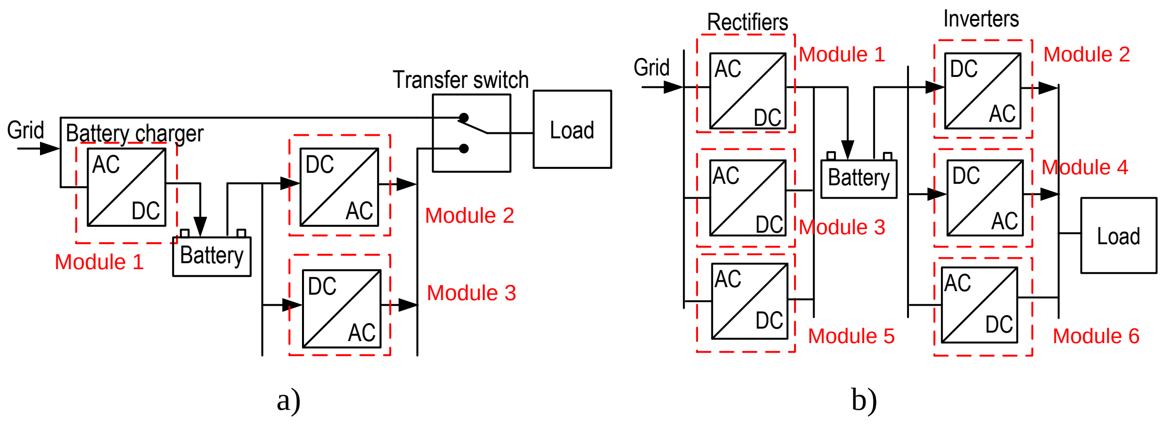

Fig. 1.62. Implementation of versatile modules for UPS assembly; a) 2X powerful “standby” UPS topology, b) 3X powerful “on-line” UPS topology.

1.6. Summary

In this chapter:

- power grid problems and described UPS topologies that they eliminate are discussed
- common energy sources that are used in UPS systems and electrical power circuits that commonly used to interconnect specified energy source to general system are discussed
- reliability of the system is discussed and more reliable system consistence of 3 or more energy sources is proved as well as the fact that in some cases traditional energy sources (lead-acid battery) are not the best choice is concluded.
- chapter 1.5 demonstrates that versatile power module can be implemented to assemble any topology on UPSS where most of the energy sources can be used. Such assembling approach gives UPS system that is very scalable and flexible.

2. Development of VERSATILE POWER MODULE

In chapter 1.5 the necessity of versatile power module was discussed. Elaboration of VPM includes the following tasks:

1) Choice of the conductor’s system that has low stray inductances and easily connectable with other modules

2) Development of transistor driver circuit

3) Development of safe and flexible measurement circuits

4) Development of modular and robust cooling system

2.1. Power board

It was decided to develop versatile power modules with rated current up to 20- 25A that gives inverter or rectifier power up to 4-5 kW.

To develop good power board few rules must be complied. Power board of power converter must have minimum stray inductances of current conductors.

Round conductor induction can be calculated using formula [2.1]:

$$L = \frac{\mu_0 l}{2\pi}(\ln\frac{2l}{r} - 1) + L_i \tag{2.1}$$

where: l – length of wire;

μ_0 = vacuum permeability (4pi*10^-7);

Li – internal wire inductance.

Internal wire inductance can be found using:

$$L_i = \frac{\mu l}{8\pi} \tag{2.2}$$

where: μ = absolute material permeability.

If wire absolute material permeability is close to vacuum permeability then wire inductance is:

$$L = \frac{\mu_0 l}{2\pi}(\ln\frac{2l}{r} - \frac{3}{4}) \tag{2.3}$$

For short wires more precise result can give equation:

$$L = \frac{\mu_0 l}{2\pi}(\ln\frac{2l}{r} - \frac{3}{4} + \frac{128}{45\pi}\frac{r}{l} - \frac{r^2}{4l^2}) \tag{2.4}$$

As a power board of most power converters is assembled on PCB then rectangular conductor's shapes is more actual.

For rectangular conductor shape with finite thickness "L" can be calculated using:

$$L = \frac{\mu_0 l}{2\pi}(\ln\frac{2l}{a+b} + \frac{1}{2}) \tag{2.5}$$

where: l – length of wire;

a – width;

b – thickness.

In the case of small thickness when it can be neglected "L" can be calculated using:

$$L = \frac{\mu_0 l}{2\pi}(\ln\frac{2l}{a} + \frac{1}{2}) \tag{2.6}$$

From the mentioned formulas it is obvious that wire induction "L" depends on conductor length, shape and material relative magnetic conductivity, but mostly it is an air, PCB textolite, a cooper that has "μ" permeability close to that of vacuum. From this formula it can be concluded that length of conductors in power converter must be as short and thin as possible (keeping wire cross section at the acceptable level).

Using the above mentioned formulas it is given graphical comparison (fig. 2.1) of wire inductance dependence on its length. In all the cases conductor cross section is equal.

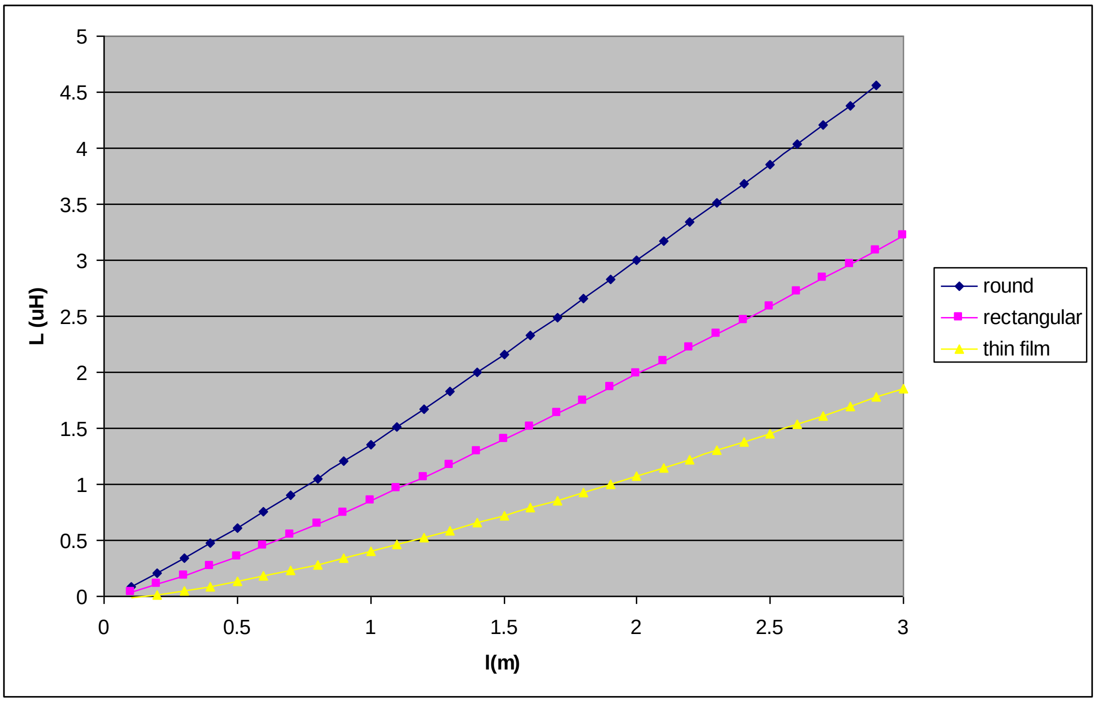

Fig. 2.1. Conductor inductance dependence on its length.

The next important point is relative position of two conductors.

Inductance for two parallel round conductors can be calculated using:

$$L = \frac{\mu_0}{\pi}(\ln\frac{d}{r} + \frac{1}{4}) \tag{2.7}$$

where: *d* - distance between conductor centres;

r – radius of conductors.

In the case when $d >> r$:

$$L = \frac{\mu_0}{\pi}(\ln\frac{d}{r}) \tag{2.8}$$

For more precise calculation it can be used:

$$L = \frac{\mu_0}{\pi}(\ln\frac{d}{r} - \frac{r^2}{d^2} - \frac{3}{2}\frac{r^4}{d^4}) \tag{2.9}$$

As it was mentioned above for conductor inductance calculation in power converter the equations for rectangular shapes is more actual. On PCB conductors in one layer and parallel different layers (fig.2.2. and fig.2.3) can be placed in parallel.

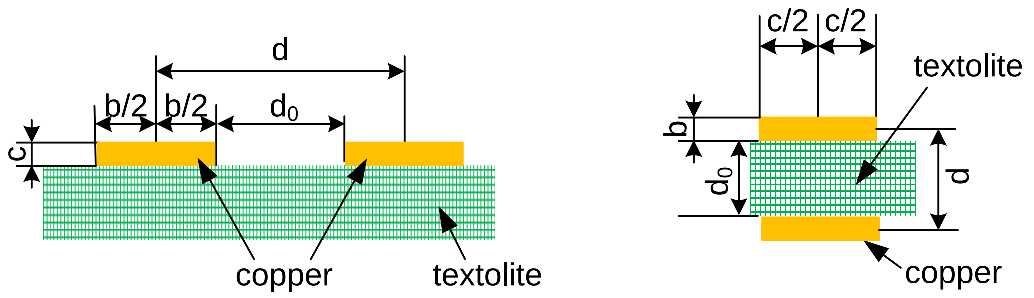

a) b)

Fig.2.2. Finite thickness conductor displacement. a) in on layer, b) in different layers

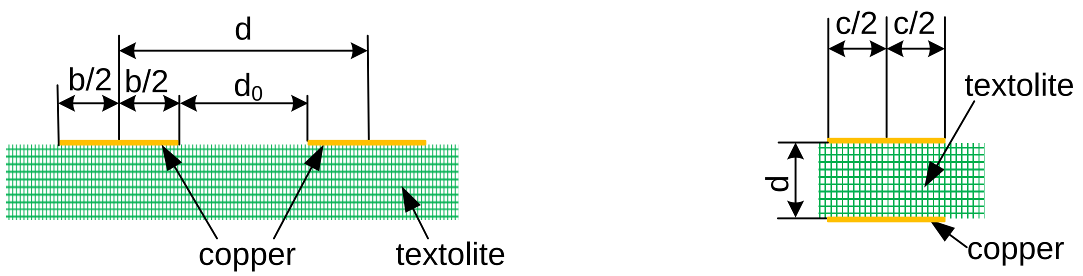

a) b)

Fig.2.3. Infinite small thickness conductor displacement. a) in on layer, b) in different layers

Inductance (for length unit) of two finite thickness parallel conductors placed in one layer (fig.2.2.a) can be calculated as:

$$L = \frac{\mu_0}{\pi}\left(\ln\frac{d}{b+c} + \frac{1}{2}\left(\frac{1}{\beta}+1\right)^2 \ln(1+\beta) + \frac{1}{2}\left(\frac{1}{\beta}-1\right)^2 \ln(1-\beta)\right) \quad (2.10)$$

where: $\beta = \dfrac{b}{d}$

For infinite small thickness conductor (2.3.a) can be used:

$$L = \frac{\mu_0}{\pi}(\ln\frac{d}{b} + \frac{1}{2}(\frac{1}{\beta}+1)^2\ln(1+\beta) + \frac{1}{2}(\frac{1}{\beta}-1)^2\ln(1-\beta)) \quad (2.11)$$

For inductance calculation of finite thickness parallel conductors placed in different layers (2.2.b) can be used:

$$L = \frac{\mu_0}{\pi}(\ln\frac{d}{b+c} + \frac{\gamma^2-1}{2\gamma^2}\ln(1+\gamma^2) + \frac{2}{\gamma}arctg(\lambda)) \quad (2.12)$$

where: $\gamma = \frac{c}{d}$

For inductance calculation of infinite small thickness parallel conductors placed in different layers (2.3.b) can be used:

$$L = \frac{\mu_0}{\pi}(\ln\frac{d}{c} + \frac{\gamma^2-1}{2\gamma^2}\ln(1+\gamma^2) + \frac{2}{\gamma}arctg(\lambda)) \quad (2.13)$$

Fig.2.4. represents a graphical comparison of two conductor inductance dependency on its shape and distance between its centres.

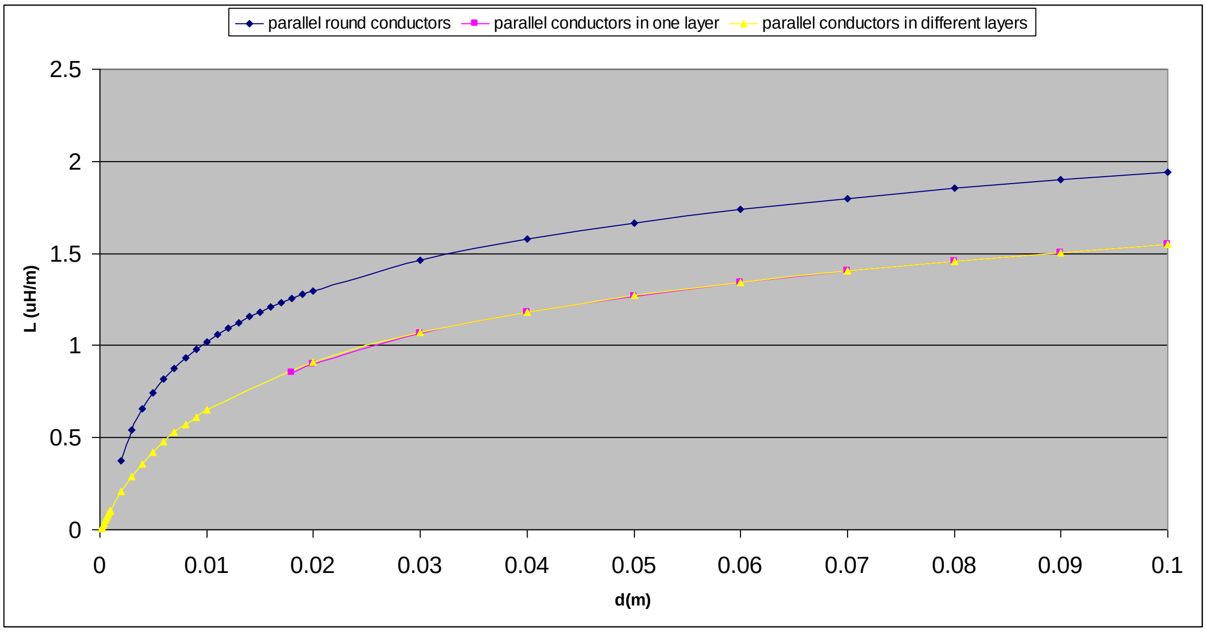

Fig.2.4. Comparison of two conductor inductance dependency on its shape and distance between its centres.

As it can be seen from fig.2.4 the lowest inductance (begins almost from “0”) has two parallel conductors that are placed in different layers of PCB (bus bar construction) and thus distance between its centres can be very small. Copper thickness on PCB is in range 18-120μm, and insulator thickness can be in range 100-500μm. Due to that power board that are made as bus bars can have very small stray inductions of current conductors. This approach ensures smaller overvoltages on semiconductor switches during switching and increase reliability of power board.

Using bus bar approach power board of versatile power converter was developed. Fig.2.5 represents sketch-up of PCB, transistor and heat sink placing. There are 2 PCBs that are insulated with special thin 0.15mm paper. The layers that are below and above the paper are used as the DC-link bus.

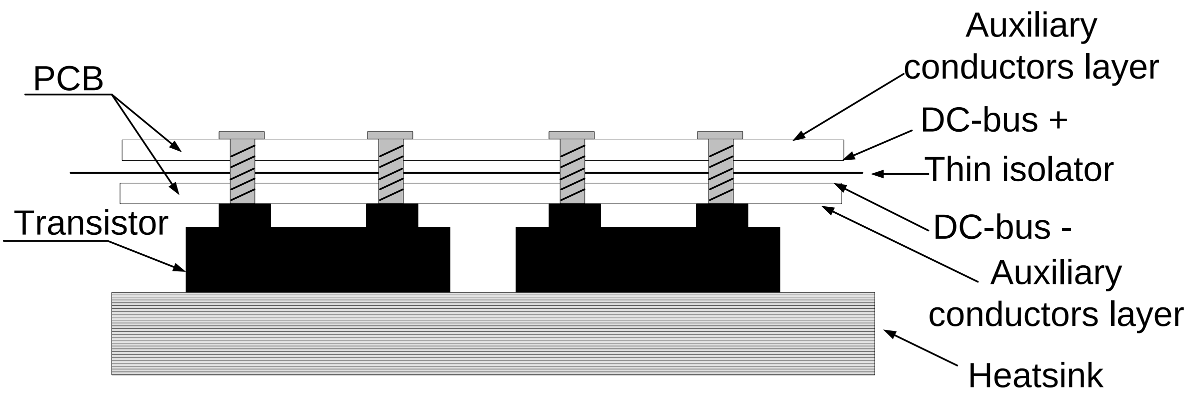

fig.2.5. Cross-section of power board of versatile power converter.

The DC-link “+” and “-” buses were placed close to each other with the purpose to minimise stray inductances of current commutation loops. In fig.2.6 equivalent circuit of the power board is depicted. It is obvious that there are few inductances that totalize the stray inductance Ls:

a) Lcap – capacitor inductance
b) Ldc-link – DC-link conductor inductance
c) Lcon – transistor and it connections inductance

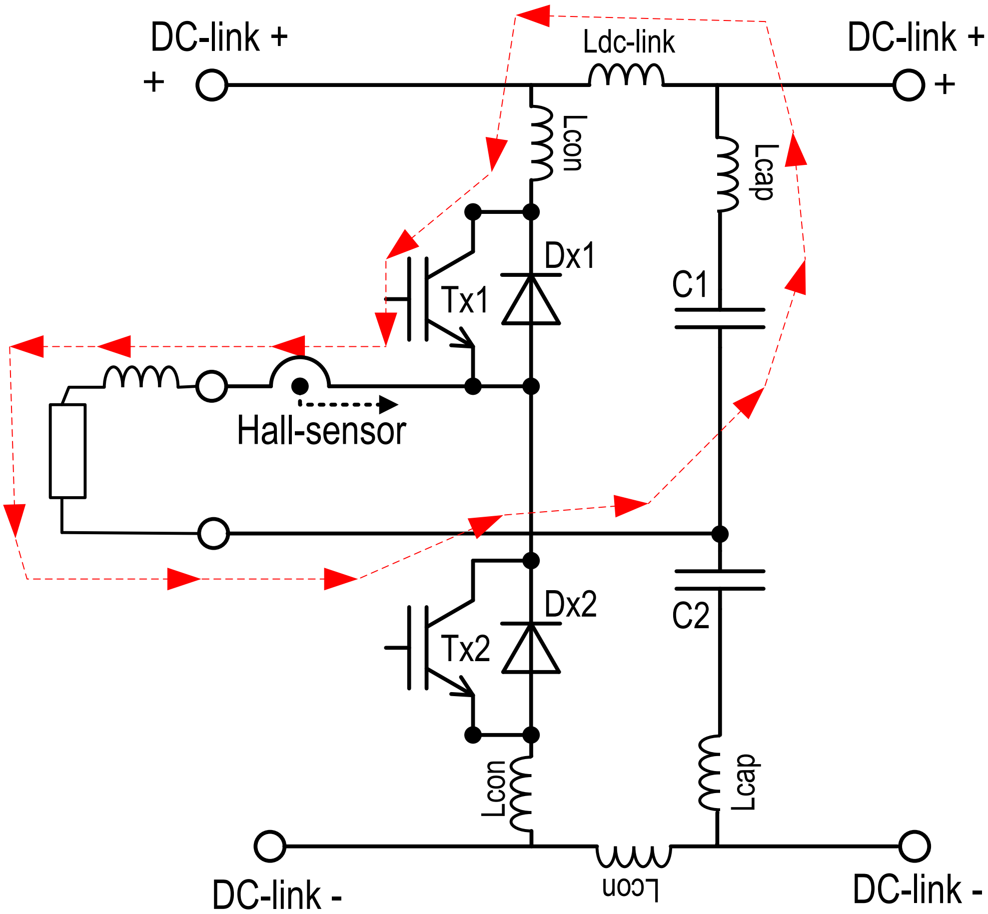

Fig. 2.6. Equivalent circuit of the power board with current commutation loop example

To minimise “Ls” each of its composite elements has to be minimised. Capacitors (RIFA PEH200) with very low equivalent series inductance (ESL) that is only 16nH is chosen. To minimise Lcon the transistors cases (SOT227) were connected directly to PCB with screws (fig.2.5). To minimise Ldc-link inductances PCB with bus bar structure shown in fig.2.7 was developed. Power board schematics and layout can be found in Appendix A.

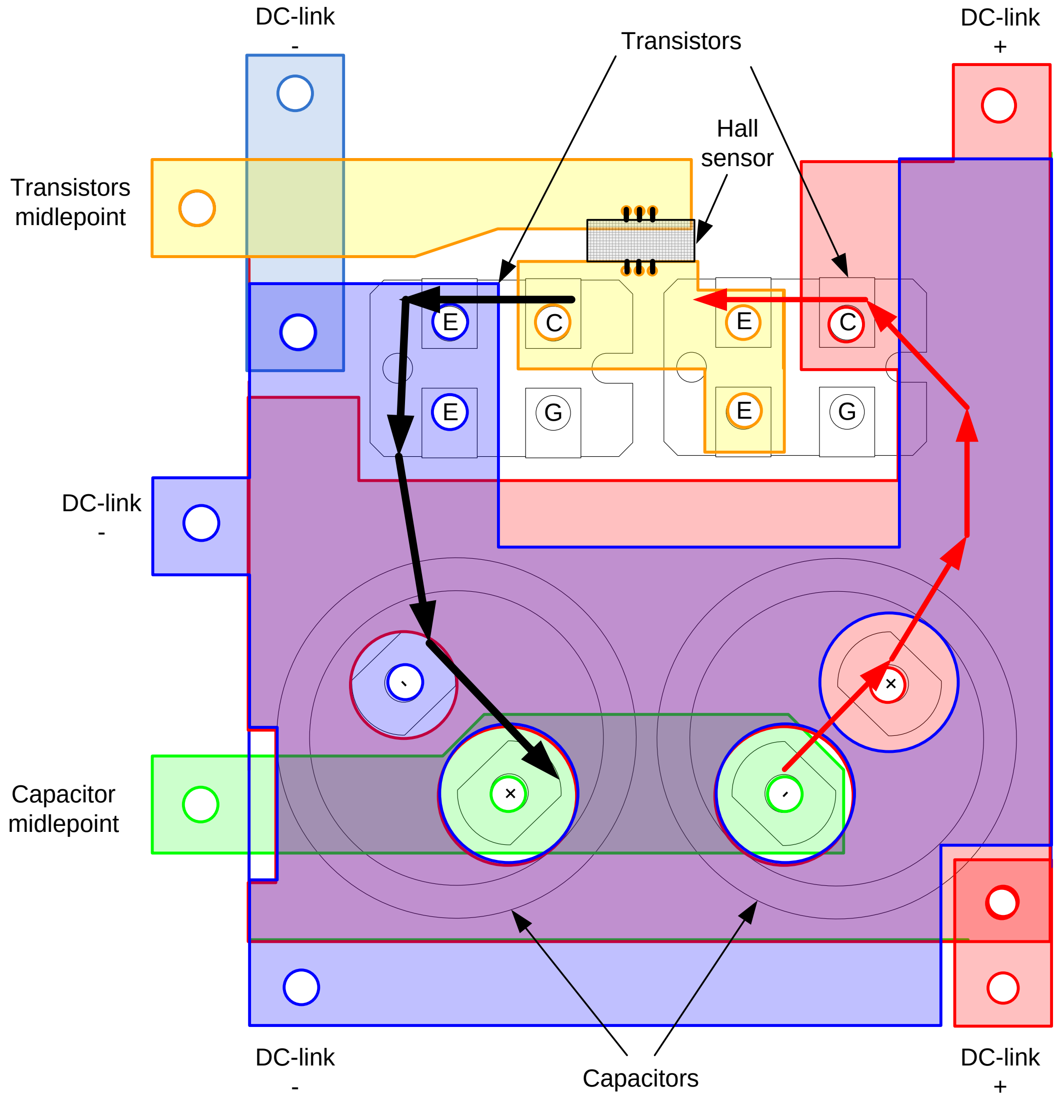

Fig. 2.7. The power board of versatile power converter.
(Red – DC-link „+”; Blue – DC-link „-”; Green – capacitor middle point; Yellow – transistors middle point; red arrows show current path that totalize ”Ls” for “Tx1” transistor, black arrows show current path that totalize ”Ls” for “Tx2” transistor)

As it can be seen in fig. 2.7 the current commutation loops are very short.

Sketch-up of power board of versatile power converter is given in fig. 2.8. There another additional parts of power board can be seen:

- resistive dividers for voltage measurements
- hall sensor (LEM LTS 15-NT, ±48A) for current measurement
- Two connectors for driver and measurement boards

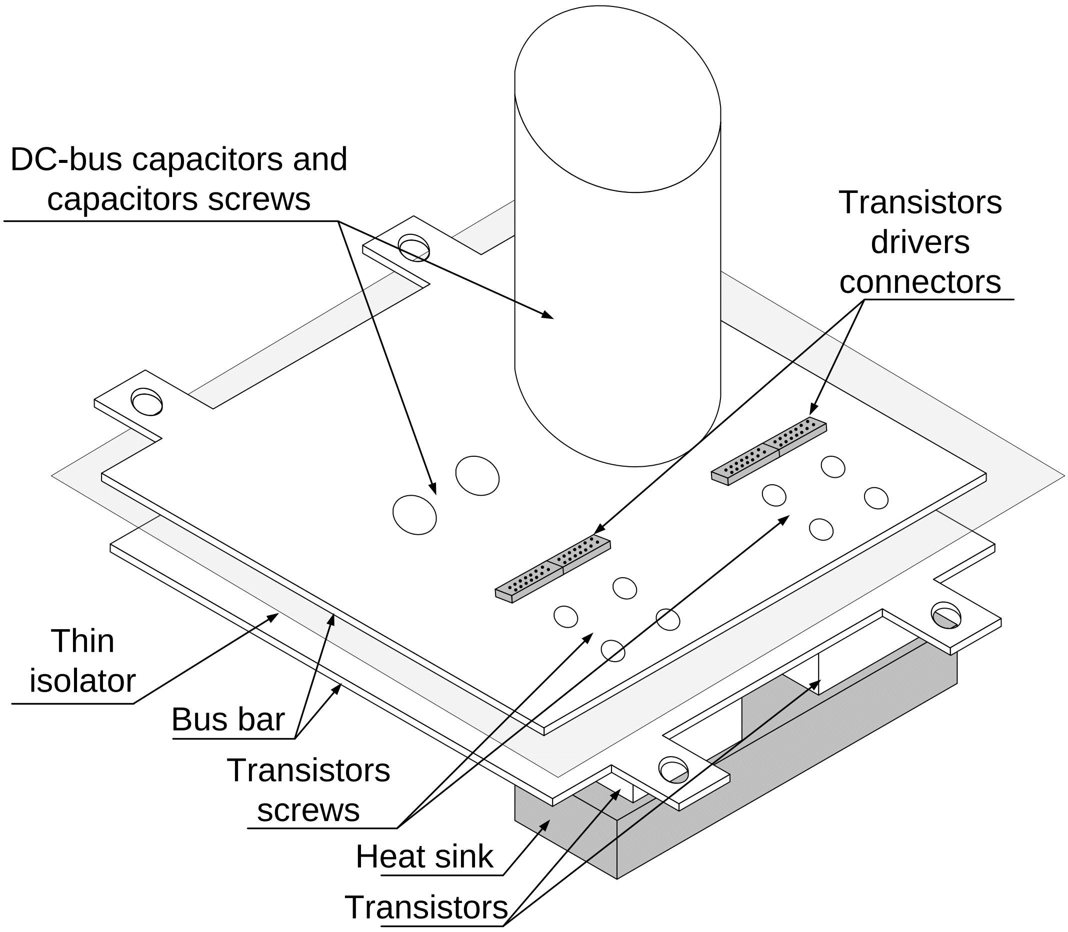

Fig.2.8. Sketch up of power board construction of versatile power converter

Assembled power board of versatile power converter is shown in fig.2.9.

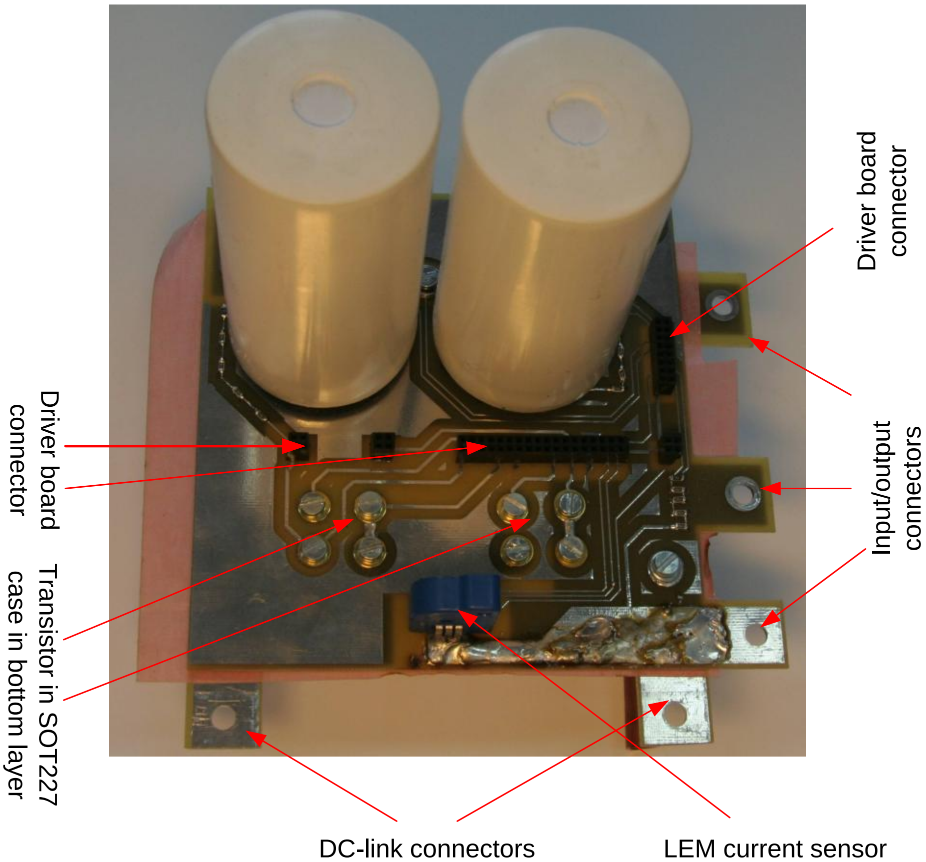

a)

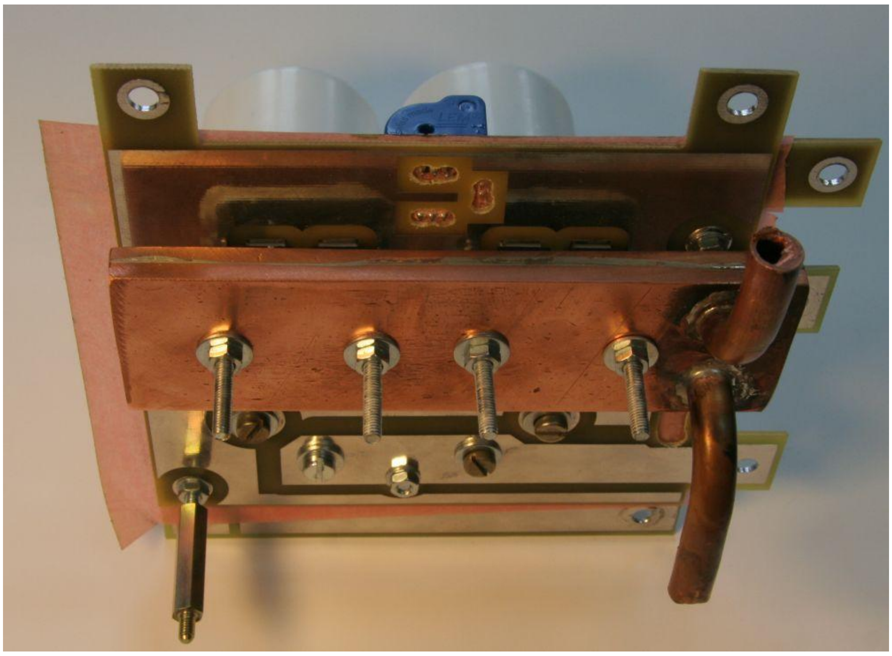

b)

Fig.2.9. Versatile power converter without driver and measurement boards

a) top side; b) bottom side

As the input/output current of power module is close to 20-25A DC-link current at 4-5 kW will be close to 10A for full-bridge configuration (300-400V) and close to 5A for half-bridge configuration (600-800V). All current conductors size was calculated with the assumption of 30A/mm^2 for outer layers and 20A/mm^2 for inner layers [21,22] and copper thickness 70 microns + 30-40 microns solder alloy. It means that 10-15 mm width track can be able to conduct up to 30-40A depending on the layer position.

All clearances between track were calculated regarding to [21,22], stating that PCB with rated voltage up to 830V clearance between track must be from 2mm to 3,5mm. Bus bar insulating paper was tested up to 1200V.

As it is “VERSATILE” power converter such elements like capacitors and transistor must be calculated for the worst cases. Capacitors rated voltages were chosen on the assumption of DC-link voltage (800V) for half-bridge configuration and 400V for full-bridge configuration. Capacitors were chosen with maximal capacity that was available for given sizes (6-7cm in diameter) that was specified by power board maximal size (15cm x 15cm). For smaller power loses it was chosen low ESR capacitors. Taking into account all about mentioned it were chosen RIFA 450V, 1000uF low ESR and ESL capacitors.

Transistor rated voltage determines DC-link voltage in half-bridge configuration (800V). For such high voltage IGBT transistors have better parameter. For easier mounting to primary heat sink SOT227 case (also known as ISOTOP) was chosen with screw terminals (fig.2.10.) and screw montage holes. As well they are easy-to-use and installing because mostly they have insulated cooling base from collector (no need in additional thermal conducting voltage insulator).

Fig.2.10. SOT227 case (ISOTOP)

Figure 2.11 demonstrates experiential data of switching of transistor and diode. Experiments were made with DC-bus voltage 550V and commutation current 25A. Testing with higher voltage (at 25A current) is not allowed by laboratory equipment.

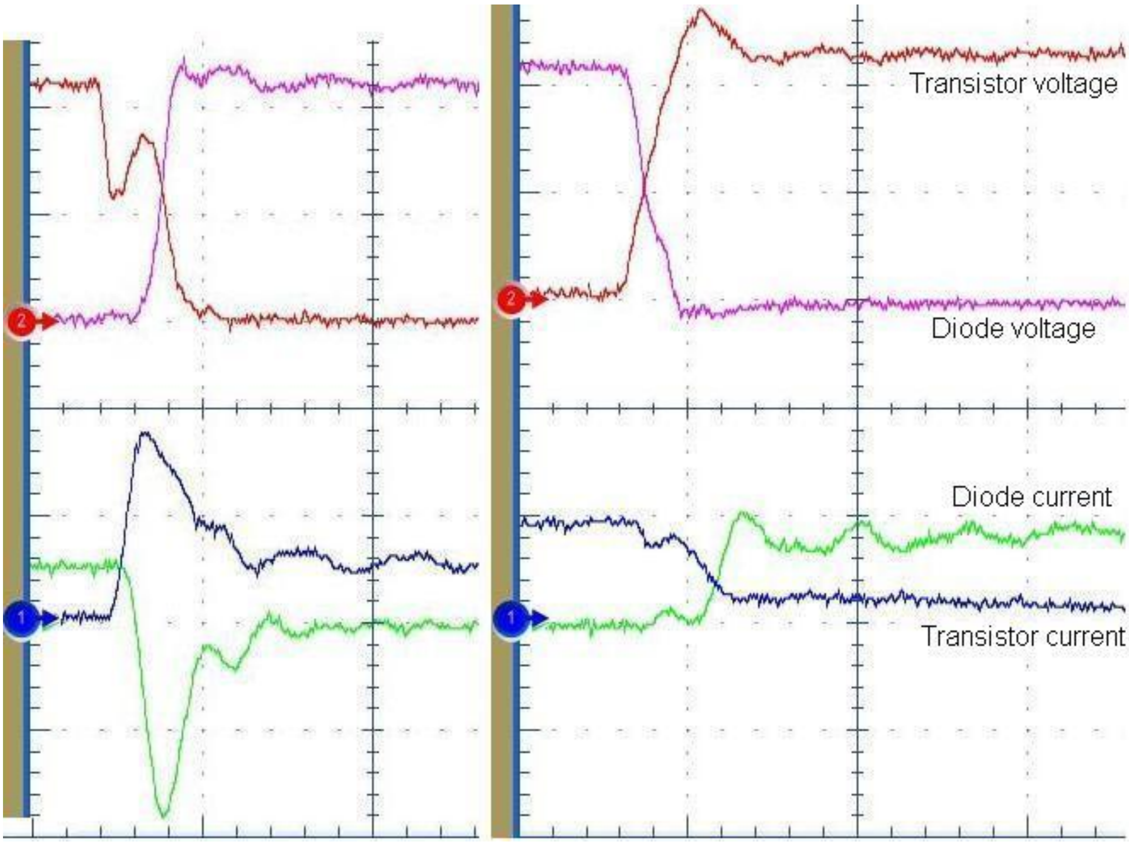

Fig. 2.11. Transistor and diode switching (time scale is 200ns per division, Voltage scale is 250V/div, current scale is 25A per division)

As can be seen during diode close overvoltage on transistor is relatively small (15-20% of rated voltage). Due to this 1200V transistors can be safely used with DC-link voltage up to 800V.

2.2. Driver board

Driver board has to ensure safe and reliable control interface and local protection from incorrect control signal. Driver board schematics and layout can be found in Appendix B.

To ensure mentioned demands the driver board (fig.2.13., fig.2.14) contains:

- Galvanic isolated power converter, that converter high DC-link voltage (800V) to 15V. 15V are necessary to supplied transistor driver.

- 15V to 5V DC/DC power converter, that supplies opto-recivers, opto-transmiters, and logic elements
- Two channel transistor drivers (Scale 2SD106A-17_E drivers manufactured by „CT Concept”)
- Opto-recievers and opto-transmiters, that ensure galvanic (optical) isolation of control signals and transistor status signals
- Logic elements to ensure protection over simultaneous opening of transistors

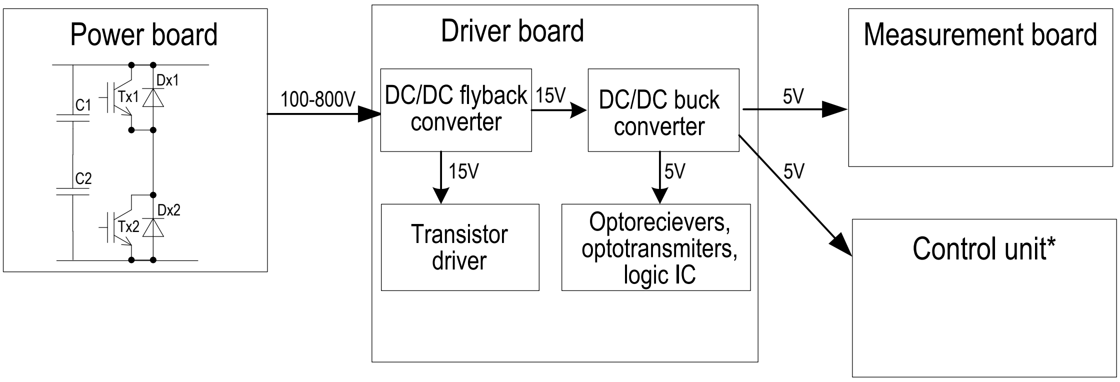

Fig.2.12. Driver board diagram and its interconnection with other boards of versatile power converter

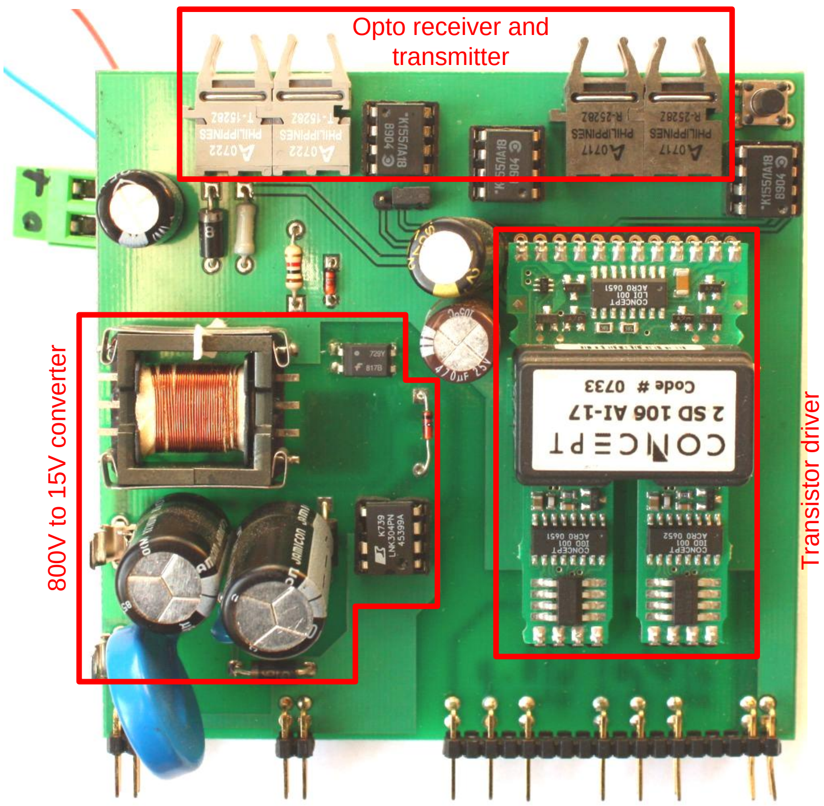

a) Top side

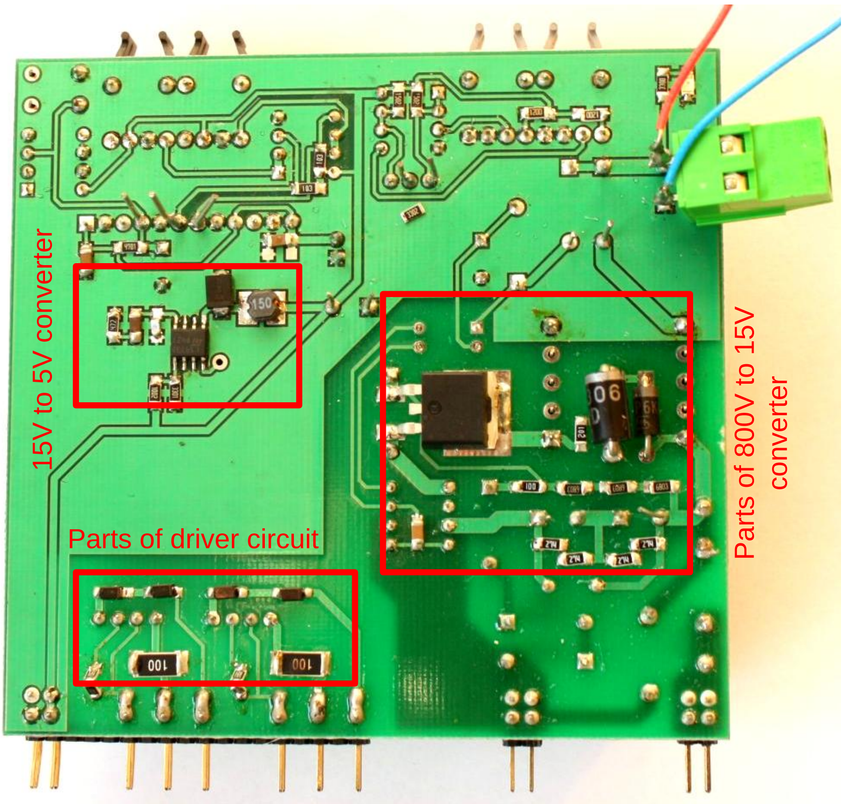

b) Bottom side

Fig.2.13. Photo of driver board

a) High-voltage (100V-800V to 15V) fly-back converter

To ensure power supply to auxiliary circuits additional power converter supplied from DC-link and convert high-voltage (up to 800V) to 15V is necessary. Total maximum power consumption of auxiliary circuits can be up to 4W (table 2.1.), but taking into account efficiencies of auxiliary power supplies and small reserve 5W power supply was developed.

Table. 2.1.

Power consumption calculation of auxiliary circuits of versatile power converter

Board	Elements	Power (W)
Driver board	1xDriver [23] 2xHFBR-2528Z Receiver [48] 2xHFBR-1528Z Transmitter [48] Logic 1xHall-sensor LEM LTS 15-NP Efficiency of auxiliary DC/DC converter (15V to 5V) is close to 90%	- 2W - 2x16mAx5V=0.16W - 2x20mAx5V=0.2W - very small - up to 60mA x 5V = 0.6W 2.96W/0.9 = 3.3W
Measurement board	3xHCPL7800 3xDC/DC power supplies AM1L-0505D-N with efficiency 75%	- Primary current up to 15.5mA - Secondary current up to 14.5mA 3x15.5mAx5V/0.75=0.3W 3x14.5mAx5V=0.22W 0.52W/0.9=0.58W
Adaptor board (can be supply externally or from driver board)	2xHFBR-2528Z Receiver [48] 2xHFBR-1528Z Transmitter [48] Logic	2x16mAx5V=0.16W 2x20mAx5V=0.2W Very small 0.36W/0.9=0.4W
Total		3.84W, but taking into account auxiliary converters the efficiency is 4.3W

To develop the high voltage DC/DC converter “Power Integrations” “LinkSwitch” IC for fly-back DC-DC converters was used. To increase input voltage range fly-back converter (fig.2.14) with the StackFET configuration [42] was used. To choose correct parts and their values it was used [41, 43, 44, 45].

This topology has some advantages:

- a wide input voltage range
- built in open-loop protection
- short-circuit protection
- thermal overload protection
- high bandwidth that provides fast turn-on without overshoot
- no additional transformer bias winding is needed since the U1 is powered directly from its drain pin.

-the voltage feedback allows keeping output voltage constant at any load current.

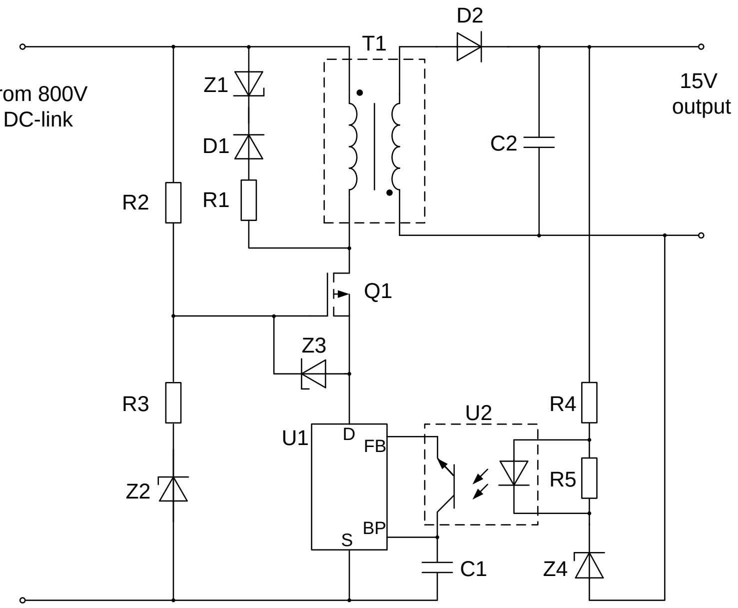

Fig.2.14 High voltage fly-back converter diagram

Converter has been developed, assembled and tested (fig.2.16). Experimental data shows that it could start up even at 50V on input with low load (up to 50% from rated) (fig.2.15 a,b). At higher load (load current 300mA or 4.5W) it starts up at input voltage about 200V (fig.2.15. c).

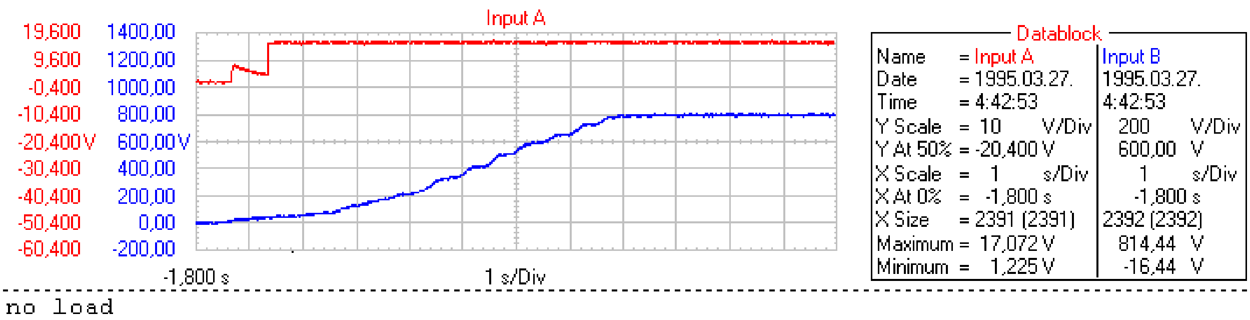

a) no load

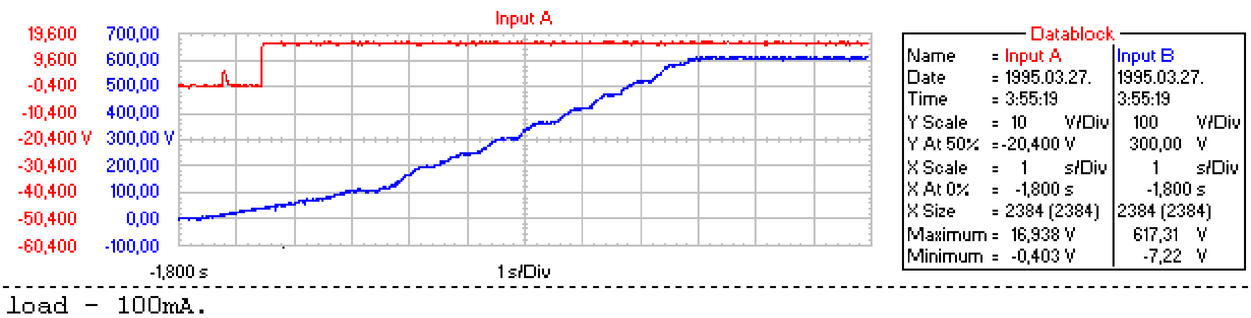

b) 100mA load

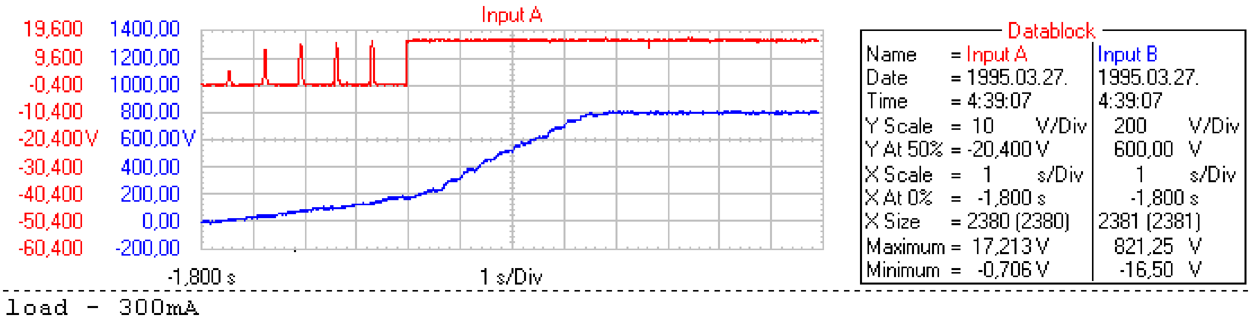

c) 300mA load

Fig.2.15. High voltage fly-back converter starting up.

Output voltage – red curve, input voltage – Blue curve

b) 15V to 5V buck converter

For low voltage conversion (15V to 5V) “STMicroelectronics” L5973D IC [46] was chosen. The L5973D is a step down monolithic power switching regulator with current limit 2.5A. It is easy applicable, robust IC that occupies very small area on PCB and has high conversion efficiency (about 90%).

c) Transistors driver and its interface

fig.2.16. transistor driver Scale ”2SD106A-17_E”

“Scale” driver (fig.2.16.) ensures fast (gate current up to 6A) and correct switching within wide range of frequencies (up to 100kHz). It protects against overloads and short circuits. It measures transistor voltage drop in opened condition and if voltage drop exceeds specified level driver switches off the transistor. Maximum voltage drop can be determined by correctly chosen resistors [23]. In addition driver gives the possibility to specify voltage level of control signal (between 5V and 15V). To ensure protection from incorrect control signal (when both channels are set to high level) some additional logic ICs are connected to driver and give the signal to switch off the transistor in faulty control signal.

Control signals for the drivers as well as backward status signals are provided through optical fibers and optical transmitters/receivers “Avago technologies “, fig.2.17.

Fig.2.17. Photo of opto-transmiter “HFBR-1528” and opto-reciever “HFBR-2528”

Optical interface is necessary to protect control device from high voltage in the case of accident as well as to improve noise immunity of the control signal. Thus the control signal and transistor status signal can be received/transmitted for long distance (up to 50m) in high EMI environment without any signal quality degradation. This transmitter can be operated up to 10 MBd using a simple driver circuit.

Receiver “HFBR-2528Z” consists of a silicon PIN photodiode and digitizing IC to produce a logic compatible output. It can operate from DC to 10 MBd.

The experiments demonstrating signal delay were made. Total signal delay (driver board and adaptor board) is shown in fig.2.18.

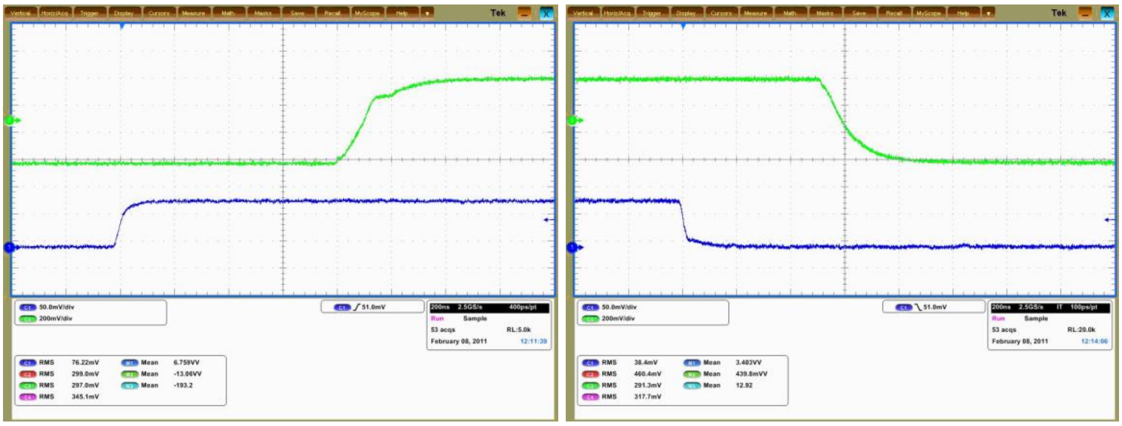

a) b)

Fig.2.18. Driver board and adaptor board signal delay.
Green– transistor gate voltage, blue – control signal: a) rising signal b) falling signal.

As it can be seen, signal delay is quite short (600-800ns). Such signal delay does not affect converter regulation precision.

2.3. *Measurement board*

Measurement board (fig.2.19., fig.2.20) provides feedback for control system and galvanic isolation of measured signals. It has 3 channels with 3 BNC connectors that ensure both capacitors and input/output voltages measuring and one BNC for input/output current measuring. Measurement board schematics and layout can be found in Appendix C.

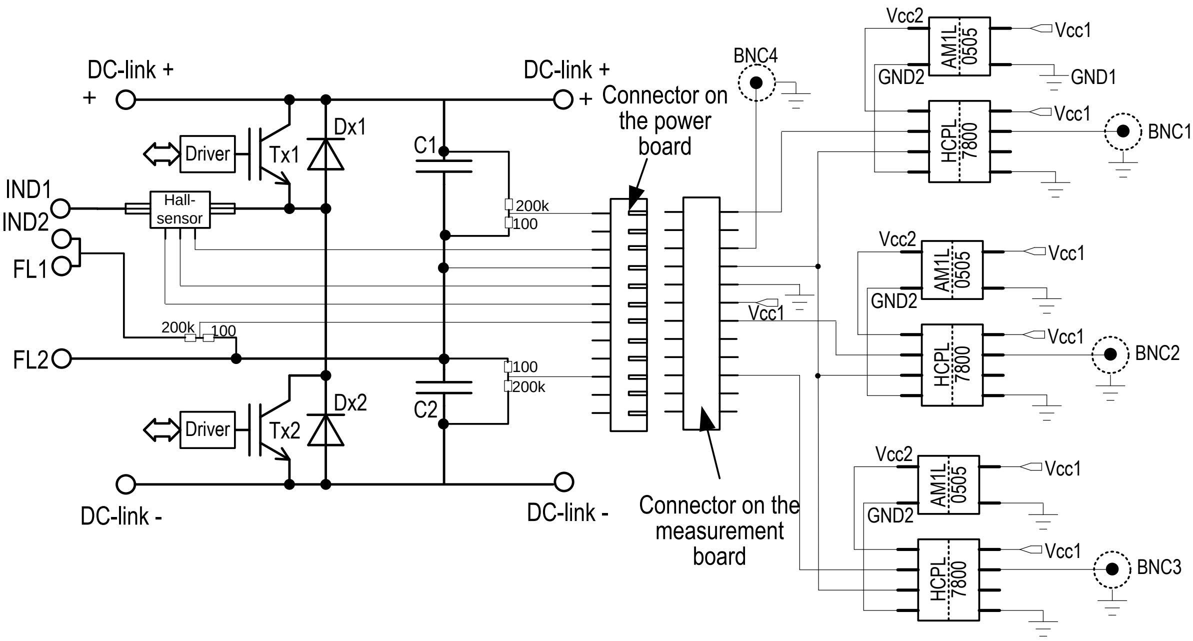

Fig.2.19. Principal electrical diagram of measurement board

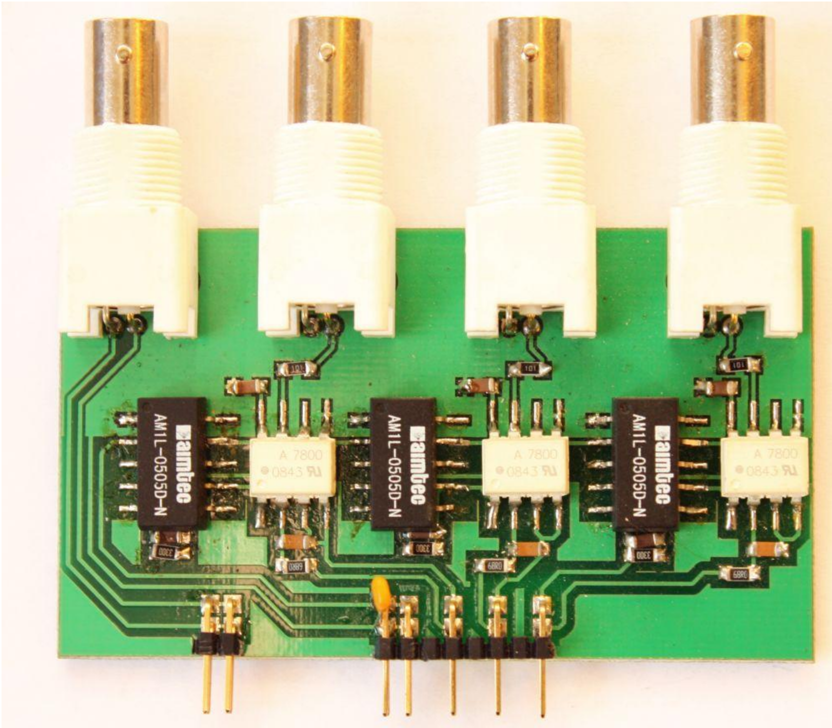

Fig.2.20. Photo of measurement board

Voltages from capacitors and input/output voltage are divided by resistive divider by 2000 times. The divided voltages are measured and amplified 4 times by isolation amplifiers HCPL7800 that are depicted in fig.2.21. [49].

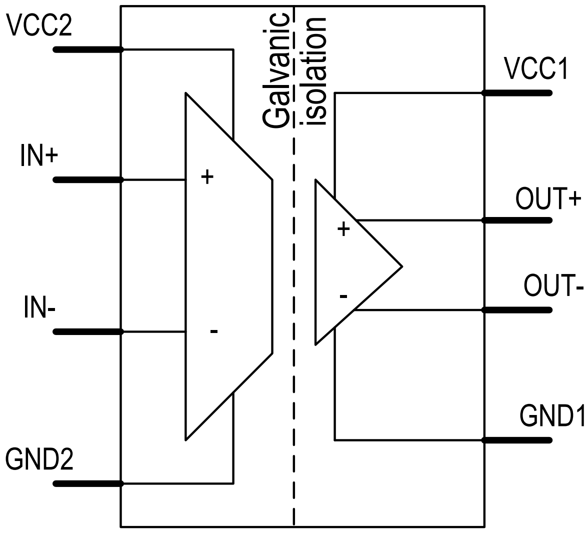

Fig.2.21. Functional diagram of HCPL-7800 isolation amplifier [24]

Fig.2.22. Photo of HCPL-7800 isolation amplifier

The isolation amplifier needs galvanic isolated power supply +5V of input side. This element also adds 2.5V offset. Therefore taking into account all voltage divisions and amplifications the output voltage of the measurement board may be expressed with the equation:

$$U_{HCPL} = 2.5 + \frac{U}{500} \tag{2.14}$$

In the case of capacitor voltage 400V the isolation amplifier will give on its output:

$$U_{HCPL\_\max} = 2.5 + \frac{400}{500} = 3.3V \tag{2.15}$$

In case of -400V the output voltage is:

$$U_{HCPL\_\min} = 2.5 + \frac{-400}{500} = 1.7V \tag{2.16}$$

Zero voltage across the capacitors give 2.5V at the output of the isolation amplifier.

As the current is measured with hall-sensor (LEM LTS 15-NT is placed on power board) this signal does not need any additional galvanic isolation [50]. It is measured by the control system directly. The maximum measured value of current of the hall-sensors is ±48A. Like

HCPL7800 the hall-sensor (LEM LTS 15-NT) also has voltage bias +2.5V. Output signal of LEM LTS 15-NT can be expressed with the equation:

$$U_{lem} = 2.5 + 0.04167 \cdot I \tag{2.17}$$

Variations in input/output current from -45A to 45A will give LEM signal variation from 0.62V to 4.38V.

Of course all additional conversion of measured signal gives additional delay. Delay of measurement circuit (about 4.6 microseconds) can be seen in fig. 2.23.

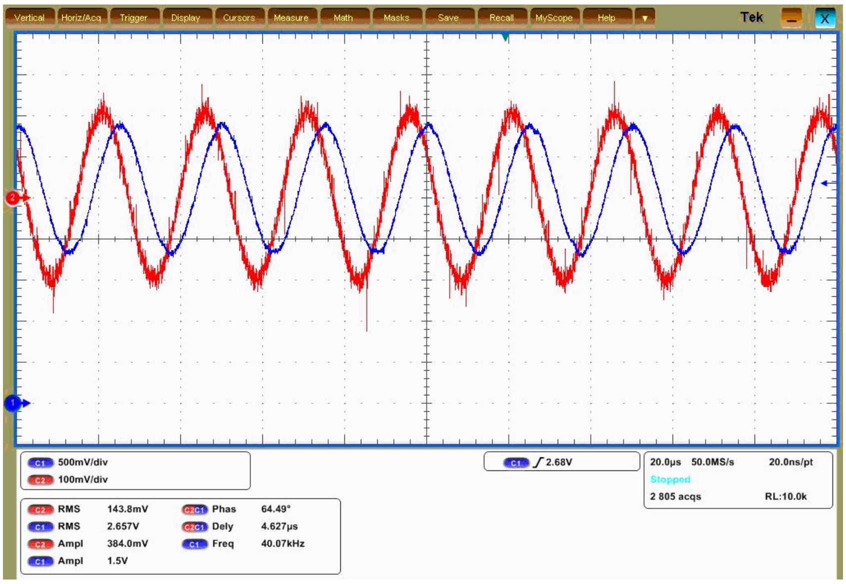

Fig.2.23. Measurement board signal delay for sine wave.

Red is input signal. Blue is output voltage of the isolation amplifier.
(delay can be seen in left bottom corner)

Bandwidth of the measurement circuits also was tested experimentally. In fig.2.24 frequency cut-off characteristics are given. As it can be seen -3dB (frequency cut-off) is about 90kHz. Such high bandwidth is fast enough for feedback signal measurement.

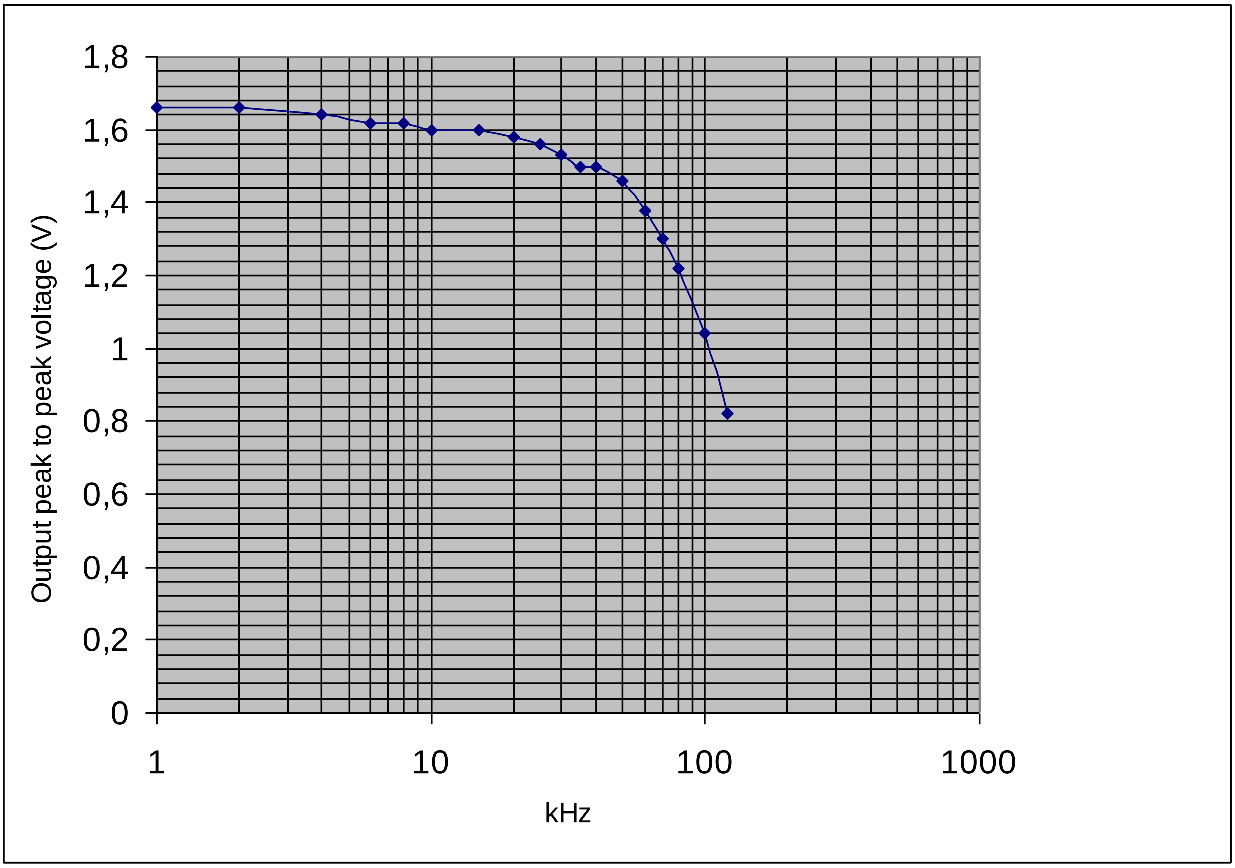

Fig.2.24. Frequency cut-off of measurement board

2.4. Adaptor board

In future the “Versatile power modules” will be controlled with DSP board, but for much faster development of control algorithms and its simple debugging it was decided to use real-time controller dSpace DS1103.

As a control device and measurement board can have different signal levels it is necessary additional elements to equalize levels of measured signals. The adaptor board (fig.2.25, fig.2.26) receives measured signals through BNC connectors, but voltages dividers with potentiometers allow adjust signal levels. Driver board schematics and layout can be found in Appendix D.

In order to transmit control signal it is necessary to drive relatively powerful LED in opto-transmitter (HFBR-1528) that consumes current up to 40mA, but not each microcontroller or DPS can give such current directly from digital port. Due to that the adaptor board has transmitter LED driver.

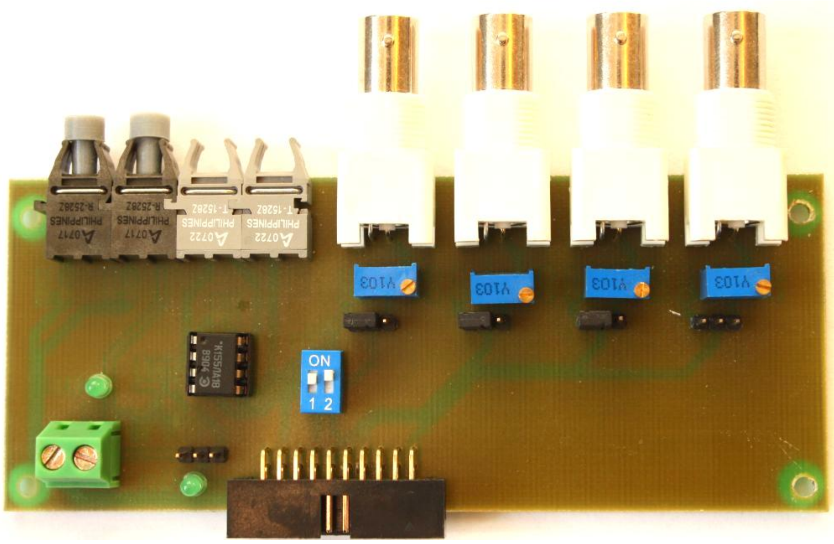

Fig.2.25. Top side of adaptor board

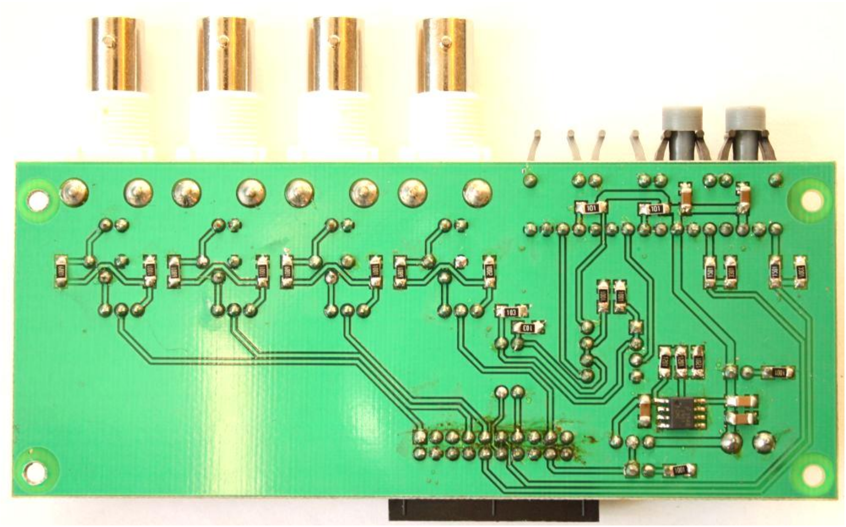

Fig.2.26. Top side of adaptor board

Adaptor board signal delay already is included in signal delay of driver board that is shown in fig.2.23.

2.5. Cooling system

Cooling system must dissipate all heat energy that is generated due to the losses in semiconductor devices. It means that power dissipating in cooling system must be equal or higher than all the losses in power converter. Power losses in power converter must be calculated for the worse operating case.

Power loses can be found in different ways:

- Power converter can be simulated in computer using such software as Pspice, Matlab Simulink, PSIM etc. This is a fast calculation method, but it could not be very precise, due to the program's restrictions. In some programs it is not easy to create model of semiconductor and other elements that behave like real device.
- Losses can be calculated using mathematical equations. Disadvantage of this method is the necessity to spend much time to calculate all the equations.
- Power losses could be taken from datasheets. Datasheet usually gives the losses of one switching for typical conditions. Multiplying it by frequency the losses can be found. It is very fast and quite precise method, but usually data given only for few conditions that not always match the conditions in the given task
- Another method is to use semiconductor manufacturers special-purpose software that can calculate losses for most common used converters [25]. It is very fast and precise method. Disadvantage of this method is that not all converters types can be found there.

It was decided to use the latter method. To calculate power losses in semiconductors it was used ”SemiSel” simulation software [25]. There were all necessary converters types. Below table.2.2 with power loses for different converters is given.

Table.2.2.

Power loses for different converters.

Converter topology	Circuit parameters	Loses in whole converter	Loses in each semiconductor
Inverter (full bridge)	Output current 25A, Output voltage 230V, Cos(f)=0.8	222W	Transistor – 46W Diode – 9.7 W In whole devices – 55.7W
Active rectifier (full bridge)	Output current 25A, Output voltage 230V, Cos(f)=1	225W	Transistor – 48W Diode – 8.5W In whole devices – 56.5W
Buck	Output current 25A, Output voltage 125V	114W	Transistor (upper device) - 76 Diode (lower device) - 38
Boost	Input current 25A, Output voltage 375V	118W	Transistor (lower device) - 93 Diode (upper device) - 25

As it is obvious the transistor has the highest losses in boost configuration. Due to the fact that any versatile power module can operate as boost converter the heat sinks must be designed for the worst case. It means that heat sinks must be able to cool down semiconductors with power losses 100W.

Modular construction of power converter means also modular construction of heat sinks. To create compact and modular heat sink it was decided to develop water cooling system. Basic water cooling system consists of:

- primary heat sink/heat sinks
- water pump
- secondary heat sink (heat exchanger)
- thermometers and protection devices

There are two types of water cooling systems:

- with parallel connected heat sinks (fig.2.27-a)
- with serial connected heat sinks (fig.2.27-b)

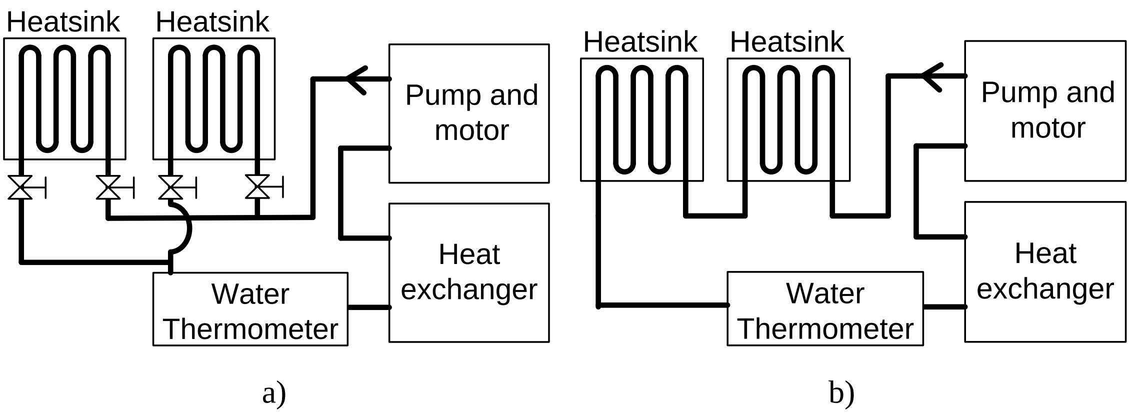

Fig.2.27. Cooling systems: a) parallel connection; b) serial connection;

Disadvantage of such connection is a necessity in more powerful water pump than in a system with serial connection. In such system water flows in each heat sink can be different due to heat sinks non-idealness, but it will affect cooling capability. Disadvantage of serial connection is that each next heat sink gets more warmed water. But as the given below calculation shows the temperature difference between heat sink's input and output water in most of the cases is below $1C^0$. It means that even 5-8 connected in series heat sinks will give temperature difference only in $5\text{-}7C^0$. Due to the mentioned fact it was decided to develop cooling system with connected heat sinks in series.

Design of cooling system mean:

- chose/design of primary heat sink
- chose/design of water pump
- chose/design of secondary heat exchanger
- chose/design of protection systems

Secondary heat exchanger

Secondary heat sink (heat exchanger) is necessary to chill water and dissipate losses energy in ambient environment. The secondary heat sink available on local markets was chosen.

Diagram of dissipation power versus input water temperature (at water capacity 2 l/min) was experimentally tested and its characteristic is given in fig.2.28. Water temperature was limited up to 60 C^0, because maximum safe temperature of all pipes that are used in water cooling system is 65 C^0.

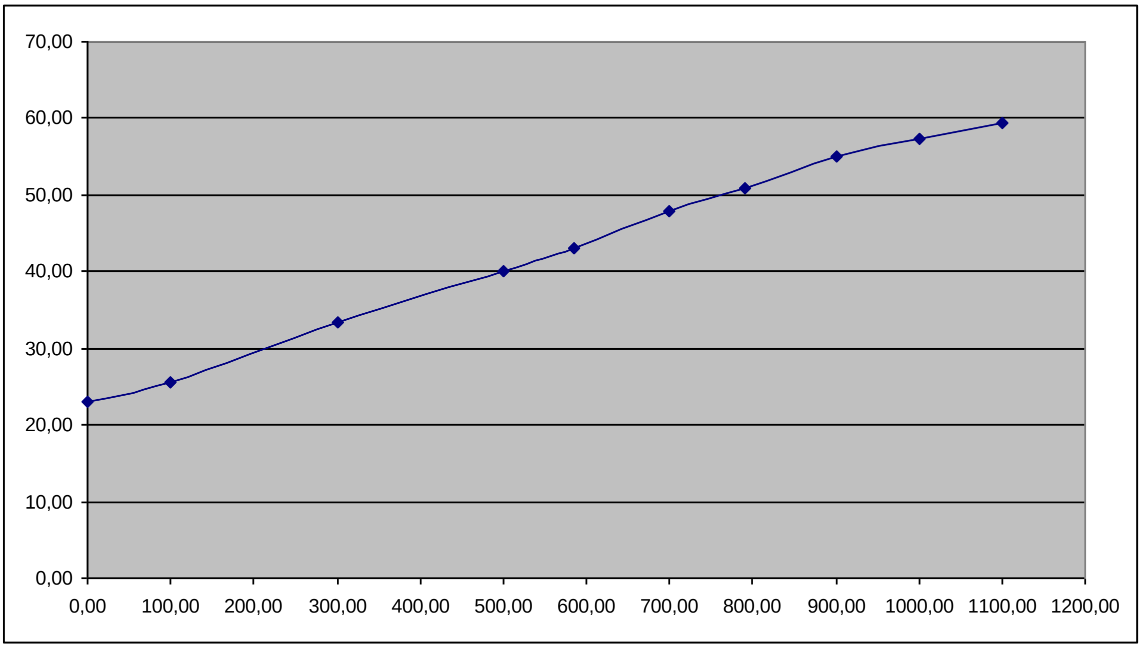

Fig. 2.28. Secondary heat exchanger dissipation power versus input water temperature at pump capacity 2 l/min and ambient air temperature about $25C^0$

As it can be seen, heat exchanger can dissipate up to 1000 W of heat at ambient temperature 25^0C and water temperature does not exceed 60^0C. It means that such secondary heat sink will allow dissipation of power from 6-8 modules, that is enough to assemble any UPS configuration with power up to 4kW.

Primary heat sink

As it was mentioned above each module has 2 semiconductor devices connected into the phase leg. As there are two close placed switches, they can be put both on the same heat sink. As it is hard to find not expensive heat sink with specified sizes it was decided to develop primary heat sink. There are two available methods of quick and relatively cheap manufacturing of the heat sinks: a) use a milling machine for channels cutting; b) solder or weld heat sinks from copper sheets and tubes. To find better heat sink construction it was designed and calculated 4 different primary heat sinks constructions (fig.2.29.). Heat sinks are developed for IGBT transistors in SOT227 case (also known as ISOTOP).

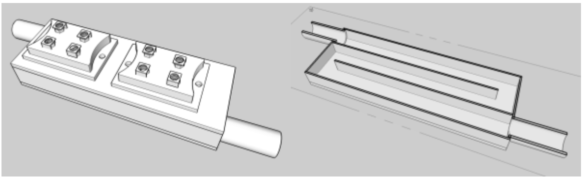

a)

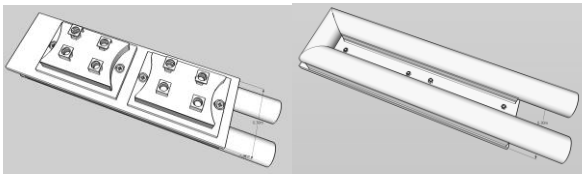

b)

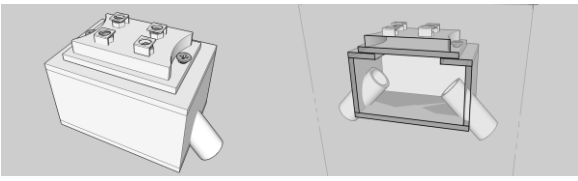

c)

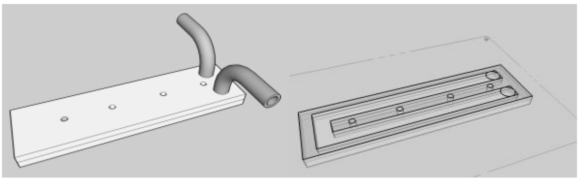

d)

Fig. 2.29. Heat sinks constructions

Heat sink in fig.2.29.a consists of two 2mm surface sheets separated with channels made of 0.7mm thin sheets. Lateral wall are also made of 2mm sheets. Number of channels depends on cooled device width. In case of SOT227 transistor it is rational to use 3 channels.

Heat sink in fig.2.29.b consists of one 2mm thick sheet and one bend tube (diameter 10mm) that is soldered on the sheet with big amount of cooper solder to increase thermal conductivity between the tube and the sheet. The copper solder is preferable because it has 4-6 times better thermal conductivity then the tin solder. (thermal conductivity of copper is 401 W/m*K, but tin -66.6 W/m*K).

Heat sink in fig.2.29.c is a box soldered of 2mm thin copper sheets. The sheet under semiconductor device has a window that provides a possibility of direct cooling. The power switches and heat sinks are sealed to avoid any coolant leakage from the system.

Heat sink in fig.2.29.d consists of two 5mm thin sheets where 3mm deep channels are milled. Diameter of milling cutter is 10mm. When both sheets are soldered together channel size is 6x10mm. In one sheet two 10mm holes for tubes are drilled.

Heat sinks calculations were made using thermodynamics laws [26,27,28,29].

To start calculate heat sinks the task should be formulated. For better understanding of the task a thermal equivalent circuit of few connected modules (two modules operate in inverter mode, one module operate in boost mode) was made with additional load 660W to fully load secondary heat exchanger fig.2.30.

- main task to hold transistor and diode junction temperature below $150C^0$

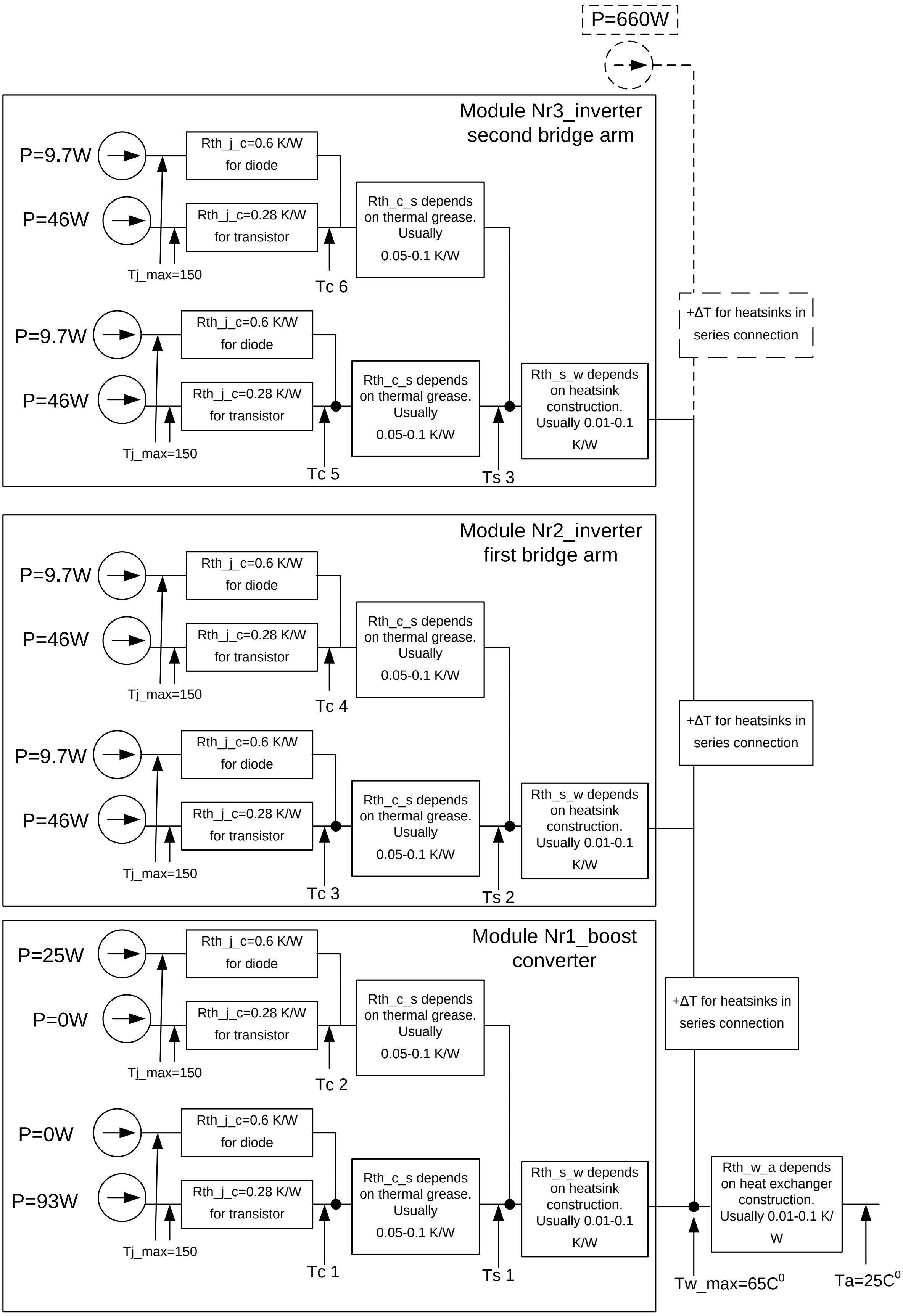

Fig.2.30. Versatile power modules thermal equivalent circuit

Calculation example is shown for milled heat sink (fig.2.29.d).

Firstly such water flow velocity must be found that gives turbulent flow in heat sink. Turbulent water flow ensures heat exchange in water occur due to convection, but not due to conduction. Type of water flow in pipe can show Re (Reynolds number) [30].

$$R_e = \frac{V \cdot L}{\nu} \tag{2.18}$$

where V – velocity of fluid (m/s);

L – characteristic linear dimension (m);

ν - is the kinematic viscosity (ν = μ / ρ) (m²/s).

Re is dimensionless number that shows the ratio between inertial forces and viscous forces in liquids and gases. For fluid flow in a pipe (also for square pipe with equivalent hydraulic diameter Dh=4S/P [31]) with diameter D laminar flow occurs when Re < 2300 and turbulent flow occurs when Re> 4000. Between 2300 and 4000, laminar and turbulent flows are possible and depend on other factors, such as pipe shape, roughness and flow uniformity. To find flow velocity in square channel where it is fully turbulent the following equation can be used:

$$V = \frac{R_e \nu}{D_h} = \frac{2R_e \nu (a+b)}{4ab} \tag{2.19}$$

where Re=4000,

ν - kinematic viscosity of fluid at rated temperature (as a total losses is about 1000W than, water temperature take at 60C^0 and it has ν =0,475*10^{-6}),

a, b – dimensions of channel (6x10mm).

$$V = \frac{R_e \nu}{L} = \frac{2 \times 4000 \times 0.475 \times (0.006 + 0.01)}{4 \times 0.006 \times 0.01 \times 10^6} = 0.253 m/s \tag{2.20}$$

Taking into account channel dimensions, pump capacity must be higher than:

$$H = V \cdot a \cdot b = 0.253 \times 0.006 \times 0.01 \times 1 \times 60 = 0.0009108 \ m^3/min = 0.9 \ l/min \tag{2.21}$$

Such capacity can ensure even small water pump. One of them was chosen and bought. It ensures up to 13l/min (800l/h) without load. Rated power of water pump is 10W. Its load characteristic is given in fig.2.31.

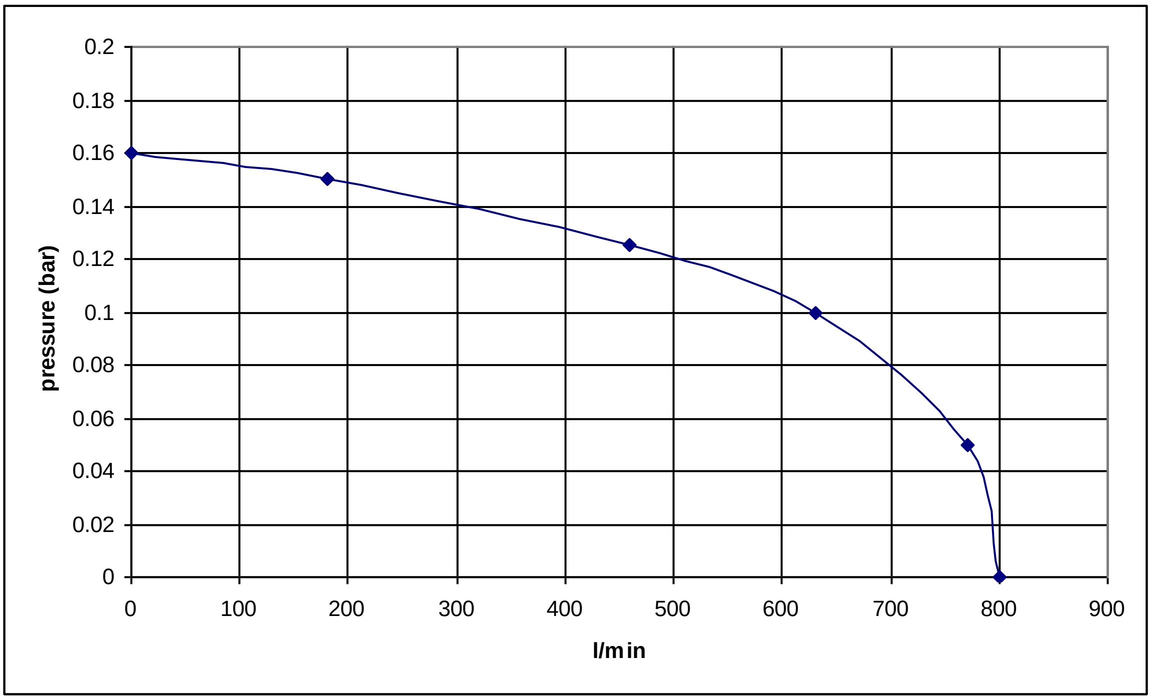

Fig.2.31. Water pump capacity/pressure chart

To get pump capacity in cooling system it is necessary to know pressure drop of the whole cooling system. Calculation of pressure drop on pipe with bends (in our case heat sinks) is quite a complicated task, due to many factors which influence it (fluid type, length of channels, diameter of channels, fluid velocity, fluid temperature, material type of channel, internal pipe roughness, shape and number of bends in pipe). Pressure drop equation [33]:

$$\Delta p = \lambda \cdot \frac{L}{D} \cdot \frac{\rho}{2} \cdot \overline{w}^2 \tag{2.22}$$

where: L-length of pipe;

D-diameter of pipe;

ρ-fluid density;

w-fluid velocity;

λ – pipe friction coefficient.

The pipe friction coefficient equation is [33]:

$$\frac{1}{\sqrt{\lambda}} = -2 \cdot \lg\left(\frac{2.51}{\mathrm{Re} \cdot \sqrt{\lambda}} + \frac{k}{D} \cdot 269\right) \tag{2.23}$$

where: k – absolute roughness.

If in pipe (in our case heat sinks) there are bends, elbows, reducers, valves and etc than their pressure drop can be found [33]:

$$\Delta p = \zeta \cdot \frac{\rho}{2} \cdot \overline{w}^2 \tag{2.24}$$

where: ζ – coefficient of resistance of bend (or elbow, reducer, valve etc) and usually it is determined experimentally.

But simpler and more precise way to find pressure drop is to use special purpose programs. One of the examples can be “Pipe flow wizard” [32]. Such parameters as flow capacity, length, diameter, material of pipe, number of bends (or elbows, reducers, valves) can be entered and the program calculates pressure drop for given pipe, Reynolds number, flow type, friction factor. Using this program for heat sink fig.2.29.d a diagram of pressure drop versus water capacity (fig.2.33.) was built. The diagram was built for water temperature 60C^0.

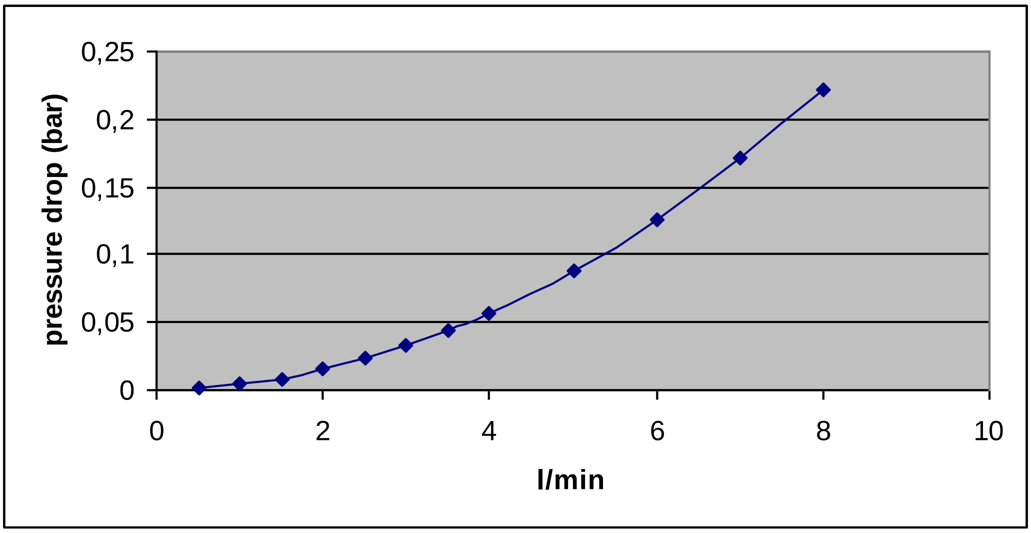

Fig.2.33. Heat sink pressure drop versus water capacity

Also the pipes that connect pump, secondary heat exchanger and all primary heat sinks also have pressure drop and its diagram is shown in fig. 2.34.

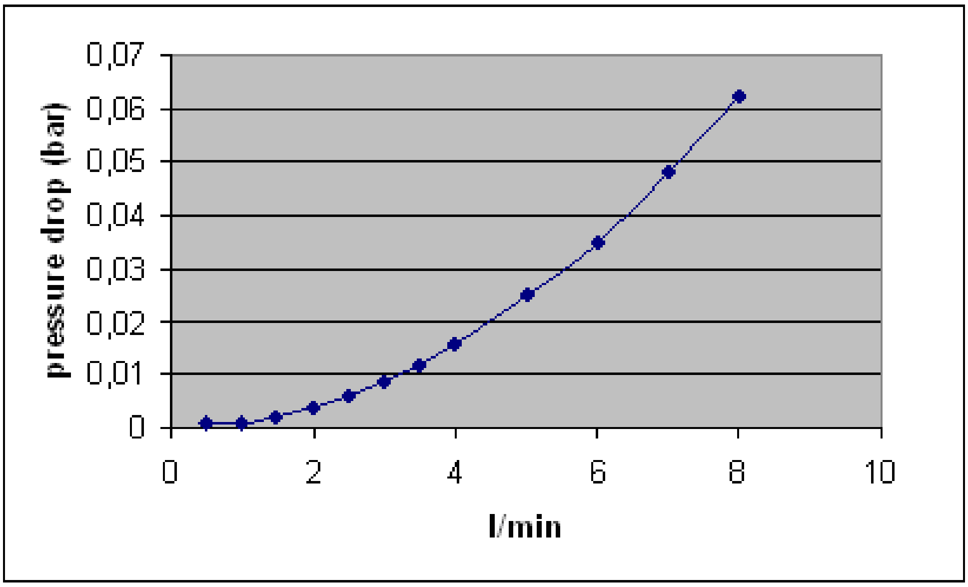

Fig.2.34. connecting pipes pressure drop versus water capacity

Secondary heat exchanger pressure drop diagram is shown in fig. 2.35.

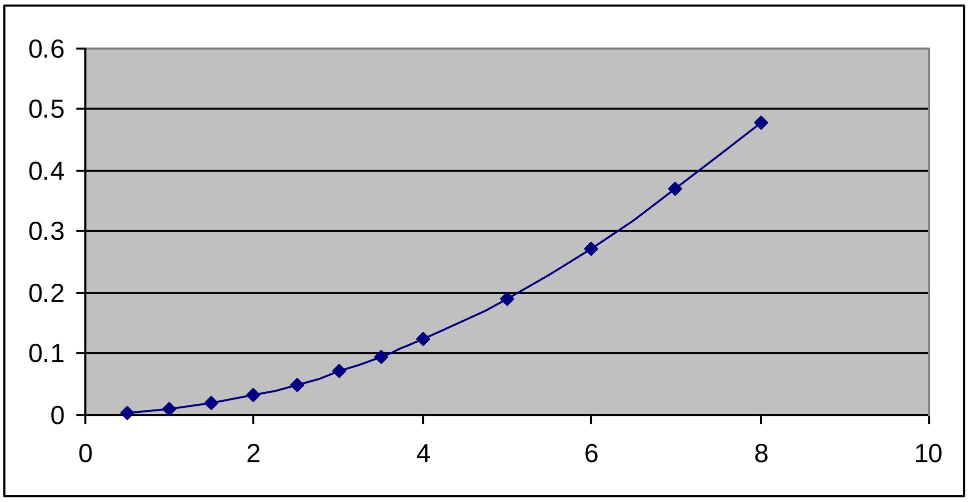

Fig. 2.35. Secondary heat exchanger pressure drop VS water capacity

To find pump capacity in the given cooling system (worst case is cooling system with 8 primary heat sinks, 1 pump, 1 secondary heat exchanger) diagrams of "pump capacity VS pressure" and "total system pressure drop VS water capacity") must be drawn in one plot and intersection point will be pump capacity in the given system (fig.2.36).

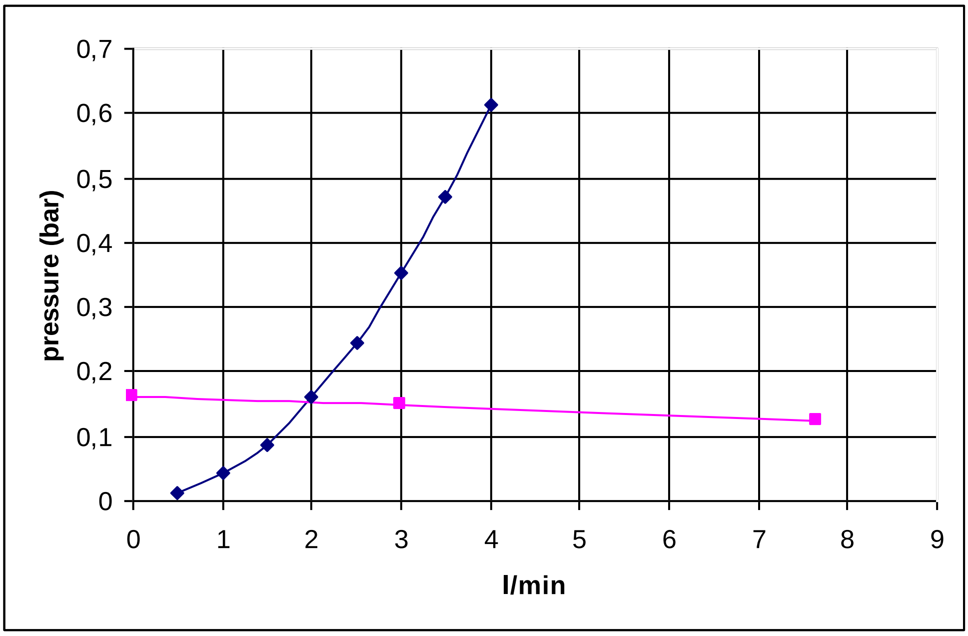

Fig.2.36. Connecting pipes pressure drop versus water capacity (blue – total system pressure drop, red – pump capacity)

Diagram shows that approximate pump capacity in the given system will be 2 l/min. All the following calculations will be made with pump capacity 2 l/min.

In system with water capacity 2 l/min water flow velocity in primary heat sink will be 0.755 m/s. Reynolds number in heat sink for this flow velocity will be:

$$R_e = \frac{VL}{\nu} = \frac{0.68 \times 0.0075}{0.475 \times 10^{-6}} = 11919 \tag{2.25}$$

As it was mentioned it means that water flow in heat sink is turbulent. Due to that for the Nusselt number (it shows the ratio of convective to conductive heat transfer across the boundary between the water and the pipe) Dittus-Boelter equation [34] can be used:

$$\frac{1}{Nu} = 0.023 \mathrm{Re}^{0.8} \mathrm{Pr}^{n} = 65{,}01 \tag{2.26}$$

where: Pr is the Prandtl number (for water at $60C^0$ Pr=2.99 [35]);

n = 0.4 for heating of the fluid, n = 0.3 for cooling of the fluid.

The equation (2.26) can be used in cases when:

$0{,}7 \le \mathrm{Pr} \le 160$, $\mathrm{Re} > 10000$ and $\frac{L}{D} > 10$

After Nusselt number can be found heat-transfer coefficient (h):

$$h = \frac{k_w}{D} Nu = 5656 \tag{2.27}$$

where: k_W - thermal conductivity of the liquid (for water at $60C^0$ is 0.653 Вт/(м*K))

As copper is one of the best heat conductors for this heat sink construction can be assumed that temperature of heat sink is almost equal in all its parts. Using Newton’s law of cooling it can be drawn diagram of temperature difference between water and heat sink versus heat flux (fig.2.37):

$$q = hS(T_s - T_b) \tag{2.28}$$

where S – surface area of the pipe (Spipe=Dh*π*l)

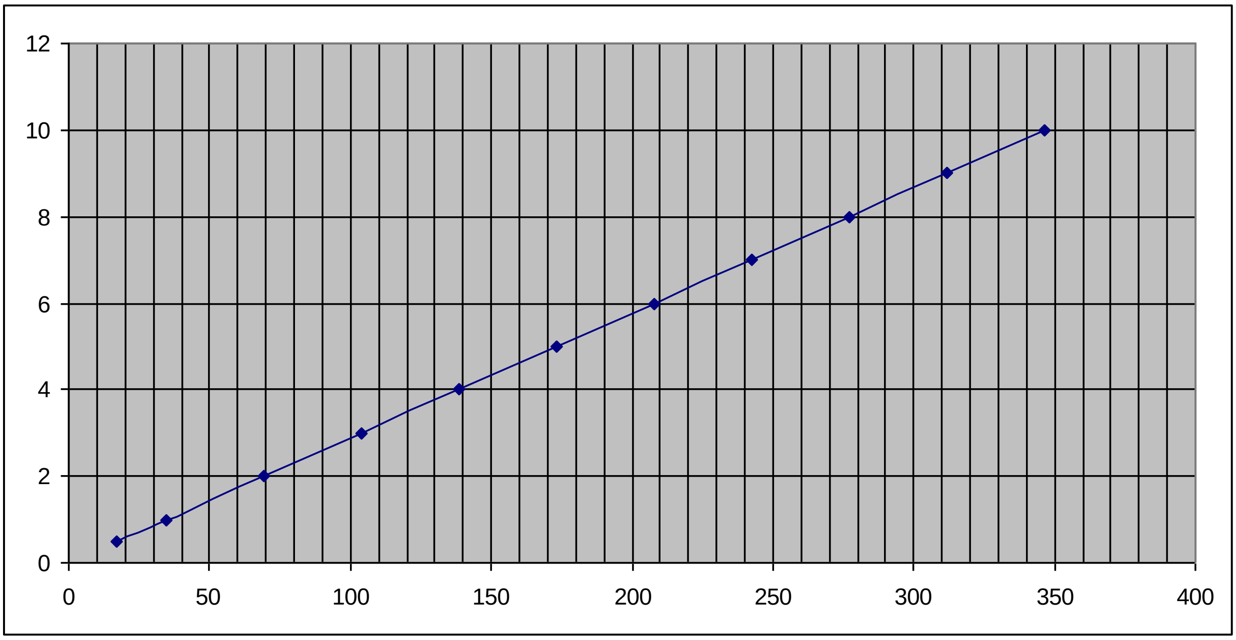

Fig. 2.37. Temperature difference between water and heat sink versus heat flux (for water $60C^0$)

As it is known thermal resistance (Rth) equation is:

$$R_{th} = \frac{\Delta T}{P_{th}} \tag{2.29}$$

But as previously drawn diagram is linear, any point can be taken to calculate primary heat sink R_{th}:

$$R_{th} = \frac{\Delta T}{P_{th}} = \frac{10}{346{,}3} = 0.0289 K/W \tag{2.30}$$

Now when heat sink is known thermal resistance can be calculated state task (fig.2.5.4). All total losses in the system are about 1000W. As it was experimentally tested at this input power water temperature will be $60C^0$. In means that the first heat sink input water will be also $60C^0$. As total power losses in the first heat sink is 118W it temperature will be 60+118*0.0289=63.4 C^0. It means that first transistor junction temperature will be 63,4+0.28*93=89.44C^0. Temperature of the second diode junction will be 63.4+0.6*25=78.4 C^0.

First heat sink output water temperature will be 60C^0 +ΔT, but

$$\Delta T=Q/(C*m) \qquad (2.31)$$

where C is water heat capacity 4185 *(J/(kg*K))*, Q – energy losses in transistor and diode during one second (118Ws or J), m – water weight that flow through heat sink in one second (2*0.983/60=0.0328 kg).

$$\Delta T=Q/(C*m)=118/(4185*0,0328)=0.86\ C^0 \qquad (2.32)$$

Second heat sink input power will be 60.86 C^0. Due to the losses in transistors and diodes in second module(111,4W), heat sink temperature will be 60.86+0.0289*111.4=64.08 C^0. Assuming that mean water temperature is equal in the whole volume of the channel in transistor 5 and 6 junction temperature will be 64.08 + 0.28*46=76.96 C^0. Diode 5 and 6 junction temperature will be 64.08 + 0.6*9.7=69.9 C^0.

Second heat sink output water temperature will be 60,86C^0 +0.81C^0=61,67 C^0.

For 3rd module all calculations are the same only input water will be 61,67 C^0, it means that all junctions temperatures will be 0.81C^0 higher than in the second module.

For the last (eighth) versatile module virtual very hard regime can be taken where power loses in each transistor and each diode will be 100W. Input water temperature will be 60+(1000-400)/(4185*0,0328)=64.37 C^0. Heat sink temperature 64.37C^0+400*0.0289=75.93 C^0. 15 and 16 transistor junction temperature will be 75.93+0.28*100=103.93C^0. 15 and 16 diode junction temperature will be 75.93+0.6*100=135.95C^0. As it can be seen even in so hard regime semiconductors junctions temperatures are below 150 C^0. Water also is about 65 C^0.

In the same manner other heat sinks were calculated . Its thermal resistance is given in table 2.3. As the theoretical calculation shows that they have satisfactory R_{th}, they were manufactured and experimentally tested. Experimental thermal resistance is given in table 2.3.

Table 2.3.

Comparison of theoretical and experimental data

Heat sink	Theoretical R_{th} (C^0/W)	Experimental R_{th} (C^0/W)	Comments
Fig. 2.29-a Soldered heat sink with square channel	Heat sink to water 0,031	Heat sink to water 0,021	-Satisfactory R_{th} , experimental even better than theoretical - low reliability of construction - hard for manufacturing
Fig. 2.29-b Heat sink with soldered tube	Heat sink to water 0,032	Heat sink to water 0,05	-Easy in manufacturing -Satisfactory reliability of construction - experimental R_{th} worse than theoretical
Fig. 2.29-c Direct cooling heat sink	Case to water 0,2	Case to water 0,3	- hard for manufacturing -at the given moment not very reliable construction, but it has good potential in future -Need more research
Fig. 2.29-d Milled heat sink	Heat sink to water 0,029	Heat sink to water 0,019	-Easiest in manufacturing -Good reliability of construction -Good R_{th} , experimental even better than theoretical

As it can be seen better theoretical and experimental results show milled heat sink (fig.2.29.d). It also was the easiest in manufacturing. Due to that they were chosen for further usage.

2.6. Summary

In this chapter stages of versatile power module development were shown.

There are solved next tasks:

1) the BUSBAR conductor’s system which allows to minimise overvoltages across semiconductor switches was chosen;

2) galvanic isolated control system that protect control system in case of fault on power board. Driver board has local hardware protection system that does not allow switch-on both transistors of one half-bridge leg was developed

3) galvanic isolated measurement circuits that allow to protect control system in the case of fault on power board was developed;

4) 4 different primary heat sink constructions were designed and theoretically calculated. One construction of water cooling system primary heat sink was chosen as cheap, easy-made and robust.

3. Development of Matlab-simulink model of versatile power module its control core and elements of UPSS

Before the experiments it was decided to evaluate converters (inverters, rectifiers, step-up/step-down converters and etc) and its control algorithms using simulations in MATLAB SIMULINK.

3.1. Model development of versatile power module

Block diagram of versatile power converter is depicted in fig. 3.1. The power board has power connectors for load, supply and inductor connection as well as two lower power connectors for driver board and measurement board. Control device (through adaptor board) is connected to measurement and driver board by coaxial cables (for analog signal) and optic fibers (for digital signals).

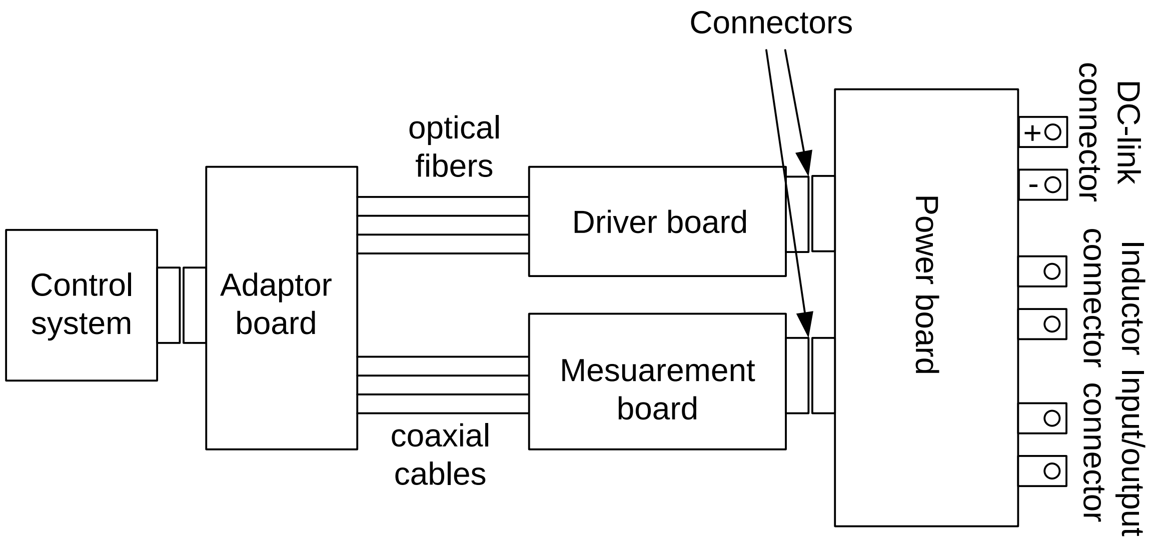

Fig. 3.1. Versatile power converter block diagram

Matlab model was built by similar topology as a real versatile power converter. Due to this Matlab-simulink model contains the same main blocks plus one auxiliary block for voltages and currents analyzing (fig.3.2):

- Power board
- Measurement board
- Driver board
- Control board

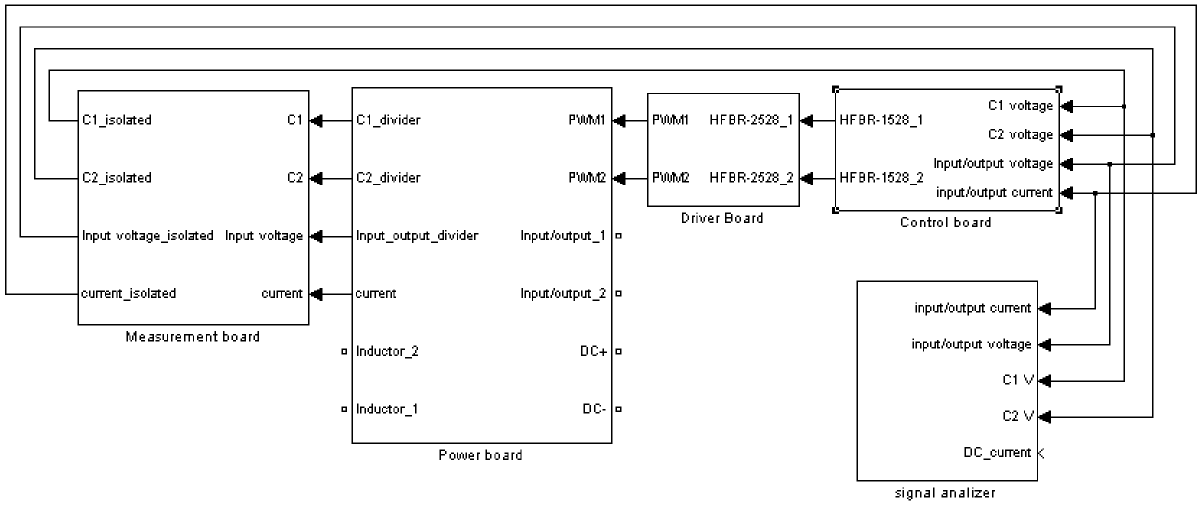

Fig. 3.2. Matlab simulink model of versatile modular power converter

3.1.1. Power board subsystem

Power board subsystem (fig.3.3.) contains the same elements like real power board converter: two power switches, two capacitors, three voltage measurements blocks (which measure voltage on resistive voltage dividers), one current measurement block, DC-link connectors, inductor connectors and input/output connectors. Parameters (capacitance and ESR) of Matlab model of capacitors are typed in the same way as it is given in datasheets or real parts (RIFA PEH200 1000uF, 450V capacitors). In addition the diodes and the transistors typed in parameters (forward voltage "Vf", resistance "Ron", current fall tame) are also taken from real elements datasheets.

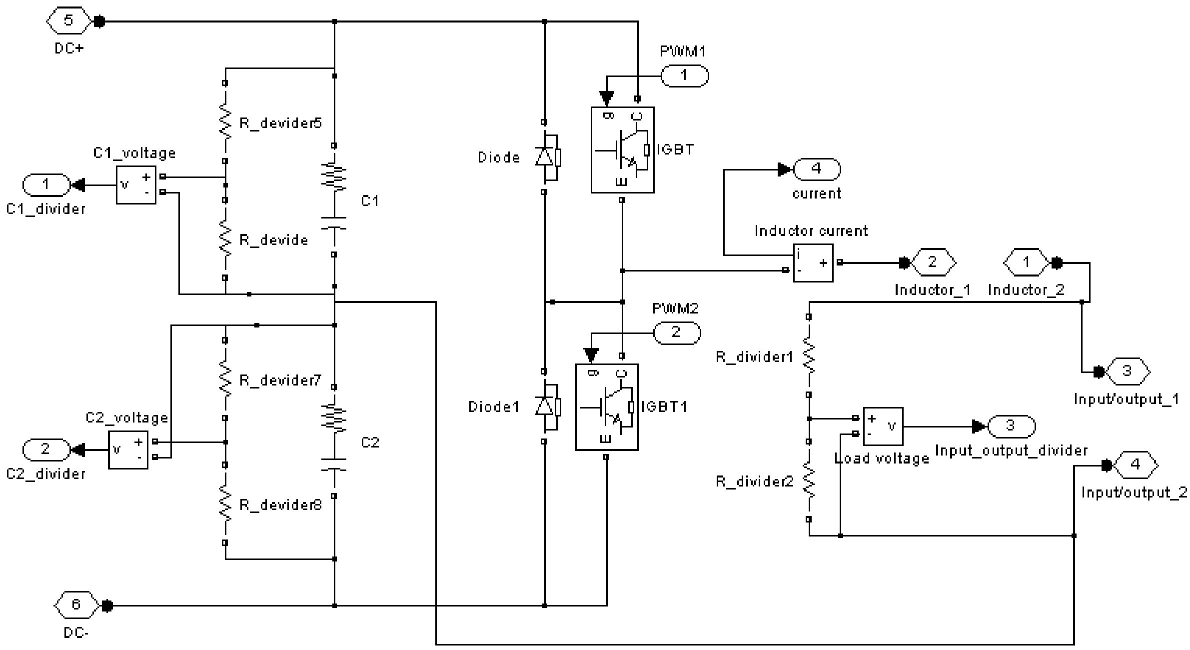

Fig.3.3. Power board subsystem circuit

Depending on the task and simulated converter some elements can be removed:

- Upper capacitor "C2" in the case of full-bridge converter topology and DC-link voltage below 450V is unnecessary. Removing of the capacitor two times increases the capacitance of DC-link and two times reduces ESR of DC-link)
- In the case of step-up or step-down converter one transistor can be removed from the model

3.1.2. Measurement board subsystem

Figure 3.4 presents the subsystem of measurement board. One of the tasks of this subsystem is to take into account bandwidth and time delay of HCPL7800 (fig.3.5.) and LEM LTS 15-NT (fig.3.6). Although in versatile converter LEM LTS 15-NT is built in the power board, but in Matlab-simulink it was decided to put it into the measurement board subsystem model. As a bandwidth of HCPL7800 (90kHz) and LEM LTS 15-NT (200 kHz) is relatively large, but the time delay (5.5us – HCPL7800, 400ns – LEM LTS 15-NT) relatively small in most of the cases subsystem signal delay can be neglected. So, the subsystems of voltage and current sensors (HCPL7800 and LEM LTS 15-NT) can be substituted only with its amplification coefficient with bias (fig.3.7. and fig.3.8.) that was mentioned in chapter 2.3. This allows to increase speed of simulation.

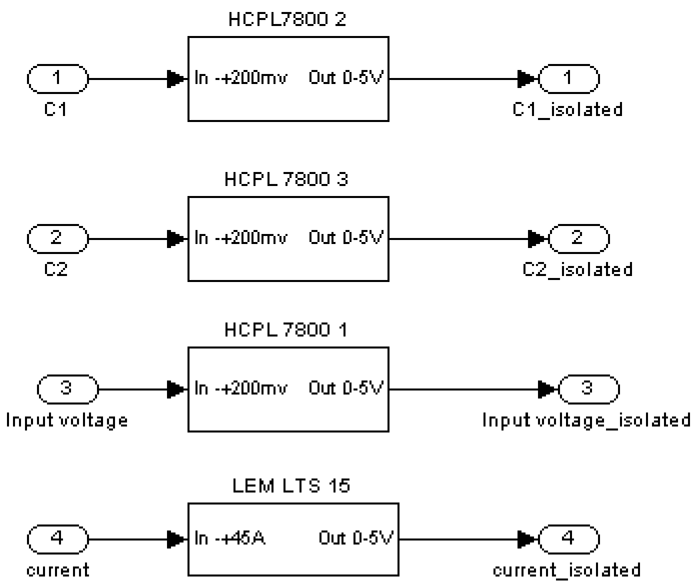

Fig.3.4 Measurement board subsystem

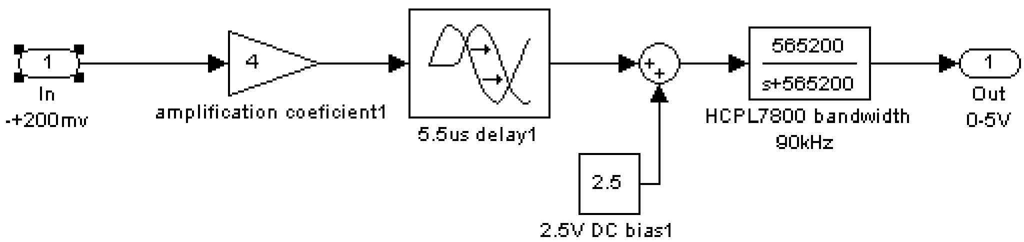

Fig.3.5. AVAGO HCPL7800 Matlab model that takes into account its amplification coefficient, bandwidth, phase shift and voltage bias.

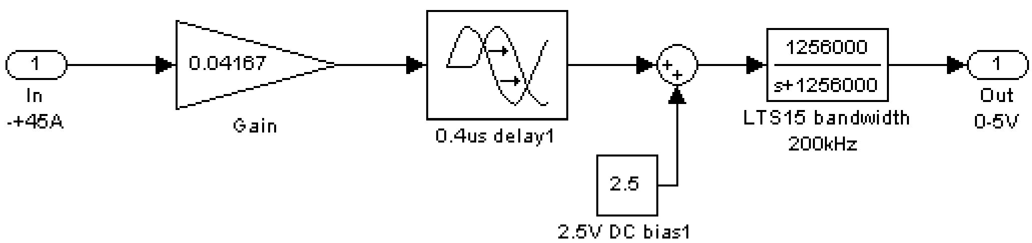

Fig.3.6. LEM LTS15 Matlab model that takes into account its amplification coefficient, bandwidth, phase shift and voltage bias.

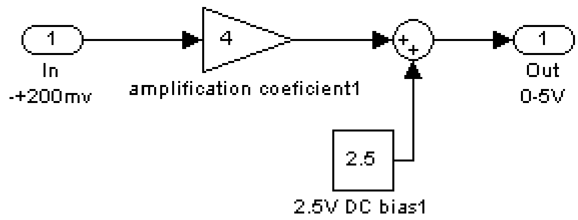

Fig.3.7. HCPL7800 Matlab model that takes into account only amplification coefficient and voltage bias

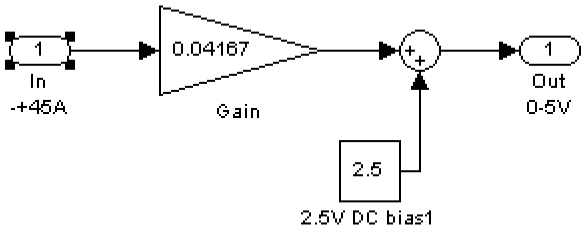

Fig.3.8. LEM LTS15 Matlab model that takes into account only amplification coefficient and voltage bias

3.1.3. Driver board subsystem

Matlab model of driver board is given in figure 3.9. The main task of this subsystem is to take into account control signal delay that was shown in fig.2.18 in chapter 2.2. These blocks include delays of all parts that are involved into control signal transmission (logic elements delays, opto-transmitter delay, opto-receiver delay, transistor driver delay). Due to the fact that the signal delay is very small (below 1 microsecond as was seen in fig.2.18.) in most of the cases it can be neglected. Thus, subsystem “Driver board” in most of the cases can be deleted at all. It minimises number of elements in model that increase speed of simulation.

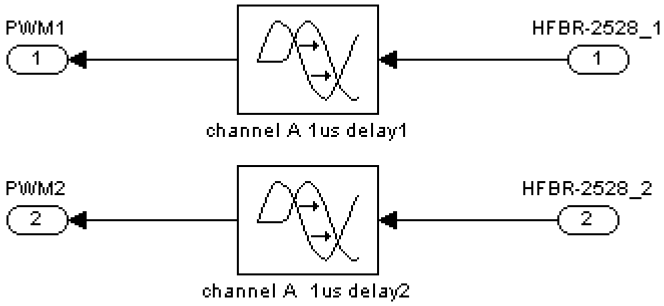

Fig.3.9. Driver board subsystem model

3.1.4. Control board subsystem

Control board subsystem represents control device. Example of "control board" subsystem is given in figure 3.10. It shows control algorithm for inverter.

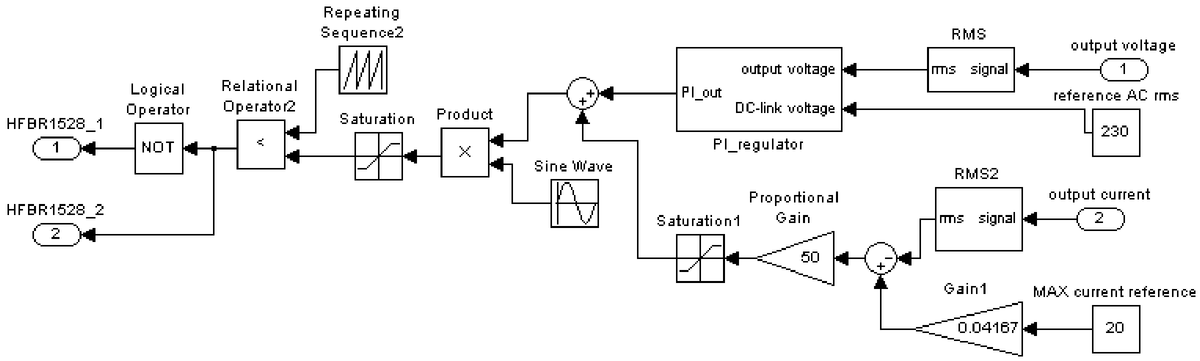

Fig.3.10. Example of control board subsystem model

3.1.5. Signals analyzer subsystem

The following parameters can be calculated in this block: active power, reactive power, total power, displacement factor, distortion factor, power factor, THD, individual harmonics amplitudes, DC-link power, converter efficiency.

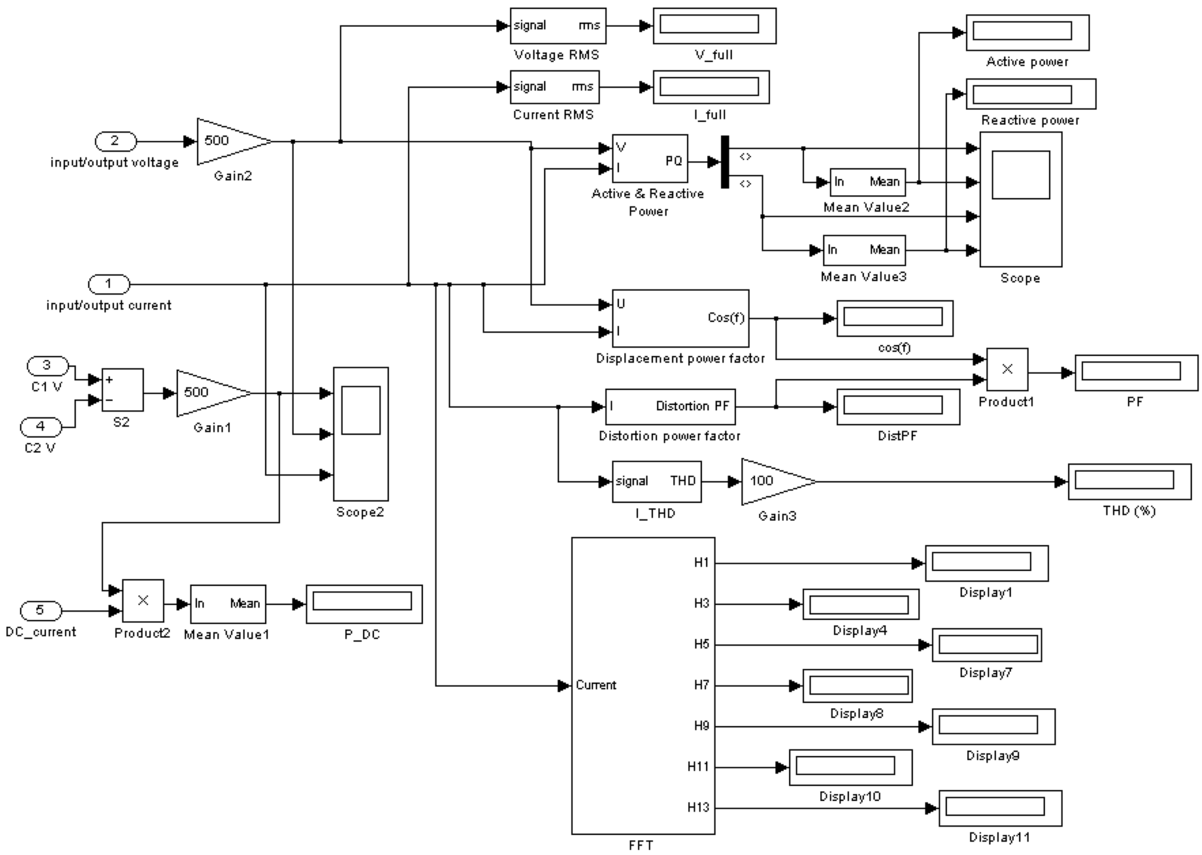

Fig.3.11. Example of signals analyzer subsystem model

3.2. Development of photovoltaic panel model

To simulate power converter for PV panel the PV panel model is necessary. In Matlab-simulink toolboxes there is no PV model. Due to this it was decided to develop it. Equivalent PV circuit is depicted in fig. 3.12. [37,39, 63]

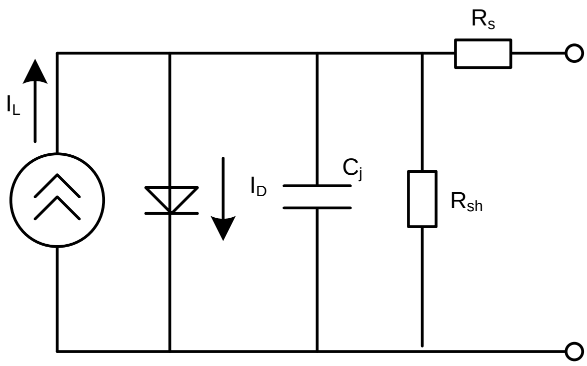

Fig. 3.12. Equivalent circuit of PV cell

Firstly it was developed PV panel Matlab-simulink model using the above given circuit that is depicted in fig.3.13.

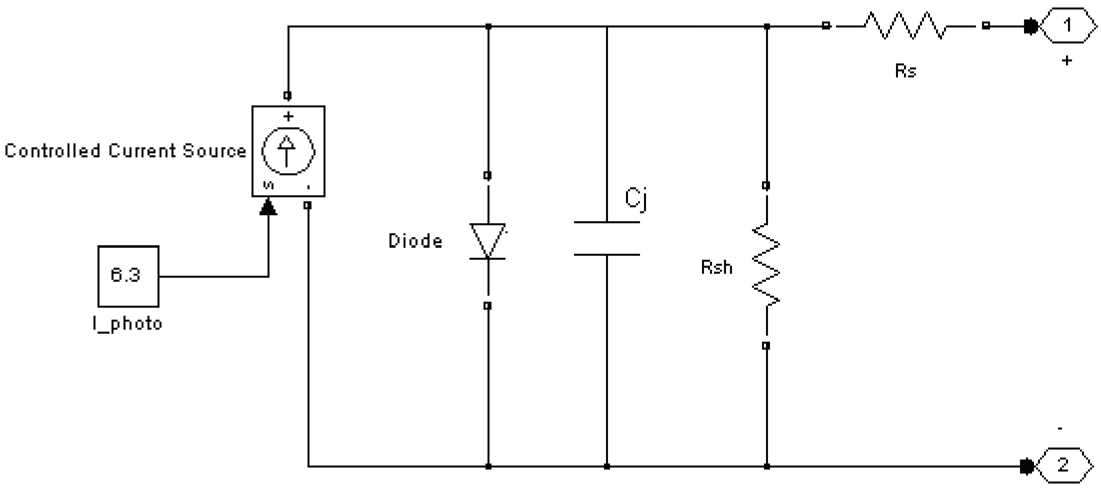

Fig. 3.13. Subsystem of Matlab-simulink PV panel model

The given model is idealized a lot, due to the idealized diode that is taken from Matlab-simulink SimPowerSystem library. PV panel open-circuit voltage depends on sum of diodes forward voltage drop and its internal series resistances. It means that open-circuit voltage can not be regulated as a function of such parameters as temperature and illumination.

Idealized Volt-Ampere (V-I) and Power-Ampere curves of Matlab-simulink model are given in fig. 3.14. Angle $\angle\alpha$ depends on Rs (the greater resistance of Rs the greater angle of slope). Angle $\angle\beta$ depends on Rsh, but they have inverse relation (the greater resistance the smaller slope of angle).

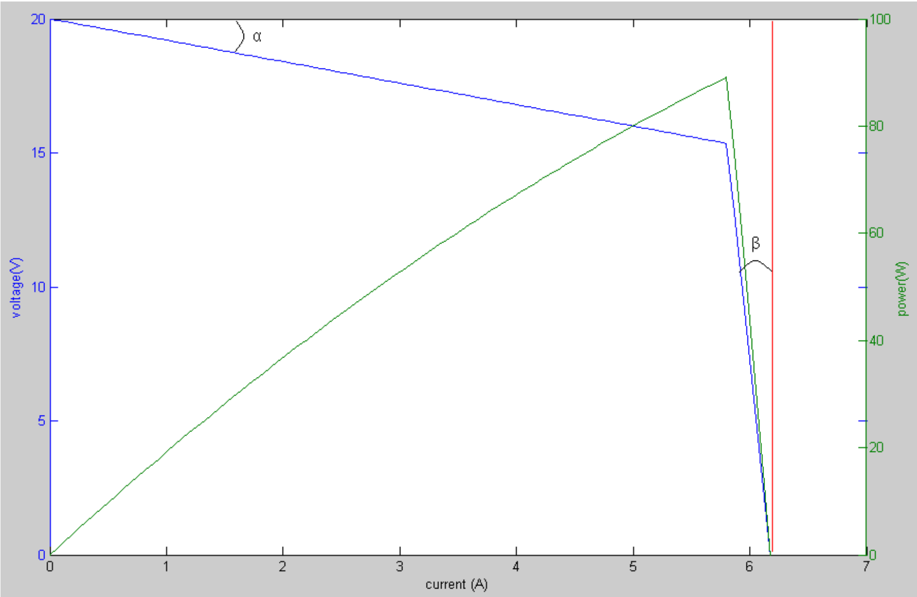

Fig.3.14. PV Matlab-simulink model V-I (blue) and P-I (green) curves

As it can be seen it is very imprecise. Due to this it was decided to use another approach of Matlab-simulink model development. It was used Matlab-simulink block "Controlled voltage source" that is controlled depending on input parameters like current, temperature, illumination [61,62].

To develop precise model of the PV panel using "controlled voltage source" it is necessary to know precise relation of its voltage and current. The following relations can be found in the literature sources:

$$I = I_L - I_0(\exp(\frac{V + IR_s}{(nkT/q)}) - 1) - \frac{V + IR_s}{R_{sh}} \qquad (3.1)$$

where: I_L=the light-generated current;

I_0=dark saturation current;

V – voltage, R_s – series resistance;

R_{sh} – shunt resistance;

T – absolute temperature;

k – Boltzmann's constant;

q – charge of electron;

n – ideality factor and usually 1<n<2.

I_0 depends on temperature and its equation is given below:

$$I_0 = BT^y \exp(\frac{-E_{g0}}{(kT)}) \tag{3.2}$$

where: B – independent on temperature,

E_{g0} – linearly extrapolated zero temperature bandgap of the semiconductor making up the cell,

y- includes the temperature dependencies of the remaining parameters determining I_0.

The main problem of these formulas is some parameters (n, I_0) that usually cannot be found in datasheets. From everything above written it can be concluded that this approach of PV panel V-I dependence cannot be implemented.

Instead of the above mentioned method a simplified method that allows to get formula for PV panel V-I curve simulation was used. PV panel V-I curve can be measured experimentally (or taken form datasheet) and using the regression methods the formula that precisely describes real PV panel V-I curve can be found.

Such experiments were made with PV panels that were available in RTU laboratory. It was measured PV panel V-I curve with two different illumination levels (fig.3.15.). The same experimental data in text view are given in table 3.1. PV panel has 36 PV cells in series and they temperature during the experiments was about 60^0C.

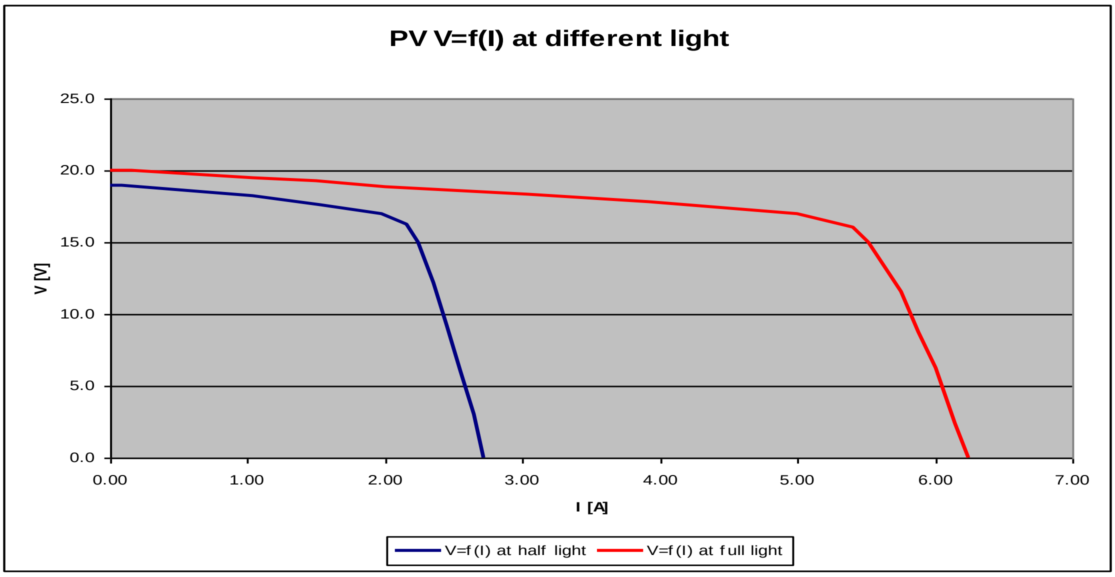

Fig. 3.15. PV panel V-I curves for full illumination level and half illumination level

Table 3.1.

Experimental I-V curves for rated and partial illumination

Panel rated illumination (100%)		Panel partial illumination (43%)	
Current (A)	Voltage (V)	Current (A)	Voltage (V)
0.00	20.0	0.00	19.0
0.16	20.0	0.08	19.0
1.04	19.5	1.04	18.2
1.50	19.3	1.52	17.6
2.00	18.9	1.98	17.0
3.04	18.3	2.16	16.2
3.92	17.8	2.24	15.0
5.00	17.0	2.35	12.2
5.40	16.0	2.45	9.2
5.52	15.0	2.55	6.0
5.75	11.6	2.64	3.0
5.88	8.8	2.72	0.0
6.00	6.2		
6.15	2.4		
6.24	0.0		

Such curves can be described with formula type:

$$U(i) = a - b \cdot i - c \cdot i^{d} \tag{3.3}$$

where : a – coefficient that represents PV panel open-circuit voltage,

b – coefficient that represents resistance R_s,

c,d – coefficients

Using software “Matcad” regression of experimental data was done. The “Matcad” calculates the coefficients for such equation type using an optimized version of the Levenberg-Marquardt method. The discovered coefficients were:

a – 20: b – 0.5, c – 3.4105e-012, d – 16 (3.4)

Substituting the coefficients in expression (3.3.) we get the PV panel I-V curve expression:

$$U(i) = 20 - 0.5 \cdot i - 3.4105 * 10^{-12} * i^{16} \tag{3.5}$$

Fig. 3.16 gives the comparison of experimental curve and simulated curve that was calculated using the expression (3.5).

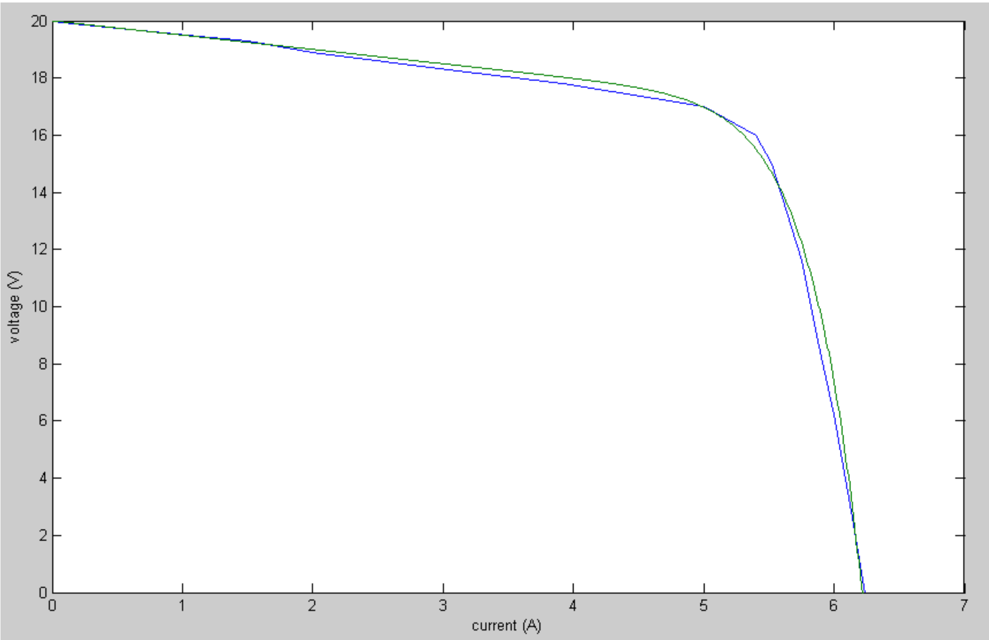

Fig.3.16. Comparison of PV panel I-V curves (
blue – experimental, green – calculated by expression (3.5))

To formula (3.5) one more variable was added to take into account light intensity. Light intensity influences open-circuit voltage and generated current. Light-generated current is directly proportional to sunlight. Idealized PV panel open-circuit voltage dependence can be described with:

$$V_{oc} = m * \frac{kT}{q} * \ln(\frac{I_L}{I_0} + 1) \tag{3.6}$$

where: m – number of cells in series in PV panel,

I_L – light-generated current that is equal to sort-circuit current.

Using experimental data the equation (3.14) can solved for I_0.

$$20 = 36 * \frac{1.38 \cdot 10^{-23} \cdot 333}{1.602 \cdot 10^{-19}} * \ln(\frac{6.24}{I_0} + 1) \tag{3.7}$$

$$I_0 = 2.4217 \cdot 10^{-8}$$

Where:I_0 – dark saturation current for idealized case at 60^0C.

Substituting in equation (3.6) I_0 with the found number open-circuit voltage at another light intensities can be found.

Final PV panel V-I dependence is:

$$U(i) = 36 \cdot \frac{333 \cdot k}{q} \cdot \ln\left(\frac{6.24 \cdot E}{I_0} + 1\right) - 0.5 \cdot i - \frac{3.4105 \cdot 10^{-12} \cdot i^{16}}{E} \qquad (3.8)$$

where: E – light intensity in fractions from experimental current at full illumination (6.24A). Practical illumination range is 0<E<2.

PV panel subsystem is depicted in fig.3.17.

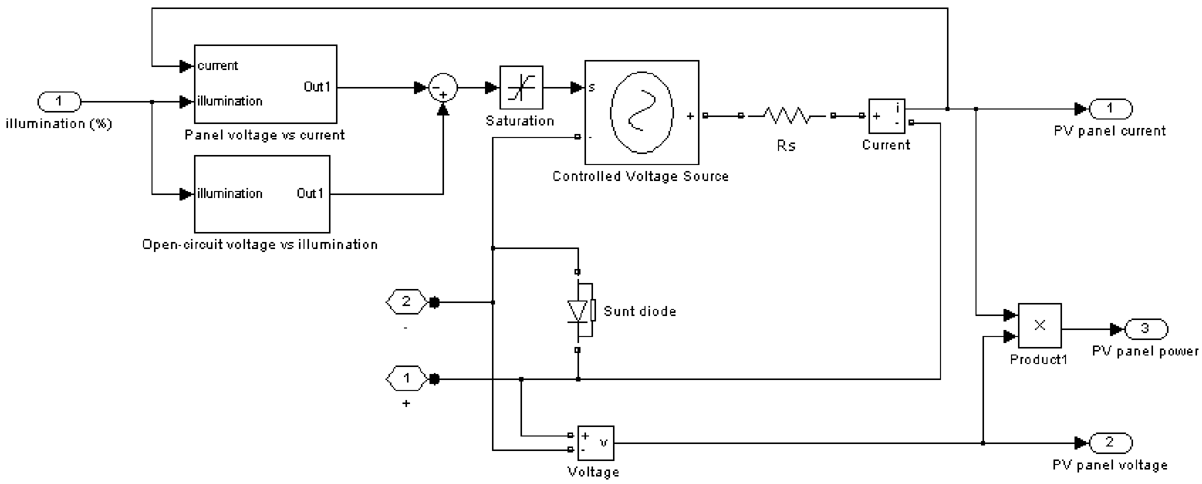

Fig.3.17. Matlab-simulink model of photovoltaic panel

There is voltage source controlled with the help of two functions. Subsystem “Open-circuit voltage vs illumination” (fig.3.18) represents the first term of equation (3.8). Series resistance “R_s” represents the second term of equation (3.8). Subsystem “Panel voltage vs illumination” (fig.3.19) represents the third term of equation (3.8).

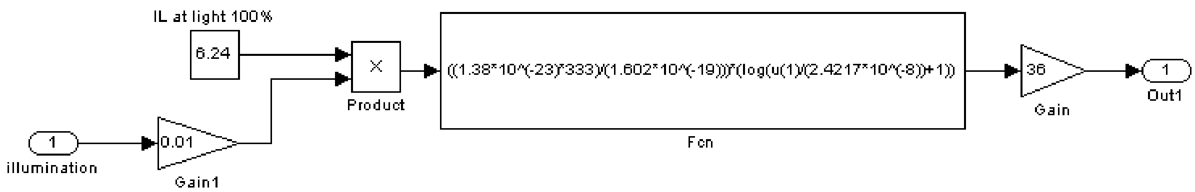

Fig. 3.18. Subsystem that represent open circuit voltage dependence on illumination

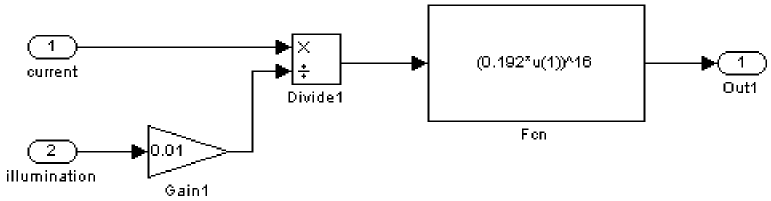

Fig.3.19. Subsystem that represent voltage dependence on current

Comparison of experimental and simulated data is given below in fig.3.20.

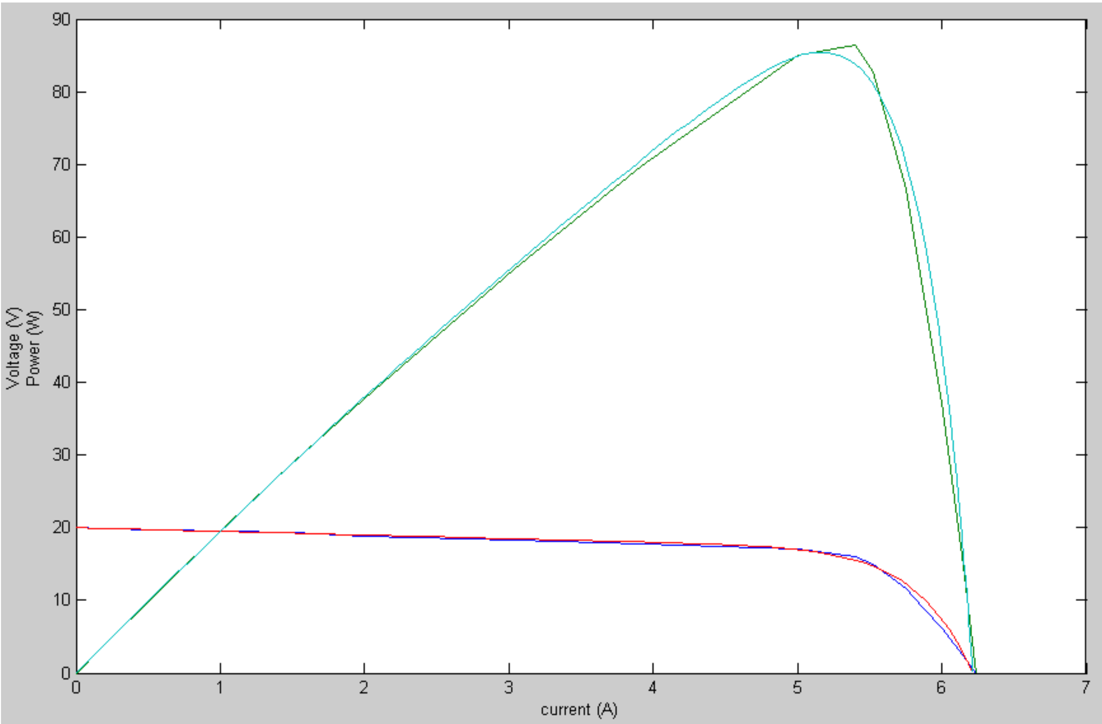

Fig. 3.20.Comparison of experimental and simulated data of PV panel's I-V and I-P curves at full light

(dark blue - experimental I-V curve, red - simulated I-V curve, green – experimental I-P curve, light blue – simulated I-P curve)

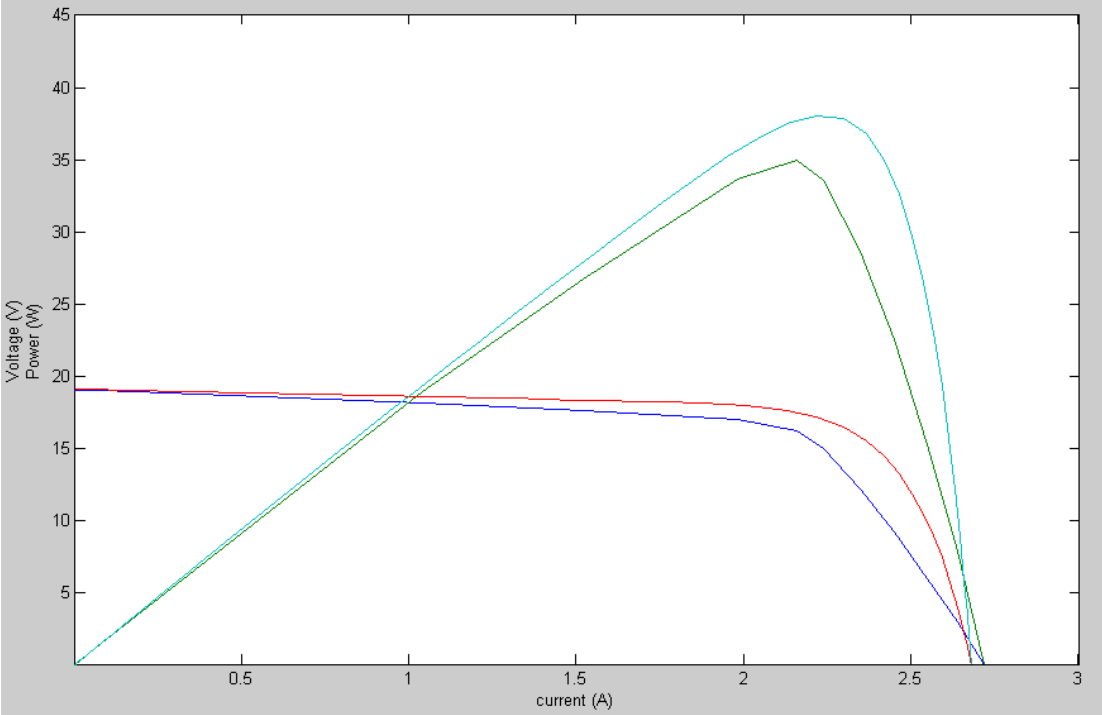

Fig. 3.21.Comparison of experimental and simulated data of PV panel's I-V and I-P curves at partial light.

(dark blue - experimental I-V curve, red - simulated I-V curve, green – experimental I-P curve, light blue – simulated I-P curve)

As it can be seen the experimental and simulated curves at partial light do not fully match but it is enough close to understand the behaviour of PV panel under different conditions. Quite important is the operation of PV array in the case of partial shading of one panel or few panels. Fig.3.22. depicts such a case. There is a simulation of the behaviour of PV array with 4 PV panels connected in series. 3 PV panels have rated illumination (100%) and one has partial illumination (50% of rated). As it is obvious Matlab-simulink model of PV array gives the adequate enough results [62].

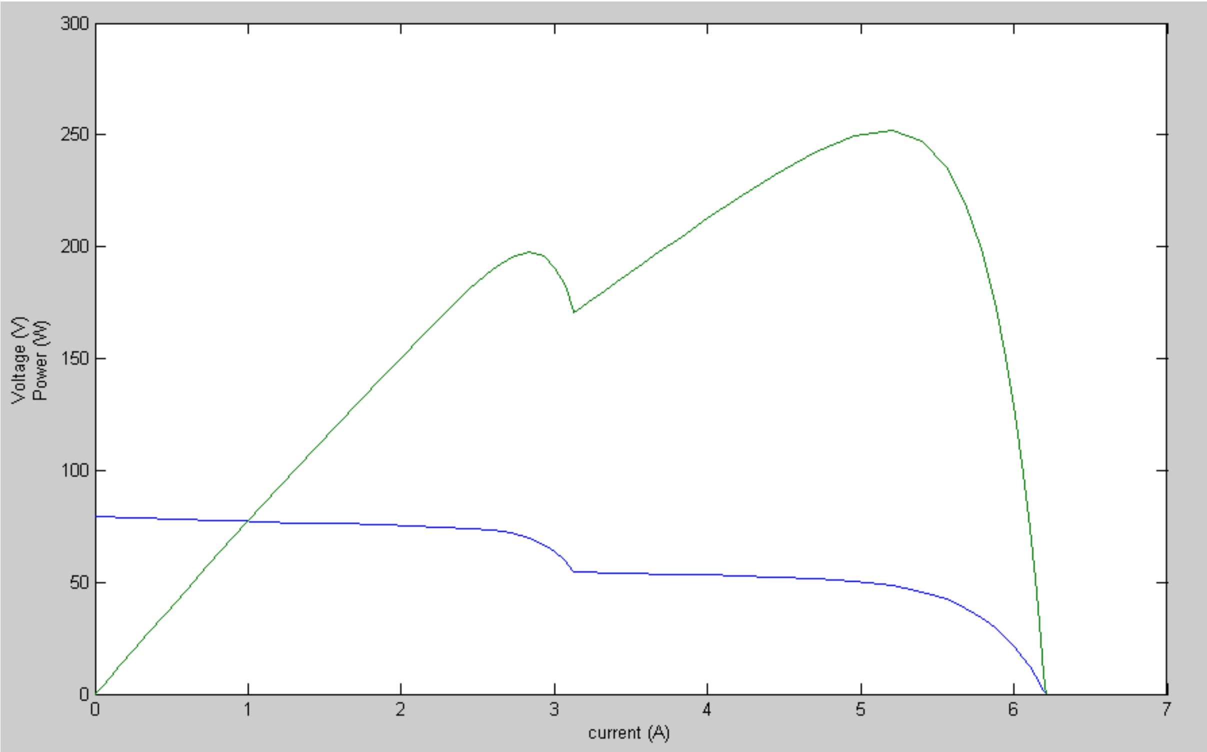

Fig.3.22. I-V and I-P curves for 4 panels connected in series for the case when one PV panel is partially shaded (50% of rated light intensity).

4. Versatile power module application for the UPSS assembling

4.1. Inverters simulation

There are two conventionally used types of inverter:

- Half-bridge
- Full-bridge

Both these types have advantages and disadvantages. The half-bridge inverter has high DC-link voltage, but due to small number of semiconductor it can have higher efficiency. The full-bridge inverter has 2 times lower DC-link voltage, but it has two times more semiconductors on current patch.

To find inverter topology that fits well both inverters topologies were simulated.

a) The half-bridge inverter

Configuration of versatile power converter for half-bridge inverter is shown in fig.4.1.

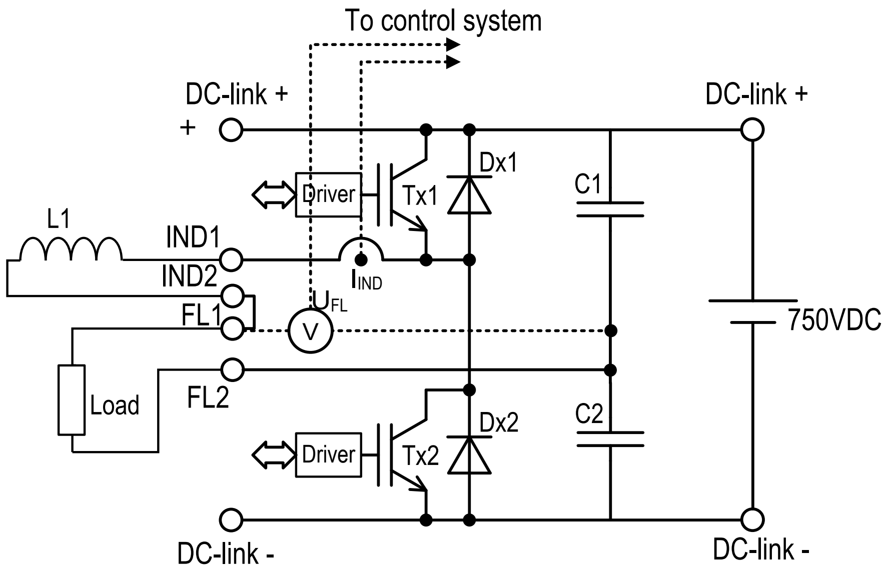

Fig.4.1. Versatile power converter configuration for half-bridge inverter

Matlab-simulink model of half-bridge inverter is shown in figure 4.2.

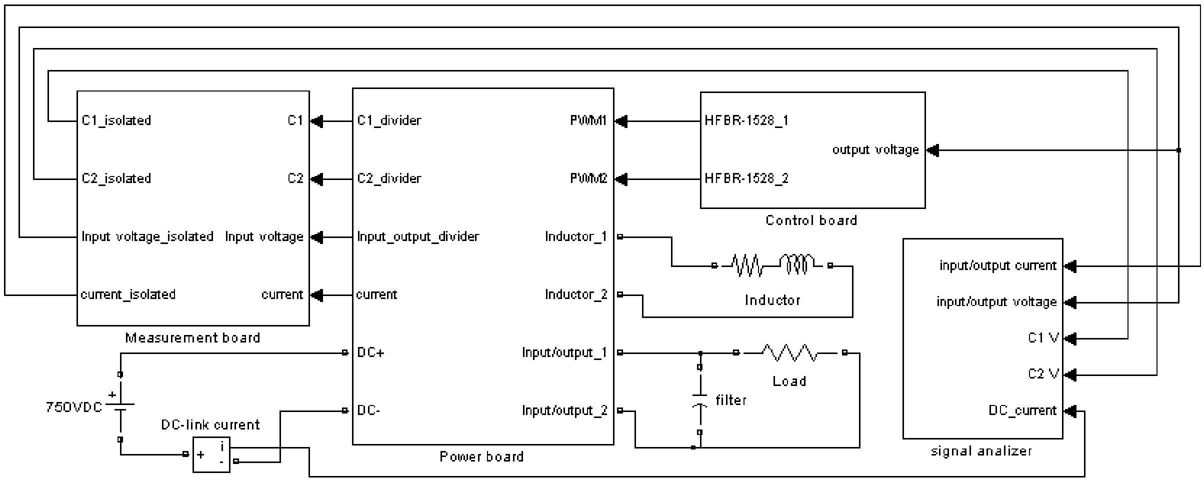

Fig.4.2. Simulink model of half-bridge inverter

The following equipment is connected to versatile power converter:

- DC voltage source 750V
- Inductor (L -2 mH, internal resistance - 0.13 Ohm)
- Resistive load
- Auxiliary current measurement block “DC-link current” that is necessary only in MATLAB-simulink for input power metering and converter efficiency calculation

To regulate output voltage few control algorithms can be used. Simple control algorithms measure only output voltage and control it (fig.4.3).

Slightly complex control system with 2 feedback signals is depicted in fig.4.4. There are the output voltage and output current measured in this scheme. Output current is measured to prevent overload and short circuits.

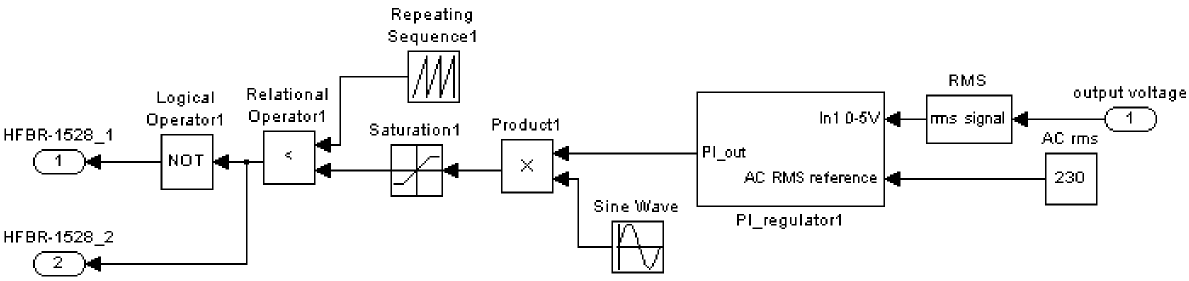

Fig.4.3. Full-bridge inverter simples control system with 1 feedback signal

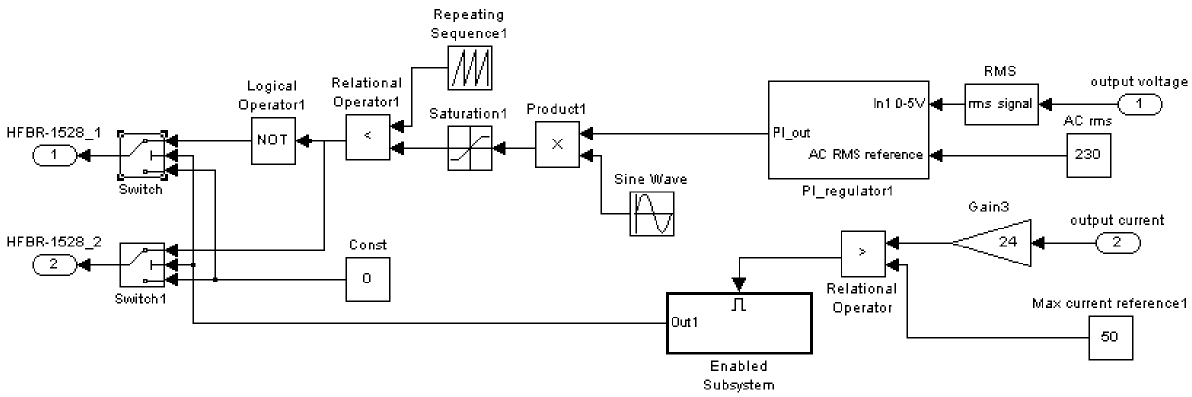

Fig.4.4. Full-bridge inverter control system with 2 feedback signals

All these control methods give similar results in normal operation mode. Simulation results are given for output power 4000W in figure 4.5. Figure 4.6. presents simulation results for highly non-linear load.

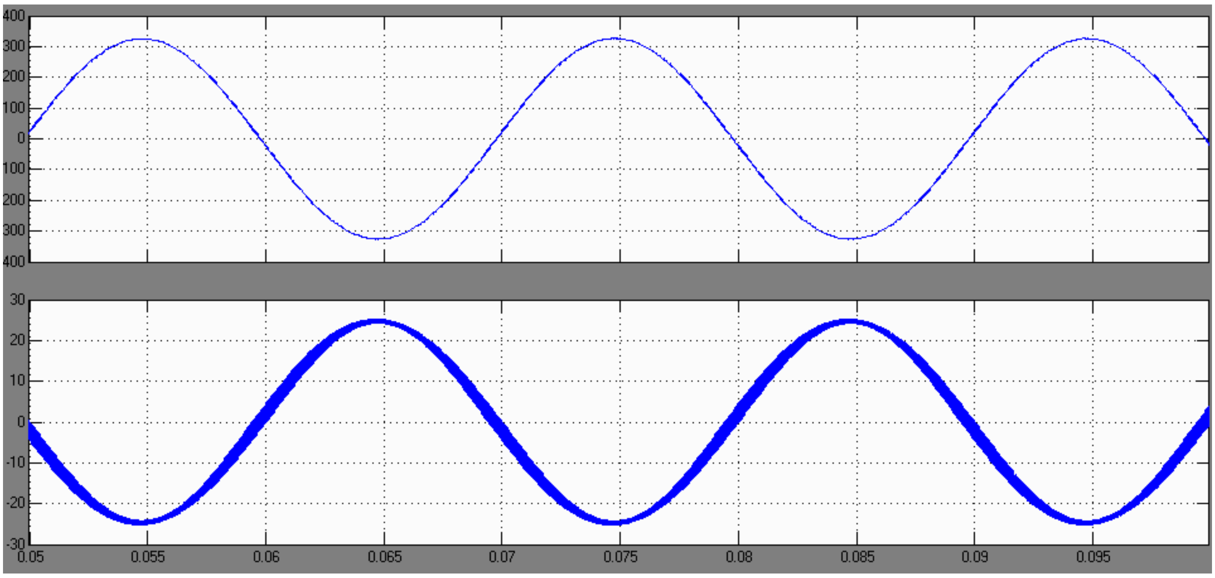

Fig.4.5. Simulation results at 4000W. Upper curve is load voltage, but lower is inductor current. The inductor current THD is 5.2%. But due to additional output filter (4.7uF capacitor) load current has THD below 1%.

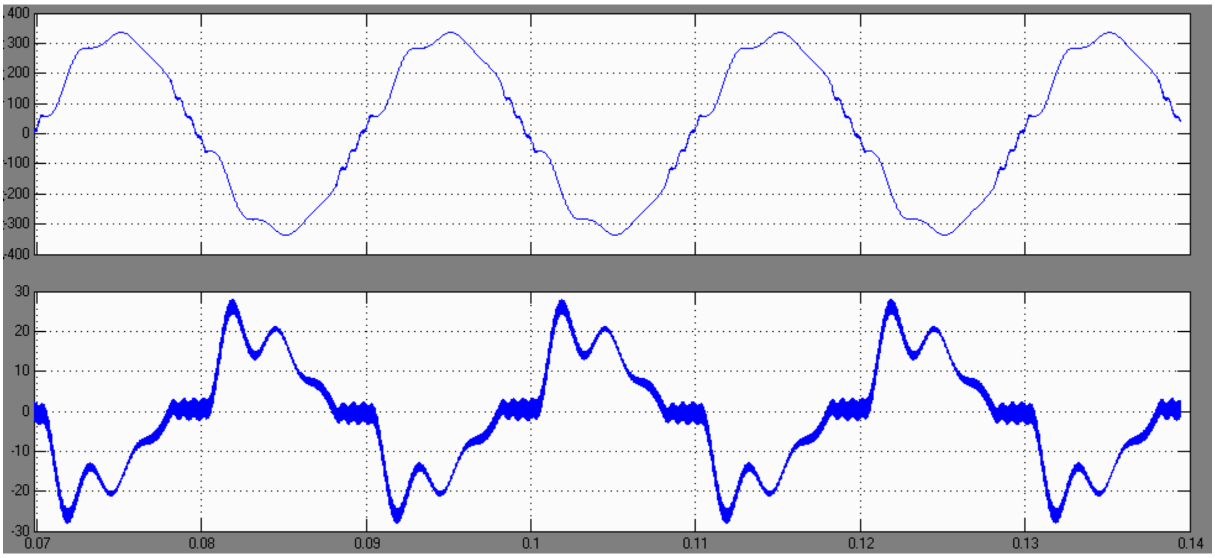

Fig.4.6. Simulation results with non-linear load. Upper curve is load voltage, but lower is inductor current. The inductor current THD is 36.7%. Cos(f) =0.91; PF=0.86.

In fig. 4.7. feedback system reaction on short-circuit is shown. Output voltage of the inverter is 230Vrms. At time 0.1s the inverter output is shortened. Current limiter is tuned on 50A (peak). To prevent transistor damage the control system switches off both transistors.

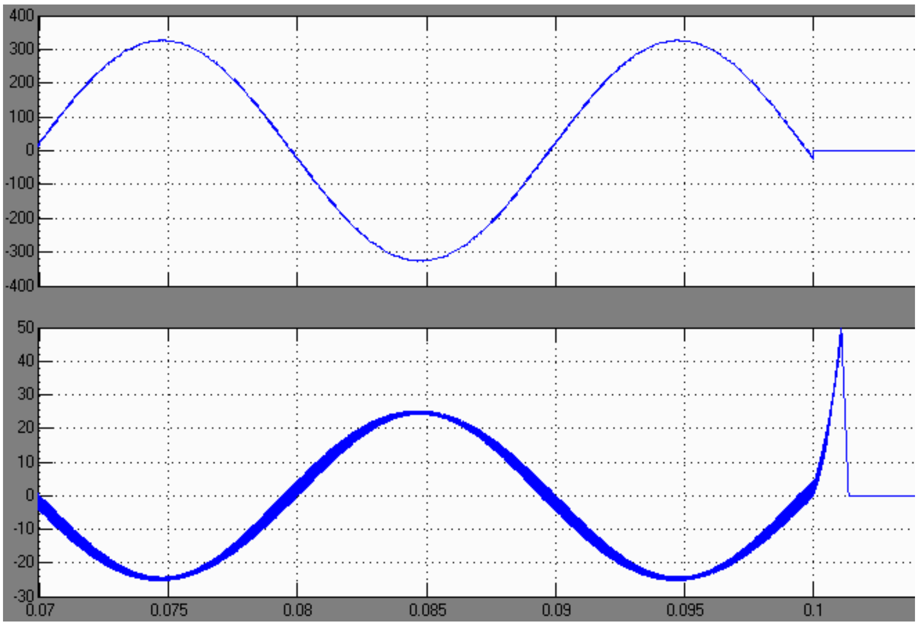

Fig.4.7. Simulations results of reaction on short-circuit in time 0.1s (upper – load voltage, lower – inductor current)

Simulation data for different loads are given in table 4.1.

Table 4.1.

Simulation results of half-bridge inverter with different loads

Power (W)	Current (A)	Output voltage THD (%)	Converter efficiency (%)
1000	4.4	1	95.7
2000	8.7	1	96
3000	13.1	1	96
4000	17.5	1	96.5

Simulation results in table 4.1. show higher inverter efficiency. The reasons of inverter high efficiency are not full equivalences of Matlab-Simulink models to real elements. Mainly it concerns to magnetic elements and semiconductors. The inductor basic Matlab-simulink model does not take into account magnetization losses. But in some cases the magnetization losses are so small (below 20% of total inductor loses) that it can be neglected.

The transistor Matlab-simulink model has idealized switching process. Fig.4.8 shows switching process of the transistor. As it can be seen it does not take into account turn-on losses. As well voltage of the transistor is not fully correct.

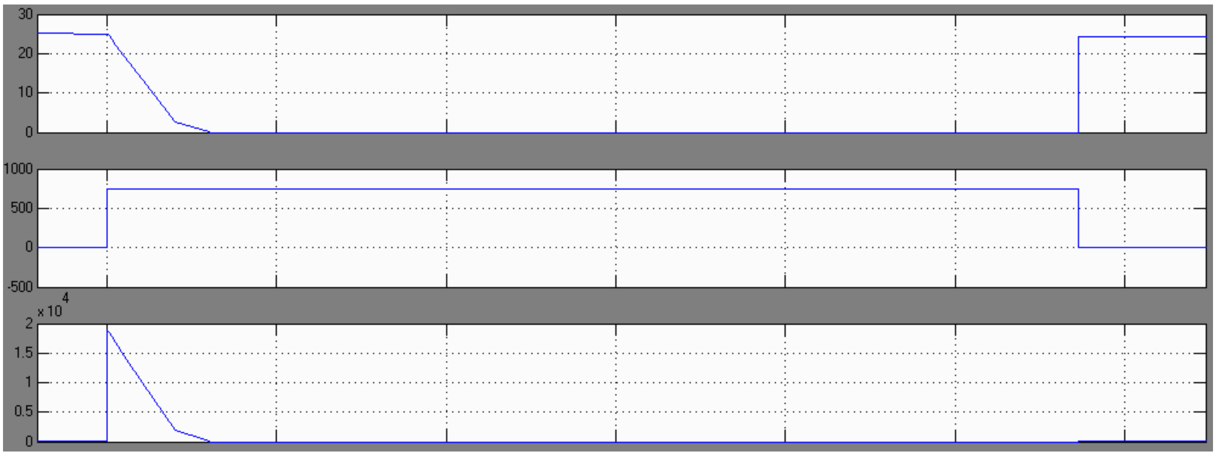

Fig.4.8. Switching process of Matlab-simulink transistor model. Curves from the upper one: switching current, switching voltage, momentary power losses

Due to the described above drawback the mean power losses in transistor (fig.4.9) can not be accepted as fully correct.

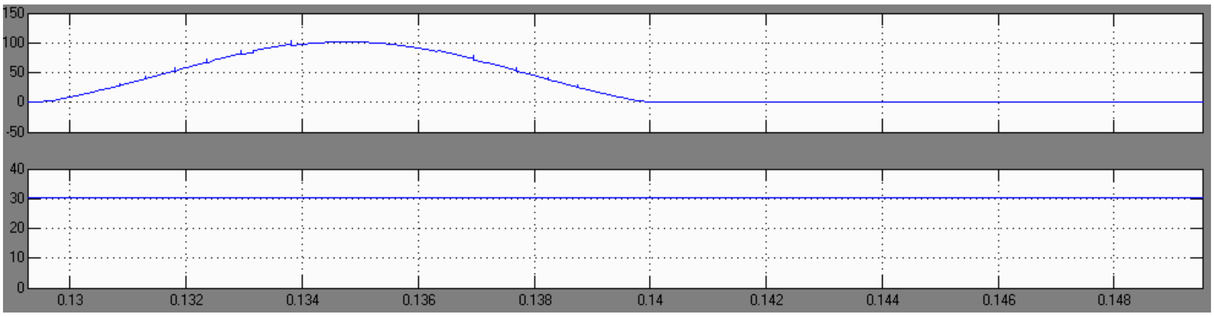

Fig.4.9. Switching losses of transistor. Curves from above: switching period mean power losses, mean power losses (about 30W)

Similar situation exists with Matlab-simulink diode model. Simulated mean power losses of the diode are only 2W. Switching process of the diode is given in fig.4.10.

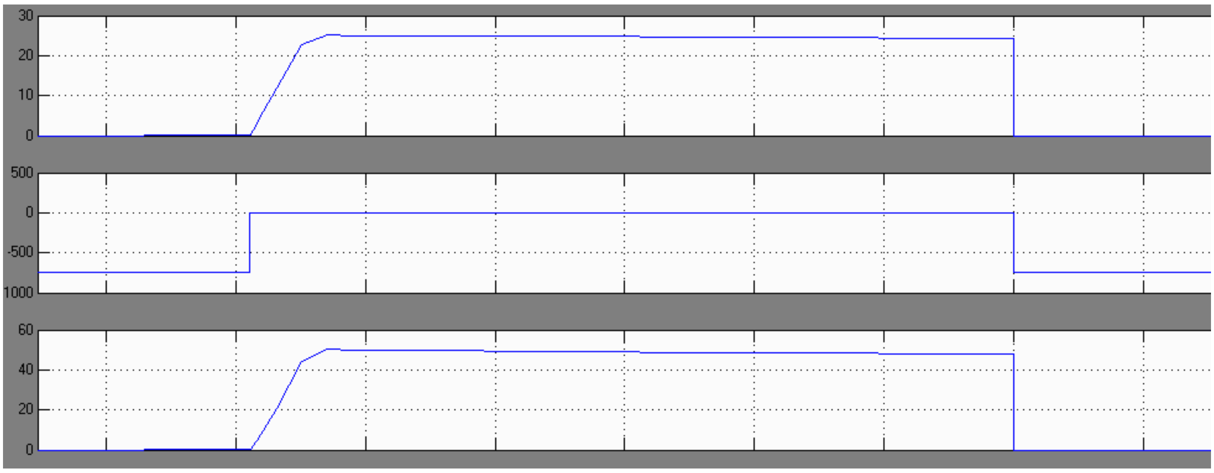

Fig.4.10. Switching process of Matlab-simulink diode model. Curves from above: switching current, switching voltage, momentary power losses

From all the above written we can conclude that Matlab is hardly implementable for converter adequate efficiency evaluation with current models of the semiconductors.

b) the full-bridge inverter simulation

To assemble the full-bridge inverter 2 versatile power converters are necessary (fig.4.11). As the full-bridge topology has no need in capacitor middle point and DC-link voltage is lower (375V) one of the DC-link capacitors can be shunted. That gives double DC-link capacity of each module.

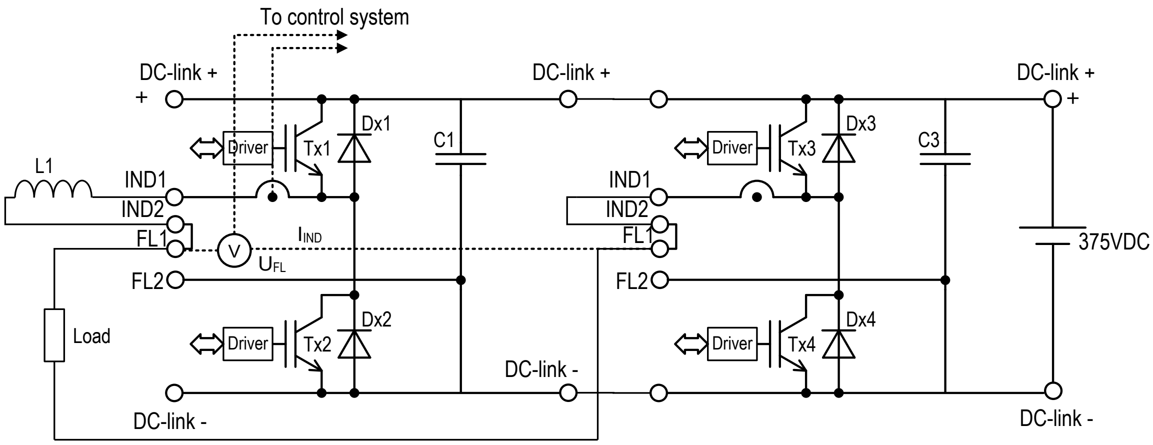

Fig.4.11. Two versatile power converters configuration for full-bridge inverter

Matlab-simulink model of the full-bridge inverter is given in figure 4.12.

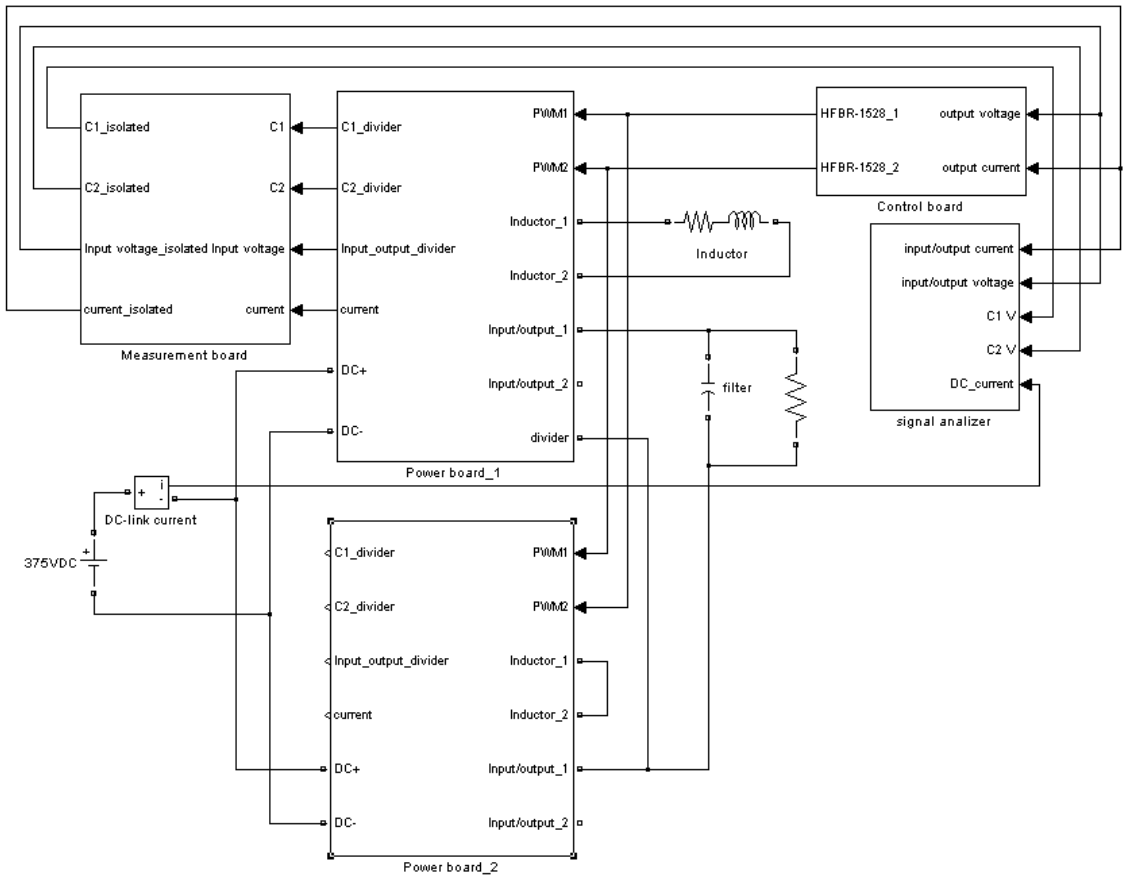

Fig.4.12. Matlab-simulink model of full-bridge inverter

For the regulation of output voltage the same control algorithms like those for half-bridge inverter can be used.

All voltage and current curves are very similar to half-bridge inverter simulated curves. Mostly difference is only in switching losses of transistors and diodes due to lower DC-link voltage (fig.4.13). In each individual semiconductor the mean losses are lower, but due to higher number on semiconductors in full-bridge converter the total efficiency of the whole converter is a bit lower.

Generally speaking these two inverter topologies are very similar according to their output voltage and current parameters. Main difference is in DC-link voltage and numbers of semiconductors and DC-link capacitors. So, in the case of high (750V-800V) DC-link voltage half-bridge inverter can be applied, but in the case of lower (350V-400V) DC-link voltage full-bridge inverter has to be used.

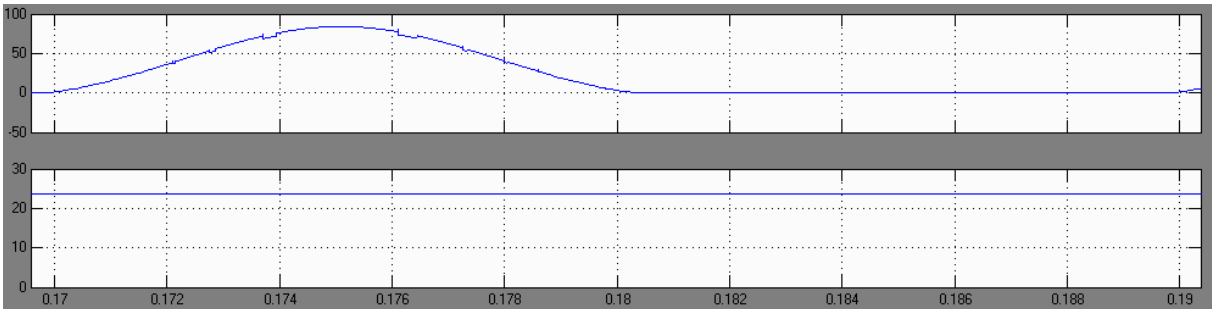

Fig.4.13. Switching losses of transistor. Curves from the upper: switching period mean power losses, mean power losses (about 23W)

Simulation data for different loads are given in table 4.2.

Table 4.2.

Simulation results of full-bridge inverter with different loads

Power (W)	Current (A)	Output voltage THD (%)	Converter efficiency (%)
1000	4.5	0.8	96.5
2000	8.7	0.8	96.8
3000	13.1	0.8	96.7
4000	17.5	0.8	96.4

4.1.1. Active PFC Rectifiers simulation

As it was mentioned in the second chapter there are many different topologies of active rectifiers:

- Boost PFC
- Boost interleaved PFC
- Bridgeless PFC converter
- Bridgeless totem PFC converter
- Full-bridge PFC rectifier/inverter
- Half-bridge PFC rectifier/inverter

All these converters have advantages and disadvantages. To find better PFC rectifier topology for uninterruptible power supply system they were simulated and compared.

a) Boost PFC topology

Boost PFC topology (fig.4.14.) is the most popular topology of active PFC rectifiers. It is often used for high power factor rectifiers in power supplies and electric drive applications.

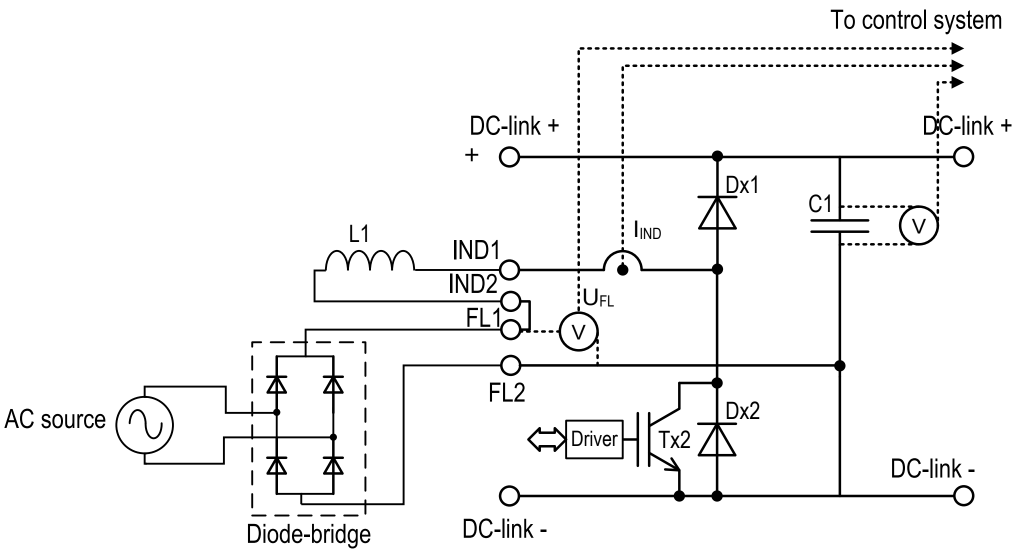

Fig.4.14. Versatile power converters configuration for boost PFC rectifier

The line current simultaneously flows through three semiconductors that is the most significant disadvantage of boost PFC. For this reason the overall efficiency of such converters usually is lower than that of the other topologies.
Matlab-simulink model of the boost PFC converter is shown in Fig. 4.15. For this converter simulation one versatile power converter plus one diode-bridge rectifier are used.

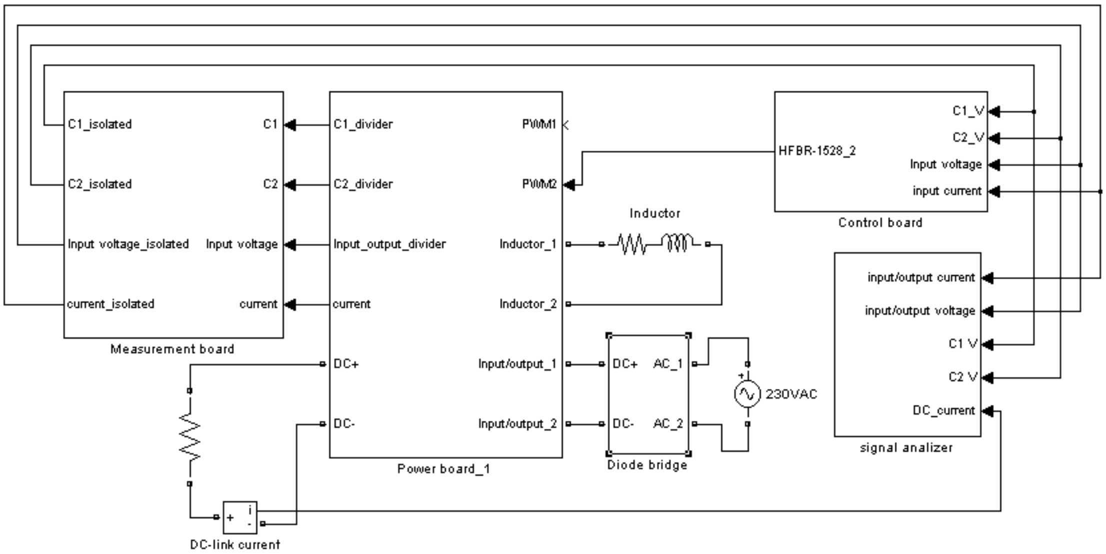

Fig. 4.15. Matlab model of subsystem "power board" for boost PFC converter

The following are connected to the versatile power converter:

- AC voltage source (230V rms) that simulates the grid
- Diode bridge that rectifies grid voltage
- Inductor (L -2 mH, resistance - 0.13 Ohm)
- Variable resistive load to get different powers and input currents
- Auxiliary current measurement blocks "DC-link current" that are necessary only for output power metering and converter efficiency calculation

The boost PFC topology needs only one DC-link capacitor due to that "C2" capacitor is shunted. It also increases twice the DC-link capacitance relatively to two capacitors in series. It has to be noted that the DC-link has higher voltage than input amplitude voltage [64].

$$V_d > \hat{V}_s \tag{4.1}$$

where : V_d – DC-link voltage,

$\hat{V}_s$ - voltage amplitude value

As a boost PFC can be considered as 2 different converters (diode bridge and boost DC/DC converter), the relation of input voltage and output can be written as:

$$\frac{V_d}{|v_s|} = \frac{1}{1-d(t)} \tag{4.2}$$

where: d – duty cycle

thus,

$$d(t) = 1 - \frac{\hat{V}_s \cdot |\sin(\omega t)|}{V_d} \tag{4.3}$$

The equation shows that in the case of $V_d = \hat{V}_s$ the d(t) will be within the range from 0 to 1 (fig.4.16).

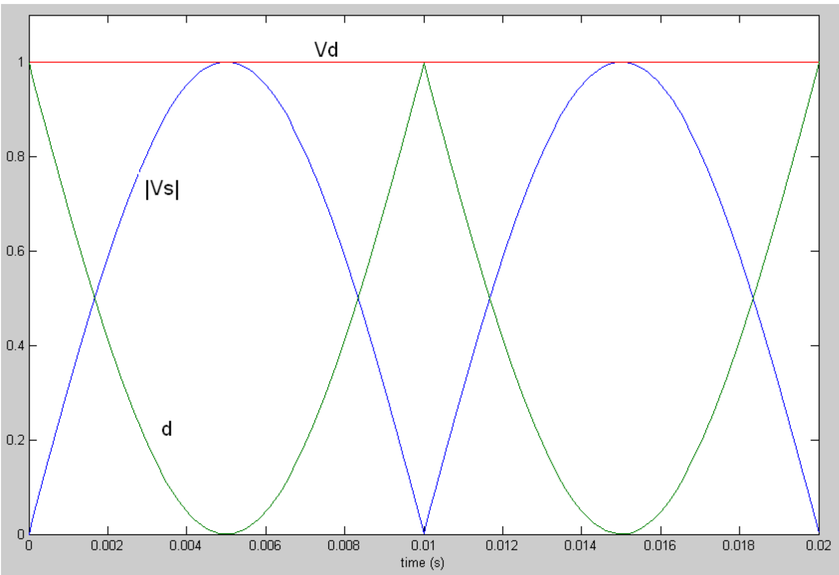

Fig.4.16. Boost converter PWM duty cycle in the case if $V_d = \hat{V}_s$

(red - DC-link voltage, blue – boost converter input voltage, green – duty cycle)

In practice the DC-link voltage is higher of $\hat{V}_s$ thus duty cycle:

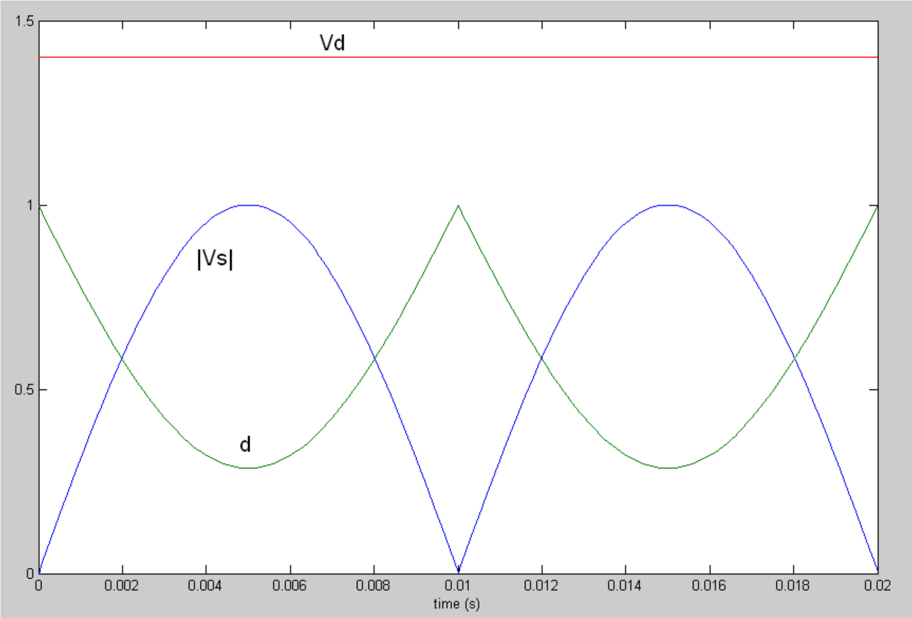

Fig.4.17. Practical boost converter PWM duty cycle (red - DC-link voltage, blue – boost converter input voltage, green – duty cycle)

The control circuit of boost PFC is given in fig. 4.18. Main task of this algorithm is to form the current of boost converter similar to the rectified voltage shape, and in phase with it. In such way power with cos(f) about 1 and current with very low THD (below 5%) can be consumed. As a feedback the DC-link voltage is used with the possibility to be regulated close to 375V.

Also the control algorithm has protection from DC-link over-voltage and transistor over - current. In the case of exceeding one of the limits the transistors switches-off.

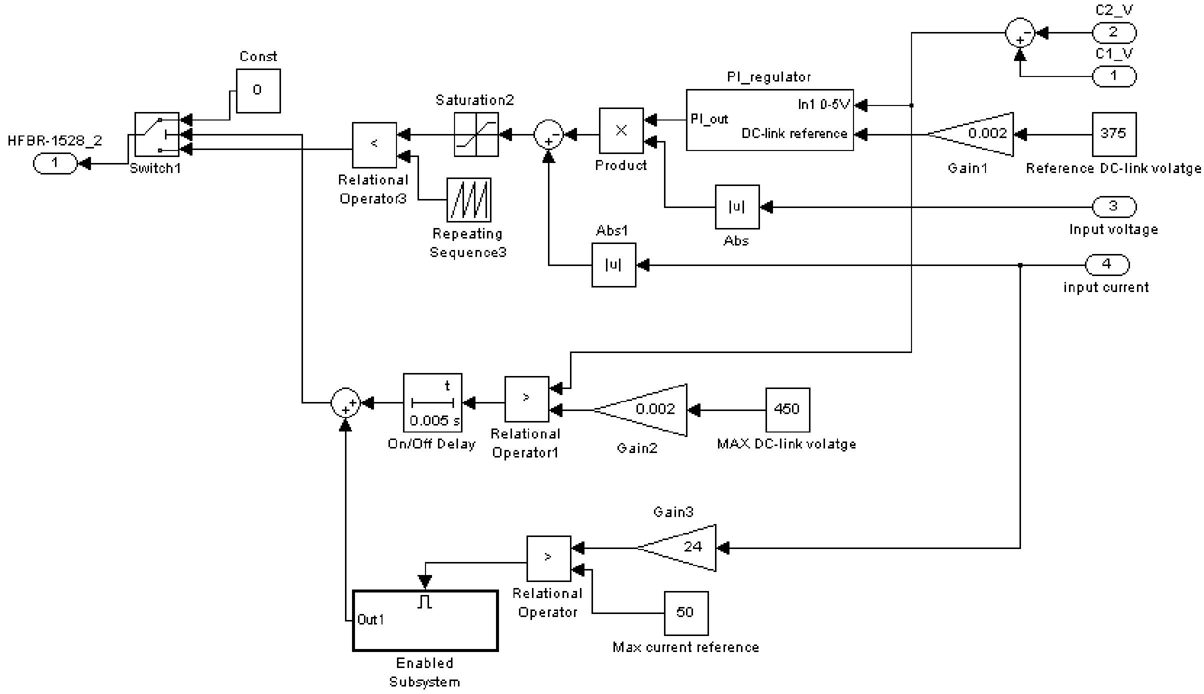

Fig. 4.18. Matlab-simulink model of control board for boost PFC rectifier

The diode mean current for switching period can be expressed with [64]:

$$\bar{i}_d(t) = (1-d)\bar{i}_L(t) = \frac{\hat{I}_L \hat{V}_s \cdot |\sin(\omega t)|^2}{V_d} \tag{4.4}$$

where: $\bar{i}_L$ - inductor mean current for switching period,

$\hat{I}_L$ - amplitude value of inductor current

Substituting the $|\sin(\omega t)|^2 = \sin^2 \omega t = 1/2 - \cos(2\omega t)/2$

$$\bar{i}_d = \frac{\hat{I}_L \hat{V}_s}{2V_d} - \frac{\hat{I}_L \hat{V}_s \cdot \cos(2\omega t)}{2V_d} \tag{4.5}$$

where: first term of equation is DC component I_d and second term $i_{d2}(t)$ is second-harmonic component. Assuming that through the load only I_d current flows then the capacitor voltage ripple is:

$$v_{d2}(t) = \frac{1}{\omega C}\int i_{d2} \cdot d(\omega t) \tag{4.6}$$

Substituting i_{d2} from (4.5)

$$v_{d2} = -\frac{1}{\omega C}\frac{\hat{I}_L \hat{V}_s}{2V_d}\int \cos 2\omega t \cdot d(\omega t) = -(\frac{\hat{I}_L \hat{V}_s}{4\omega C V_d})\sin(2\omega t) \tag{4.7}$$

where:

$$\hat{V}_{d2} = \frac{\hat{I}_L \hat{V}_s}{4\omega C V_d} \tag{4.8}$$

The equation represents peak value of output capacitor. In the simulation the capacitor with capacitance 1mF was used. Substituting all other variables with numerical values the output capacitor voltage ripples being 21V can be calculated. The same output capacitor ripple can be viewed in fig.4.19 depicting the simulation results for the rated power (4kW). Simulation results for other powers values (100%, 75%, 50%, 25%, 10%, 5%) are given in table 4.3.

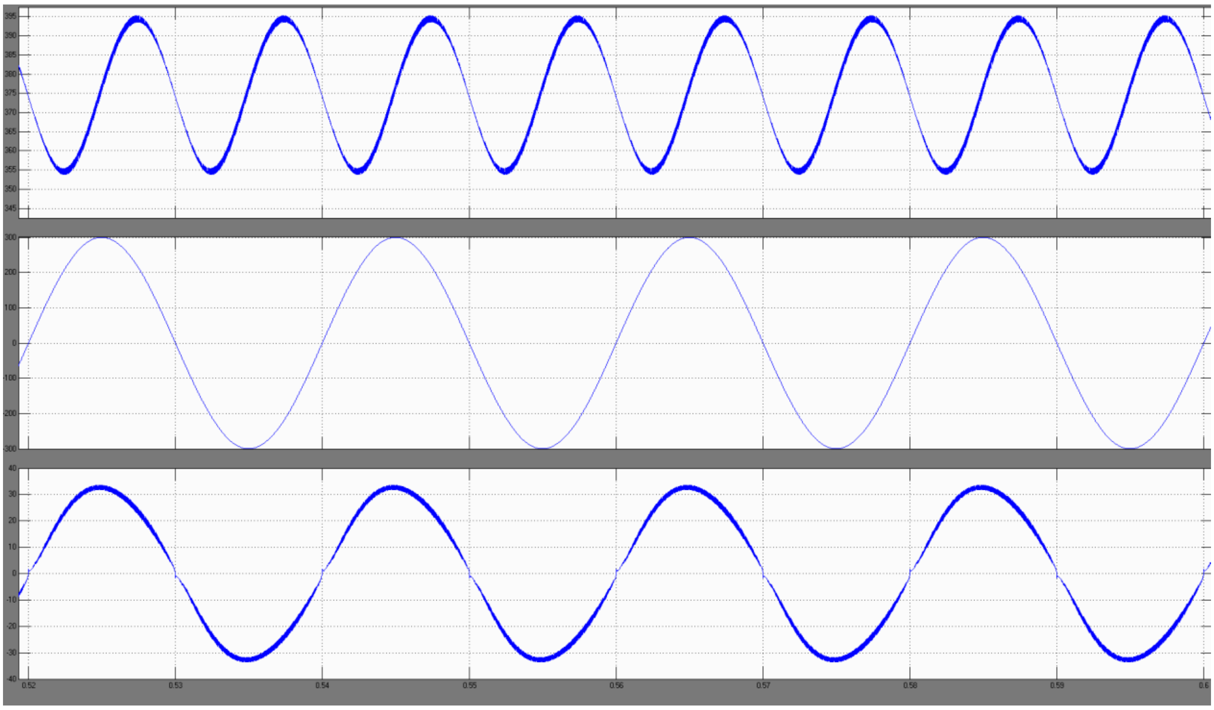

Fig. 4.19. Simulated date of boost PFC converter (upper – DC-link voltage, middle – input voltage, lower – input current). THD= about 5%, cos(f)=1.

Table 4.3.

Boost converter simulated data

Output power (W)	Input current (A)	Input current THD (%)	Converter efficiency (%)	Cos(f)
1100	5	13.6	96.7	1
2200	10	6.9	96.6	1
3300	15	4.7	96.2	1
4400	20	3.9	95.8	1

Voltage limiter operation is shown in fig.4.20.a,b. At load disconnection the PI regulator in the algorithm without voltage limiter can be unsuccessful and DC-link voltage can exceed permitted ranges (4.20.a). In the algorithm with protection the function does not allow exceeding of the voltage limits (4.20.b).

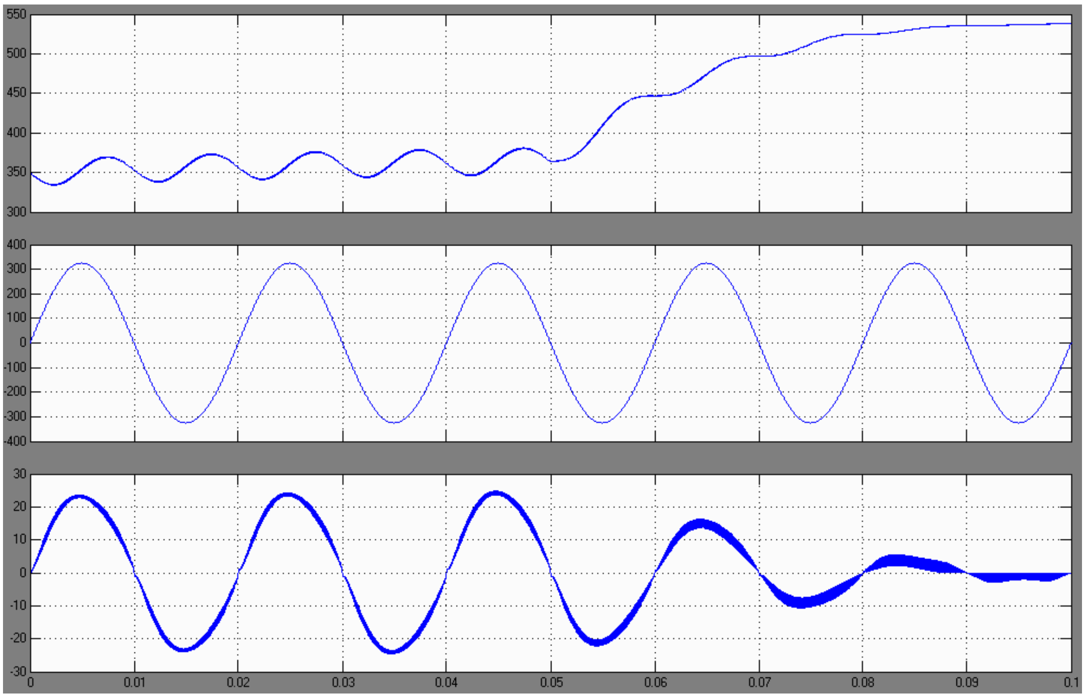

a)

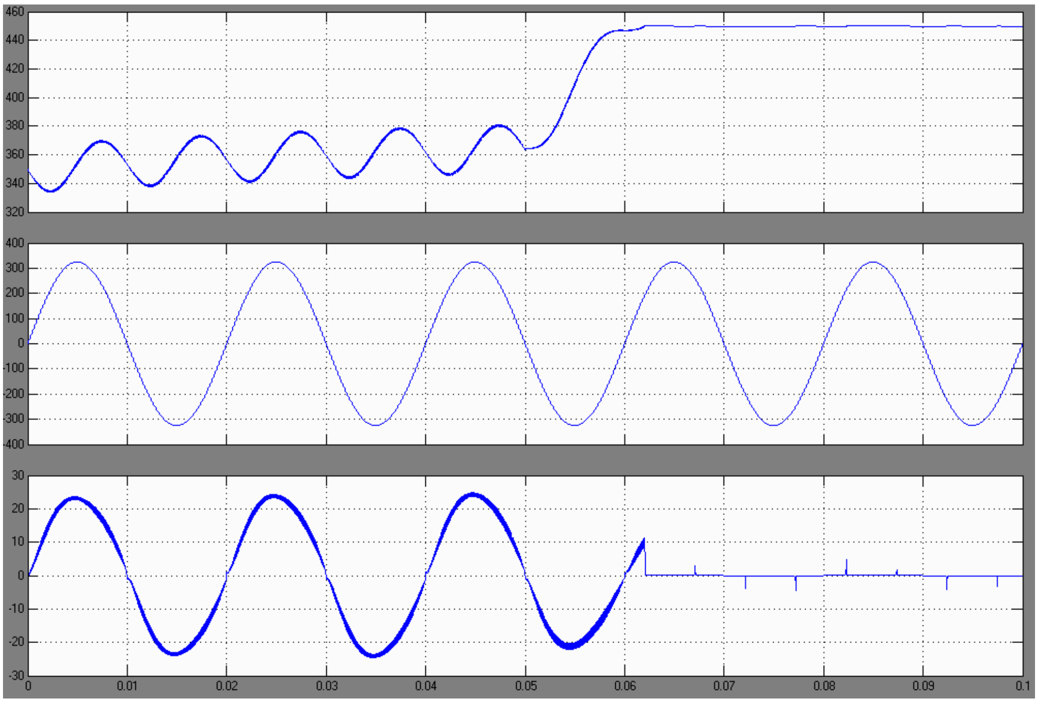

b)

Fig.4.20. Voltage limiter operation. a) the case without voltage limiting circuits in the control algorithm and DC-link voltage exceeds 450V, b) the case with voltage limiting circuits in the control algorithm and DC-link voltage does not exceed 450V.

b) Boost interleaved PFC

This topology is similar to the previous, but it has 2 boost stages (fig.4.21) that are controlled by shifted signals with equal duty cycle (fig. 4.22.). This control algorithm gives current pulsations in inductors with shift as well. Due to that total input current has lower pulsations than in each individual inductor. In the case of duty cycle 50%, the pulsations of currents are shifted exactly by the half of modulation period. In the resulting current these pulsations are, therefore, compensated and the total input current is without any pulsations.

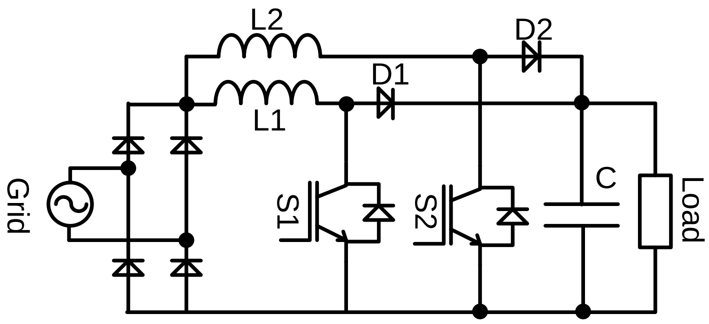

Fig. 4.21.. Boost PFC converter

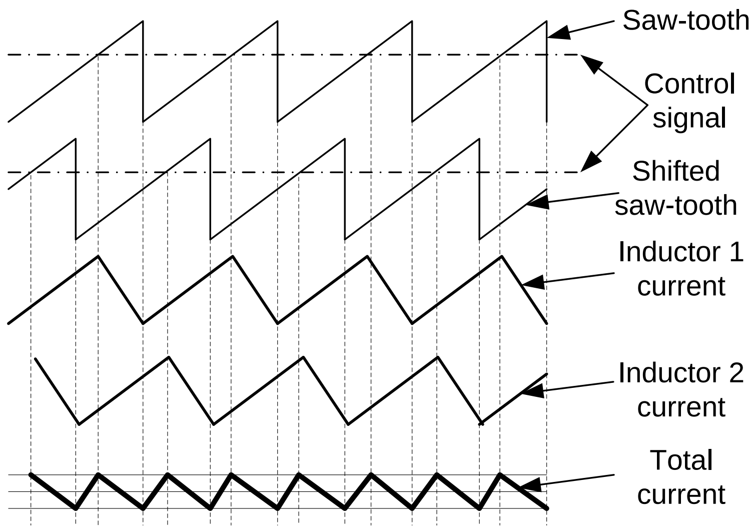

Fig. 4. 22. Control signals of interleaved boost

The power board subsystem of Matlab model for this converter is shown in Fig. 4.23. To realize this active rectifier two versatile power converters are necessary.

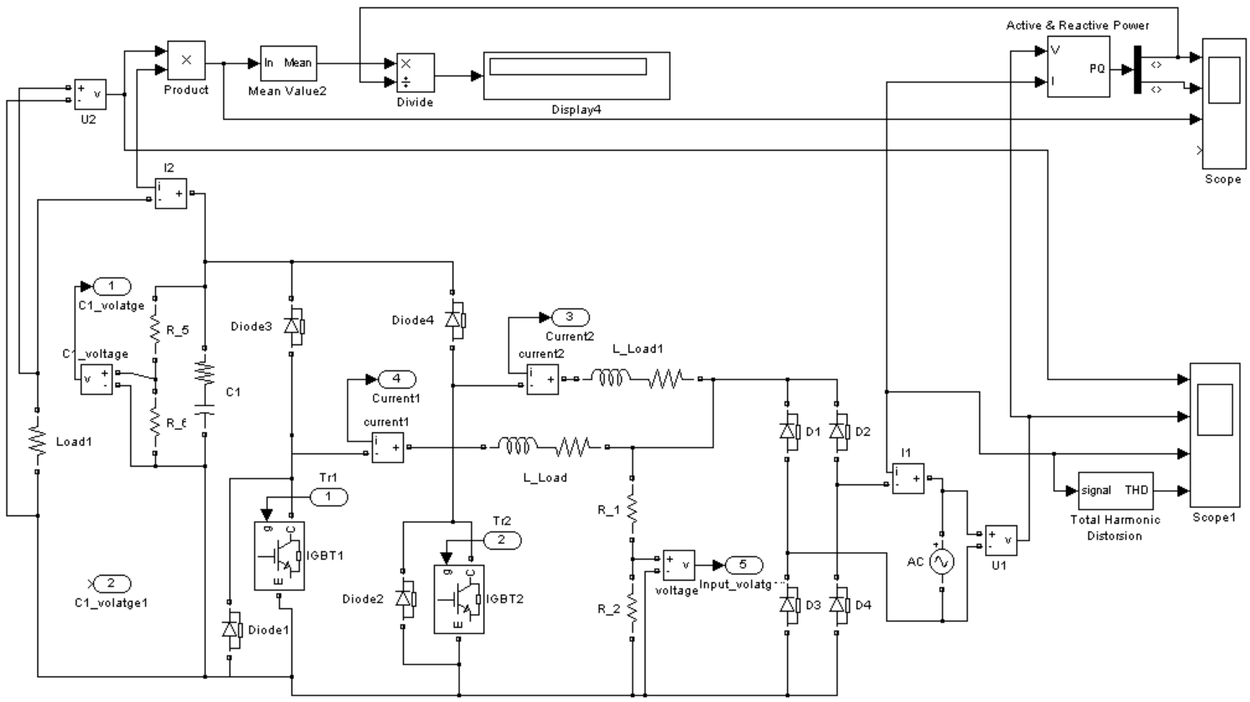

Fig. 4.23. Matlab model of subsystem “power board” for boost PFC converter

The next auxiliary elements are added to the basic elements:

- AC voltage source (230V rms) that simulates the grid
- Diode bridge

- Inductor (L -2 mH, resistance - 0.13 Ohm)
- Variable resistive load to get different output powers
- Auxiliary voltage and current measurement blocks U1, U2, I1,I2 that are necessary for input and output power metering and converter efficiency calculation
- Auxiliary ”total harmonic distortion” block for output voltage THD metering

The control circuit of boost PFC is given in fig. 4.24. Main task of this algorithm is to form the current of boost converter similar to the rectified voltage shape, that is sine wave, and in phase with voltage. In similar way cos(f) about 1 and current THD close to 0 can be obtained. DC-link voltage that must be regulated to 375V is used as a feedback.

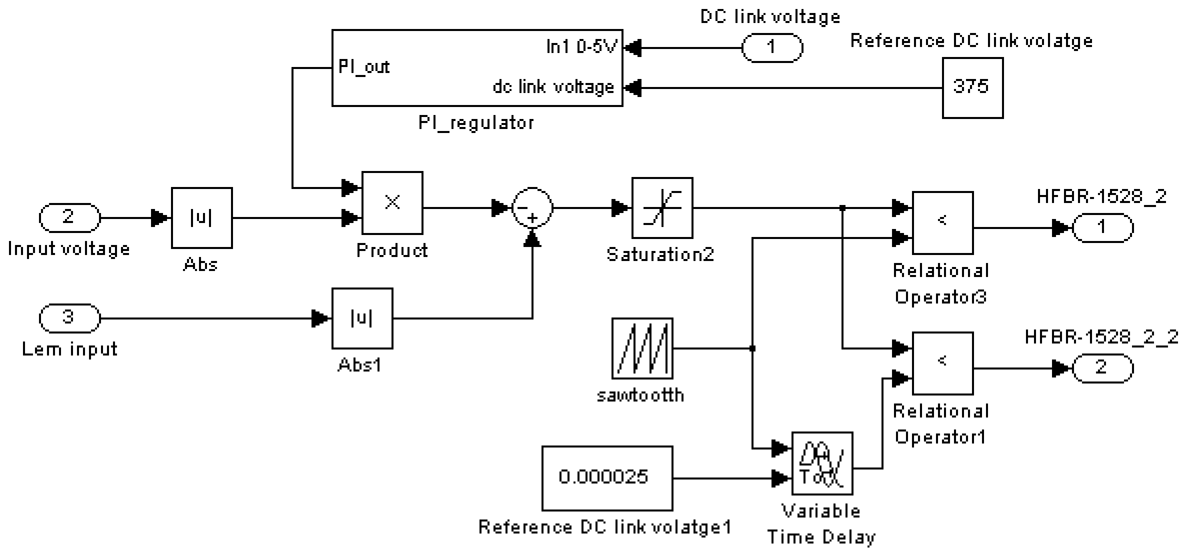

Fig. 4.24. Control circuit of boost interleaved rectifier

In figure 4.25 for few milliseconds simulated inductors currents and input current are shown. There can be seen that inductors currents have 2.2A pulsation, but input current has 0.8A pulsation. But input current pulsation is not constant and depends on PWM duty cycle depending in its turn on sine wave position. As it can be seen from fig.4.26 input current has minimum pulsation close to 2 ms and 8ms when duty cycle is about 50%.

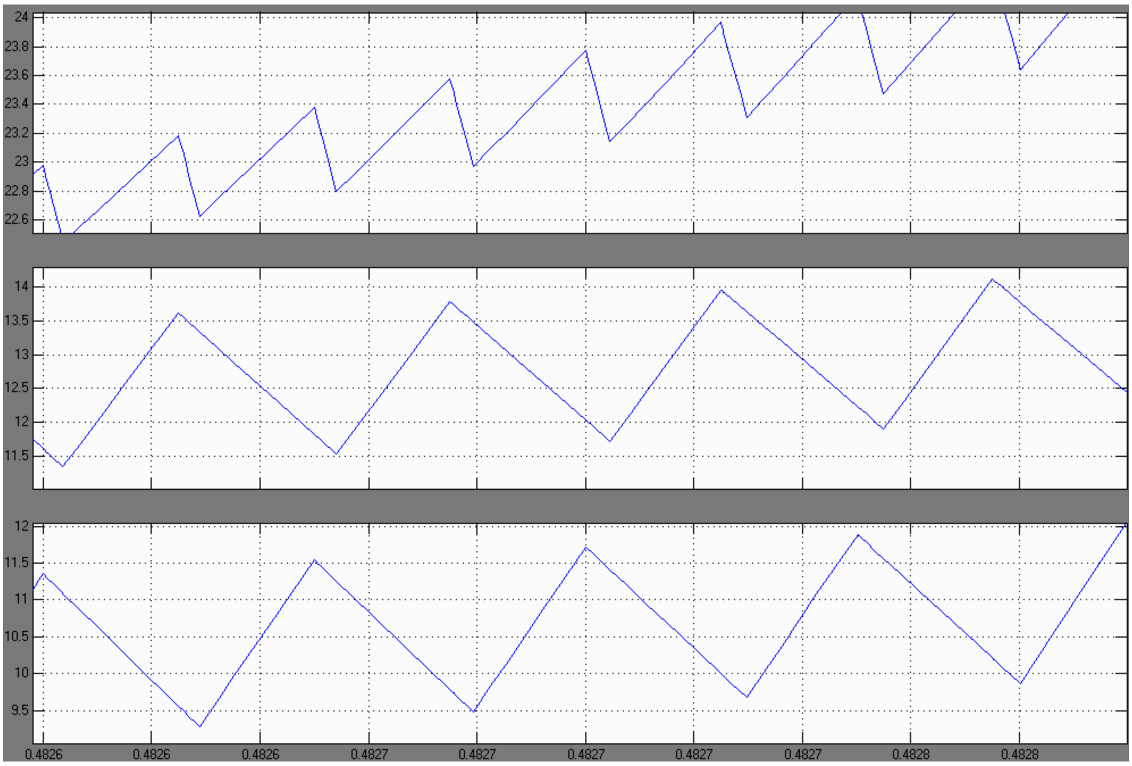

Fig. 4.25. Simulated inductors and input currents (upper – input current, middle and lower – inductor currents)

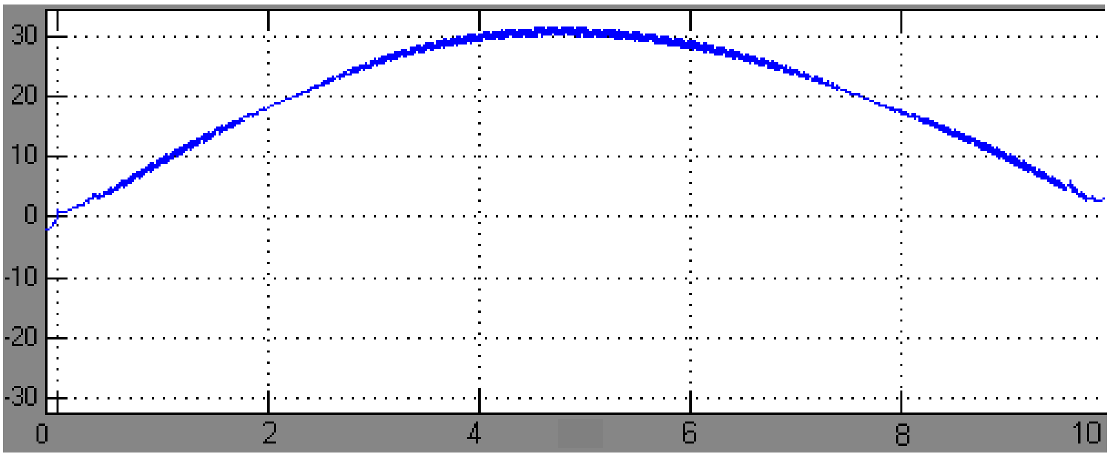

Fig. 4.26. Half period of simulated input current of boost interleaved converter

Simulation results for rated power (4400W) are given in fig.4.27.. and for different powers (100%, 75%, 50%, 25%, 10%) are given in table 4.4.

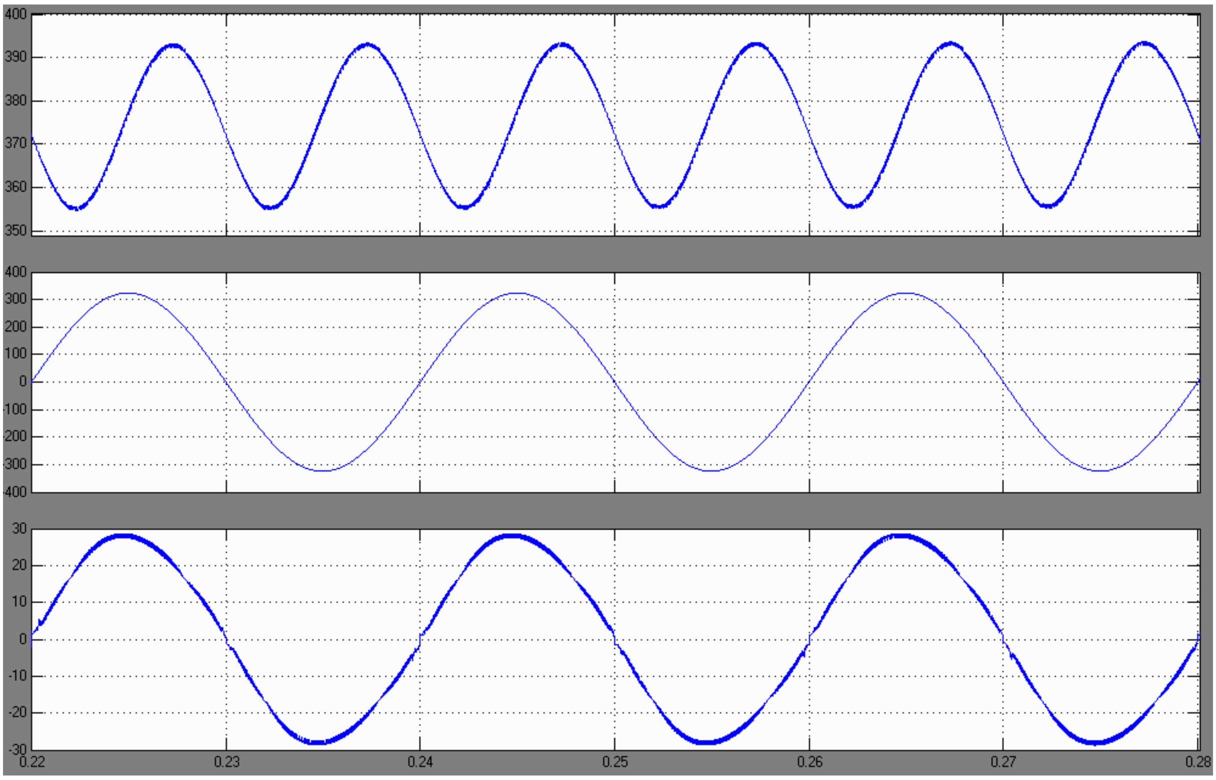

Fig. 4.27. Simulated data of boost interleaved rectifier (4400W)

(upper – DC-link voltage, middle – input voltage, lower – input current)

Table 4.4

Simulated data of boost interleaved PFC converter

Output power (W)	Input current (A)	Input current THD (%)	Converter efficiency (%)	Cos(f)
1100	5	8	96.6	1
2200	10	4.4	96.8	1
3300	15	3.6	96.7	1
4400	20	3	96.4	1

c) Bridgeless PFC

The main advantage of this active PFC rectifier is absence of the diode bridge (Fig. 4.28). That is why the line current simultaneously flows through 2 semiconductor switches that could ensure higher efficiency of the converter.

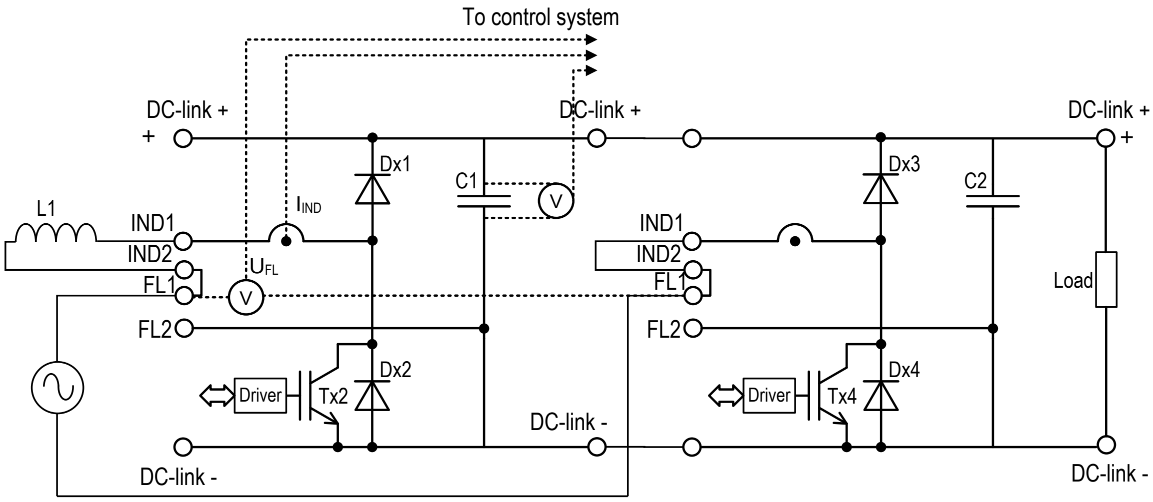

Fig. 4.28. Bridgeless PFC rectifier assembling with two versatile power converters

To assemble bridgeless PFC converter 2 versatile power converters are necessary. Matlab-simulink model of bridgeless PFC rectifier is shown in fig. 4.29.

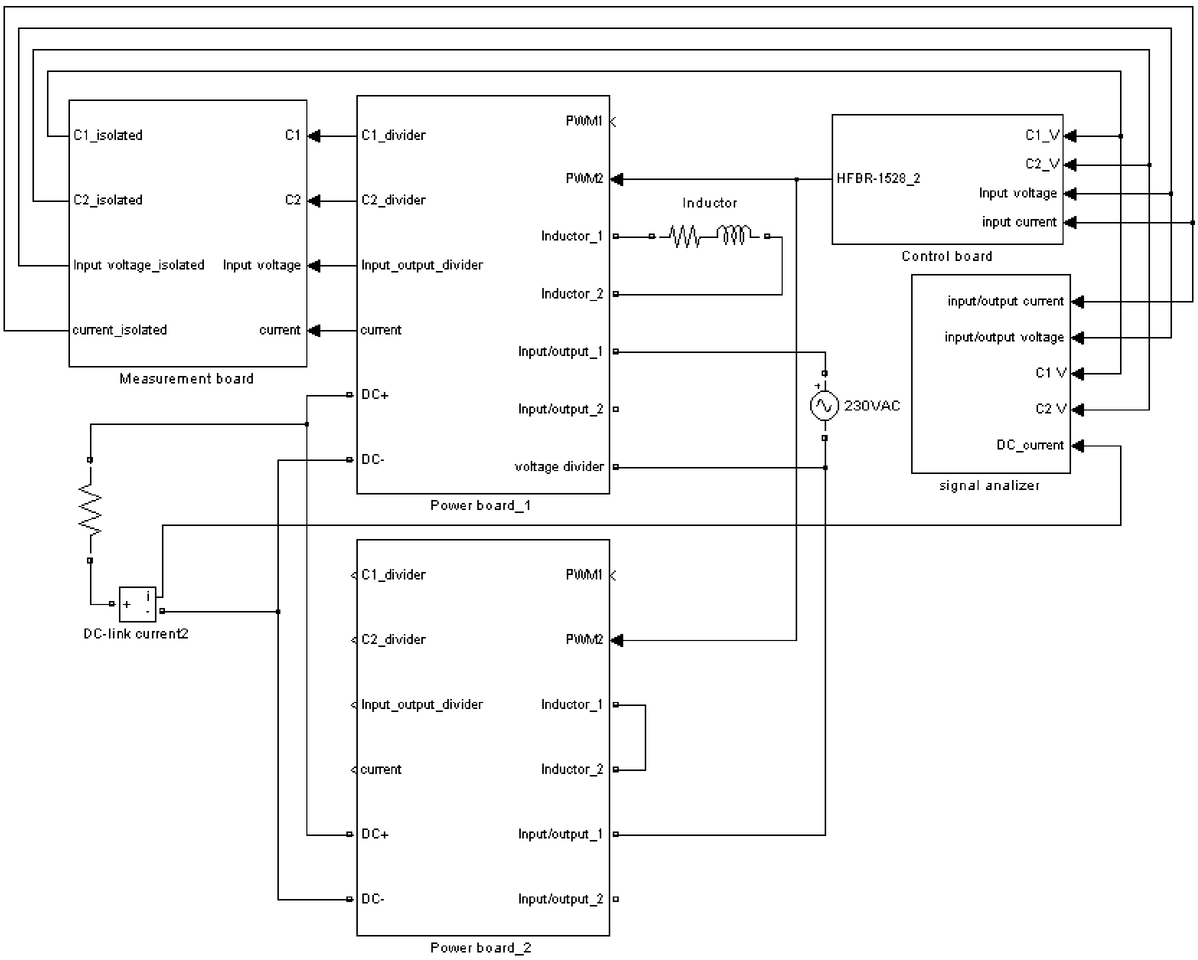

Fig. 4.29. Matlab-simulink model of subsystem "power board" for bridgeless PFC converter

The following elements are connected to basic versatile converters:

- AC voltage source (230V rms) that simulates the grid
- Inductor (L -2 mH, resistance - 0.13 Ohm)
- Variable resistive load to get different output powers
- Auxiliary voltage and current measurement blocks "DC-link current" that are necessary for output power metering and converter efficiency calculation

The bridgeless PFC rectifier can be controlled by the same control algorithm like boost PFC rectifier. Both switches can be controlled with the same signal and in real converter they can be driven by the same driver. It is the advantage of this PFC rectifier.

Simulation results for the rated power are given in fig.4.30. Is it similar to boost PFC rectifier simulation results, but voltage pulsations are lower due to higher DC-link capacity. Current shape is highly sinusoidal with THD about 5% and cos(f) about 1. For different powers simulation results are given in table 4.30.

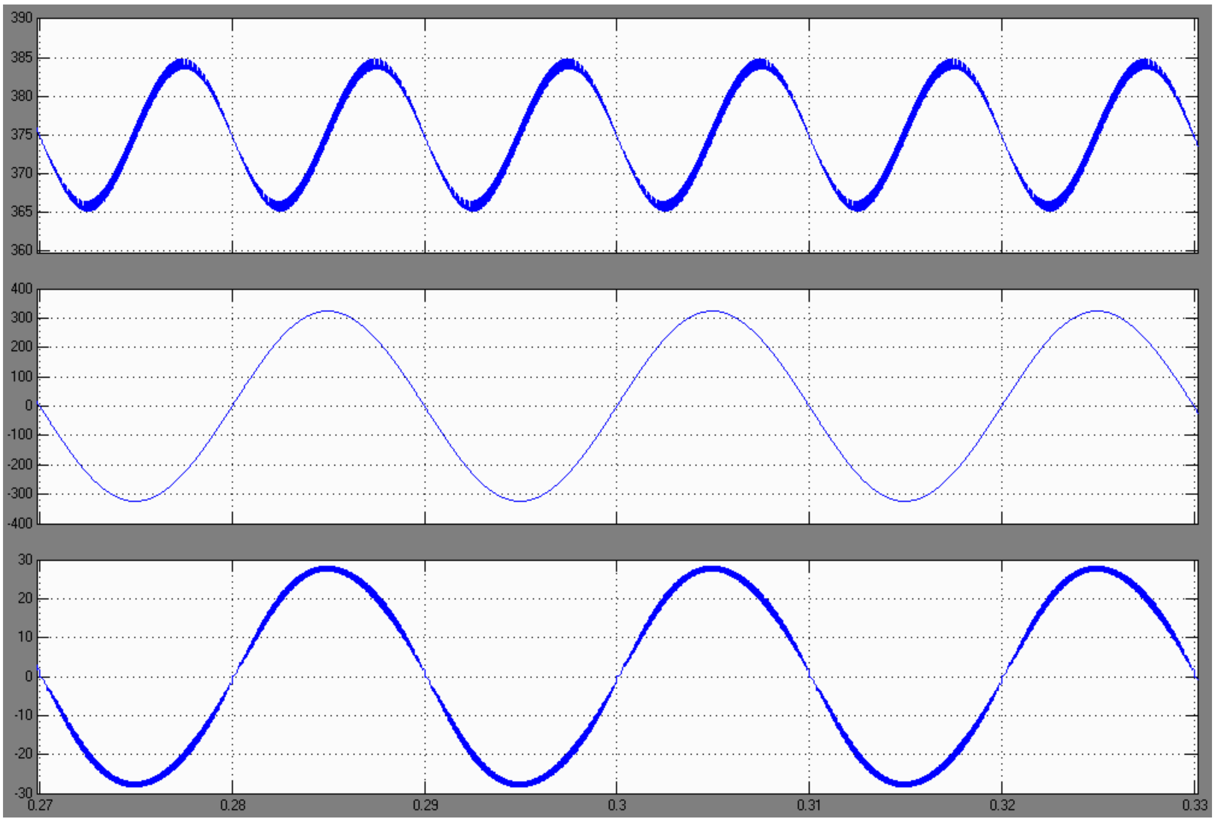

Fig. 4.30. Simulated data of bridgeless PFC rectifier (4400W)

(upper – DC-link voltage, middle – input voltage, lower – input current)

Table 4.5.

Simulated data for bridgeless converter

Output power (W)	Input current (A)	Input current THD (%)	Converter efficiency (%)	Cos(f)
1100	5	13.4	96.1	1
2200	10	6.8	96.8	1
3300	15	4.66	96.6	1
4400	20	3.7	96.3	1

d) Bridgeless-totem PFC

The main advantage of the bridgeless-totem PFC converter is the same like in bridgeless PFC converter has - absence of the diode bridge (Fig. 4.31.). The bridgeless-totem PFC converter includes transistors controlled by different drivers and different signals. Each of these transistors operates only within one half-wave.

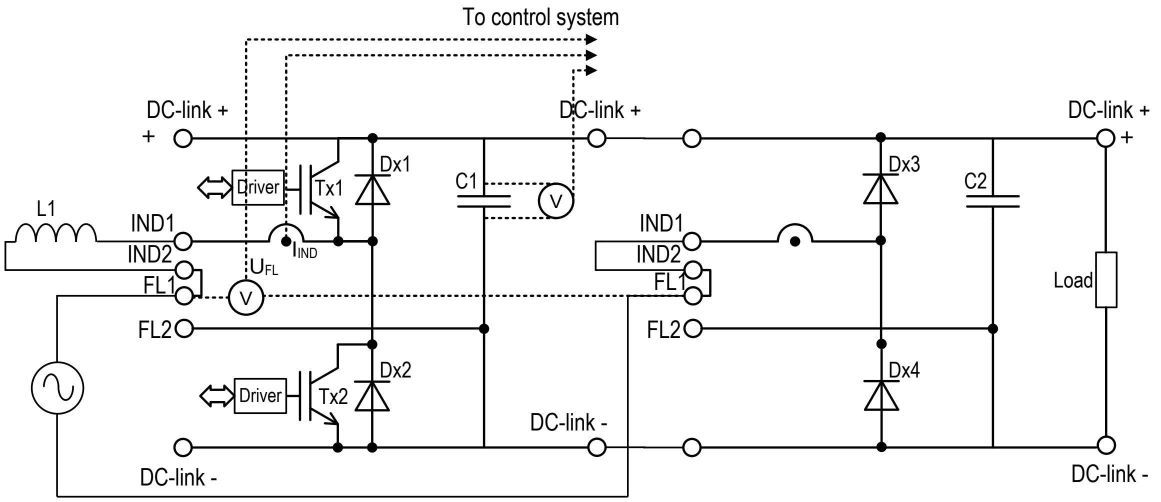

Fig. 4.31. Bridgeless-totem PFC rectifier assembling with two versatile power converters

Bridgeless totem PFC converter power board Matlab-simulink subsystem model is shown in fig. 4.32.

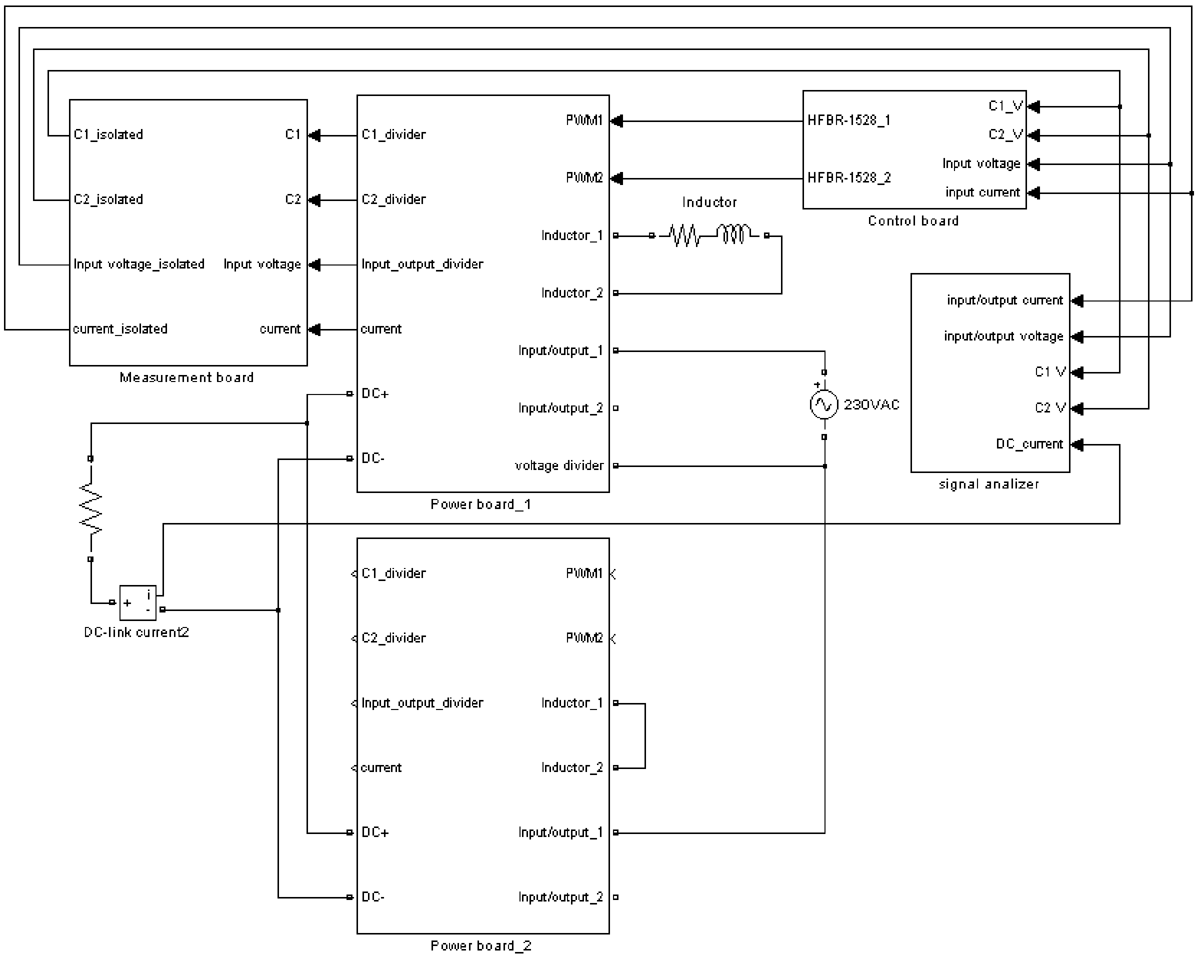

Fig. 4.32. Matlab-simulink model of bridgeless-totem PFC rectifier with two versatile power converters

Few auxiliary elements are added to versatile power converters basic elements:

- AC voltage source (230V rms) that simulates the grid
- Inductor (L -2 mH, resistance - 0.13 Ohm)
- Variable resistive load to get different output powers
- Auxiliary current measurement blocks “DC-link current” that are necessary for output power metering and converter efficiency calculation

The control circuit of bridgeless-totem PFC is given in fig. 4.33.

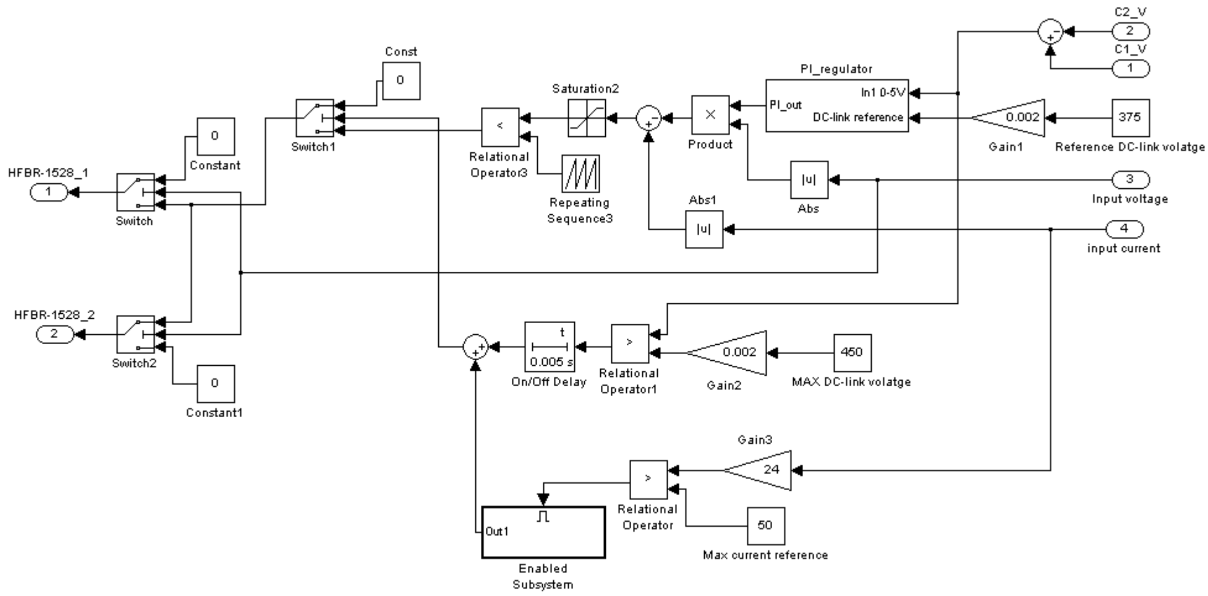

Fig. 4.33. Control circuit of bridgeless totem PFC converter

Simulations diagram is similar to that for bridgeless PFC rectifier that is why they are not depicted here. Simulation results for bridgeless-totem PFC rectifier are given in table 4.6.

Table 4.6.

Simulated data of bridgeless totem PFC converter

Output power (W)	Input current (A)	Input current THD (%)	Converter efficiency (%)	Cos(f)
1100	5	13.5	96.2	1
2200	10	6.8	96.8	1
3300	15	4.6	96.6	1
4400	20	3.6	96.3	1

e) Full-bridge PFC

Like bridgeless and bridgeless totem PFC converters the full-bridge PFC converter does not need diode bridge (Fig. 4.34). Line current also simultaneously flows through 2 semiconductor switches that ensures higher efficiency of the converter.

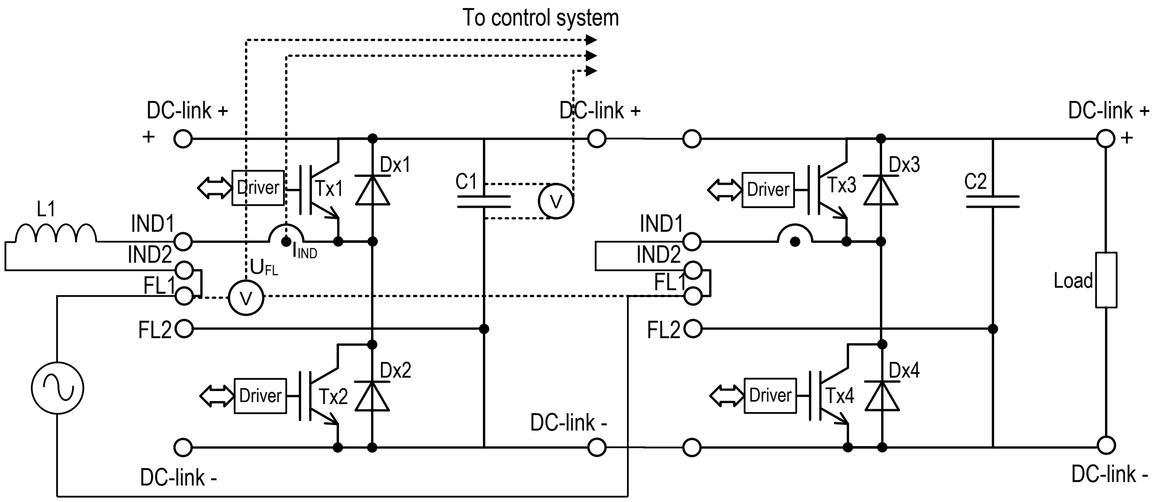

Fig. 4.34. Full-bridge PFC rectifier assembling with two versatile power converters

Matlab-simulink model of full-bridge PFC rectifier is shown in fig. 4.35.

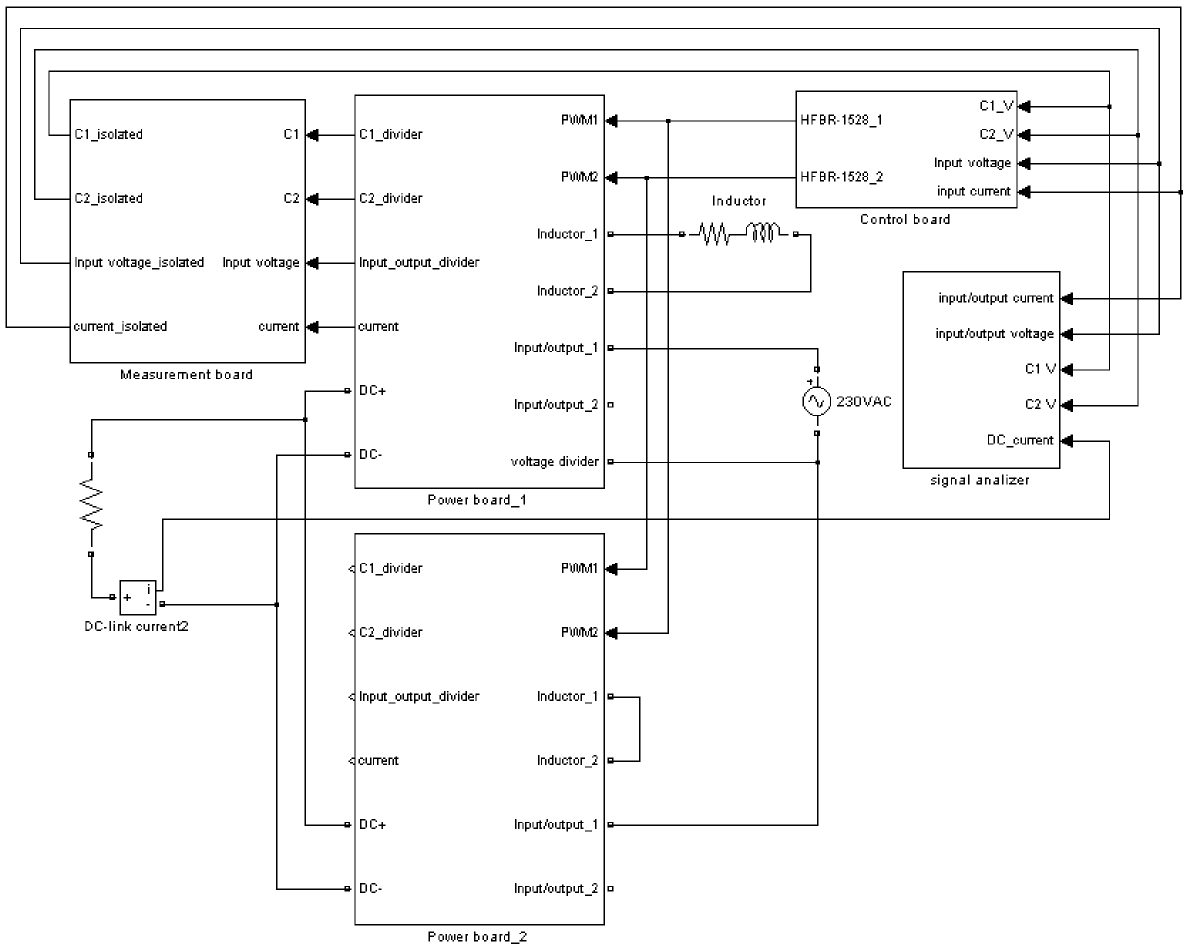

Fig. 4.35. Matlab model of subsystem “power board” for boost PFC converter

Few auxiliary elements are added to basic elements:

- AC voltage source (230V rms) that simulates the grid
- Inductor (L -2 mH, resistance - 0.13 Ohm)
- Variable resistive load to get different output powers
- Auxiliary current measurement blocks “DC-link current” that are necessary for output power metering and converter efficiency calculation

The control circuit of full-bridge PFC converter is given in fig. 4.36.

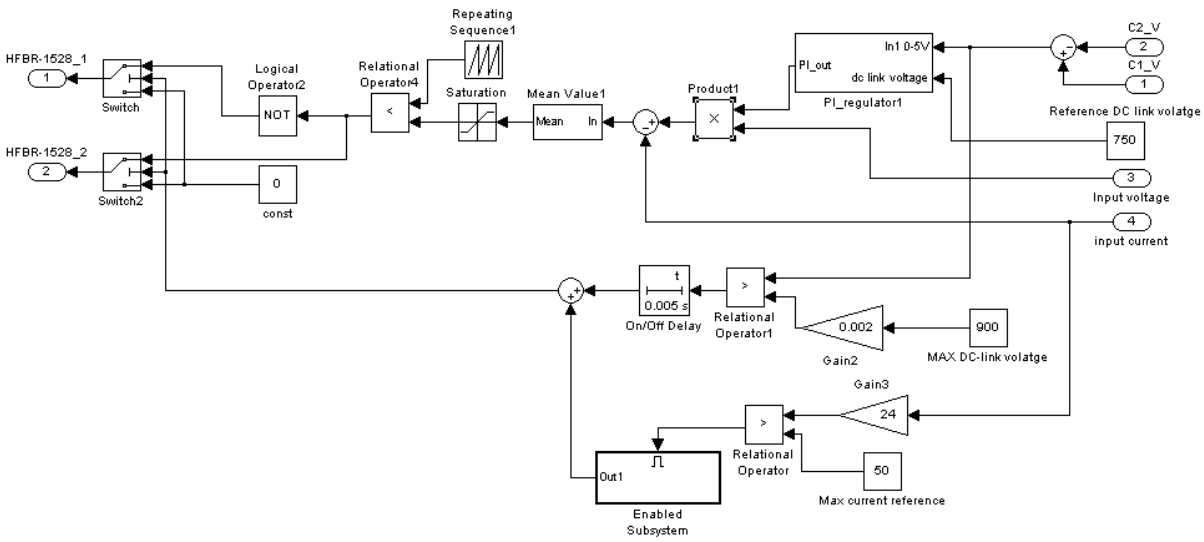

Fig. 4.36. Control circuit of full-bridge PFC rectifier

Simulation results are given in table 4.7.

Table 4.7.

Simulated data of full-bridge PFC converter

Output power (W)	Input current (A)	Input current THD (%)	Converter efficiency (%)	Cos(f)
1100	5	19.5	94.9	1
2200	10	10	94.8	1
3300	15	6.6	95.4	1
4400	20	54.8	95.3	1

f) Half-bridge PFC

The main advantage of the half-bridge PFC converter is that the current passes through only one semiconductor device (Fig. 4.37).

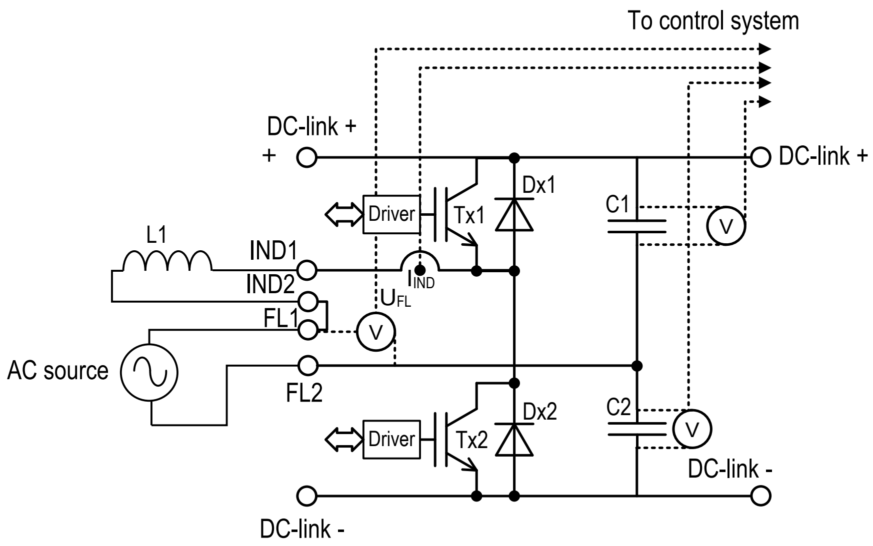

Fig. 4.37. Half-bridge PFC rectifier assembling with one versatile power converter

Half-bridge PFC converter power board Matlab-simulink subsystem model is shown in fig.4.38.

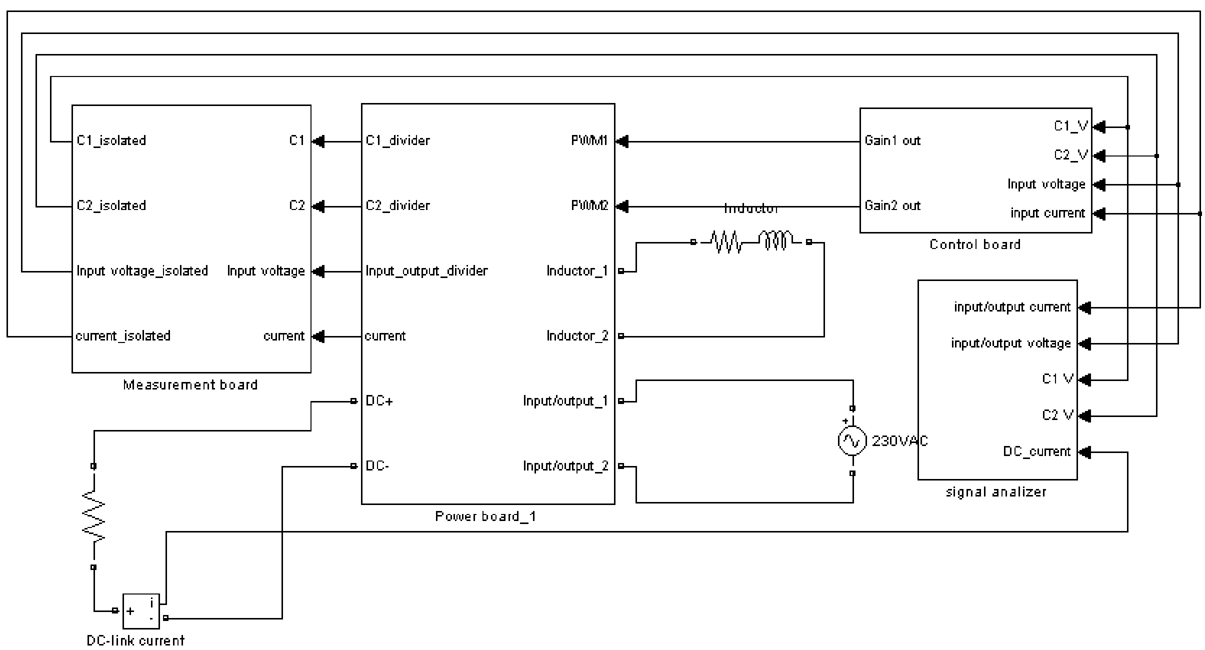

Fig. 4.38. Matlab-simulink model of half-bridge PFC rectifier

To versatile power converter the following elements are connected:

- AC voltage source (230V rms) that simulates the grid
- Inductor (L -2 mH, resistance - 0.13 Ohm)
- Variable resistive load connected to DC-link to get different output powers
- Auxiliary current measurement blocks “DC-link current” that are necessary for output power metering and converter efficiency calculation

The control circuit is given in fig. 4.39.

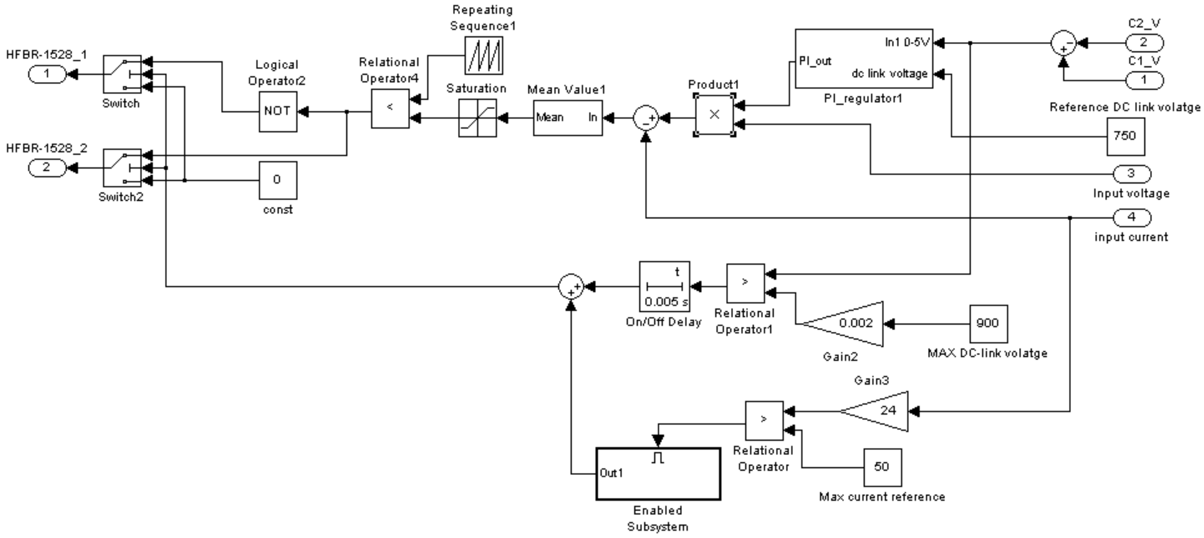

Fig. 4.39. Control circuit of half-bridge PFC rectifier

Simulation results are given in table 4.8

Table 4.8.

Half-bridge PFC converter simulated data

Output power (W)	Input current (A)	Input current THD (%)	Converter efficiency (%)	Cos(f)
1100	5	19	96.3	0.99
2200	10	9.7	96.2	0.99
3300	15	6.5	95.9	0.99
4400	20	4.9	95.6	0.99

4.1.2. Charging/discharging converters

As it was mentioned in the first chapter, there are different possible backup energy sources. In order to make the UPSS more flexible it is necessary to make the bidirectional DC/DC power converter to be able to work with any type of the DC energy source or DC backup storages. The bidirectional DC/DC converters can be assembled by means of as many VPM.

Output power of the boost converter must be equal to the inverter input power. As inverter output power is 4kW and its efficiency is close to 0.95, output power of boost converter must be close to 4.2kW. On the basis of this the energy storages that can provide such power were purchased.

For research targets 2 supercapacitors and lead acid batteries were purchased:

- 48.6V, 165F, 0.007 Ohm
- 125V, 63F, 0.018 Ohm
- 6x12V=72V, 17Ah, 6x0.012=0.072 Ohm

As it was mentioned above there are two types of inverters: full-bridge and half-bridge. They have important difference: DC-link voltage of full-bridge inverter has to be close to 375V, but DC-link voltage of half-bridge inverter has to be close to 750V. Using Matlab simulink possibility of building DC/DC converter for both levels of voltages with the above mentioned storages will be tested. DC/DC converter Matlab-simulink model is given in fig. 4.41.

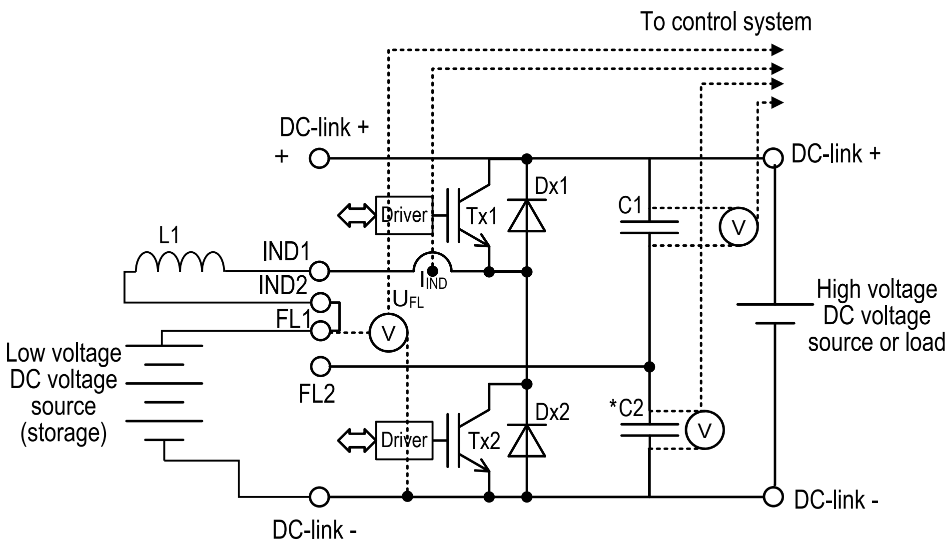

Fig.4.40. bidirectional DC/DC power converters

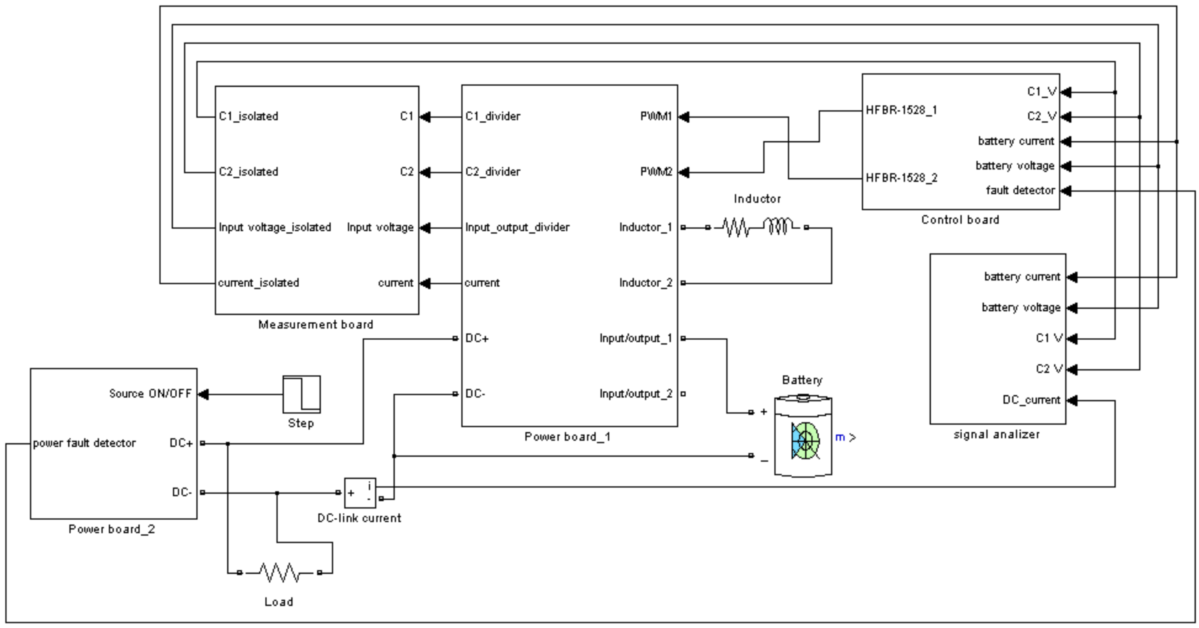

Fig.4.41. Bidirectional DC/DC converter Matlab-simulink model

To versatile power converter the following elements are connected:

- Energy storage (battery, supercapacitor, flywheel, fuel-cell)
- Inductor (L -1 mH, resistance - 0.05 Ohm)
- Voltage source that supplies DC-link and in the case of failure it gives failure signal to the control system
- Resistive load in DC-link
- Auxiliary current measurement blocks “DC-link current” that are necessary for output power metering and converter efficiency calculation

In figure 4.42.a control board of DC/DC converter is given. As it can be seen it is divided into two parts. In figures 4.42.b.c the enabled subsystem algorithms of boost and buck converters are given. When the battery is charged the buck converter control is operating and transistor IGBT1 is driven. When the battery is discharged the boost converter control is operating and transistor IGBT2 is driven.

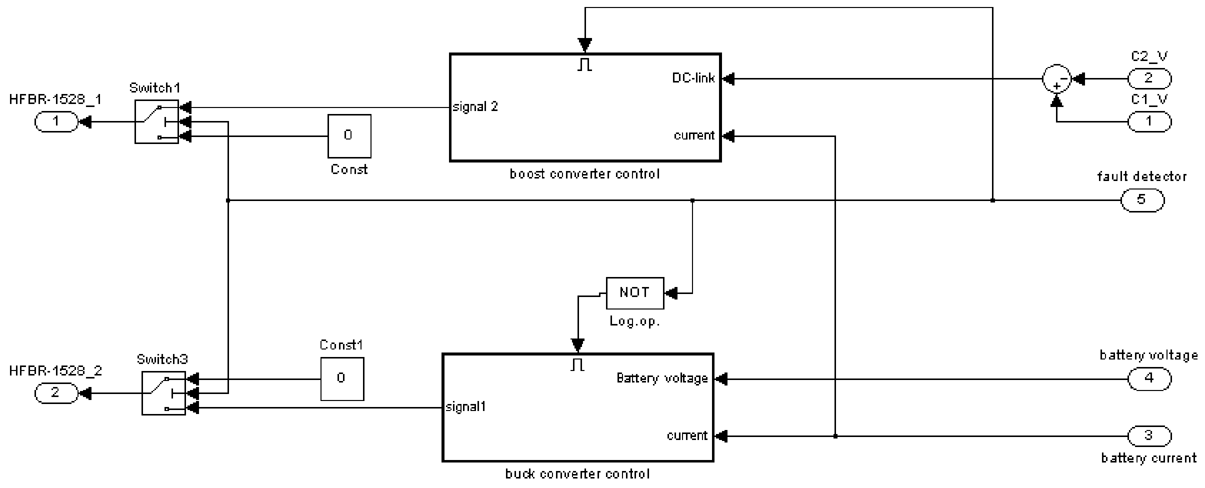

a)

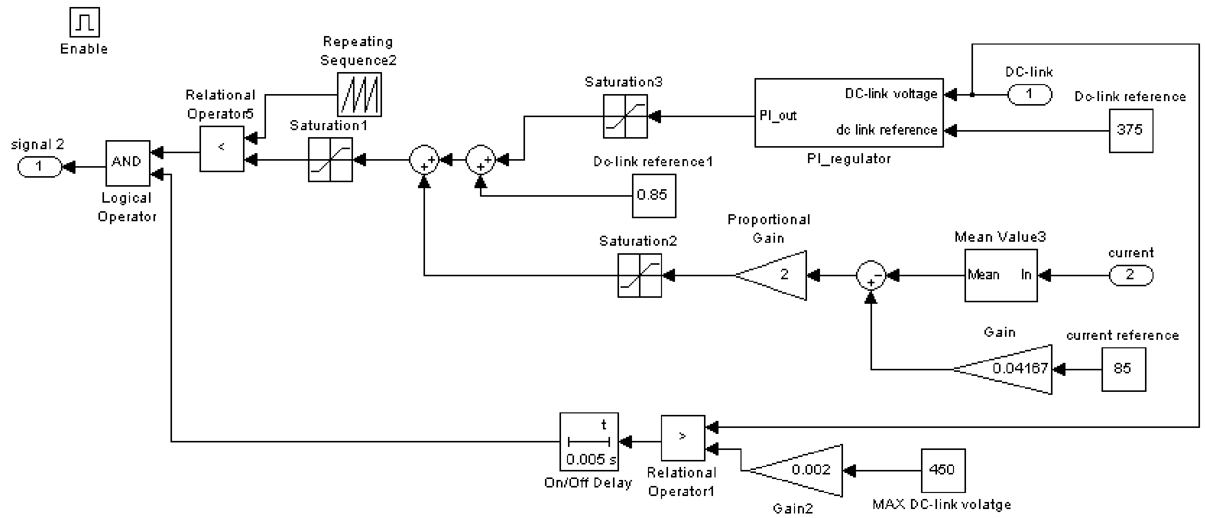

b)

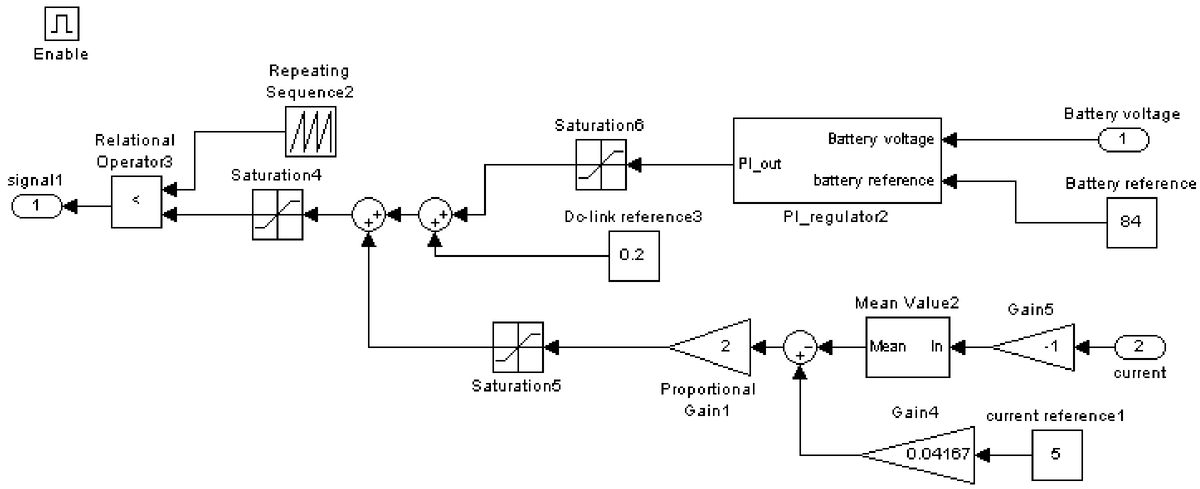

c)

Fig.4.42. control algorithm: a) control board of DC/DC converter, b) subsystem “boost converter control”, c) subsystem “bust converter control”

For boost converter as a feedback 2 signals are used: DC-link voltage and energy storage current. There are two regulators: for voltage proportional-integral (PI) regulator is used, but to prevent overcurrent proportional (P) regulator is used. PI-regulator regulates DC-link voltage, and if it tries to exceed maximum allowable current of backup source the proportional regulator reduces duty cycle of PWM signal and prevents overcurrent. Similarly there is a protection from DC-link capacitor overvoltage. In the case if there is load response to very low load or open circuit the PI regulator has no time to compensate it and the DC-link capacitor can be overcharged. Thus if the DC-link voltage exceeds 450V, the transistor control is stopped until PI regulator is able to control converter correctly.

For buck converter as a feedback also 2 signals are used: battery (or another backup energy storage) voltage and current. Like in boost converter there are two regulators: for voltage regulation and overcurrent prevention.

Figure 4.43. shows the operation of bidirectional DC/DC converter. There are few stages: battery charging (0-0.1s), supply fault (0.1s), battery discharging (0.1-0.2s), load disconnection(0.2), protection algorithms response(0.21-0.3).

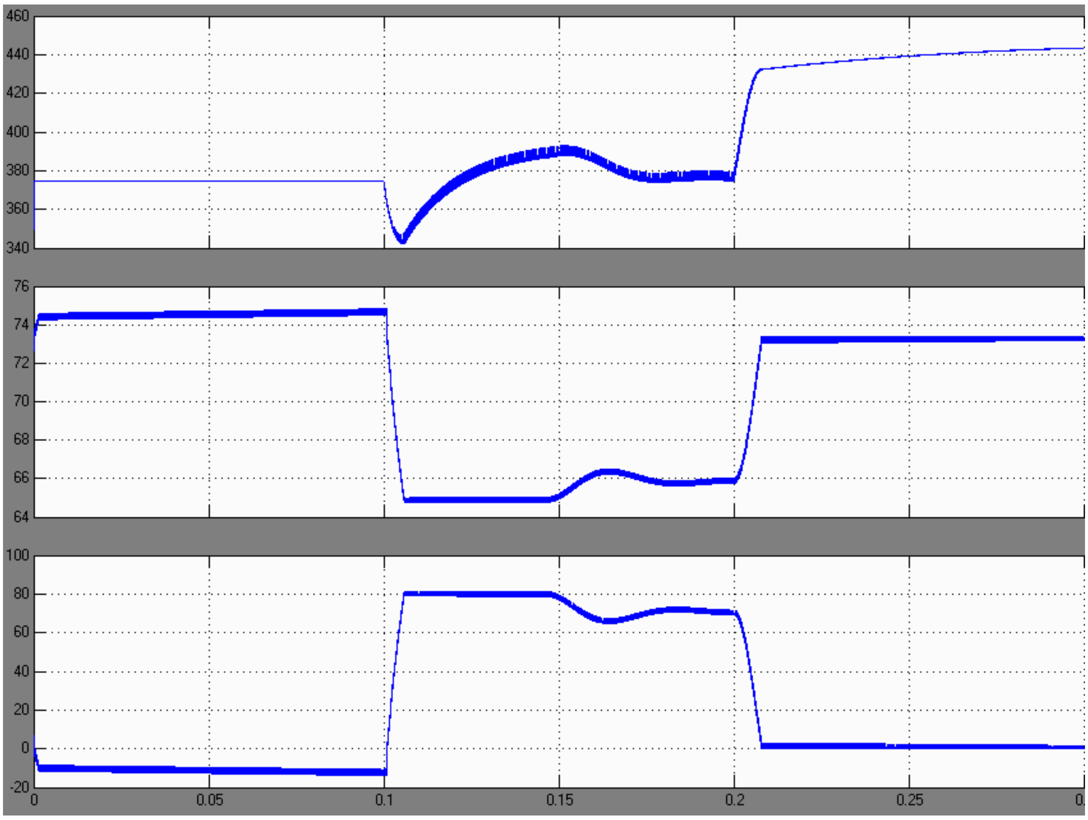

Fig.4.43. Simulated characteristics of boost converter (upper – DC-link voltage, middle – battery voltage, lower – battery current)

In table 4.9. other Matlab-simulink simulation results of different operation mode and with different energy storages are given. As the boost converter supplies the inverter its power must be higher than that of inverter input. In the worst case the inverter efficiency is close to 90% due to that boost power must be close to 4.4kW.

Table.4.9.

Charger/discharger simulation

Operation mode / Energy storage	Boost mode 375V, output power – 4.4kW	Boost mode 750V, 4400W	Buck mode 375V,	Buck mode 750V
Battery, 72V, 17Ah Rint – 0.12 Ohm At full load output voltage will be 63V.	Iin – 74A Ubat=68.5V conversion Eff=87%	Iin – 80A Ubat=66.5V conversion Eff=82%	charging current 10A, Ibat – 72V conversion Eff=94.5%	charging current 10A conversion Eff=92%
Supercapacitor 48.6V, 165F Rin - 6.3mOhm At 4.4kW discharge: 48.6V-40V - 12.8s 48.6V-35V - 19s 48.6V-30V - 24.6s	Simulation shows that it is not possible to use this storage in this configuration	Simulation shows that it is not possible to use this storage in this configuration	charging current 20A, charging voltage 30V-48.6V conversion Eff=88%	charging current 20A, charging voltage 30V-48.6V conversion Eff=87%
Supercapacitor 125V, 63F Rin - 18mOhm At 4.4kW discharge: 125V-100V - 36s 125V - 80V- 59s 125V-60V - 77s	Usc=99V I_{bat}=48A Conversion Eff=92.7%	Usc=99V I_{bat}=49A Conversion Eff=91%	charging current 20A, charging voltage 60V-125V conversion Eff=93%	charging current 20A, charging voltage 60V-125V conversion Eff=91%

Simulations show that 48.6V supercapacitor is not possible to be used with this configuration of bidirectional DC/DC converter, but these simulations did not take into account transistors and inductors thermal regimes. So it was decided to check thermals regimes of other configurations.

To calculate thermal regimes and losses of transistors and diodes it was used “Semikron” “Semisel” software [25]. Water temperature was taken $60C^0$ and heat sinks parameters taken from the 2nd chapter. In calculation the switching frequency was 20kHz.

Table.4.10.

Calculated thermal regimes of DC/DC bidirectional converter

Operation mode / Energy storage	Boost mode 375V, output power – 4.4kW	Boost mode 750V, 4400W	Buck mode 375V,	Buck mode 750V
Battery, 72V, 17Ah Rint – 0.12 Ohm At full load output voltage will be 63V.	Pcond tr – 224W Psw tr - 220W Ptr – 444W Pcond d – 25W Psw d – 35W Pd -60W Ptot – 504W Ts -60^{0}C Tc -85^{0}C Ttr – 205^{0}C Td – 121^{0}C	Pcond tr – 382W Psw tr - 1006W Ptr – 1388W Pcond d – 12W Psw d – 75W Pd -87W Ptot – 1475W Ts -60^{0}C Tc -133^{0}C Ttr – 506^{0}C Td – 185^{0}C	charging current 10A Pcond tr – 4W Psw tr - 22W Ptr – 26W Pcond d – 10W Psw d – 8W Pd -18W Ptot – 44W Ts -60^{0}C Tc -62^{0}C Ttr – 69^{0}C Td – 73^{0}C	charging current 10A Pcond tr – 2W Psw tr - 62W Ptr – 64W Pcond d – 11W Psw d – 12W Pd -23W Ptot – 87W Ts -60^{0}C Tc -64^{0}C Ttr – 81^{0}C Td – 78^{0}C
Supercapacitor 125V, 63F Rin - 18mOhm At 4.4kW discharge: 125V-100V - 36s 125V - 80V- 59s 125V-60V - 77s	Pcond tr – 98W Psw tr - 124W Ptr -- 222 Pcond d – 21W Psw d – 24W Pd -45W Ptot – 266W Ts -60^{0}C Tc -73^{0}C Ttr – 133^{0}C Td – 100^{0}C	Pcond tr – 141W Psw tr - 437W Ptr – 578W Pcond d – 10W Psw d – 42W Pd -52W Ptot – 631W Ts -60^{0}C Tc -92^{0}C Ttr – 248^{0}C Td – 123^{0}C	charging current 20A Charging voltage 125V-60V Pcond tr – 7W Psw tr - 46W Ptr – 53W Pcond d – 23W Psw d – 13W Pd -36W Ptot – 89W Ts -60^{0}C Tc -64^{0}C Ttr – 79^{0}C Td – 86^{0}C	charging current 20A Charging voltage 125V-60V Pcond tr – 4W Psw tr - 134W Ptr – 138W Pcond d – 24W Psw d – 22W Pd -46W Ptot – 184W Ts -60^{0}C Tc -69^{0}C Ttr – 106^{0}C Td – 97^{0}C

(red – configuration can not work, blue - configuration work in not desirable mode, green – normal operation mode)

As it can be seen from table 4.10. only low voltage configuration with 125V supercapacitor has acceptable operation temperatures. This means that versatile power converters in configuration of DC/DC bidirectional converter cannot be used safety to convert 4.4kW. Due to this it was decided to recalculate thermal regimes for 2 parallel connected versatile power converters (table 4.11).

Table.4.11

Calculated thermal regimes of DC/DC bidirectional converter (2 parallel modules)

Operation mode / Energy storage	Boost mode 375V, output power – 4.4kW	Boost mode 750V, 4400W
Battery, 72V, 17Ah Rint – 0.12 Ohm At full load output voltage will be 63V.	Pcond tr – 68W Psw tr - 85W Ptr – 153W Pcond d – 9W Psw d – 17W Pd -26W Ptot – 180W Ts -60^{0}C Tc -69^{0}C Ttr – 110^{0}C Td – 85^{0}C	Pcond tr – 85W Psw tr - 270W Ptr – 355W Pcond d – 5W Psw d – 30W Pd -35W Ptot – 390W Ts -60^{0}C Tc -79^{0}C Ttr – 175^{0}C Td – 100^{0}C
Supercapacitor 125V, 63F Rin - 18mOhm At 4.4kW discharge: 125V-100V - 36s 125V - 80V- 59s 125V-60V - 77s	Pcond tr – 35W Psw tr - 54W Ptr – 89W Pcond d – 8W Psw d – 13W Pd -21W Ptot – 111W Ts -60^{0}C Tc -66^{0}C Ttr – 90^{0}C Td – 78^{0}C	Pcond tr – 44W Psw tr - 160W Ptr – 204W Pcond d – 4W Psw d – 21W Pd -25W Ptot – 230W Ts -60^{0}C Tc -71^{0}C Ttr – 127^{0}C Td – 87^{0}C

(red – configuration cannot work, blue - configuration work in not desirable mode, green – normal operation mode)

As table 4.11 shows for 2 parallel versatile power converters the configuration with DC-link voltage 375V is more preferable. In the case of higher DC-link voltage (750V) it is better to decrease switching frequency (down to 10kHz) therefore reducing losses in transistor and diode and as a result the temperature of PN junctions. Disadvantage of switching frequency reduction is size increasing of such elements like inductors and capacitors.

4.1.3. Power converter simulation for photovoltaic energy source

Using the developed in chapter 3 the PV panel model simulation of MPPT (maximal power point tracking) control algorithm was made. The versatile power converter was configured as the boost converter and connected to its PV array that consists of 4 PV panels (with total rated power 360W). The load is supplied by DC-link (rectifier) and solar energy is injected to DC-link that is why the rectified power is decreased proportionally to the power injected from PV array.

Temperature of PV panel was accepted constant on different illumination levels. Due to that voltage variation from illumination is not very high and it means that maximum power point will be at definite voltage on most illumination levels. Fig.4.44. provides experimental data where it is obvious that maximum power for half-illumination and full-illumination is about 16.5 volts. That allows the application of one of the simplest MPPT algorithms – to keep constant voltage (16-16.5) of the PV panel. For 4 panels in series maximum power will be at 64-66V.

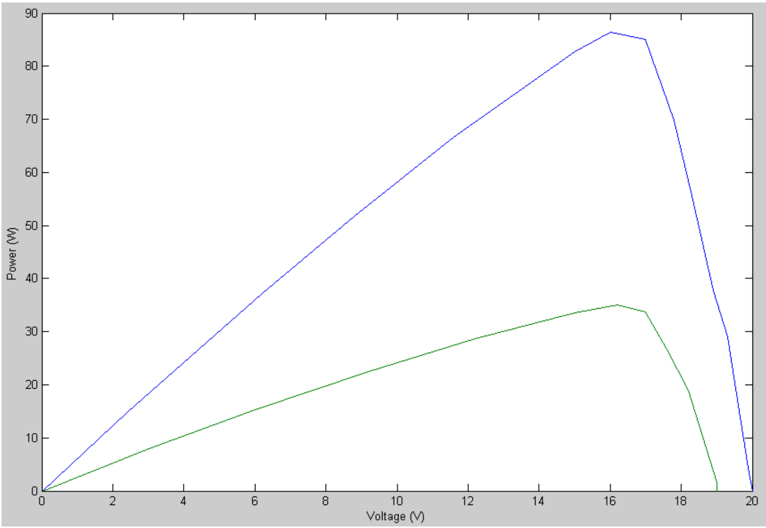

Fig.4.44. PV P-U curve. (blue – 100% illumination, green – half-illumination)

Described MPPT control algorithm is depicted in fig.4.45. DC/DC boost converter pumps such amount of current from PV array to keep voltage about 65V. It stops only in the case when DC-link voltage exceeds 450V.

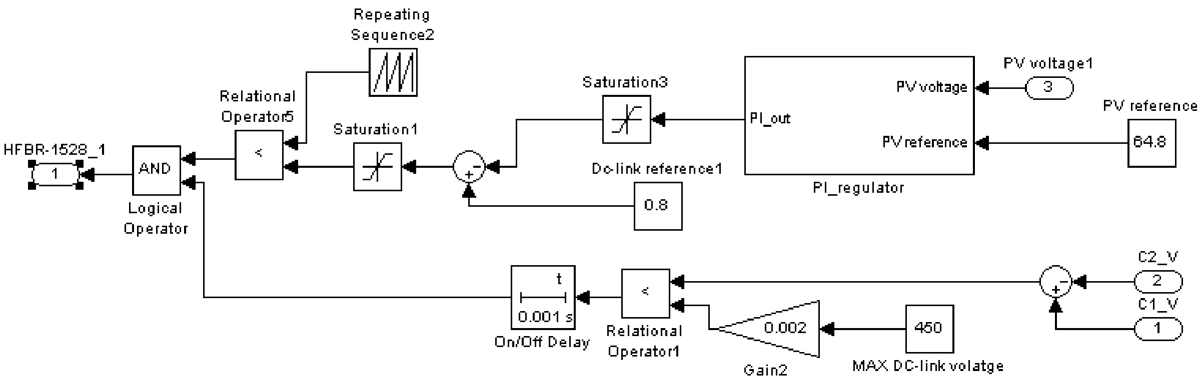

Fig.4.45. MPPT control algorithm

This algorithm will not work properly in the case if PV panels of PV array have unbalanced illumination. In the case of small PV array it is almost impossible or quite rare situation. Simulation data with different illumination levels are given in fig.4.46. There is simulated DC/DC boost power converter with MPPT control algorithm. Fig.4.46 gives power consumption curve from PV array at different illumination levels (0s-0.1s – 100% (1000W/m^2); 0.1s-0.2s – 50% illumination; 0.2s-0.3s – 120% illumination).

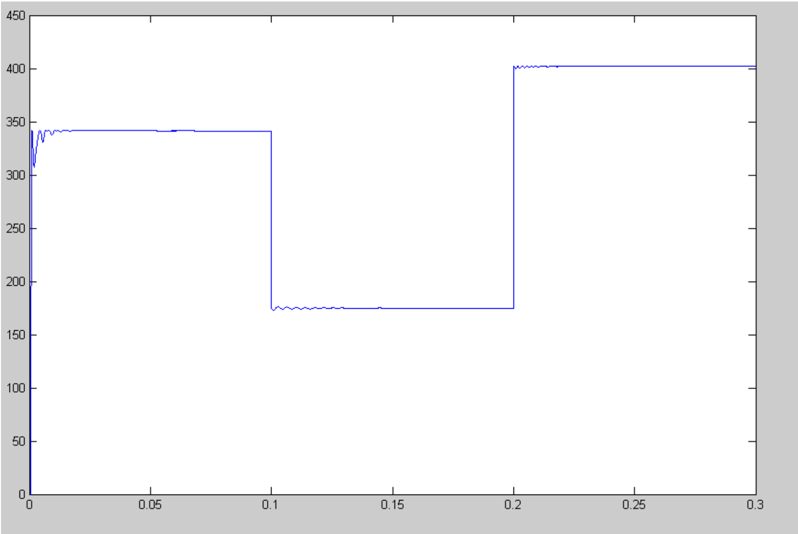

Fig.4.46. Simulated power consumption from PV array depending on illumination level

The simulation shows that the MPPT algorithm allows to utilize almost all generated power by PV array even at different illumination levels.

Table 4.12.

Comparison of PV array generated power and collected power by power converter with MPPT

Illumination level (%)	Generated	Simulated MPPT
100	342	340
50	177	170
120	404	402

4.1.4. “Online” UPS topologies and it simulation

In the previous chapters provide the descriptions of inverters and rectifiers and their simulations. From the converters description we can conclude that there are two possible voltage levels for UPS DC-link: with lower (375V) DC-link voltage and higher (750V) DC-link voltage. This means that the half-bridge inverter can be coupled only with half-bridge PFC rectifier, but full-bridge inverter can be coupled with another 5 mentioned PFC rectifiers. The boost PFC topology needs 1 versatile power converter and other topologies need 2 versatile power converters. To minimize the number of the power converters the boost topology was chosen for the second UPS topology. Both UPS topology configurations were simulated. Matlab-simulink model of first UPS topology with DC-link voltage 750VDC is depicted in figure 4.47. Its simulation results are depicted in fig.4.48.

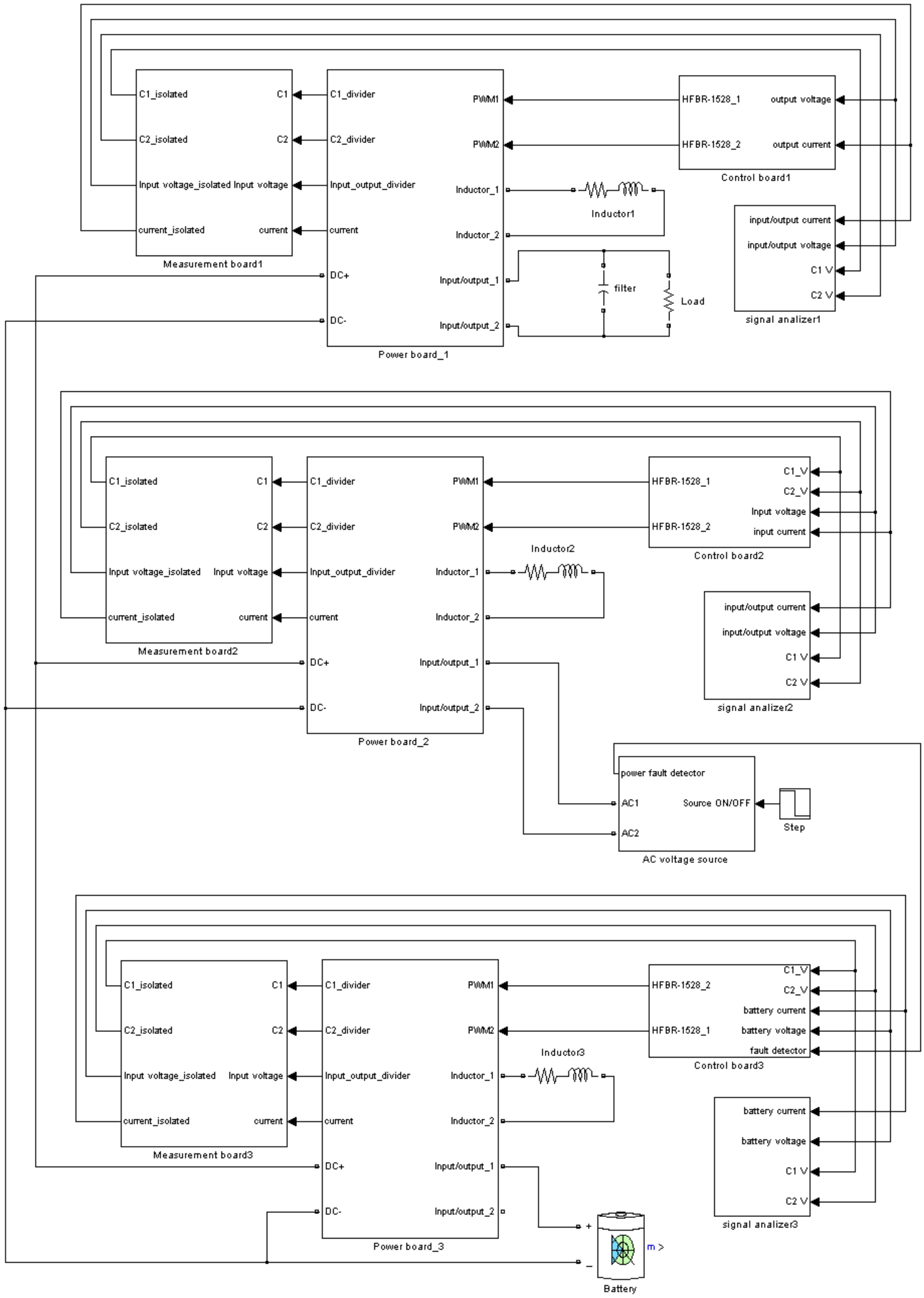

Fig.4.47. Matlab-simulink model of half-bridge UPS topology

The startup process of the UPS is simulated. As it can be seen the input current of the half-bridge PFC rectifier is sinusoidal with THD=5% and cos(f) about 1. The output voltage of the inverter also is sinusoidal with THD about 1% with resistive load and voltage RMS value close to 230V in spite of DC-link voltage variations. Overall simulated efficiency of double conversion is 0.93, but as it was mentioned above (chapter 3.1) the simulated efficiency with current models of semiconductors is not very precise.

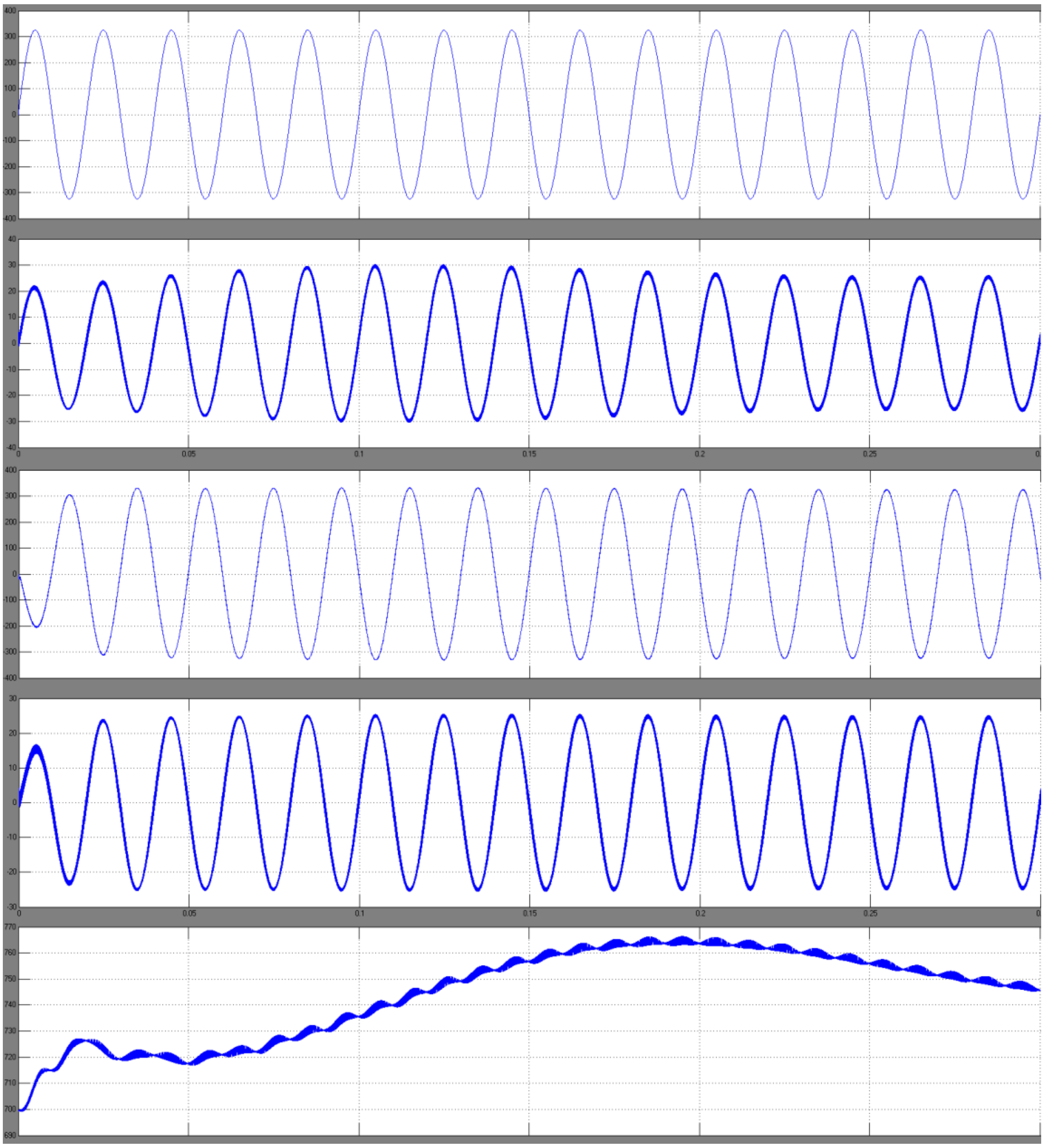

Fig.4.48. Simulated results of the half-bridge UPS topology. From the upper: input voltage, input rectifier current, inverter output current with resistive load, inverter output voltage, DC-link voltage.

Matlab-simulink model of second UPS topology with DC-link voltage 375V is depicted in figure 4.49. There is also startup of the UPS simulation and its simulation results are depicted infig.4.50.

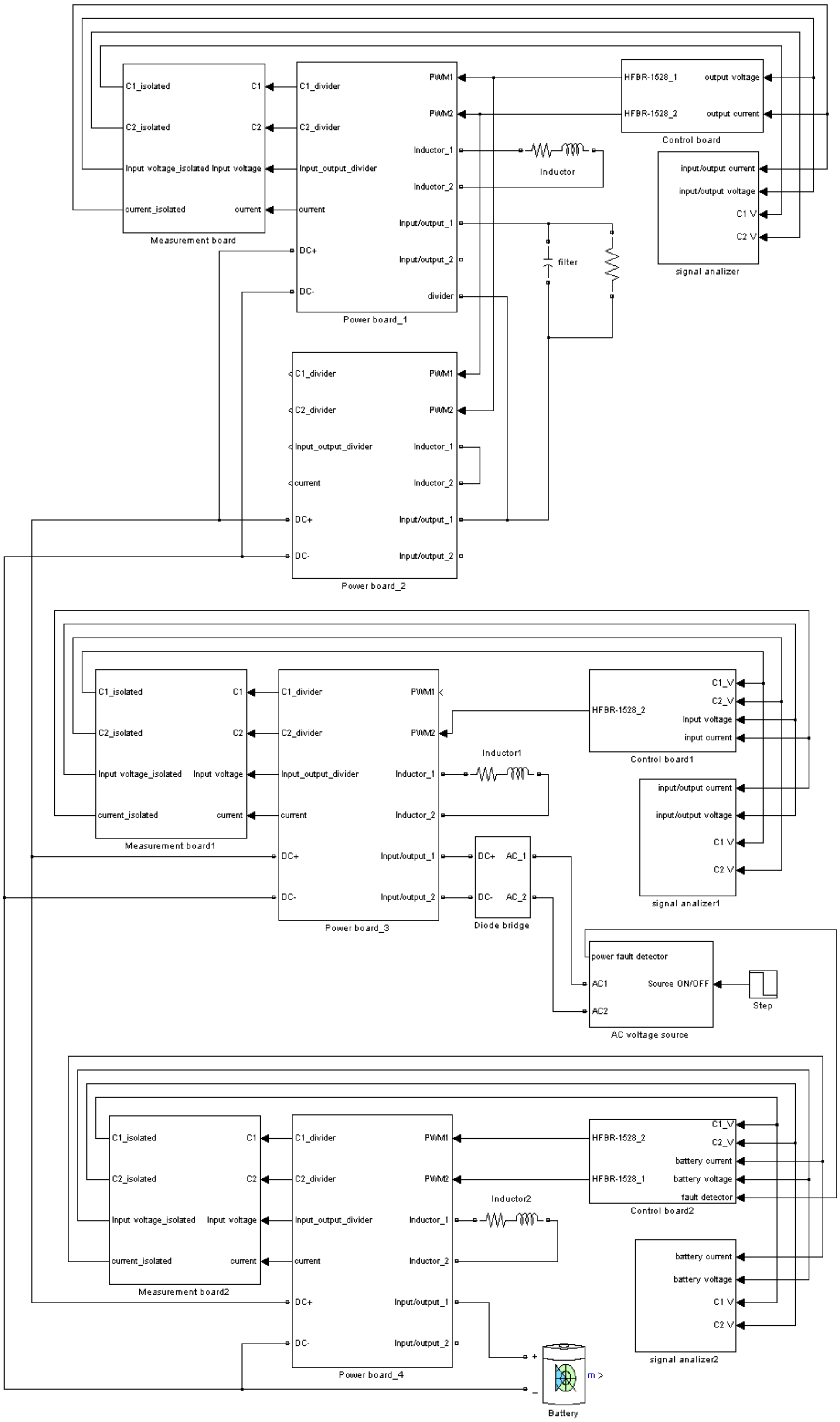

Fig. 4.49. Matlab-simulink model of “online” UPS with DC-link voltage 375V

Similar to previous topology the rectifier current is sinusoidal (THD is about 5%) and in phase with the voltage. So, the rectifier input power factor is close to 1. The inverter output voltage is also sinusoidal (RMS value about 230V) and its THD is about 1%. Overall simulated efficiency of double conversion is also about 0.93.

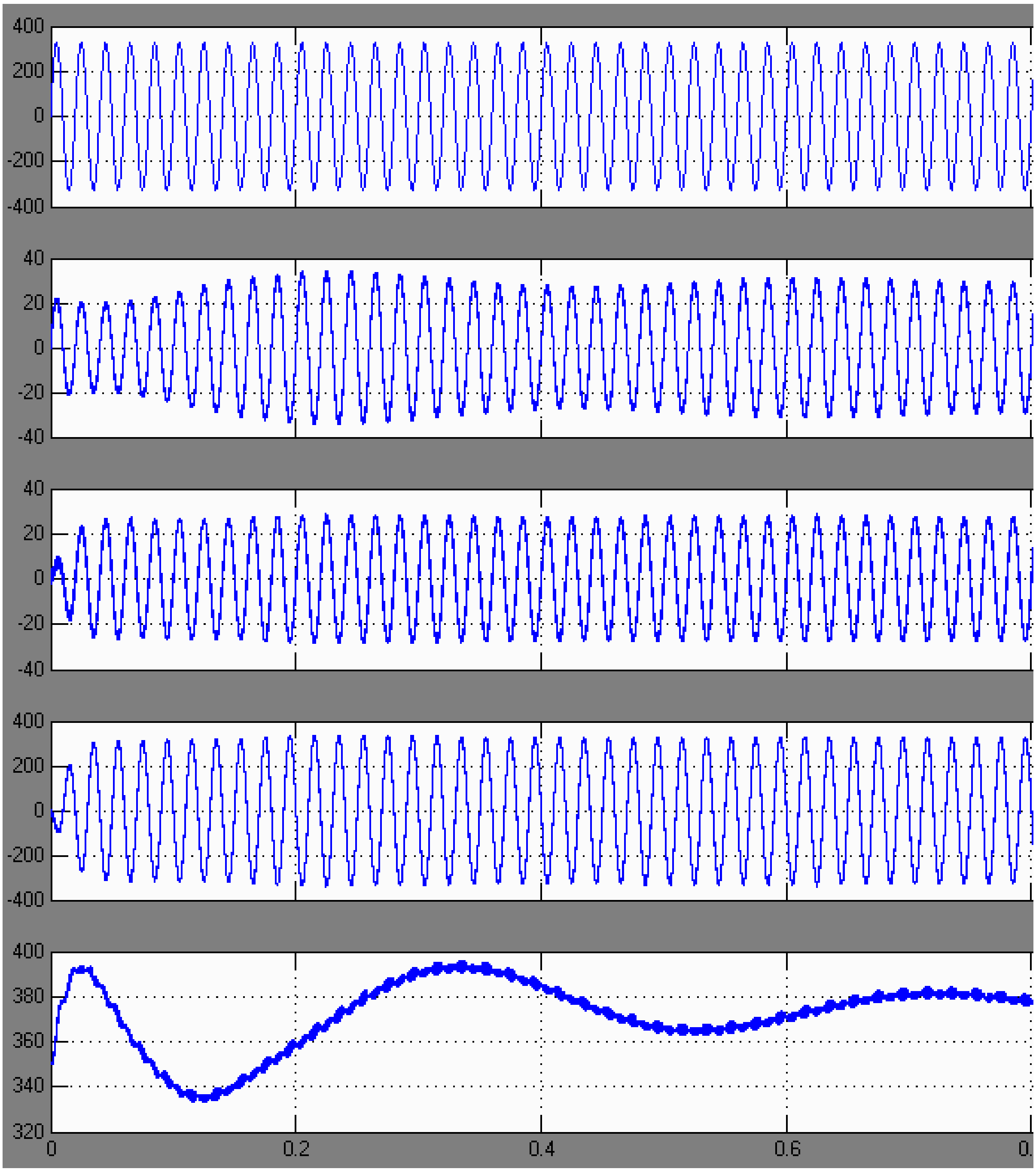

Fig.4.50. Simulated results of UPS topology with the full-bridge inverter. From the upper: input voltage, input rectifier current, inverter output current with resistive load, inverter output voltage, DC-link voltage.

4.2. *Experimental approbation of versatile power modules*

As it was mentioned, the simulation results can not be reviewed as precise results concerning to the converters efficiency. That is why it was decided to test experimentally most of the above mentioned converters topologies.

Real-time controller system “dSpace DS1103” was used for this purpose. This is a laboratory tool for converter control and testing. It has many digital inputs and outputs, many ADC inputs, DAC outputs, PWM outputs etc. It is connectable to personal computer and compatible with Matlab-simulink. Thus the control algorithms from Matlab-simulink with slight changes can be used to compile code for “dSpase” system.

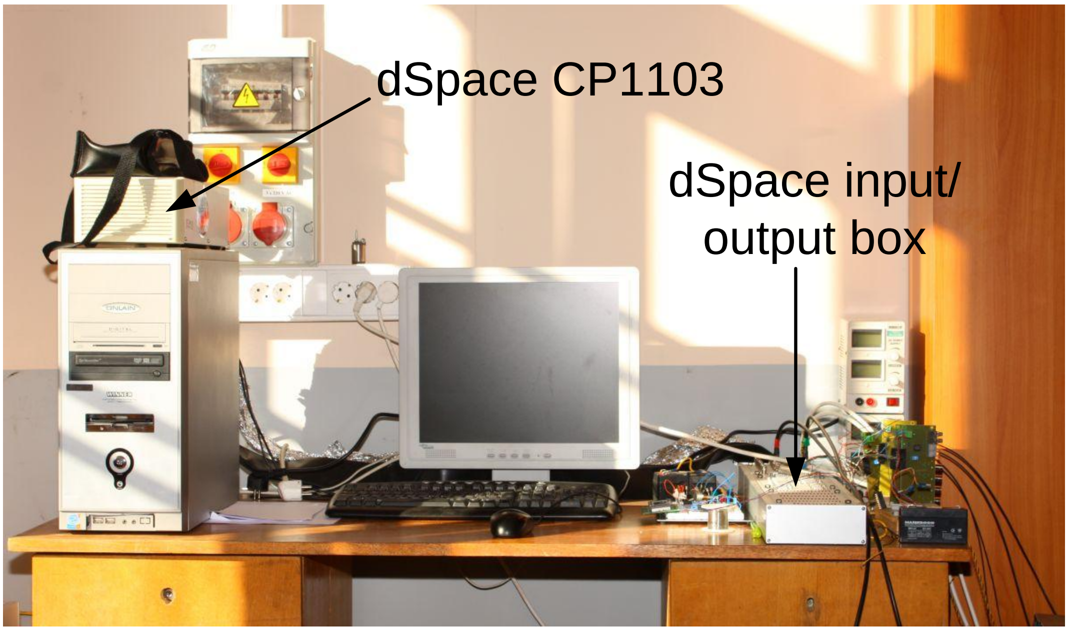

Fig. 4.51. dSpace DS1103 with personal computer

Additionally to “dSpace” program “dSpace ControlDesk” can be used (fig.4.52.) that allows to build visual control interface to:

- see measured feedback signals like on oscillograph
- control and change reference signals
- follow to control signals
- etc

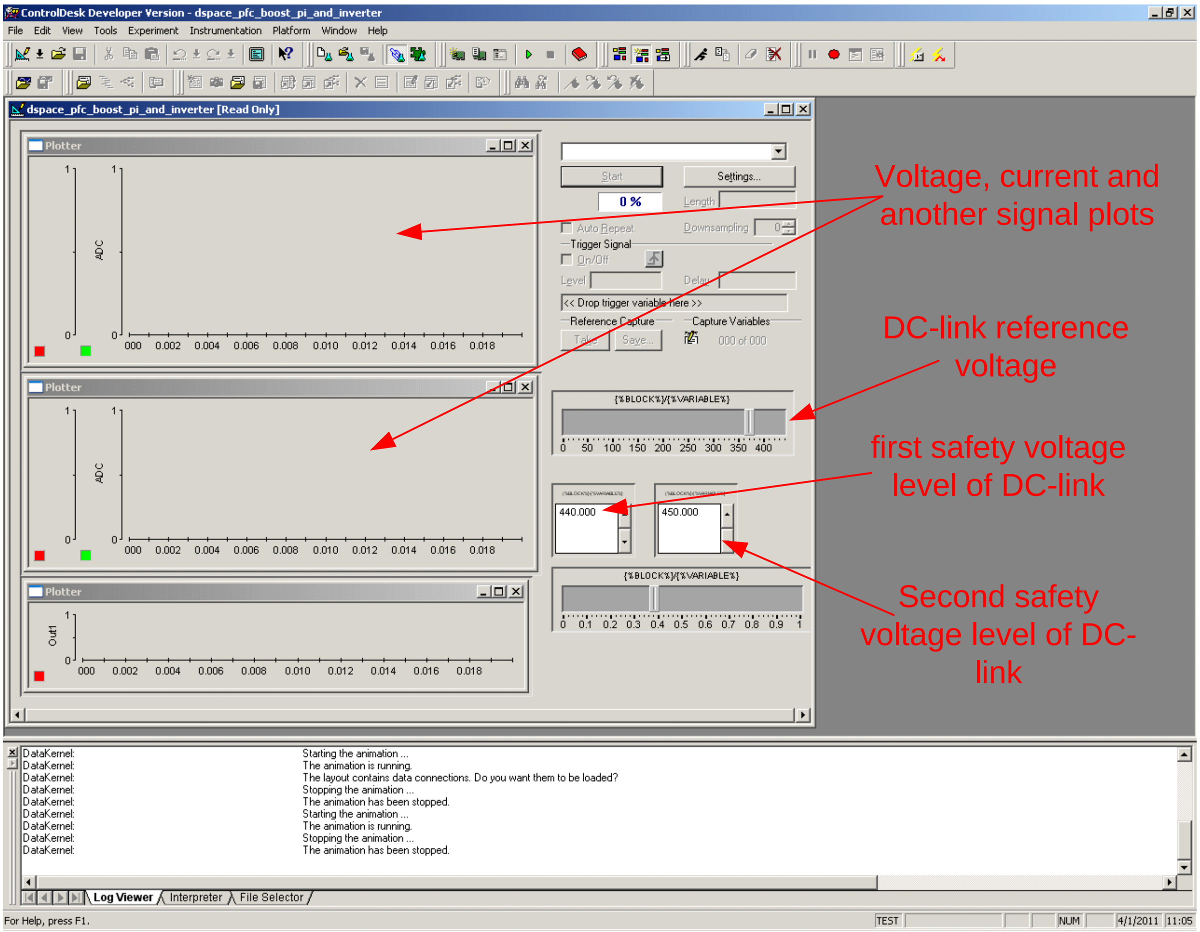

Fig.4.52. Example of window of “dSpace ControlDesk” for boost PFC rectifier

4.2.1. Rectifier testing

a) Boost PFC topology

One versatile power module was taken being interconnected with grid, inductor, and load as it was depicted in fig.4.14. The driver board and measurement board were interconnected with “dSpace” module with fiber-optic and coaxial cables.

The Matlab-simulink model of control board for boost PFC rectifier was used as the basic control algorithm for the real PFC rectifier control. The prepared Matlab-simulink control algorithm for code compiling for “dSpace” module is depicted in fig.4.53. There are used special purpose blocks from Matlab-simulink special library for “dSpace” module (it installs together with “dSpace” software):

- PWM generation block where switching frequency and dead times are configured
- ADC blocks which are linked-up to real ADC inputs.

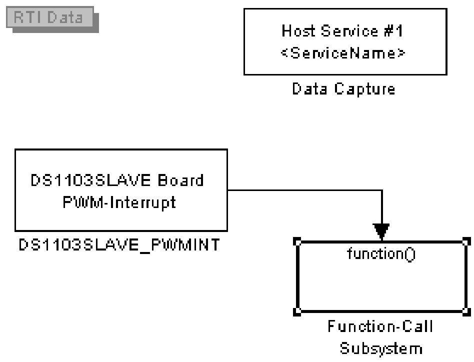

a)

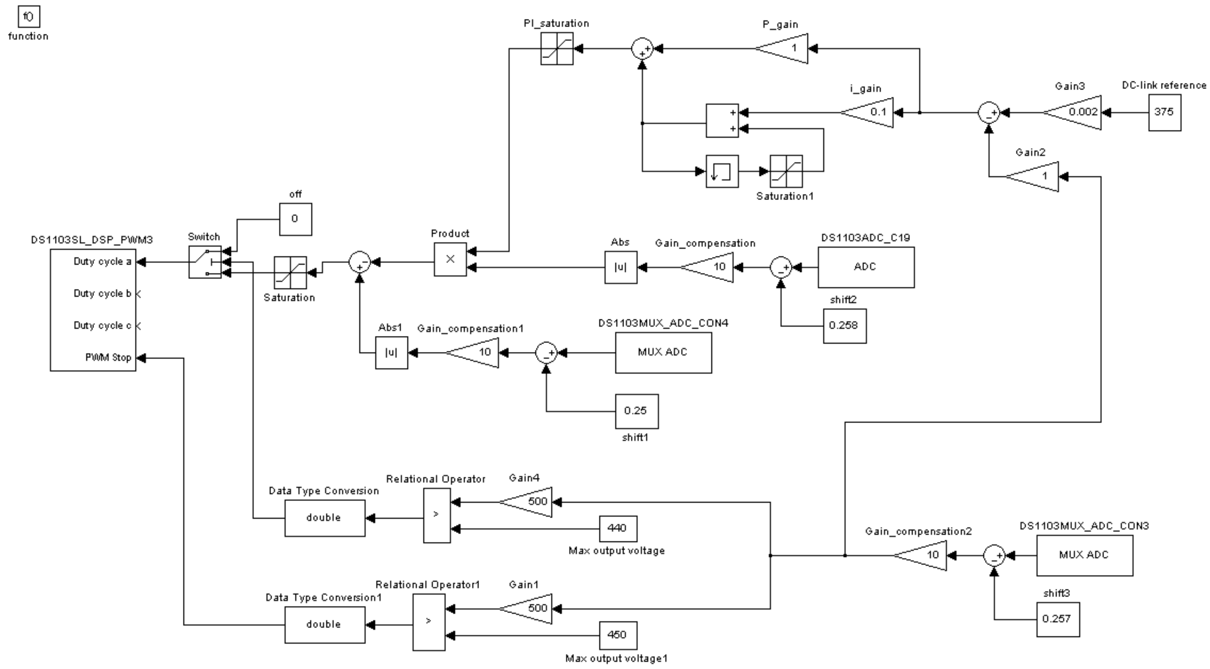

b)

Fig.4.53. Prepared Matlab-simulink model for code compiling for “dSpace” module; a) main block; b) function-call subsystem.

Control algorithm has 2 protection stages from DC-link overvoltage. In the case when DC-link voltage exceeds 440V at the first stage boost PFC rectifier transistor control is switched off only for a short period. At the second stage, in the case when DC-link voltage exceeds 450Vall PWM control signals are, switched off for longer period of time until its operation is restarted.

The example of experimental input current and input voltage of boost PFC rectifier is given in fig.4.54. The current spectral analysis is given in fig.4.55. Such harmonical distortions meets the requirements of EN 50160 standard.

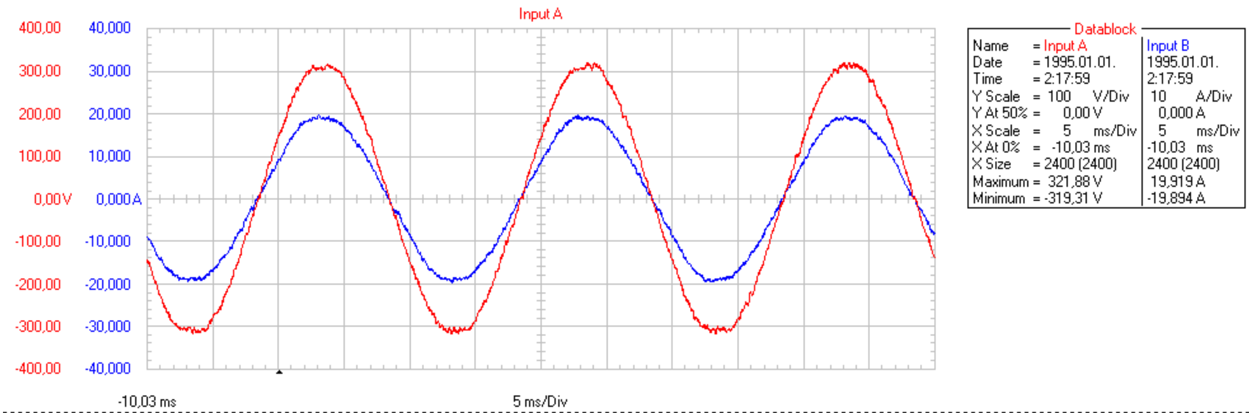

7, DC=377,1V, Rload=50 Ohm, Uin=223, Iin=13,9A

Fig. 4.54. Experimentally measured date of boost PFC converter at 75% of rated load (red – input voltage, blue – input current). Current THD= 2.2%, cos(f) close 1.

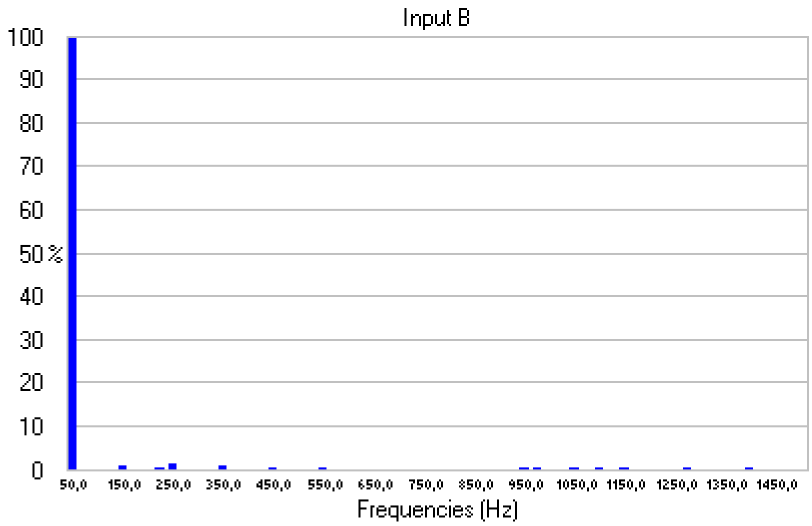

Fig.4.55. Current spectral analysis of boost PFC converter at 2.8kW

Table 3.2.2 presents the data with different loads.

Table 4.13.

Experimentally measured data

Output power (W)	Input current (A)	Input current THD (%)	Converter efficiency (%)	Cos (f)
706	3.4	7.2	0.94	0.99
2144.3	10.1	4.1	0.93	0.99
2842.6	13.7	2.2	0.93	0.99

In similar ways like with boost PFC rectifier other PFC rectifiers were tested (table.4.14 - table.4.17).

b) Bridgeless PFC topology

Table 4.14.

Bridgeless PFC experimentally measured data

Output power (W)	Input current (A)	Input current THD (%)	Converter efficiency (%)	Cos (f)
705	3.4	10	0.92	0.99
2115	10.3	5.3	0.93	0.99
2804	13.9	3.7	0.94	0.99

c) Bridgeless-totem PFC topology

Table 4.15.

Bridgeless-totem PFC experimentally measured data

Output power (W)	Input current (A)	Input current THD (%)	Converter efficiency (%)	Cos (f)
703	3.4	10	0.92	0.99
2115	10.3	5	0.92	0.99
2820	14	3.7	0.92	0.99

d) full-bridge PFC topology

Table 4.16.

Full-bridge PFC experimentally measured data

Output power (W)	Input current (A)	Input current THD (%)	Converter efficiency (%)	Cos (f)
700	3.3	20	0.9	0.99
2110	10	14	0.91	0.99
2812	13.8	13	0.91	0.99

e) half-bridge PFC topology

Table 4.17.

Half-bridge experimentally measured data

Output power (W)	Input current (A)	Input current THD (%)	Converter efficiency (%)	Cos (f)
705	3.4	9	0.9	0.99
2118	10	5	0.91	0.99
2828	14.5	3.8	0.9	0.99

As experimental data show other PFC topologies also consume sinusoidal current from the grid. As it was expected the highest efficiency is provided by the bridgeless topology, but it must be noted that the accuracy of these measurements is ±0.5% for voltage and ±2.5% for current.

As well, as was expected, the experimental data have shown lower efficiency than simulated data. This is because of imperfection of Matlab transistor model. Mostly it can calculate conduction losses, but switching losses it calculates incorrectly.

4.2.2. Inverter testing

The “dSpace” module was used for inverters control. The control algorithm for full-bridge inverter and half-bridge inverters are similar (fig.4.56).

At the given time there is lack of laboratory high voltage DC voltage source (800V, 5A) and due to this it was tested only full-bridge inverter.

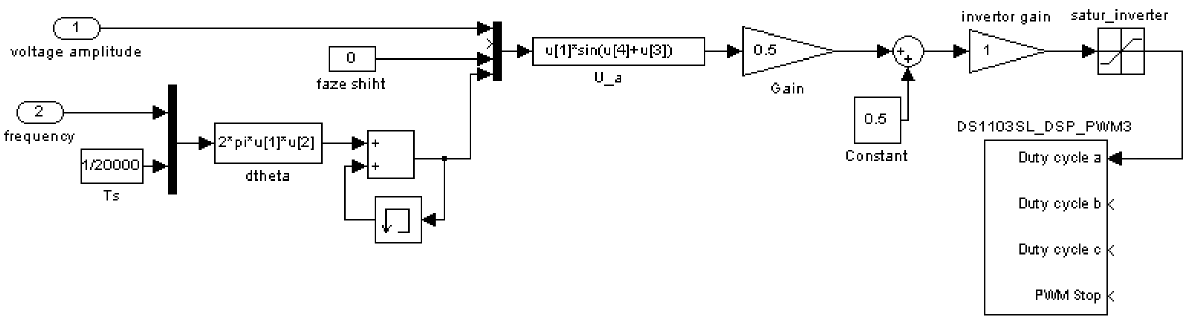

Fig.4.56. Inverter control algorithm

Experimentally measured current and voltage of full-bridge inverter with linear load are depicted in fig.4.57. Inverter output RMS voltage is 226V. The resistance of 12.5 Ohm was applied to get 4 kW load. Efficiency of voltage invention was 94.6%.

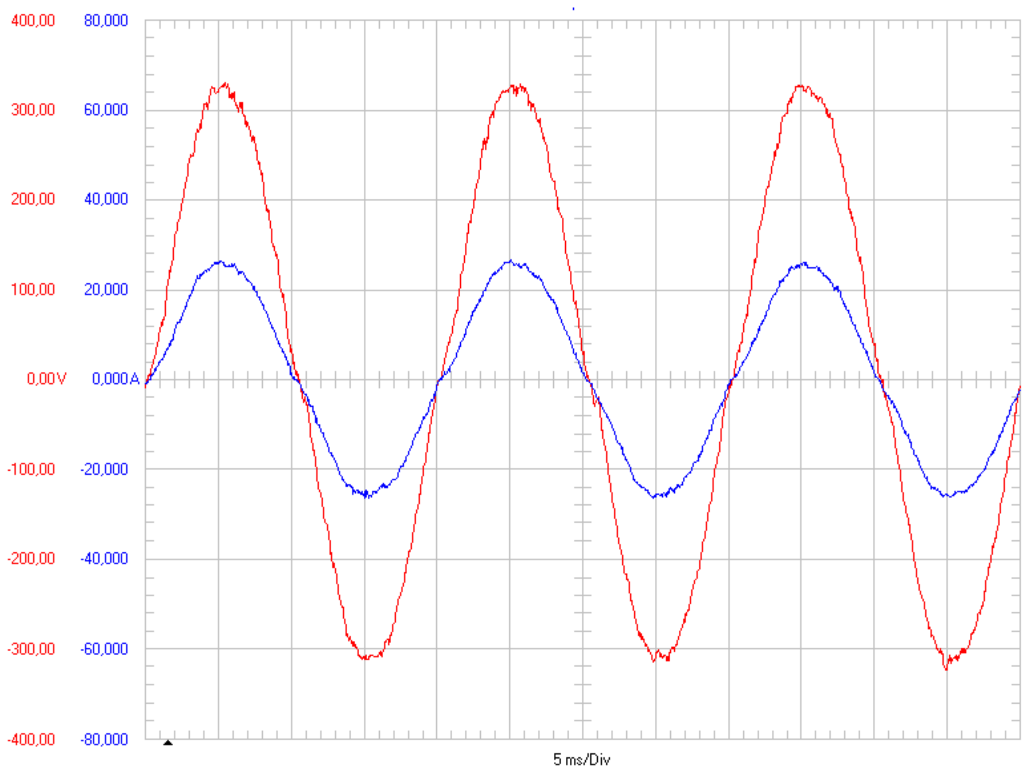

Fig. 4.57. Inverter current and voltage with linear load
(blue - current – 20A/div, red - voltage – 100V/div)

Spectral analysis of inverter voltage is given in fig.4.58. THD of inverted voltage is 4%.

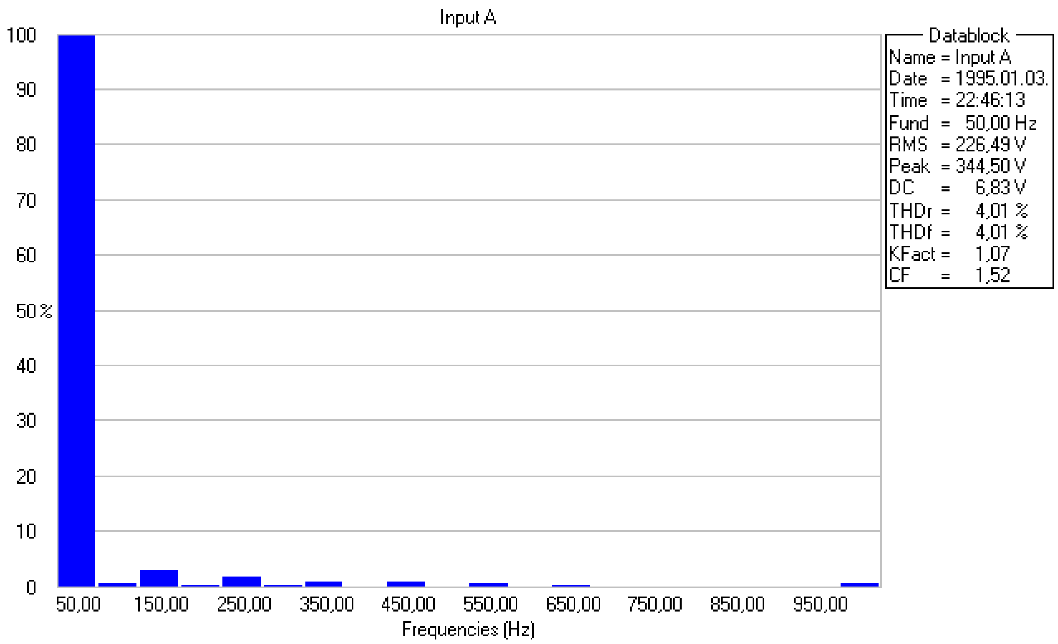

Fig. 4.58. Loaded with linear load inverter voltage spectral analysis

Experimentally measured current and voltage with non-linear load are depicted in fig.4.59. RMS value of current is 7.7A. Voltage RMS is 209V.

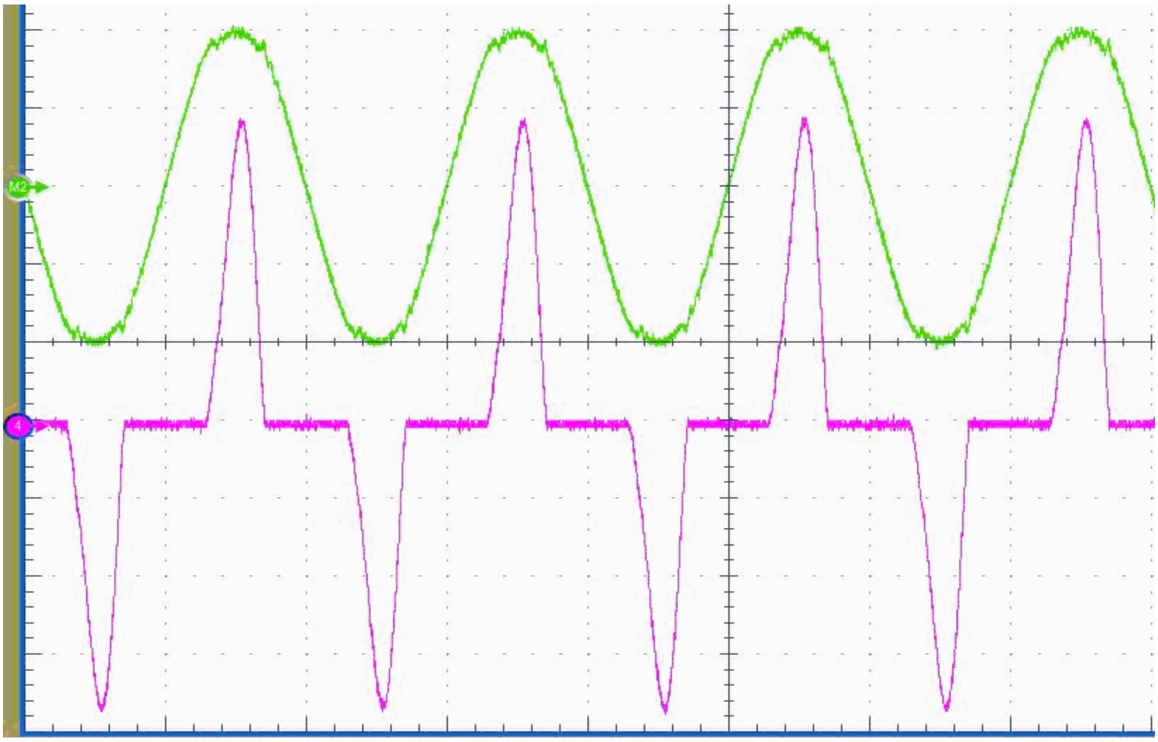

Fig. 4.59. Inverter current and voltage with non-linear load
(purple-current – 5A/div, green-voltage – 150V/div)

4.2.3. Online UPS testing

After the separate converter testing "on-line" UPS was experimentally tested. For this purpose "online" UPS topology with DC-link voltage 375V was used. Its realisation needs 4 versatile power modules as a minimum:

- boost PFC rectifier (1x)
- DC/DC energy storage charger/discharger (1x)
- Full-bridge inverter (2x)

“Online” UPS assembly is depicted in fig.4.60.

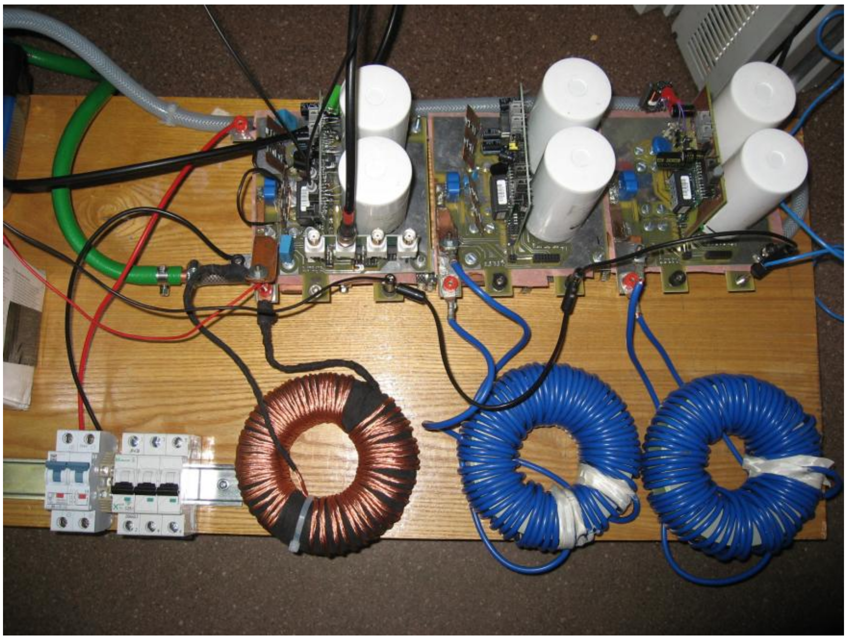

Fig.4.60. On-line UPS assembly with 4 versatile power modules

As a control device the “dSpace” module was used. Control algorithm is depicted in fig. 4.61. The control algorithm contains subsystems for each converter: inverter, PFC rectifier, charger (buck converter), discharger (boost converter). Each of these subsystems contains the algorithms already mentioned in the previous chapters.

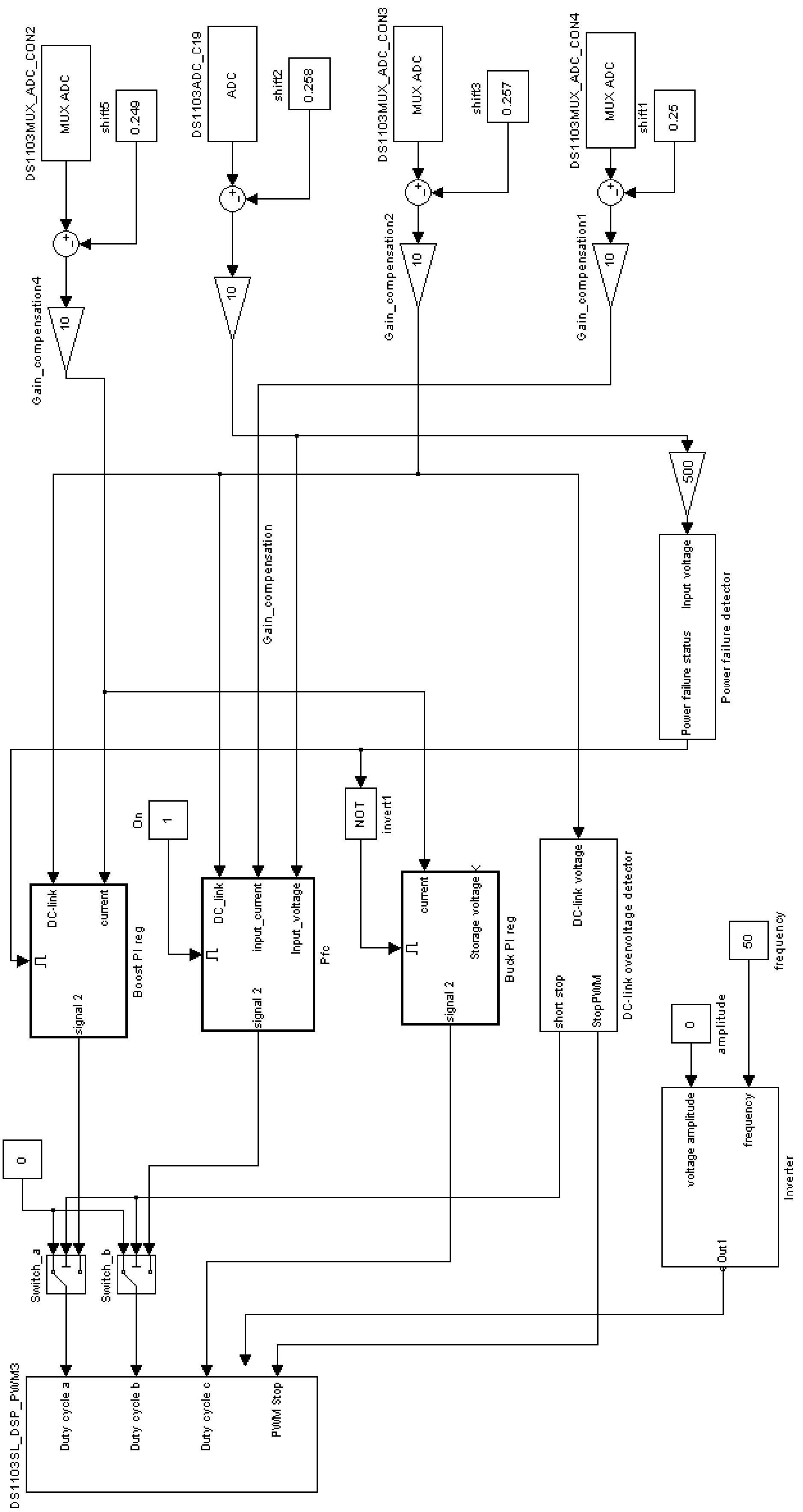

Fig. 4.61. “Online” UPS control algorithm

Fig. 4.62., fig. 4.63., fig. 4.64., represent “online” UPS operation with rated voltage (220V-230V), undervoltage (180V), overvoltage (250V) at 50% of the rated load (statistic shows that most UPS loaded on 40-70%). The figures show that output voltage does not depend on input voltage shape and amplitude. It is obvious that input voltage shape is distorted due to many nonlinear loads in RTU grid (voltage THD about 8%), but the output voltage is corrected and it THD is about 3-4%.

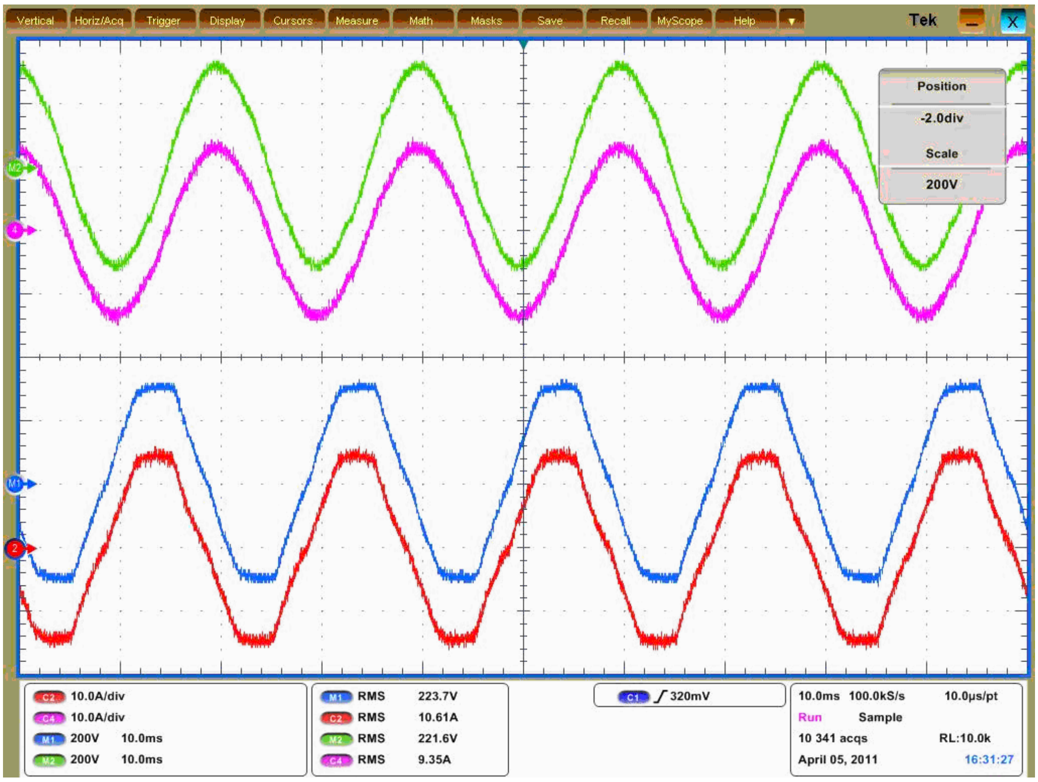

Fig. 4.62. UPS voltages and currents with rated input voltage.

(Input voltage-blue, input current- red, output voltage - green and output current – purple)

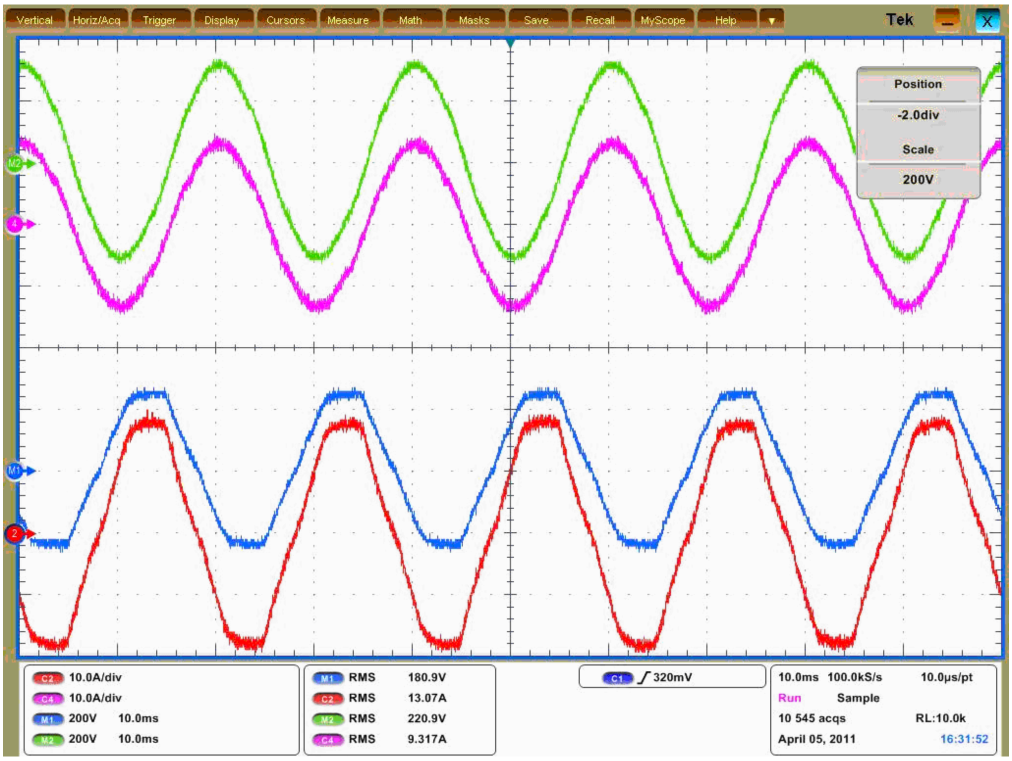

Fig. 4.63. UPS voltages and currents at low (180V) input voltage.

(Input voltage-blue, input current- red, output voltage - green and output current – purple)

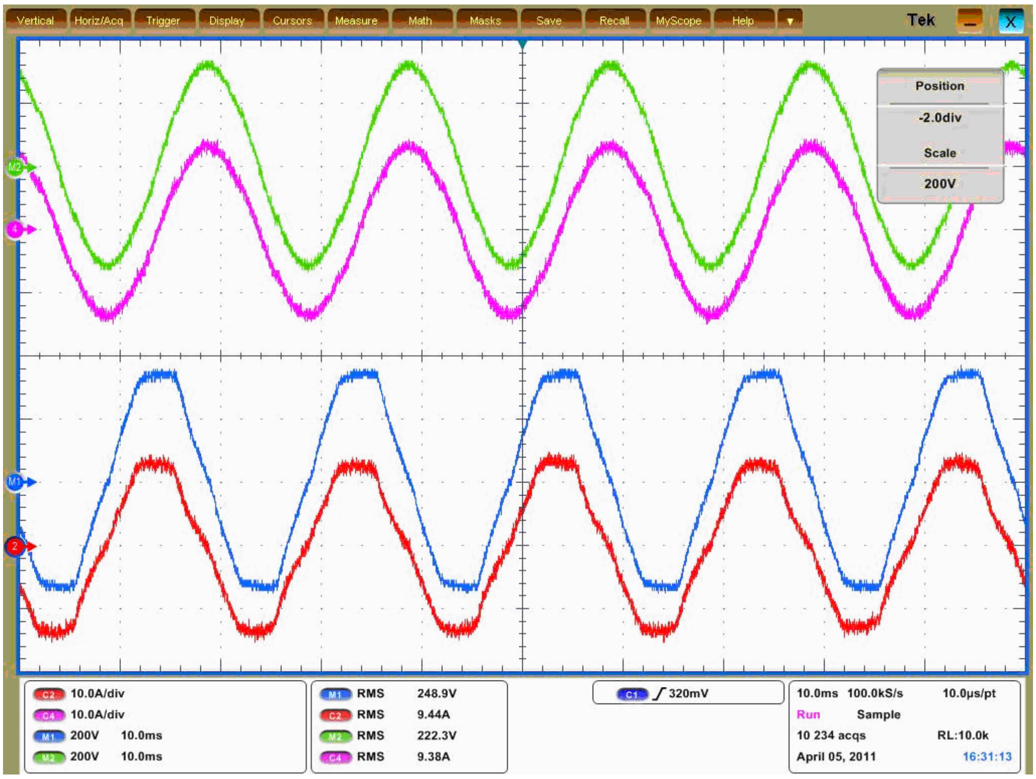

Fig. 4.64. UPS voltages and currents at high (249V) input voltage.

(Input voltage-blue, input current- red, output voltage - green and output current – purple)

The next pictures represent operation of assembled “online” UPS with non-linear loads. As it can be seen the input current is sinusoidal.

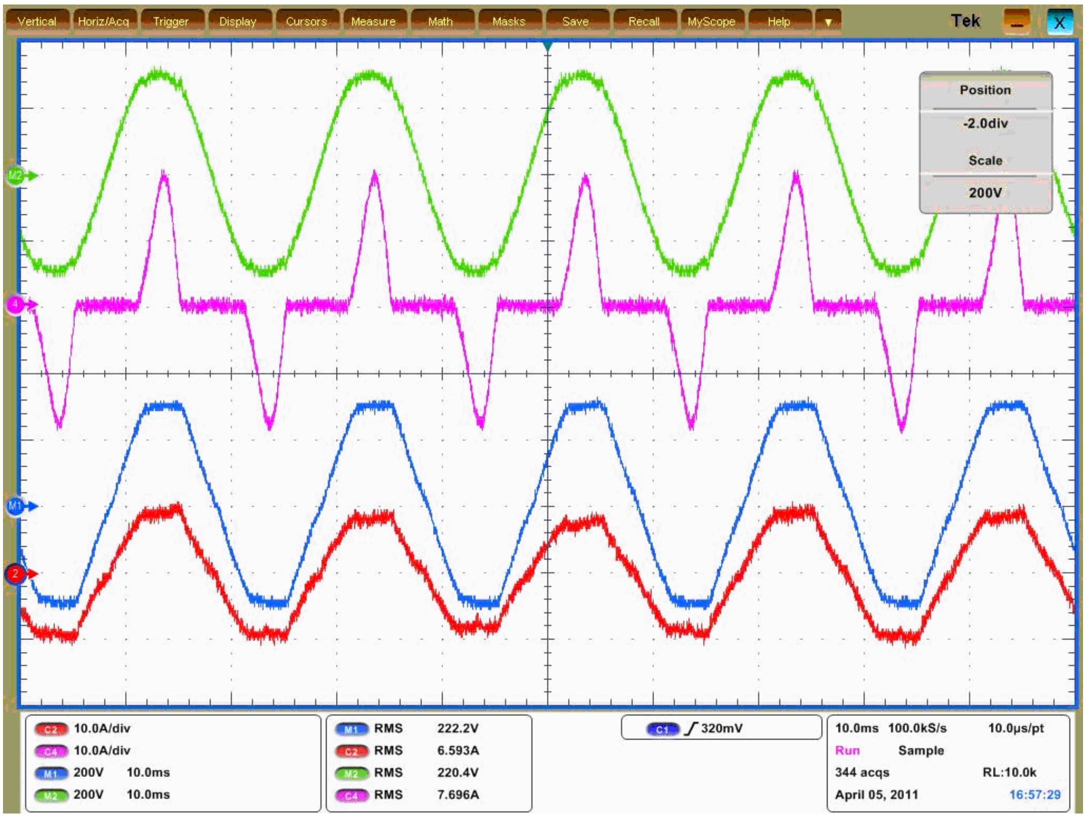

Fig. 4.65. UPS voltages and currents at rated input voltage and non-linear load.
(Input voltage-blue, input current- red, output voltage - green and output current – purple)

Another important parameter of UPS is switching time to backup storage. For these reasons the UPS control algorithm includes subsystem “Power failure detector” (fig.4.66). It is necessary to detect the presence of input voltage and in the case of power failure it switches the UPS to backup storage mode.

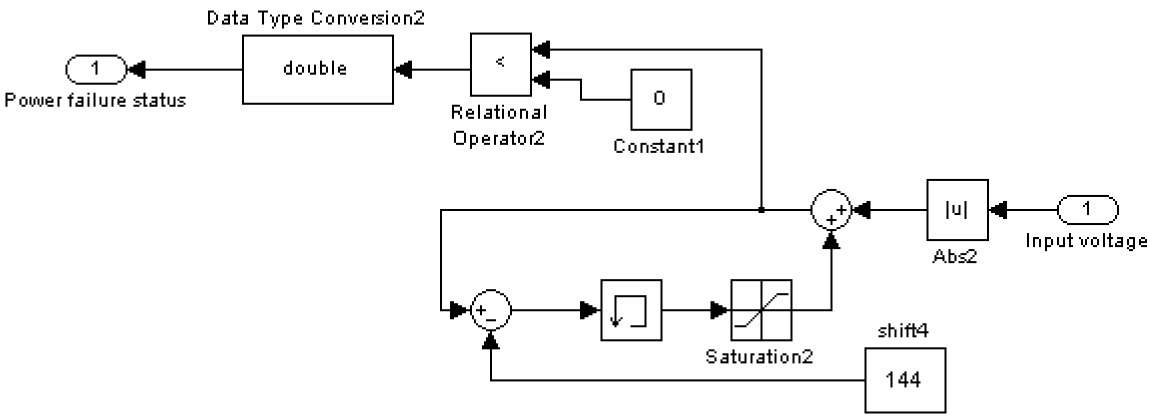

Fig. 4.66. Subsystem of power failure detection

As it was mentioned in the second chapter, measurement board output magnitude value of the measured input voltage is:

$$U_{mm} = \frac{U_m}{500} \cdot \sin(\omega t) + 2{,}5 \qquad (4.9)$$

where: U_m- magnitude of input voltage,

500 – total dividing coefficient of measurement system,

2.5 – DC bias of measurement board. So, if the input voltage has magnitude value 325V, the magnitude value of measured signal in “dSpace” module will be 0.065V.

Magnitude value of measured signal in “dSpace” is:

$$U_{md} = (\frac{U_m}{500} \cdot \sin(\omega t) + 2{,}5)/10 \qquad (4.10)$$

where: 10 – dividing coefficient of “dSpace” module.

For more comfort use in digital way there is removed DC bias, dividend coefficients and signal is rectified. So, input signal $U_{md'}$ of subsystem “power failure detector” is:

$$U_{md'} = \left| U_m \sin(\omega t) \right| \qquad (4.11)$$

Mean value of this signal is

$$U_{aved'} = \int_0^{\pi} U_m \sin(\omega t) d\omega t = \frac{2U_m}{\pi} \tag{4.12}$$

It is accepted that the grid failed in the case if its voltage RMS value drops below 160V. Mean value of the rectified reference voltage is:

$$U_{ave\_ref} = \frac{2\sqrt{2}U_{ref}}{\pi} = 144.05 \tag{4.13}$$

To find grid status the signals $U_{aved'}$ and U_{ave_ref} are compared, its error is integrated and integration value compared with 0. Positive value means the presence of supply power, but negative value in its turn means its absence.

$$S = \int_0^{\pi} (U_m \sin(\omega t) - 144.05) d\omega t \tag{4.14}$$

To prevent large accumulation of integral value there is saturation of integral.

$$S_{sat} = \in (-b, b) \tag{4.15}$$

Observing half period of sinusoidal voltage results in conclusion that "S" is increased when sin wave voltage is higher than its mean value, but decreasing - when lower than its mean value (fig.4.67). Curves of the sine wave and its mean value are crossed within angle $\angle a$. Its value can be found as:

$$U_m \cdot \sin(a) = \frac{2U_m}{\pi} \tag{4.16}$$

From (4.16) the $\angle a$ can be expressed as:

$$\angle a = \arcsin(\frac{2}{\pi}) \quad (4.17)$$

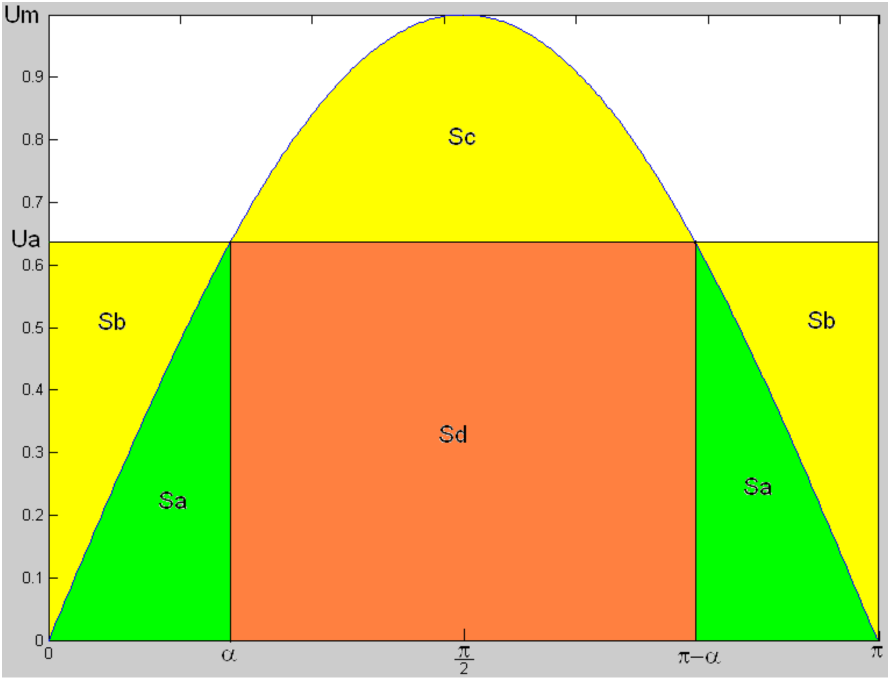

Fig.4.67. Curves of sine wane and its mean value

The areas Sb and Sc (2xSb=Sc) take part in the error accumulation.

$$S_a = \int_0^{\arcsin\frac{2}{\pi}} (U_m \sin(\omega t) d\omega t = -U_m \cdot \cos(\omega t)\,|_0^{\arcsin\frac{2}{\pi}} = 226.3 \cdot 0.2289 = 51.8 \quad (4.18)$$

Dividing it on integration time the mean value of Sa can be found:

$$U_{a\_Sa} = \frac{S_a}{\arcsin\frac{2}{\pi}} = \frac{51.8}{0.6901} = 75.061 \quad (4.19)$$

Mean value of area Sb can be found if from the U_{ave_ref} subtract the mean value of the Sa:

$$U_{b\_Sb} = 144.05 - \frac{S_a}{\arcsin\frac{2}{\pi}} = 68.989 \quad (4.20)$$

Taking into account that the control algorithm measures the voltage with frequency 20kHz and $\angle a = \arcsin \frac{2}{\pi}$ that corresponds to 2.2ms the number of measurements made by the control algorithm will be:

$$N = \frac{f}{2.2ms} = 44 \tag{4.21}$$

where: f – measurement frequency (20000 Hz)

Totally the sum will be:

$$M = 2 \cdot U_{b\_Sb} \cdot 44 = 2 \cdot 68.989 \cdot 44 = 6071 \tag{4.22}$$

That gives that saturation must be:

$$S_{sat} = \in (-6071, 6071) \tag{4.23}$$

The “power failure detector” was experimentally tested. Fig.4.68 demonstrates that detection time is close to 5ms.

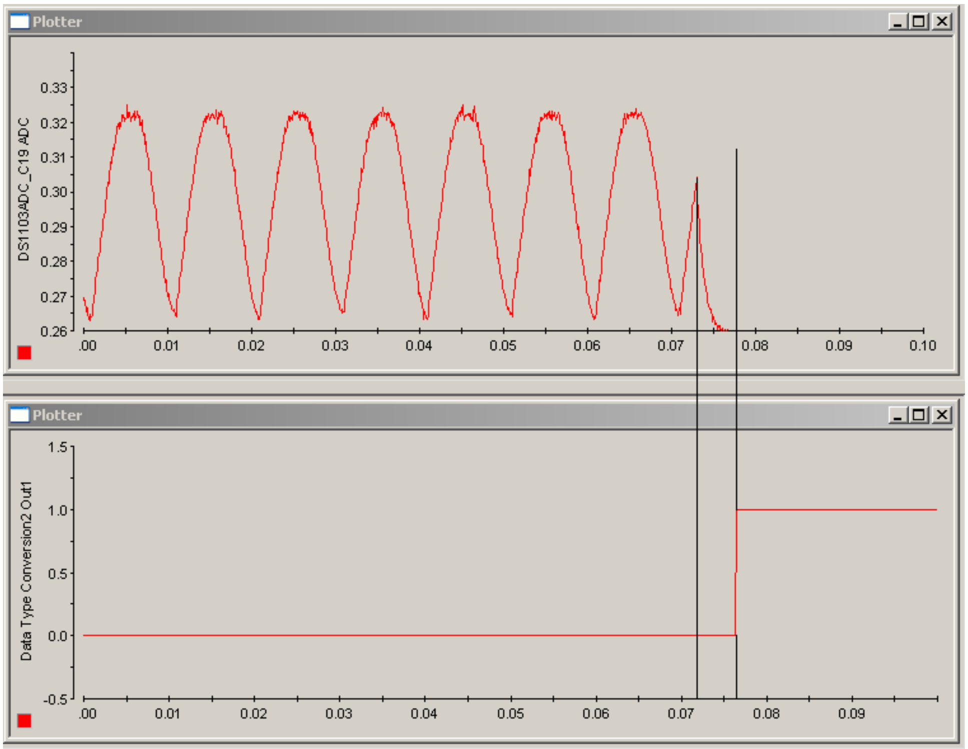

Fig.4.68. Experimental test of "Power failure detection" detection time is close to 5ms.

The operation of "power failure detector" in UPS is depicted in fig.4.69.

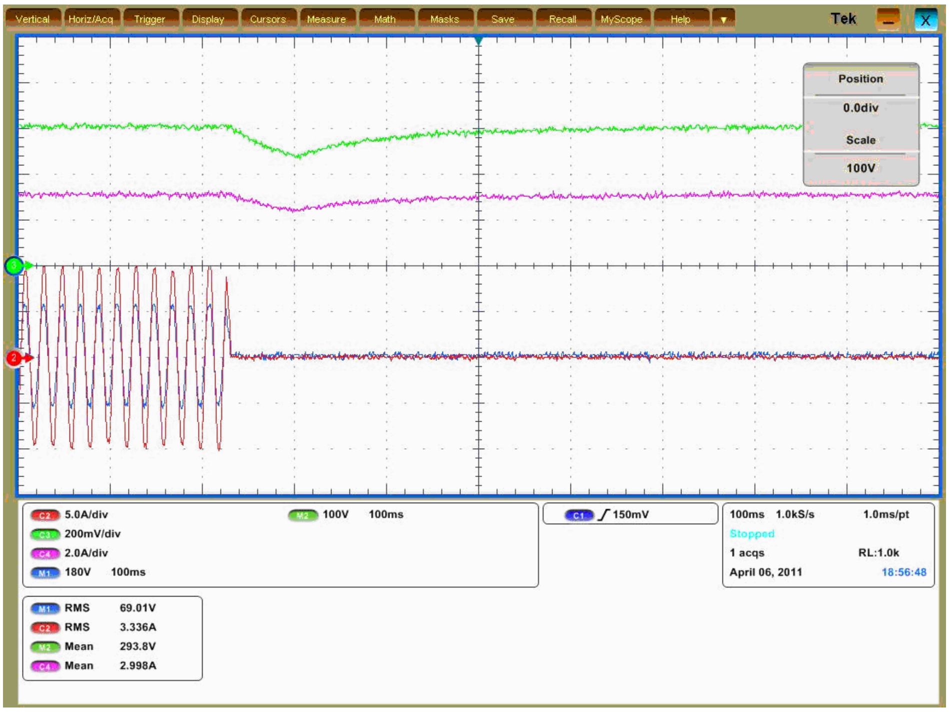

Fig.4.69. Operation of "power failure detector"

Red – input voltage, blue - input current, green – DC-link voltage

4.3. Summary

- In this chapter active rectifiers, inverters, DC/DC converters assembled with versatile power converter were simulated, analyzed and tested.
- Simulation data were used for selection of optimal topology for UPSS. It resulted in the conclusion that it is better to chose lower DC-link voltage. Due to that DC/DC converter with DC-link voltage 375V and full-bridge inverter that also has DC-link voltage 375V are used. As a rectifier the boost PFC rectifier was chosen due to lower number of necessary VPMs for its assembling. It is simple in control. The simulations results show that it has an acceptable level of THD of input current, but its efficiency is only slightly lower (0.5-1%) than that the best one have from experimentally tested.
- The selected topology of UPS was simulated and tested.

5. Cost of Versatile power module

This chapter presents cost comparison of classical UPS systems and UPS that is built with VPM. The 4kW online UPS can be assembled with 5 VPMs. Conventional "online" UPS cost is approximately 1500Ls [www.powerall.lv]. The calculation of price of UPS assembled with VPMs is given in table 5.1.

Table.5.1

'"Online" UPS costs calculation:

Power board	PCB – 20Ls Capacitors – 2x15=30Ls Transistors= 2x14+28Ls Another small items – 3Ls Total – 81Ls
Driver board	PCB – 6Ls Driver – 35Ls Opto receivers – 6x2 =12Ls Opto transmitters – 9x2 = 18Ls Transformer – 2 Another small items – 10Ls Total - 83Ls
Measurement board	PCB – 5Ls HCPL 7800 – 4x3Ls =12Ls 1W 5V power supply – 3x3Ls=9Ls BNC connector - 4x1Ls=4Ls Other small things = 2Ls Total – 32Ls
Adaptor board	PCB – 4Ls Opto receivers – 6x2 =12Ls Opto transmitters – 9x2 = 18Ls BNC connector - 4x1Ls=4Ls Other small things – 2Ls Total – 40
Total for one module – 236Ls	
Cooling system for 1 kW heat dissipation	Primary heatsinks – 10Ls Secondary heat sink – 10Ls Water pump – 20Ls Water tubes – 5Ls Connectors – 5Ls Total – 50Ls
Energy storage	Lead-acid battery for 7-10 min (420-600sec) It is connected in series 6 Panasonic17Ah and 12V

	batteries Total battery is 72Vx17Ah 6x40Ls = 240Ls Or Supercapacitor: 125V, 63F – 492kWs (used energy close to 290kWs). At 4kW discharge can supply energy close to 70sec. Price of this supercapacitor is 2600Ls
Control system	For advanced control it will be necessary DSP processor It price can be up to 300 Ls
Inductors	Inductor approximately cost 30-50LS
Total for 4kW online UPS (5 modules) – 5x236Ls + 4x10Ls+40Ls+300Ls+240Ls+3x30=1890Ls	

As it can be seen the price of developed UPS system is higher. Main reason of it is that it is cost of prototype. In the case of mass production this price can be reduced almost twice.

It must be noted that in the comparison price of classical UPS topology is given. But main reason is that VPM are developed for more complicated tasks that cannot by realized with UPS that's represent on the market.

Major results

- Uninterruptible power supply system that allows to utilize varied energy sources and storages has been proposed and developed
- Versatile power module for uninterruptible power supply system has been developed
- MATLAB-Simulink models of the proposed UPSS and its elements have been proposed, developed and validated
- Several configurations VPM based UPSS with varied energy storages and sources have been tested

Minor results

- As a result of secondary research it was developed precise Matlab-Simulink model of photovoltaic panels that are available in "Institute of Industrial Electronics and Electrical Engineering " laboratory that can be used in future researches too
- As a result of secondary research it was developed cheap and robust construction of primary hear sink for water cooling system

Conclusions

- The proposed approach of development of UPSS provides increased flexibility of utilization of alternative sources and storages
- The proposed VPM provides effective laboratory test bench for research and development of the proposed UPSS
- The utilized simulation-testing environment based on MATLAB-SIMULINK-dSpase(CP1103) even more facilitates development of UPSS hardware and software
- Simulation and experimental results prove initial assumption of easy reconfigurable versatile concept of UPSS development

References

[1] Florin Iov, Anca Daniela Hansen, Poul Sørensen, Nicolaos Antonio Cutululis, “Mapping of grid faults and grid codes”, Technical University of Denmark, July 2007

[2] Standard LVS EN 50160

[3] Muhammad H. Rashid, Power Electronics Handbook_Devices Circuits and Applications_Second Edition, Nov 8 2006

[4] Kristina Hamachi LaCommare, Joseph H. Eto, “Understanding the Cost of Power Interruptions to U.S. Electricity Consumers”, September 2004

[5] http://www.ups-info.ru

[6] “Electrical engineering Tables, Standarts, Formulas” Europa-Lehrmittel, 2008

[7] Ewald Fuchs, Mohammad A. S. Masoum, Power Quality in Power Systems and Electrical Machines, Academic Press, March 7 2008

[8] Neil Rasmussen, “The Different Types of UPS Systems”, White Paper #1, APC, 2004

[9] http://en.wikipedia.org/wiki/Eaton_BladeUPS

[10] Правила устройства электроустановок, 7 издание.

[11] https://www.automation.siemens.com/sitop/html_76/ups500.htm

[12] Stephen McCluer, Jaen-Francois Christin, “Comparing data center batteries, flywheels, and ultracapacitors”, Whitre paper #65,

[13] http://www.activepower.com/solutions/ups-systems/flywheel-technology/flywheel-vs-battery/

[14] Becker H. I., “Low voltage electrolytic capacitor”, U.S. Patent 2800616, 23 July 1957.

[15] http://www.smartgauge.co.uk/peukert_depth.html

[16] Liebert , “Five questions to ask before selecting power protection for critical systems”, A guide for it and data center managers

[17] Wendy Torell, Victor Avelar, four steps to determine when a standby generator is needed for small data centers and network rooms, White paper #52

[18] Maxwell Technologies, MC POWER SERIES 48 V MODULES datasheet

[19] D. DeCoster, 15 Seconds Flywheel Reserve or 15 Minutes Battery Reserve? The RELIABILITY difference

[20] LVS EN 62040-3 standard

[21] LVS EN 61000 standard

[22] Отраслевой стандарт - платы печатные

[23] Concept, Dual SCALE Driver 2SD106AI-17 datasheet

[24] Hewlett Packard, High CMR Isolation Amplifiers HCPL-7800 datasheet
[25] http://www.semikron.com/
[26] Fraidoon Mazda, power electronics handbook Third Edition, January 1998
[27] Lienhard J.H. “A Heat Transfer Textbook Third Edition”, Phlogiston Press; 3rd edition, August 5, 2003
[28] Nagla, J., Siltumtehnikas pamati : mācību līdzeklis LPSR augstsk. tehnisko specialitāšu studentiem, 1981
[29] Nagla, J , Siltumtehniskie aprēķini piemēros : māc. līdz. tehn. spec. stud., 1982
[30] Resources, Tools and Basic Information for Engineering and Design of Technical Applications, http://www.engineeringtoolbox.com/reynolds-number-d_237.html
[31] Инженерный справочник и таблицы, http://www.dpva.info/Guide/GuidePhysics/VicosityReynolds/HydraulicDiameter/
[32] Pipe Pressure Drop & Flow Rate, http://www.pipeflow.co.uk/public/control.php?_path=/497/499
[33] Pipes pressure drop calculator, http://www.engineersedge.com/fluid_flow/pressure_drop/pressure_drop.htm
[34] Nusselt number, http://en.wikipedia.org/wiki/Nusselt_number
[35] Prandtl's number, http://www.engineeringtoolbox.com/water-thermal-properties-d_162.html
[36] Alvis Sokolovs, “Research and Development of Integrated AC drive with Induction motor and Matrix Converter”, PhD Thesis, Riga Technical university, 2010
[37] Commercialization of Local Inverter Product: 3.4kW Single-Phase Grid-Connected Inverter
[38] List of standards, drafts and specifications specially developed for PV applications, DKE German Commission for Electrical, Electronic & information Technologies of DIN and VDE, august 2010
[39] Stuart R. Wenham, Martin A. Green, Muriel E. Watt, Richard Corkish, “Applied photovoltaics”, Earthscan Publications Ltd., 2007-02, ISBN: 1844074013, 335 pages
[40] Samuel Vasconcelos Araújo, Peter Zacharias, Regine Mallwitz, “Highly Efficient Single-Phase Transformerless Inverters for Grid-Connected Photovoltaic Systems”, IEEE transactions on industrial electronics, vol. 57, no. 9, September 2010
[41] Power Integrations home page, http://www.powerint.com/en/community/papers-circuit-ideas-puzzlers/circuit-ideas/-high-voltage-input-switching-power-supply-usi

[42] Rahul Joshi, Power Integrations, “Designing Wide Range Power Supplies for Three Phase Industrial Applications” , November 2006

[43] Power Integrations, Application Note AN-37, LinkSwitch-TN Family

[44] Power Integrations, product datasheet, LinkSwitch-TN Family, www.powerint.com

[45] Power Integrations, Flyback Transformer Design For TOPSwitch® Power Supplies Application Note AN-17

[46] Power Integrations, TOPSwitch® Flyback Transformer Construction Guide, Application Note AN-18

[47] STMicroelectronics, L5973D datasheet, 2.5 A switch step down switching regulator

[48] Avago Technologies, HFBR-1528Z,HFBR-2528Z datasheet, 10 Megabaud Versatile Link Fiber Optic Transmitter and Receiver for 1 mm POF and 200 µm HCS®

[49] Avago Technologies, HCPL-7800 datasheet, Isolation Amplifier

[50] LEM, Current transducer LTS 15-NP datasheet

[51] Piller home page, http://www.piller.com/site/8/Dynamic.asp?nav_id=115

[52] E1 DYNAMICS home page, http://www.e1dynamics.com/topology.php

[53] POWER*THRU home page, http://www.power-thru.com/22.html*

[54] Active Power, Inc. Home page, http://www.activepower.com/solutions/dc-energy-storage-systems/

[55] TEAL Electronics Corporation, BoostBridge, Short Term Ride-Through Batteryless UPS & Power Conditioning Units; 5kVa to 20kVA Models

[56] M-Field Energy Ltd., http://www.fuelcellmarkets.com/M_Field_Energy/forming_relationships/3,1,28266,18,28460.html

[57] My Ton, Brian Fortenbery DC Power for Improved Data Center Efficiency, March 2008

[58] D.A.J. Rand, J. Garche, P.T. Moseley, C.D. Parker Valve-regulated Lead–Acid Batteries, ELSEVIER, 2004

[59] Калатаров П. А., Цейтлин Л. А., „Расчот индуктивностей, справочная книга, издание третье, переработанное и даполненное”, Ленинград, Энергоиздат Ленинградское отделение, 1986. г.

[60] Maxwell technologies, K2 SERIES 650F - 3,000F ULTRACAPACITORS datasheet

[61] I. H. Altas, and A.M. Sharaf, “A Photovoltaic Array Simulation Model for Matlab-Simulink GUI Environment”, International Conference on CLEAN ELECTRICAL POWER, ICCEP '07, 21-23 May 2007

[62] Kajihara, A.; Harakawa, A.T., “Model of photovoltaic cell circuits under partial shading”, IEEE International Conference on Industrial Technology 2005, ICIT 2005, Hong Kong, 14-17 Dec., 2005

[63] HAMAMATSU Photonics, Photodiode Technical information

[64] NED MOHAN, First course on Power Electronics and drives, MNPERE, 2003

[65] Florin IOV, Frede BLAABJERG, Roger BASSETT, Jon CLARE, Alfred RUFER, Stefano SAVIO, Peter BILLER, Paul TAYLOR, Brigitte SNEYERS, “Advanced power converter for universal and flexible power management in future electricity network”, 19th International Conference on Electricity Distribution, Vienna, 21-24 May 2007

[66] Joe Oreskovic, ”The Modular UPS Responding to the Market’s Need”, Eaton Power Quality Company, INFOBATT, April 2010, Toronto

[67] Koen De Gusseme, David M. Van de Sype, Jeroen Van den Keybus, Alex P. Van den Bossche, Jan A. Melkebeek, “Fully Equipped Half Bridge Building Block for Fast Prototyping of Switching Power Converters”, 35th Annual IEEE Power Electronics Specialists Conference Aachen, Germany, 2004

[68] Frede Blaabjerg, Remus Teodorescu, Zhe Chen, Marco Liserre, “Power converters and control of renewable energy system”

Appendixes

VPM Power board schematics

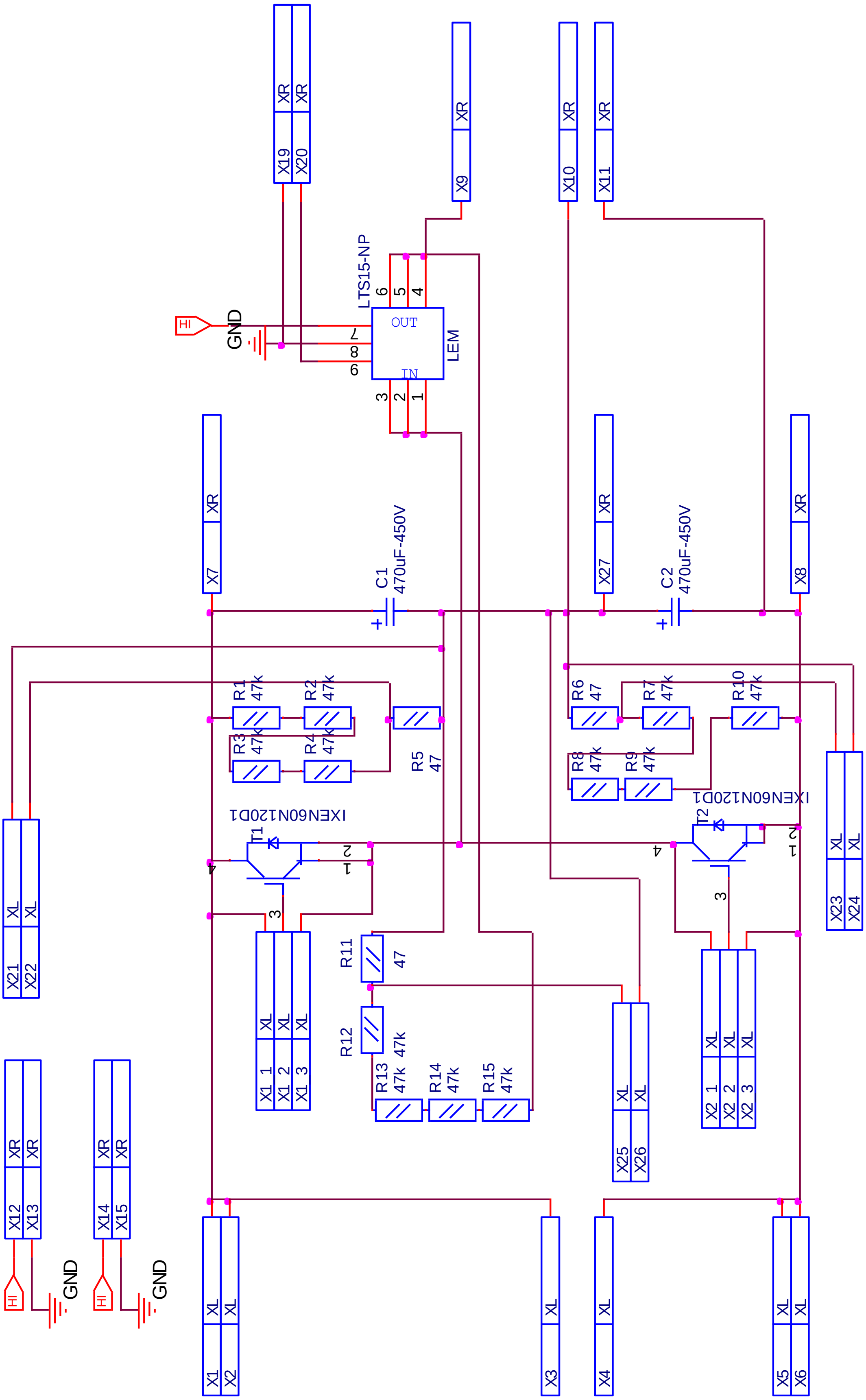

VPM Power board layout

Top layer of first PCB

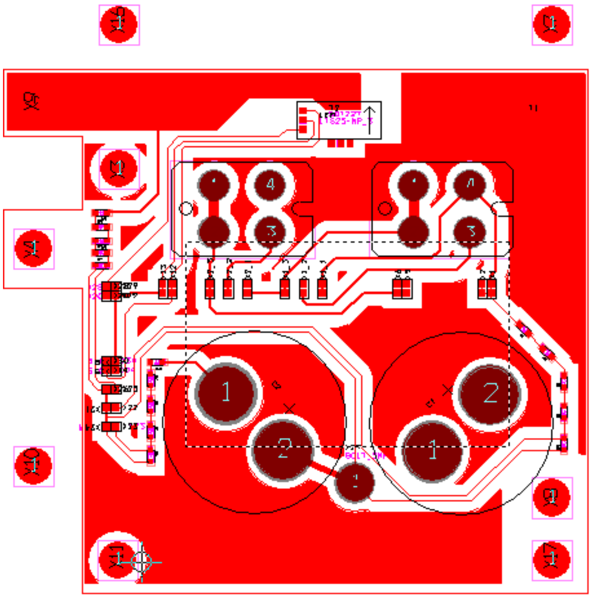

Bottom layer of first PCB

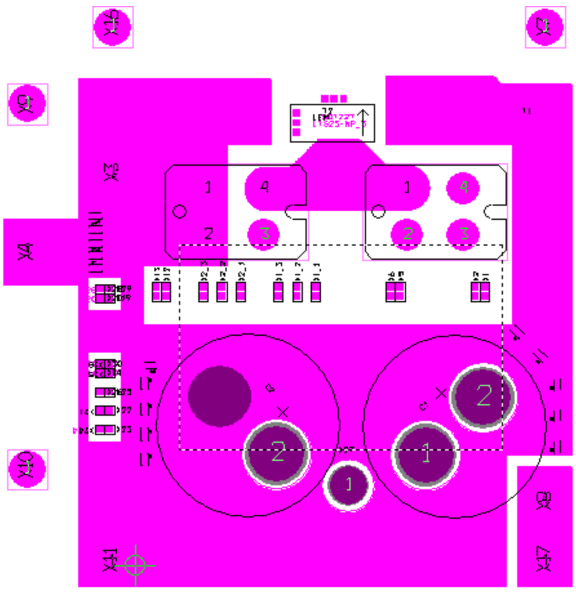

Top layer of second PCB

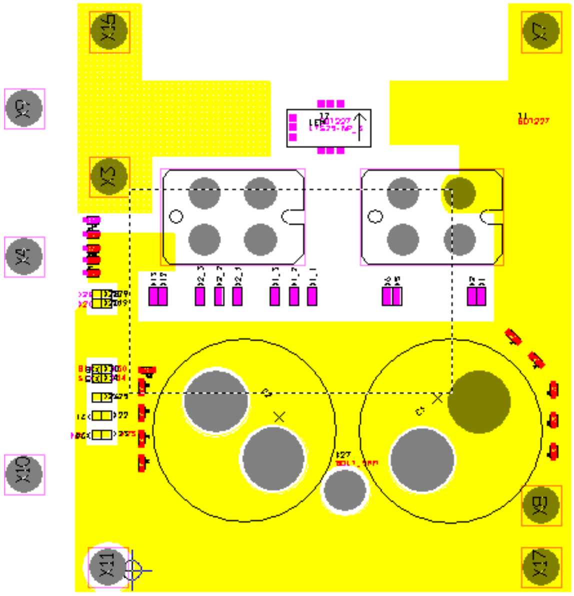

Bottom layer of second PCB

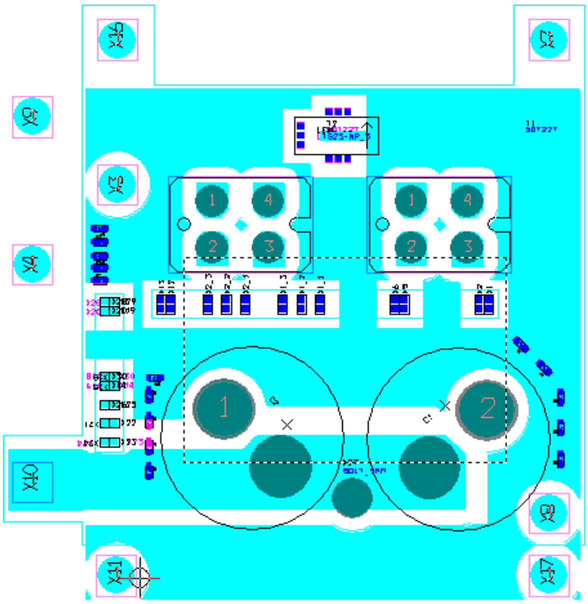

Appendix B

VPM driver board schematics

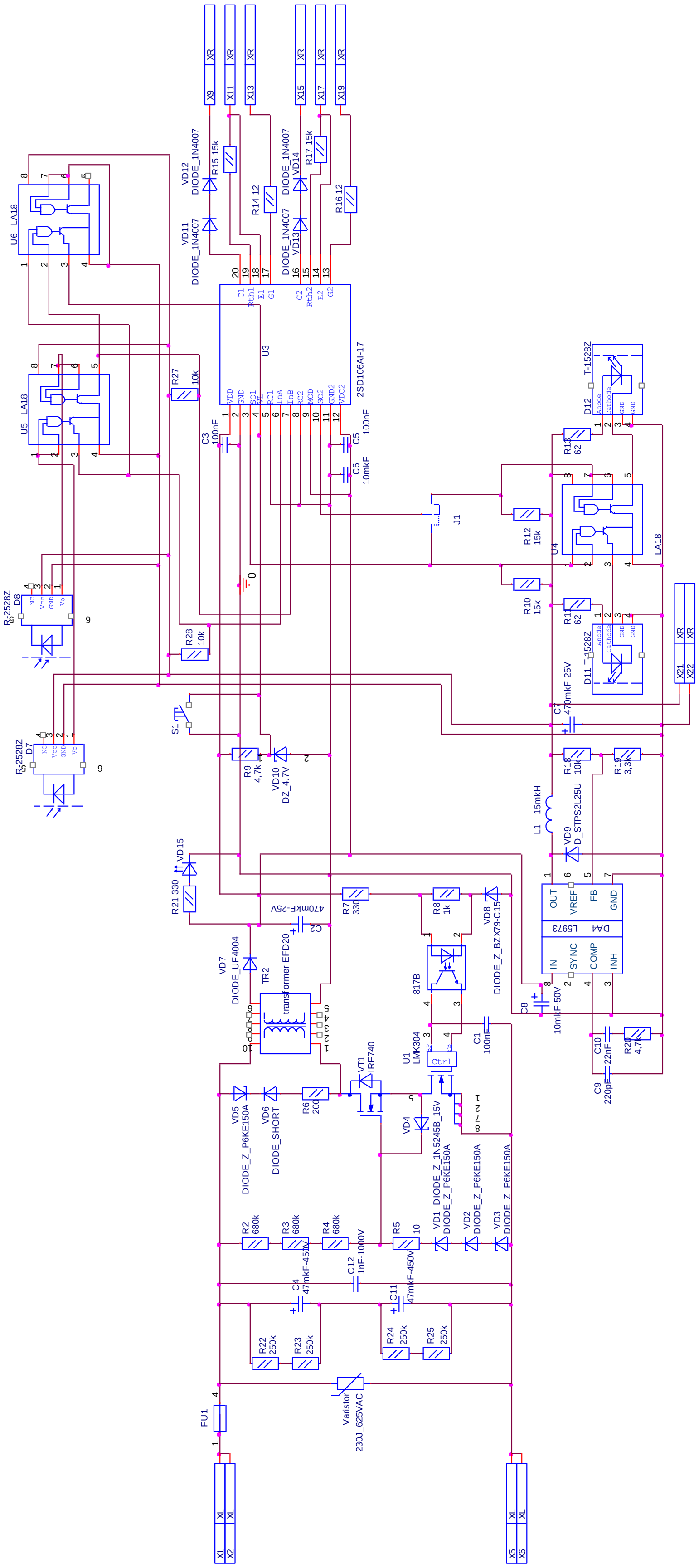

VPM driver board schematics

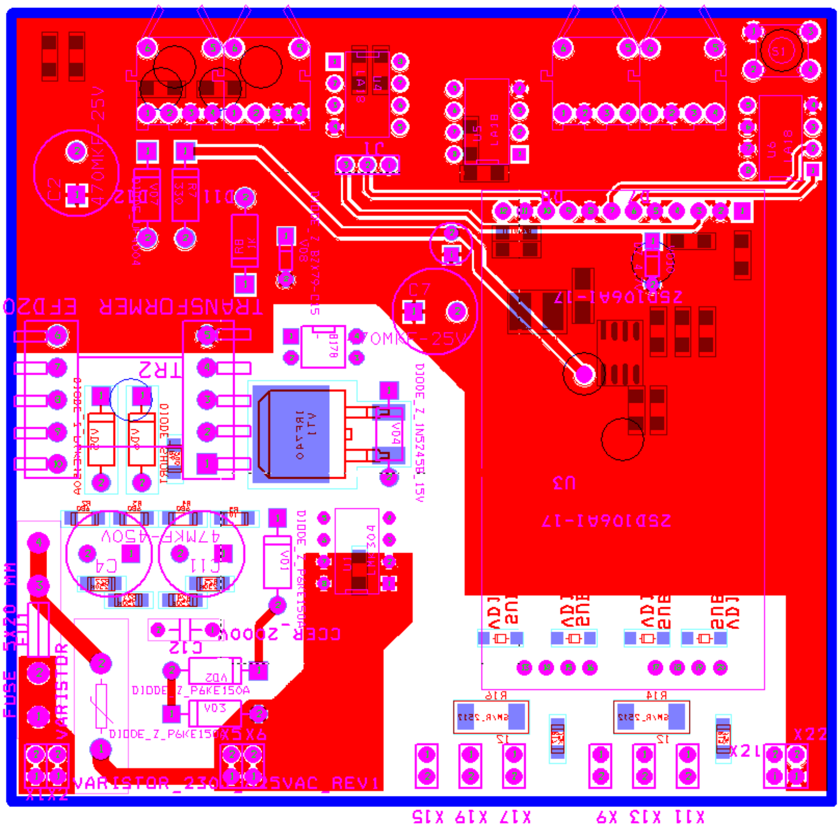

a) Top layer of driver board

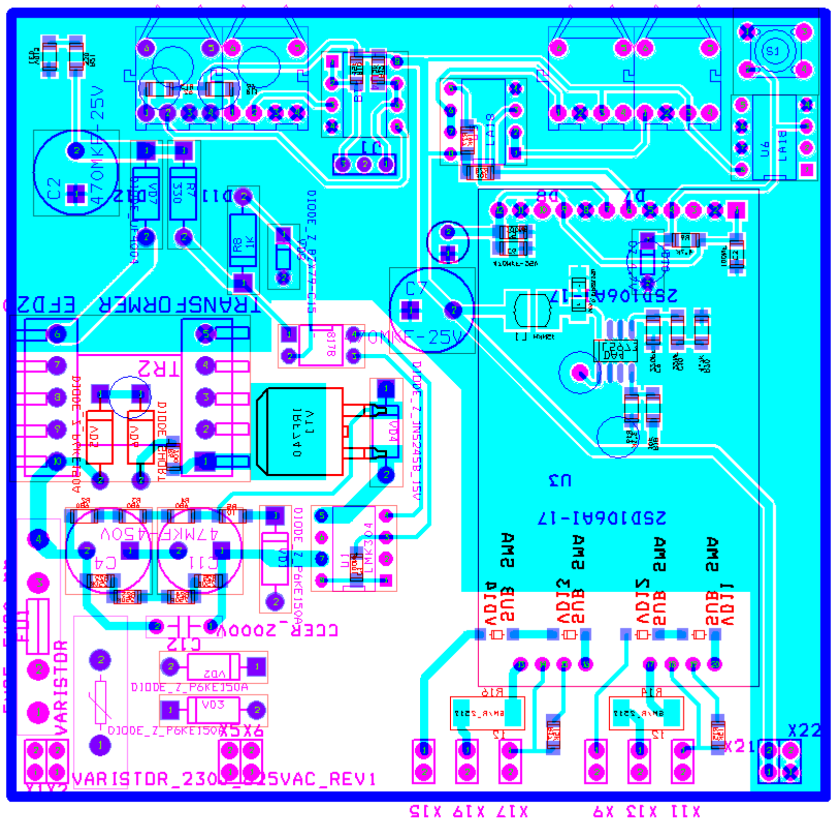

b) Bottom layer of driver board

Appendix C

VPM measurement board schematics

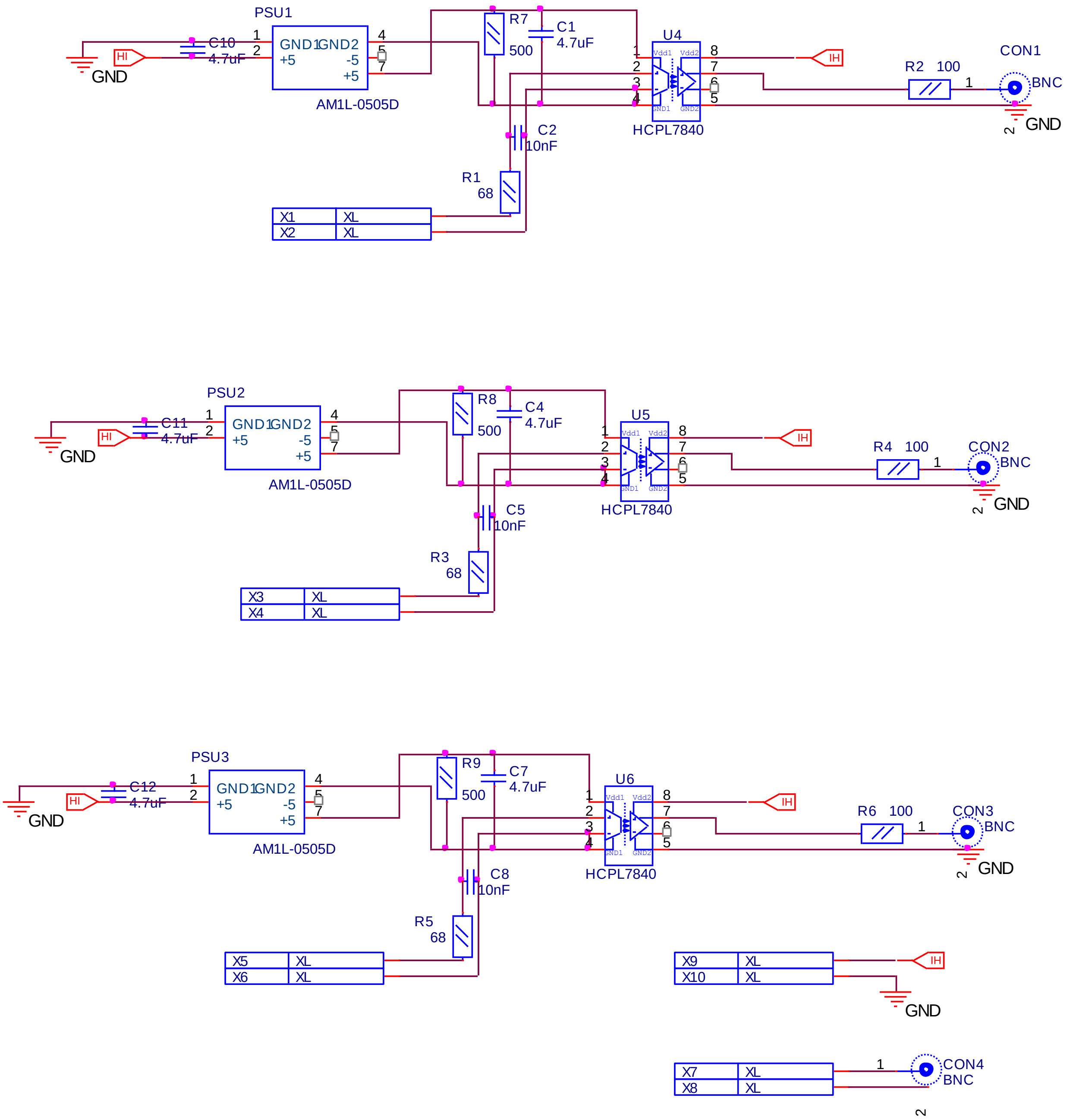

VPM measurement board layout

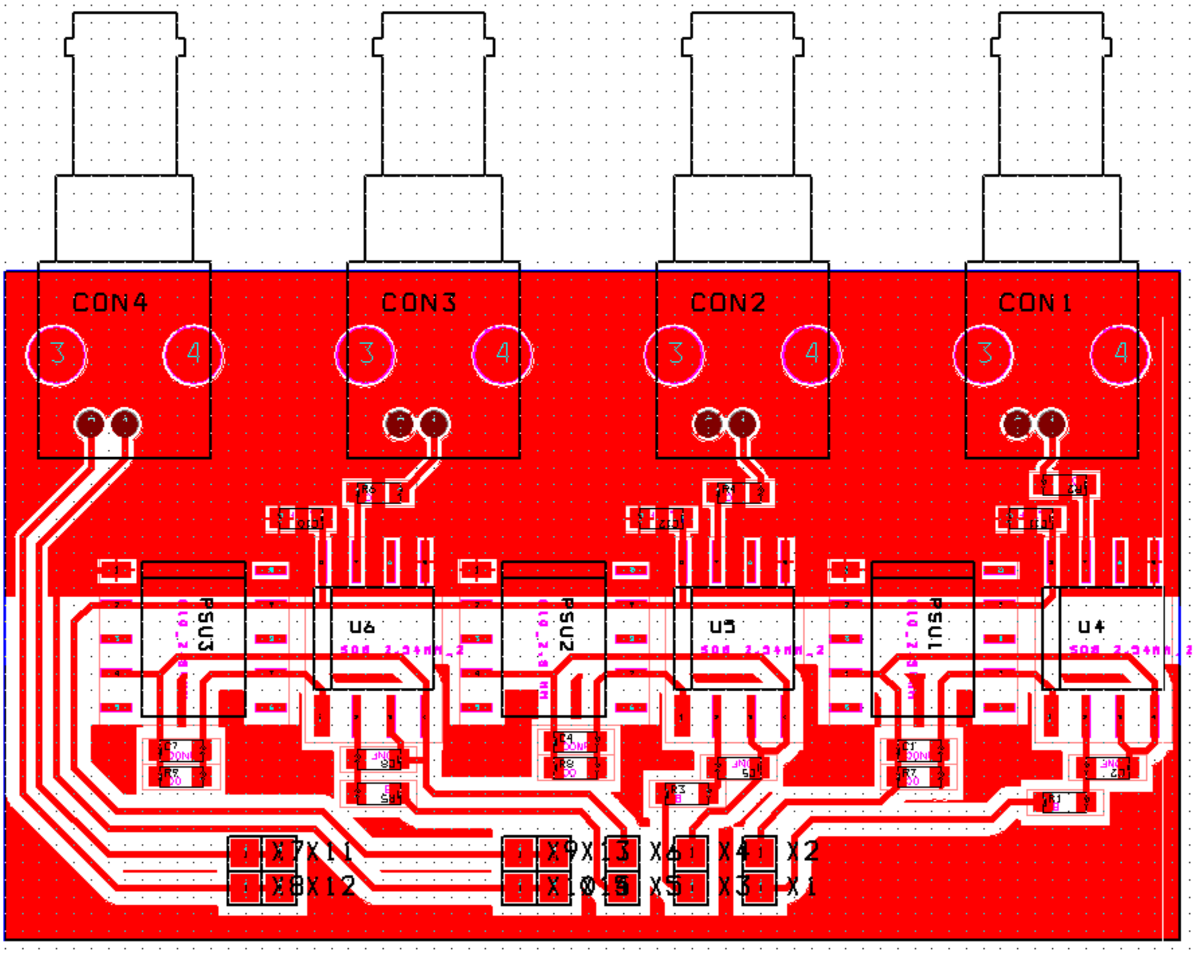

VPM adopter board schematics

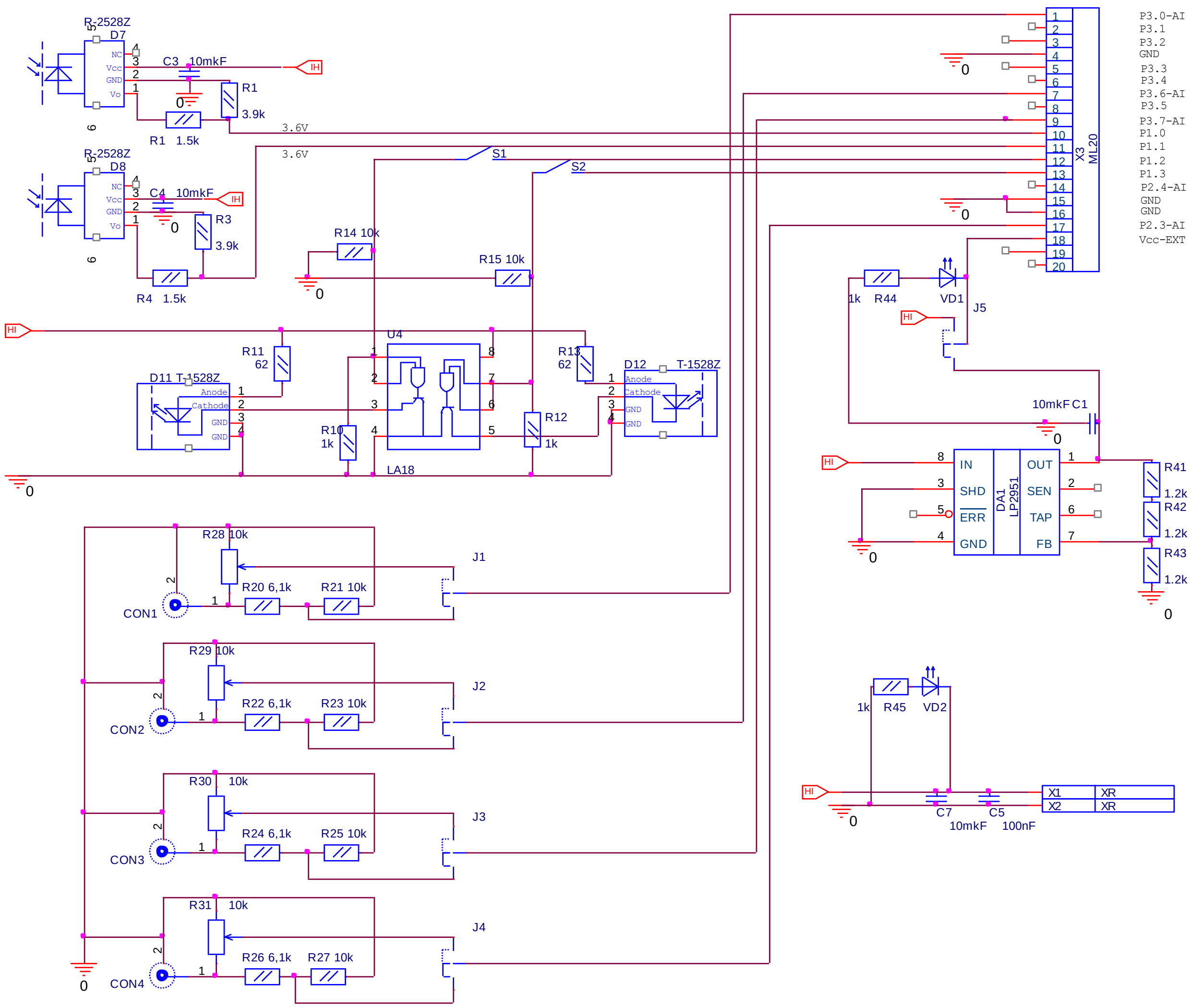

VPM adopter board layout